Departamento de Física Estelar
INSTITUTO DE ASTROFÍSICA DE ANDALUCÍA
Consejo Superior de Investigaciones Científicas

Gamma-ray burst afterglows and instrumentation for their study: From BOOTES to X-shooter

Memoria que presenta
D. Antonio de Ugarte Postigo
para optar al grado de
Doctor en Física.

Directores de Tesis:
Dr. Alberto J. Castro-Tirado
Dr. Filippo M. Zerbi

INSTITUTO DE ASTROFÍSICA DE ANDALUCÍA
junio de 2007

Editor: Editorial de la Universidad de Granada
Autor: Antonio de Ugarte Postigo
D.L.: Gr. 1442 - 2007
ISBN: 978-84-338-4389-0

Resumen en Castellano

Desde el anuncio de su descubrimiento fortuito en 1973, las **explosiones de rayos gamma** han sido uno de los mayores misterios de la Astrofísica moderna. Durante este tiempo, los avances en el conocimiento de las explosiones de rayos gamma han estado determinados por desarrollos tecnológicos que hicieron posibles nuevas y mejores observaciones. Durante casi tres décadas, la baja precisión de las localizaciones en rayos gamma y la demora en la distribución de las coordenadas impidió la detección de contrapartidas en otras longitudes de onda. El completo desconocimiento de la escala de distancias a la que se producían estos fenómenos llevó a la formulación de un gran número de modelos de la más diversa índole. El gran avance se produjo cuando, en 1997, el satélite *BeppoSAX* fue capaz de observar las contrapartidas X de varias explosiones de rayos gamma y de determinar su posición con una precisión de unos pocos minutos de arco. Esto llevó al descubrimiento de las primeras contrapartidas en bandas ópticas, milimétricas y radio y a la medida espectroscópica de su distancia, ubicándolos a distancias cosmológicas. De este modo se entró en una era de descubrimientos a través del estudio multibanda de estas contrapartidas de larga duración, las conocidas como postluminiscencias.

Observacionalmente, las explosiones de rayos gamma son breves (entre 10^{-3} y 10^{3} segundos) pero muy intensos fogonazos de fotones de alta energía (de $\sim$ 1 keV a 10 GeV) que ocurren a un ritmo de unas pocas por día en el Universo. Durante estos breves segundos se convierten en las fuentes más brillantes de todo el cielo en rayos gamma para después desaparecer. Sin embargo, la postluminiscencia de estas explosiones se puede observar en todo el rango electromagnético y pueden ser estudiadios durante periodos mucho más largos en escalas de días, semanas o incluso meses en el caso de ondas de radio. Las explosiones de rayos gamma pueden dividirse en dos clases principales, atendiendo a su duración: explosiones largas, con una duración media de unos 20 segundos y comprendiendo el 75% de los eventos y las explosiones cortas, con una duración media de 0.1 segundos representando el 25%. Se han realizado otras clasificaciones, de las cuales es mayoritariamente aceptada la división entre explosiones de rayos gamma, explosiones ricas en rayos X y fogonazos de rayos X. Esta división (referida al grupo de explosiones largas) corresponde a la diferencia de la dureza espectral en la emisión temprana, teniendo las explosiones de rayos gamma el espectro más energético y los fogonazos de rayos X el más suave. A diferencia de la división entre explosiones cortas y largas, esta división no parece distinguir entre diferentes tipos de fenómenos astrofísicos.

Hasta el año 2005, todas las postluminiscencias que se habían detectado correspondían a la clase de explosiones largas y, a día de hoy tenemos una imagen más o menos clara de su origen. Se piensa que las **explosiones de rayos gamma largas** son el resultado del colapso de estrellas supermasivas, con tiempos de vida extremadamente cortos y que acaban sus días convirtiéndose en agujeros negros y liberando enormes cantidades de energía a través de un par de chorros con expansiones ultrarelativistas que producen los rayos gamma mediante choques internos y la postluminiscencia mediante la interacción de los chorros con la materia interestelar que rodea la explosión. En el momento del colapso se produce también una explosión de supernova que, en los eventos más cercanos, puede ser observada al emerger pasadas unas semanas de la explosión inicial. Debido a su corta vida, estas explosiones se producen muy cerca de los lugares de nacimiento de las estrellas progenitoras, en las

zonas de mayor formación estelar de galaxias extremadamente azules, subluminosas y con una baja metalicidad. Por otro lado, las **explosiones de rayos gamma cortas** no están aún tan bien estudiadas, aunque se sabe que se producen en tipos de galaxias mucho más heterogéneos, con poblaciones estelares dominantes de edades típicamente mayores. Debido a la falta de componente de supernova y a la forma de la emisión gamma temprana, se piensa que son producidas, no por el colapso de estrellas supermasivas, sino por la coalescencia de un sistema binario compacto, probablemente formado por dos estrellas de neutrones o una estrella de neutrones y un agujero negro. Sin embargo, la naturaleza de estas explosiones cortas dista mucho de ser bien comprendida e incluso observaciones recientes parecen indicar que podrían no estar producidas por un único fenómeno.

En esta Tesis hemos estudiado una muestra representativa de explosiones de rayos gamma que nos dan una idea de los diferentes tipos de explosiones que se observan. Una explosión larga clásica, una explosión rica en rayos X, una explosión corta oscura y una brillante explosión corta que localizamos a alto corrimiento al rojo:

GRB 021004[1] es una explosión clásica, brillante y de larga duración que fue localizada rápidamente y con un seguimiento intenso en todas las longitudes de onda. Reunimos observaciones abarcando desde unos minutos después de la explosión hasta varios años después, cuando sólo la galaxia anfitriona podía ser detectada. La curva de luz se caracteriza por una serie de jorobas que la desvían de la evolución típica de caída según una ley de potencias predicha por los modelos estándares. Ajustamos la curva de luz, en las 14 bandas diferentes para las que tenemos datos, utilizando un modelo de bola de fuego al que hemos añadido hasta 7 inyecciones de energía. Estas inyecciones son debidas a la llegada de sucesivas conchas ultrarelativistas que se emitieron en el momento de la explosión con diferentes velocidades. La postluminiscencia estaría producida por la interacción de la concha más rápida con el medio circundante. Al irse decelerando esta por la interacción, sería alcanzada por la siguiente más rápida, produciéndose un abrillantamiento de la curva de luz. Los sucesivos episodios de inyección producirían cada una de las jorobas. Así mismo presentamos un estudio de la galaxia anfitriona de esta explosión, caracterizada por estar dominada por la baja extinción, un brote de formación estelar y una magnitud absoluta de $M_B \simeq$-22.0.

GRB 050408 es una explosión rica en rayos X, el grupo intermedio entre las explosiones de rayos gamma clásicas y los fogonazos de rayos X. Para este estudio obtuvimos una completa curva de luz multibanda, que abarca desde el mismo momento de la explosión hasta varios meses después, cuando ya solo la galaxia anfitriona es detectable. Las observaciones se completan con datos de radio y ondas milimétricas que, combinadas con los datos X de la literatura, constituyen el conjunto de datos más completo para una explosión rica en rayos X recopilado hasta la fecha. Las curvas de luz se caracterizan por una época temprana en la que la curva es plana y una intensa joroba con un máximo en torno a 6 días después de la explosión. Explicamos la primera como debida a un chorro visto ligeramente fuera de eje y la joroba mediante una inyección de energía de intensidad comparable a la explosión inicial. El análisis de la distribución espectral de energía de la postluminiscencia revela una extinción compatible con un bajo enriquecimiento químico del entorno de la explosión.

[1] Las explosiones de rayos gamma se nobran siguiendo la notación "GRB AAMMDD", siendo AAMMDD el año, mes y día en que ocurrió. GRB procede del inglés Gamma-Ray Burst (explosión de rayos gamma).

Conjuntamente con la detección de una galaxia subyacente con brote de formación estelar, típica de las explosiones largas, nuestras observaciones fortalecen la asociación entre las explosiones ricas en rayos gamma y las clásicas explosiones de rayos gamma largas.

GRB 050509B fue la primera explosión de rayos gamma corta detectada y localizada con precisión a través de rayos X por *Swift*. Los datos que recogimos para este evento abarcan desde el momento de la explosión hasta 18.8 días después. A pesar de la rápida respuesta y de la profunda campaña de seguimiento, no se consigió localizar contrapartida alguna en óptico, infrarrojo cercano u ondas milimétricas. Sin embargo, una galaxia elíptica brillante, localizada a un corrimiento al rojo de $z = 0.225$ fue identificada en el borde de la zona de error y se propuso como el candidato más probable a haber albergado la explosión de rayos gamma. A través de un estudio de la distribución espectral de flujo deducimos que se trata de una galaxia con una población estelar dominante con una edad de ~ 720 Maños, mucho más vieja que cualquiera de las galaxias anfitrionas previamente observadas para explosiones largas, dando una clara indicación de los diferentes ambientes en que se producen las explosiones largas y cortas. Durante las semanas que siguieron a la explosión, se realizó una profunda búsqueda para localizar la componente de supernova, que debería poderse observar según algunos modelos, pero no se localizó nada, imponiéndose unos límites muy estrictos. Si la explosión se produjo, tal y como parece, en las afueras de la galaxia elíptica, la ausencia de la componente de supernova favorecería las teorías que indican que las explosiones cortas se producen por la coalescencia de un sistema binario compacto. Sin embargo, durante la búsqueda de la posible supernova se identificaron varias galaxias débiles más en la zona de error de la explosión, de modo que un origen a un corrimiento al rojo mucho mayor no puede ser descartado.

El primer puñado de contrapartidas de explosiones cortas que se detectaron antes del final de 2005 fueron localizadas embebidas en galaxias subyacentes brillantes y cercanas ($z < 1$). **GRB 060121** fue la primera explosión corta para la que se detectó una postluminiscencia con un brillo claramente superior al de su galaxia anfitriona. Para este evento obtuvimos observaciones ópticas y en infrarrojo cercano, que utilizamos para obtener un corrimiento al rojo fotométrico que resultó devolver dos posibilidades: La primera, con una mayor probabilidad, correspondería a un $z = 4.6$, y la segunda menos probable a $z = 1.7$. En cualquier caso, GRB 060121 es la explosión de rayos gamma más distante para la que se ha localizado contrapartida óptica, implicando una liberación de energía comparable a la de las explosiones largas y mucho mayor de las previamente observadas para explosiones cortas. Nuestros resultados sugieren que este evento podría corresponder a una familia de eventos cortos muy energéticos, localizados a $z > 1$ y con contrapartidas más brillantes que sus galaxias anfitrionas. Así mismo discutimos la posibilidad de que esta explosión corresponda a un grupo de eventos de duración intermedia.

Como ya indicamos al comienzo de este resumen, los avances en la investigación de las explosiones de rayos gamma han sido determinados en una gran medida por los desarrollos tecnológicos. Un avance crucial fue el uso de observatorios robóticos para la observación automática de explosiones de rayos gamma tan solo unos segundos después de su detección por satélites. Uno de estos observatorios robóticos es **BOOTES** (the Burst Observer and Optical Transient Exploring System, el sistema de observación de explosiones y de exploración de fenómenos ópticos transitorios), que vio primera luz en 1998 con un único telescopio y que ahora cuenta con 3 observatorios, 5 telescopios, 9 cámaras y que continúa en crec-

imiento. El autor de esta Tesis ha participado en gran parte de las fases del proyecto, para el que se han debido abordar numerosos desarrollos tecnológicos. Una de las contribuciones fue el diseño de un espectrógrafo de campo amplio para observar el espectro de explosiones de rayos gamma durante los primeros minutos de emisión. Otra contribución importante fue el desarrollo de un paquete de programas para la reducción y el análisis de imágenes del observatorio que se describe en el párrafo siguiente. Durante los nueve años de vida de BOOTES, los observatorios han seguido más de 100 alertas, resultando en la publicación de múltiples circulares astronómicas, contribuciones a congresos y artículos arbitrados. La ciencia secundaria ha tenido también un importante papel en los observatorios de BOOTES, siendo destacable la productividad de los estudios de meteoros.

Un observatorio robótico no solo debe ser capaz de realizar observaciones autónomas, sino también de manejar los datos que se generan durante las observaciones y de usarlos para mejorar el programa de observación sin intervención humana. **JIBARO** (**J**oined ut**I**lities in **B**OOTES for the **A**nalysis and **R**eduction of **O**bservations, unión de utilidades para la reducción y análisis de observaciones en BOOTES) es un grupo de programas que fueron desarrollados en el contexto del proyecto BOOTES para reducir y analizar observaciones en tiempo real, con la capacidad de detectar nuevas fuentes tales como las contrapartidas ópticas que siguen a una explosión de rayos gamma. El resultado de las observaciones puede ser utilizado para interaccionar con el propio observatorio y para generar alertas externas que comuniquen la detección de fenómenos astronómicos relevantes a los científicos. Los programas han sido recientemente mejorados para ser utilizados con las imágenes de los telescopios de varios observatorios profesionales.

Finalmente, presentamos nuestra contribución a **X-shooter**, un espectrógrafo de segunda generación que será instalado en el foco Cassegrain de una de las unidades de 8 m del VLT, operado por el Observatorio Europeo Austral. Este instrumento será capaz de obtener un espectro de resolución intermedia que cubrirá el rango de 300 a 2,500 nm en una única exposición. Este amplio rango espectral, con una alta eficiencia, es obtenido mediante el uso de 3 espectrógrafos Echelle diferentes, cada uno optimizado para un rango diferente y alimentado a través de dicroicos que dividen el haz de luz con mínimas pérdidas. El autor ha participado como encargado del paquete de trabajo de las redes de difracción, responsable de la simulación adquisición y análisis de las redes para los espectrógrafos visible y ultravioleta. Estos dos espectrógrafos se encuentran en fase de montaje en el Observatorio Astronomico de Brera (Italia) y viajarán a la central del Observatorio Europeo Austral en Garching (Alemania) en el mes de agosto, donde se completará la integración del instrumento completo, que viajará a Chile en la primavera de 2008, estando la primera luz prevista para el verano de 2008. Este instrumento será una importante herramienta para muchas ramas de la astrofísica debido a su alta eficiencia y a su amplia cobertura espectral. Será especialmente útil para el estudio de las explosiones de rayos gamma, donde servirá para investigar el Universo más lejano con una efectividad sin precedentes.

Summary

Since the announcement of their serendipitous discovery in 1973, **gamma-ray bursts** have been one of the greatest mysteries of modern Astrophysics. During this time, gamma-ray burst advances have been determined by technological developments that made new observations possible. During almost 3 decades, their imprecise localisation in gamma-rays and the delay in the delivery of their coordinates prevented the detection of counterparts in other wavelengths. The complete ignorance on the distance scale at which they were happening led to the formulation of a large amount of models of the most diverse and exotic nature. The great leap forward came in 1997 when *BeppoSAX* was able to observe the counterpart of a gamma-ray burst in X-rays and quickly determine its coordinates with a precision of a few arcminutes. This led to the discovery of the first optical, millimetre and radio counterparts and the firm localisation of gamma-ray bursts at cosmological distances. In this way we entered into an era of discoveries through the multiwavelength study of these long living counterparts of gamma-ray bursts, the so called afterglows.

Observationally, gamma-ray bursts are brief (from 10^{-3} to 10^{3} seconds) but very intense flashes of high energy photons (from $\sim$1 keV to 10 GeV) that occur at a rate of a few per day throughout the Universe. During a few seconds they outshine every other source of gamma-rays in the sky and they then disappear. However, the afterglows of gamma-ray bursts are observed in all other wavelengths, from radio to X-rays and can be detected during much longer times, in the scale of days, weeks or even months in the case of radio wavelengths. Gamma-ray bursts can be mainly divided into two classes of bursts, according to their duration: long bursts, with an average duration of 20 seconds and representing 75% of the total number of events and short burst, with an average duration of 0.1 seconds and represent the remaining 25%. Other classifications have been attempted, of which the division between gamma-ray bursts, X-ray rich bursts and X-ray flashes is also widely accepted. This division (referred to the long group of events) corresponds to the difference in the hardness of the spectra during the early emission, having gamma-ray bursts the highest energy spectra and X-ray flashes the softest ones. Unlike the division between long and short bursts it does not seem to distinguish between different kind of astrophysical phenomena.

Up to the year 2005 all the afterglows that had been detected corresponded to the long duration class of events and a more or less clear picture is now accepted for them. **Long gamma-ray bursts** are thought to be the result of the collapse of extremely massive, short-living stars that end their lifes collapsing into a black hole and releasing a vast amount of energy through a pair of ultrarelativistic expanding jets that produce the gamma-rays through internal shocks and the afterglow by the interaction of the jets with the interstellar medium that surrounds the burst. At the time of the collapse a supernova-like explosion is also produced which, in the nearest cases, can be observed to emerge a few weeks after the burst onset. Due to their short life, these bursts happen very near to the birth place of the stars and are produced in the richest star forming regions of extremely blue, sub-luminous, low metallicity galaxies. On the other hand, **short bursts** are not so well studied, but are known to be produced in a much more heterogeneous kind of galaxies, with much older typical dominant stellar populations. Together with the lack of any supernova component and the shape of their gamma emission, they are thought to be produced, not by the

collapse of a massive star, but by the merge of a compact binary system, probably formed by a neutron star - neutron star or a neutron star - black hole pair. However, the nature of these these short events is still far from clear and some recent discoveries could indicate that short bursts are not even formed by a unique population of events.

In this Ph.D. Thesis we have studied a representative sample of gamma-ray bursts that give us an idea of the different kind of bursts that are observed. A classical long burst, an X-ray rich burst, a short dark burst and a bright high redshift short burst:

GRB 021004[2] is a "classical", bright, long duration burst that was rapidly detected and intensively followed up in all wavelengths. We gathered observations ranging from a few minutes after the burst onset to several years after, when only the host galaxy could be detected. The light curve is characterised by a number of bumps that make it depart from the typical power law evolution predicted by the standard models. We fit the light curve in the 14 different bands for which we have data using a standard fireball model to which we have added up to 7 energy injections. These injections would be produced by different ultrarelativistic shells that were released with different velocities during the initial moments of the burst. The afterglow would be driven by the interaction of the fastest moving shell with the surrounding medium. As this shell is decelerated by the interaction it would be caught by the following shell producing an energy increase and a rebrightening of the light curve. The successive episodes would produce each of the bumps. We also observed and studied the host galaxy of this burst, that resulted to be a low extinction starburst galaxy with an absolute magnitude of $M_B \simeq$-22.0.

GRB 050408 is an X-ray rich burst, the intermediate class between the hard spectrum gamma-ray bursts and the softer X-ray flashes. We obtained a comprehensive multiband optical light curve, covering the time from the onset of the burst to several months later, when only the host galaxy was detectable. The observations are completed with radio and millimetre data and combined with near infrared and X-ray observations from the literature to produce what, to our knowledge, is the completest dataset for an X-ray rich event to date. The light curves are characterised by an early flattening and an intense bump peaking around 6 days after the burst onset. We explain the former through an off-axis viewed jet and the latter with an energy injection equivalent in intensity to the initial shock. The analysis of the spectral flux distribution of the afterglow reveals an extinction compatible with a low chemical enrichment surrounding the burst. Together with the detection of an underlying starburst host galaxy, typical of long gamma-ray bursts, the observations strengthen the link between X-ray rich bursts and classical long gamma-ray bursts.

GRB 050509B was the first short duration gamma-ray burst detected and precisely localised through X-rays by the *Swift* mission. The data that we collected range from the moment of the burst to 18.8 days later. In spite of the fast response and the deep follow-up campaign, no optical, near infrared or millimetre counterpart was detected. However, a bright elliptical galaxy lying at a redshift of $z = 0.225$ was found at the edge of the error box, being identified as the most probable candidate for having hosted the gamma-ray burst. From a spectral flux distribution of this galaxy we derive a dominant stellar population with an age of $\sim$ 720 Myr, much older than any of the previously observed hosts of long

[2]Gamma-ray bursts are bubbed "GRB YYMMDD" with YYMMDD being the year month and day of occurrence.

gamma-ray bursts, giving the first clue to the differences between the environments of long and short events. During the weeks that followed the gamma-ray burst, a deep search was carried to look for any supernova component that should be observable according to some models but nothing was detected down to very strong limits. If the burst was, as it seemed produced in the outskirts of the elliptical galaxy, the lack of this supernova component would favour the theories that claimed that short bursts would be produced by the merge of a compact binary system. However, during the surveys for a supernova component, several other faint galaxies were detected in the error box of the burst, so a higher redshift origin can not be completely discarded.

The first handful of short gamma-ray burst afterglows detected before the end of 2005 were found to be embedded in nearby ($z < 1$), bright galaxies. **GRB 060121** was the first short burst observed to clearly outshine its host galaxy. We obtained optical and near infrared observations of the event and through a photometric redshift, located the burst at a most probable redshift of $z = 4.6$ with a less probable $z = 1.7$. In either case, GRB 060121 is the furthermost short duration GRB optical afterglow ever detected and implies an energy release comparable to long bursts and much larger than the previously observed for other short bursts. Our results suggest that this event may correspond to a family of energetic short events lying at $z > 1$ and with afterglows that would outshine their host galaxies. We also discuss the possibility of this burst being part of an intermediate group of events

As we stated at the beginning of this summary, the advances of gamma-ray burst science have been greatly determined by technological developments. A crutial advance was the use of robotic observatories to automatically observe gamma-ray bursts just a few seconds after their detection by satellites. One of these robotic observatories is **BOOTES** (the Burst Observer and Optical Transient Exploring System), which saw first light in 1998 with a single telescope and that now counts with 3 observatories, 5 telescopes, 9 cameras and is still growing. The author of this Thesis has participated in most of the different phases of the project, for which many technological developments had to be accomplished. One of the contributions was the design of a wide field spectrograph to observe the spectra of gamma-ray bursts during the first minutes of the emission. Another important contribution is the development of the image reduction and analysis software of the observatory which is described in the following paragraph. During the nine years of life of the BOOTES project, the observatories have followed over 100 gamma-ray bursts that resulted in the publication of several astronomical circulars, proceedings and refereed papers. Secondary science has also had an important place in the observations of BOOTES, being worth mentioning the productivity of the observation of meteors.

A robotic observatory must not only be able to do autonomous observations, but also to handle the data that is generated during the observations and use it to improve the observing plan without human intervention. **JIBARO** (**J**oined ut**I**lities in **B**OOTES for the **A**nalysis and **R**eduction of **O**bservations) is a group of programmes that we developed in the context of the BOOTES project in order to reduce and analyse astronomical images in real time, being capable of detecting new sources such as optical counterparts of gamma-ray bursts. The results of the observations can be used to interact with the observatory itself and to generate external alerts that communicate a relevant astronomical event to the scientists. The software has been now upgraded to be used with the images of large telescopes of several observatories.

Finally, we present our contribution to **X-shooter**, a second generation spectrograph that will be mounted on the Cassegrain focus of one of the 8 m units of the Very Large Telescope, operated by the European Southern Observatory. This instrument will be capable of obtaining a medium resolution spectrum that will cover the range from 300 to 2,500 nm in a single exposure. This wide range is accomplished with a very high throughoutput thanks to the use of three different Echelle spectrographs that are each optimised for a different wavelength range and that are fed by dichroics that divide the optical beam with minimum light losses. The author has been the workpackage manager responsible of the simulation, procurement and testing of the diffraction gratings of the ultraviolet and visible spectrographs. These two spectrographs are now being assembled in Brera Observatory, at Merate (Italy) and will travel to the ESO headquarters in Garching (Germany) during August, where the complete instrument will be assembled. The current schedule expects the instrument to travel to Chile during the Spring of 2008 and first light is foreseen in Summer 2008. This instrument will be a very important tool for many branches of Astrophysics due to its high efficiency and wide spectral coverage. It will be specially useful for gamma-ray burst studies, where it will serve to study the most distant Universe with an unprecedented effectiveness.

Index

Part I

Context

1

A brief history of gamma-ray bursts

Since the announcement of their discovery in 1973, gamma-ray bursts (GRBs) have been one of the greatest mysteries of modern Astrophysics. During almost 3 decades, the elusiveness of these events prevented the detection of counterparts in other wavelengths. There was an absolute ignorance of the distance scale at which they were happening, which led to the formulation of over 100 theoretical models of the most diverse and exotic nature. The great leap forward happened when, in 1997, *BeppoSAX* was able to observe the counterpart of a GRB in X-rays and quickly determine its coordinates with a precision of a few arcminutes. This led to the discovery of the first optical, millimetre and radio counterparts and the firm localisation of GRBs at cosmological distances. We had entered into an era of vertiginous research and exciting discoveries that is still ongoing.

1.1 Discovery of GRBs

After witnessing the effects of the nuclear weapons used during World War II and their rapid development (50 nuclear explosions were registered between the first nuclear test was conducted by the United States in July 1945 and the end of 1953), many voices began to rise towards the adoption of a treaty that would ban all nuclear explosions. This efforts led to a partial success when, in 1963, the Limited Nuclear Test Ban Treaty was signed. This treaty prohibited nuclear explosions in the atmosphere, underwater and even in space.

That same year, the first two of a series of satellites were launched by the United States to verify the compliance with the ban. They were named *Vela* as for the Spanish word *velar*, which means 'to guard'. These satellites where designed to detect the gamma-rays that would be generated during a nuclear explosion. Up to 6 pairs of *Vela* satellites were launched during the following decade (see Fig. 1.1). The detectors were triggered many times throughout the lifetime of the *Vela* programme by gamma-ray events, but fortunately none were due to forbidden nuclear detonations.

During the satellites lifetime, Ray Klebesadel, from Los Alamos National Laboratory in New Mexico, carried a search for the gamma-ray bursts that were supposed to be generated during the initial moments of a supernova explosion, as had been predicted by Stirling Colgate (1968). It was already 1969 when, together with Roy Olson, they were searching

Figure 1.1: Artist's impression of one of the *Vela* satellites in orbit. The first pair was launched in 1963, 3 days after the Limited Nuclear Test Ban Treaty was signed. Astronomical gamma-ray sources have to be detected by satellites or high altitude balloons, as the atmosphere is opaque to them.

through the printouts of the data collected by the two *Vela 4* satellites back in 1967. To check the veracity of the bursts they compared the events that had been registered by each of the spacecrafts, searching for simultaneous ones. Finally, when they got to the data collected on the 2^{nd} July 1967 they found a simultaneous detection by *Vela 4A* and *Vela 4B* at 14:19 UT. It was a double peaked signal lasting a few seconds (Fig. 1.2), very different from what was expected from a nuclear explosion. It did not seem to correspond to any detected solar eruption (although this could not be completely discarded) or to any detected supernova. Latter it turned out that it had also been recorded by the *Vela 3* satellites. A previously unknown astronomical gamma-ray source had been detected.

In the following years several other similar events were detected. The new generation of satellites (*Vela 5* and *Vela 6*) had a more accurate timing that allowed to measure the different arrival times of the signal to the satellites. This differential arrival time allowed to obtain a rough localisation of the bursts through triangulation and it was immediately evident that they were not produced by the Sun, Moon or planets, showing a seemingly random distribution in the sky. The discovery of these 'gamma-ray burst of cosmic origin' was reported in a paper published by Klebesadel, Strong and Olson in *The Astrophysical Journal Letters* on 1973, where they presented the analysis of 16 of these events. The first event of July 1967 was not included in this publication, as a solar origin could not be completely discarded (although it is now recognised as the first ever detected GRB). The light curve of the 1967 event was latter presented in a paper by Strong and Klebesadel (1976). Once that these new phenomena had been detected it was time to study them and identify the source that generated them. But the answer was not going to be immediate nor simple.

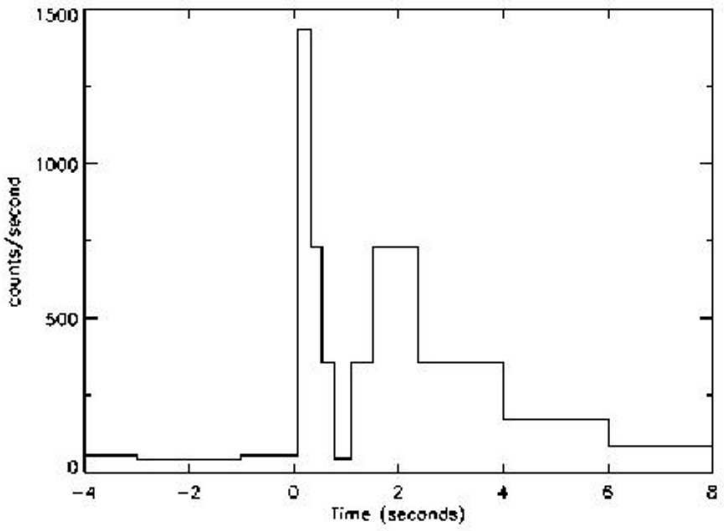

Figure 1.2: Light curve of GRB 670702, the first GRB ever detected (Strong & Klebesadel 1976).

1.2 Dark years

Several balloon experiments in the mid 1970's (Fishman & Derrickson 1975) and early 1980's (Wilson et al. 1982) showed that bigger detectors were needed to be flown to Space in order to observe enough number of GRBs to draw statistical conclusions on their nature. The KONUS instruments aboard *Venera 11* and *12* missions were launched in 1978 and provided over 150 GRB localisations, giving the first indication that GRB were isotropically distributed in the sky. However, in order to identify the astronomical sources that were generating GRBs, astronomers needed to search for something unusual going on in the region in which the events were happening by means of observations at shorter wavelengths. But this was not easy, as the localisations obtained by the satellites were very imprecise, with uncertainties of several degrees and the searches for transients in these error boxes turned out to be unfruitful. The answer to this problem could come from the use of a larger baseline between the detectors, what would be known as the *InterPlanetary Network* (*IPN*). It was proposed by Kevin Hurley, who was working at the time at the Centre d'tude Spatiale des Rayonnements (CESR) in Tolouse. At the end of 1978 the first IPN began to work with 5 space probes carrying gamma-ray detectors. The IPN did succeed in providing localisations of GRBs with uncertainties of the order of arc minutes, but even the deepest surveys failed to find anything unusual in the error boxes (Schaefer 1992; Schaefer 1994). The bursts lasted for only a few seconds in gamma-rays and if we were observing the fields several weeks or months later it could be that whatever had happened was already over at the time of the follow-up observations.

Gerald Fishman and Charles Meegan, from the Marshall Space Flight Center in Huntsville, Alabama proposed and got accepted in 1978 what would come to be BATSE, the Burst And Transient Source Experiment (Fishman 1981). BATSE was an all sky gamma-ray monitor to be installed on one of NASA's 'Great Observatories', the *Compton Gamma*

Ray Observatory (*CGRO*) and that would detect and localise hundreds of GRBs per year. But it would still have to wait until 1991 to be launched.

At the end of the 1980's a few hundred GRBs had been detected, mostly by the *Vela* satellites, the KONUS experiment and the IPN but their nature was almost as obscure as it was at the early 1970's (Higdon & Lingenfelter, 1990). Many theories had been formulated, but without knowing the distance scale at which they were happening a relativistic solar particle interacting with interplanetary matter in our Solar System or a white hole in a distant galaxy were equally valid explanations (see Nemiroff 1994 for a compilation of over 100 GRB models).

1.3 BATSE & the great debate

On the 5^{th} April 1991 finally *CGRO*, the heaviest ever scientific satellite was launched by the Atlantis space shuttle (Fig. 1.3). On board it carried BATSE, which was composed of eight detectors that were placed in each of the corners of the satellite to observe the complete sky. They were sodium iodide scintillators of 51 cm in diameter with three photomultipliers that registered the faint flashes that were produced each time a gamma-ray photon stroked. These detectors also react to cosmic rays, which are much more common than gamma-rays. In order to discriminate them a thin plastic scintillator that reacted to cosmic rays but not to gamma-rays was placed in front of the detector. Only those events that triggered the main detector but not the other one were considered.

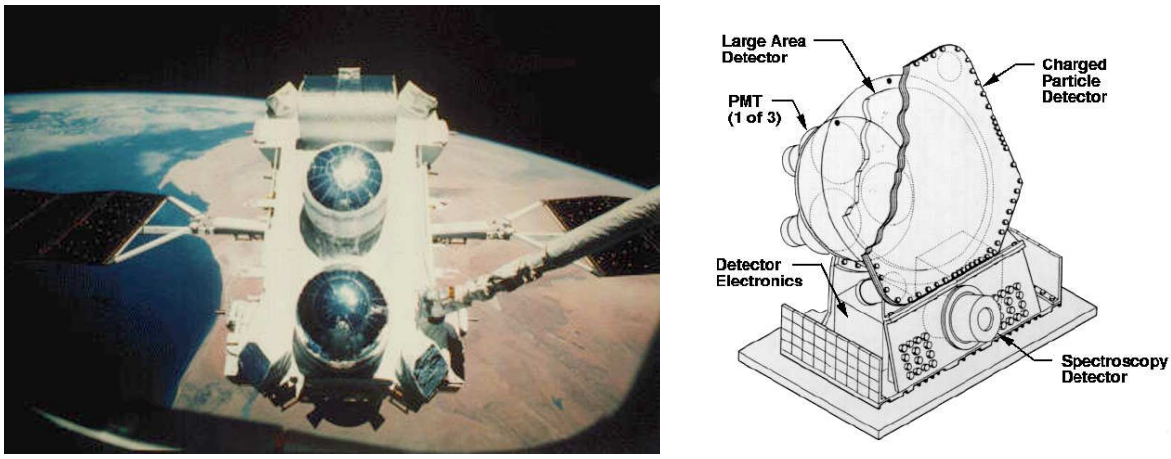

Figure 1.3: Left: Image of *CGRO* as it was being placed in orbit by Shuttle Atlantis. BATSE detectors can be seen at the corners of the satellite. Right: Diagram showing the structure of one of the BATSE detectors.

At the time of the launch of *CGRO* the general opinion of the GRB community was that they were generated by neutron stars. If this was true, we would expect GRBs to follow a distribution on the sky similar to that of the already detected neutron stars, with a concentration towards the disk of the galaxy. This was not the case of the detections from the early experiments. However, the sensitivities of the detectors that had been used were still too small to be capable of detecting the edge of the distribution (Higdon, Meegan

& Cline, 1984; Hurley, Cline & Epstein, 1984), so we would only be seeing the nearest population of GRBs. On the other hand, the neutron star hypothesis was reinforced by claims of the detection of cyclotron lines (implying strong magnetic fields), as expected in the neutron star scenario, in the spectra of several GRBs which had been detected by the *Venera* and *Ginga* satellites (Mazets et al. 1981a; Murakami et al. 1988; Fenimore et al. 1988).

It was believed that BATSE would be sensitive enough to show the distribution of GRBs along the Milky Way and that it would finally close the debate about the distance scale. Surprisingly, as the first BATSE observations were analysed during the Spring of 1991 the results continued to point to a uniform distribution, even in the faintest bursts (Fig. 1.4). Furthermore, there was a turnover in the cumulative distribution of GRBs towards a lack of faint bursts. All this together meant that we were in the centre of a uniformly spherical distribution of which we were already seeing the edges (Meegan et al. 1992).

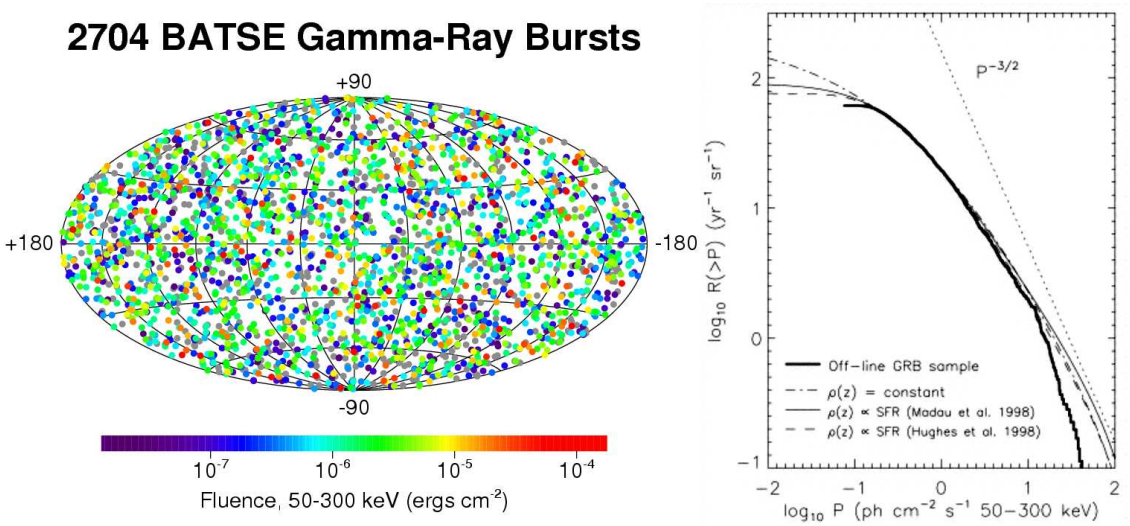

Figure 1.4: Left: Localisation of BATSE GRBs in the sky, showing an isotropic distribution. Right: Cumulative peak flux distribution of BATSE bursts, showing a lack of faint bursts (Kommers et al. 2000).

These results were shocking for the vast majority of the GRB community that expected to see a disk-like distribution in BATSE detection maps. But the debate was not yet over, there seemed to be other evidences for the neutron star theory and after all, they could still be distributed spherically along the halo of our Galaxy.

The discussion on the distance scale of GRBs resembled the classical debate that was held in 1920 between Harlow Shapley and Herber Curtis about the distance scale of spiral nebulae. So it was seen by Robert Nemiroff, who organised a similar debate in the same auditorium and precisely 75 years later, on the 22^{nd} April 1995. This time, the two contenders were Don Lamb, defending the local theory (Fig. 1.5) and Bohdan Paczyński, supporting the cosmological origin (Fig. 1.6).

Galactic Halo

Galactic objects would be initially expected to be concentrated towards the bulge and disk of the Galaxy. However after the observations from BATSE showed an isotropic distribution, it was proposed that if they were indeed located in our galaxy they should be distributed throughout an extended halo with a radius of at least 100 kpc, so that the offset of the Sun in the Galaxy would not show up in the distribution. The lack of any concentration of bursts towards the Andromeda galaxy gives further constrains on the size of the halo. Lamb explained this lack of bursts assuming that the emission of the neutron stars that were generating these bursts was collimated and that they had to be pointing in our direction to be seen. If we assume that the neutron stars were accelerated at their time of birth along their rotational axis, we would statistically see most of the GRBs happening in the Milky Way, while only a very small fraction of those happening in Andromeda. Using this information the halo, or 'Galactic Corona' as it was called, was estimated to lie between 100 and 300 kpc. This halo had not yet been observed and was said to be formed by the arrival of high-velocity neutron stars. A higher limit to the emission energy of GRBs, assuming isotropic emission at a distance of 300 kpc would be of the order of $\sim 10^{43}$ erg s^{-1} (using a typical GRB flux of 10^{-6}erg s^{-1} cm^{-2}). For more details see Lamb (1995).

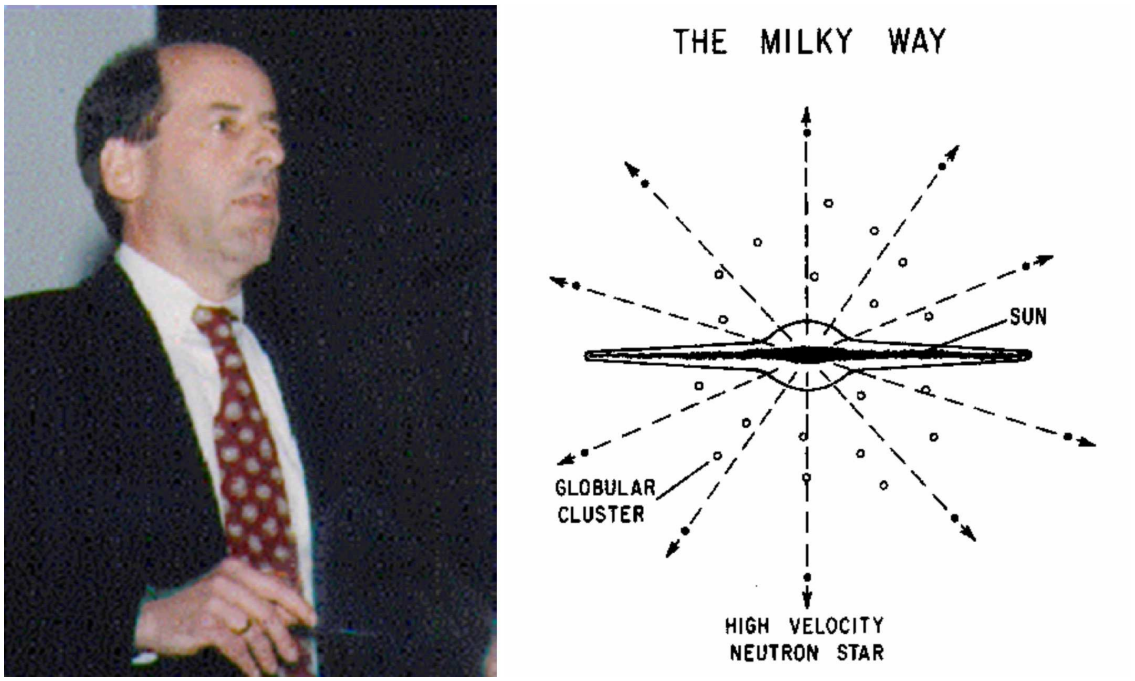

Figure 1.5: Left: D.Q. Lamb during his presentation. Right: Diagram explaining the origin of GRBs in the 'Galactic Corona' (Lamb 1995).

Cosmological distance

At distances of the order of Gpc and over, the observed distribution of any sort of astronomical objects is uniform and isotropic. Furthermore, a cosmological distribution of GRBs would naturally show a deficiency of weak sources due to relativistic effects that cause the count rate to be lower at high redshift. The strong GRBs have an intensity distribution consistent with the number density independent of the Euclidean space. Weak ones are scarce, meaning that their number density is reduced at larger distances, or that the space in which they are happening is not Euclidean. If GRBs are at cosmological distances, then the weakest ones should be redshifted, their duration should be longer and their spectra should be softer than for strong bursts. If a typical burst was produced at $z = 0.5$ it would mean an isotropic release of the order of 10^{51} erg s^{-1} making them the most energetic events detected in the Universe. For more details see Paczyński (1995).

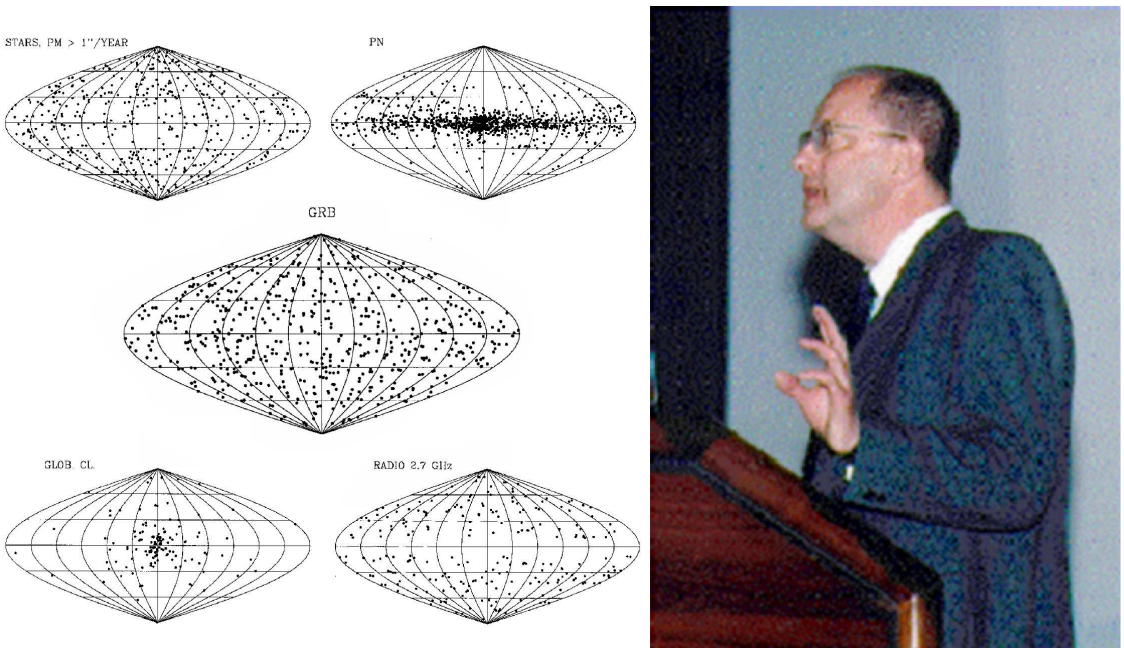

Figure 1.6: Left: Comparison of the distribution of objects at different distance scales (Paczyński 1995): Local stars top left; planetary nebulae top right; globular clusters bottom left; distant radio galaxies bottom right; GRBs centre. Right: B. Paczyński defending his model.

As in the classical spiral nebula debate, there was not a clear winner and similarly to it, the answer would come just a few years later.

1.4 *BeppoSAX*: The first counterparts

It was clear that the accurate localisations would be the key to solve the problem. *HETE* (Ricker et al. 1988) was expected to be the satellite that would finally unveil the mystery of GRBs. It was the first mission specifically designed to study these phenomena. After several delays it was finally launched on the 4^{th} November 1996. However, due to a failure in the uncoupling of the satellite, it was lost when it had already reached Earth orbit. Another 4 years would have to go through until a second unit (dubbed *HETE-2*) was built and finally launched in 2000.

In the mean time an Italian-Dutch high energy satellite, named *BeppoSAX* (Satellite per Astronomia X, 'Beppo' in honour of the Italian physicist Giuseppe Occhialini, Boella et. al 1997) had been launched on the 30^{th} April 1996, after a 10 year delay (Fig. 1.7). Its main characteristic was the wide spectral coverage, ranging from 0.1 up to 600 keV. Its primary science was not GRBs, but it turned out to be the mission that would finally disentangle the mystery of the afterglows. *BeppoSAX* carried the GRBM (Gamma-Ray Burst Monitor) that would roughly determine the coordinates of a GRB in the energy range 60-600 keV. Additionally there were two Wide Field Cameras (WFC, Jager 1997) that, observing in the range 2-30 keV would be able to determine the location of an X-ray source with an uncertainty of about 5 arcminutes. So it would be possible, if the burst occurred in the field of one of the WFCs, to detect the gamma event and search for a counterpart in X-rays. This lower energy counterparts where known to exist, having been detected for the first time by *GRANAT* for GRB 920723 (Terekhov et al. 1995).

Figure 1.7: Artist's impression of *BeppoSAX* satellite in orbit

On the 20^{th} July 1996 a burst was detected by both instruments. It happened less than 3 months after the launch, and the lack of experience in the analysis of the data delayed the communication of the result. On the 3^{rd} September 1996 Piro et al. published an IAUC (6467) anouncing the detection of X-rays associated with GRB 960720 using the WFCs aboard *BeppoSAX*. On that same day further observations were made, but the X-ray

counterpart was no longer detected (in IAUC 6480 Piro et al. claimed a detection of an X-ray counterpart, but it was later found to be unrelated to GRB 960720). After these results the efforts of *BeppoSAX's* team were aimed at reducing the response time from a month to less than a day. Several months would have to go by before they had a new opportunity to show their improved skills.

On the 11^{th} January 1997 a GRB finally happened in the field of the WFC. The position was distributed less than 24 hours later. No counterpart was detected in optical or radio, in spite of the fast response. Alberto Castro-Tirado & Javier Gorosabel (1997) imaged the field just 19 hours after the burst with the 2.2m telescope at Calar Alto Observatory in Almería, Spain, but detected no counterpart down to magnitude $R \sim 22.6$. It seemed that detecting a counterpart was not going to be as straight forward as expected.

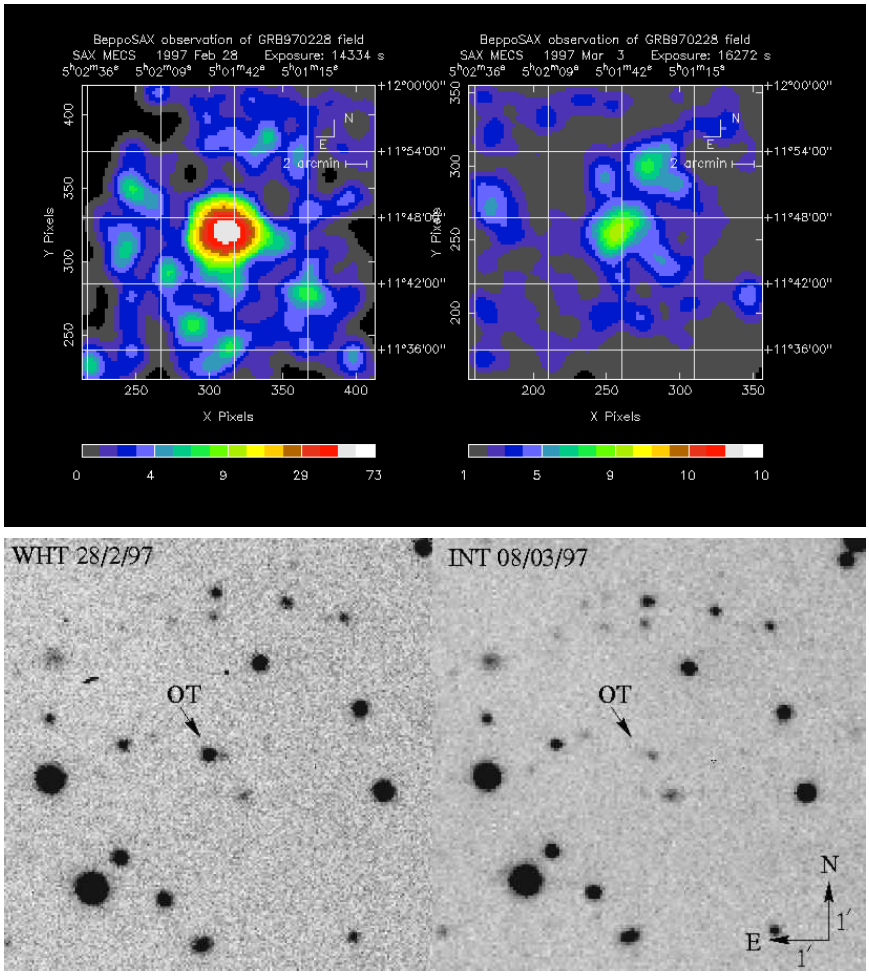

Figure 1.8: Top: X-ray counterpart detected by WFC/*BeppoSAX*. Bottom: Optical counterpart (van Paradijs et al. 1997).

The next chance came the following month, on the 28^{th} February 1997 and this time an optical counterpart (Fig. 1.8) was finally pinpointed by Jan van Paradijs' team (Groot

et al. 1997; van Paradijs et al. 1997). As it faded away, in the following days, an underlying extended object was discovered and was proposed as the host galaxy that would be sheltering the burst at a cosmological distance although, without a spectra to prove it, the cosmological origin was not more than a mere hypothesis. In spite of the efforts, a radio counterpart was not detected for this event.

GRB 970508 was not particularly powerful or long, but it would be a decisive event. The afterglow was not an easy one to detect. It initially maintained its brightness and then increased to later decay. This was the reason why, although several teams had imaged the field they did not dare to claim that raising object as the counterpart of the GRB. It was Howard Bond (see Heise et al. 1997) who, with his observations obtained from a 90cm telescope, finally claimed the discovery on the 10^{th} of May. On that same night a spectra of the afterglow was obtained with one of the 10m Keck telescopes by Mark Metzger. A redshift of 0.835 (Metzger et al. 1997a; Metzger et al. 1997b) was determined and set an end to a 30 year old mystery (Fig. 1.9).

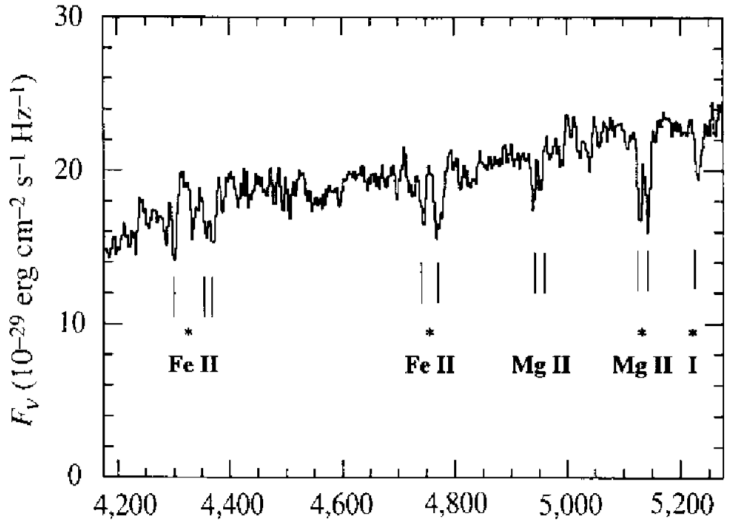

Figure 1.9: The second[2] spectrum of a gamma-ray burst afterglow, GRB970508, showing iron and magnesium absorption lines redshifted to $z = 0.835$ (Metzger et al. 1997b).

But there were still more discoveries to be made with this burst. It was the first radio counterpart ever detected at centimetre wavelengths, by Dale Frail et al. (1997) with Very Large Array and at millimetre band with the Plateau de Bure interferometer, by Michael Bremer et al. (1998). Although the first efforts were unfruitful, Frail finally managed to detect the counterpart in 3.5, 6 and 21 cm, once he knew the afterglow coordinates and could concentrate the power of the radio telescopes at the precise position. Their team also detected fluctuations in the light curve, even from day to day, that were explained as scintillation due to the very small angular size of the emitting source. The scintillation seemed to stop one month after the GRB, meaning that its angular size had increased over 3 microarcseconds, implying a shell expanding at nearly the speed of light.

1.5 Unveiling the nature of long GRBs

Now that the distance scale problem was solved, there was a mystery not easier to solve. If GRBs happened at cosmological distances, the amount of energy that was being released would be enormous. The size of the source that was generating this energy had to be, however, very small; from the microsecond fluctuations that could be detected in the gamma-ray light curves it could be inferred that the size of the engines generating the GRB had to be smaller than a few hundred kilometres. All this together implied a large amount of matter in a very reduced space. And hot dense material is not transparent, leading to the *compactness problem* (see chapter 3). The problem now relied in finding the mechanism that would allow so much radiation to escape from the progenitor.

1.5.1 Fireball model

The answer was found in a relativistically expanding fireball (Goodman 1986; Paczynski 1986; Paczynski & Rhoads 1993; Meszaros & Rees 1997), were huge amounts of matter are being expelled at almost the speed of light. The model is based on a central explosion of the order of 10^{52} ergs, which leads to an optically thick radiation-electron-positron plasma with initial energy much larger than its rest mass (Piran 1996; Piran 1999), the 'fireball'. During the explosion shock waves are generated due to the differential velocities of the ejected matter. At the places where the slower material is caught up by faster one internal shocks are generated compressing and heating the material to the point of emitting the initial gamma-rays that we observe.

The expanding fireball (Fig. 1.10) then collides with the interstellar medium, creating a forward shock wave, which emits from X-rays to radio waves during longer periods of time with a synchrotron spectrum. This is what we know as the afterglow of the GRB. Additionally, a reverse shock can be produced when part of the energy of the forward shock bounces back towards the centre of the explosion interacting with the ejecta.

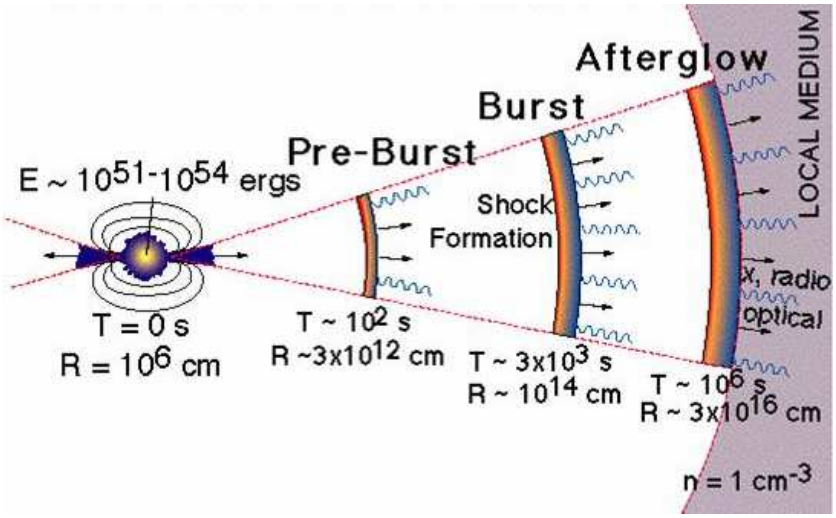

Figure 1.10: Diagram showing the structure of a fireball. Adapted from Piran (1999).

This relativistic fireball can also explain the extremely rapid increase in brightness observed in GRBs through relativistic effects. The emitting material expelled by the burst travels towards us at nearly the speed of light. This produces a very strong time compression, of a factor of over 10^4, where two photons observed with an interval of 1 second in the light curve would have been emitted with a difference of several hours (see Chapter 3 for a description of the relativistic effects involved in a GRB).

1.5.2 Beaming

On the 14^{th} December 1997 a new burst was observed by *BeppoSAX* and an optical counterpart was detected. This time the redshift was measured to be 3.42, which implied an energy release of 3×10^{53} ergs. This numbers were becoming to be too large to be explainable by the models that were being considered. If the emission was collimated (Fig. 1.11) we could expect to have numbers two or three orders of magnitude smaller than had been initially thought. James Rhoads (1997;1999) showed that the collimated outflow would lead to a break that would steepen the light curve after some time. This would happen when the Lorentz factor of the outflow decreased bellow $1/\theta_j$, being θ_j the opening angle of the jet. This steepening was first suggested to be seen in GRB 990123 (Castro-Tirado et al. 1999; Kulkarni et al. 1999) and later regularly detected in other GRBs.

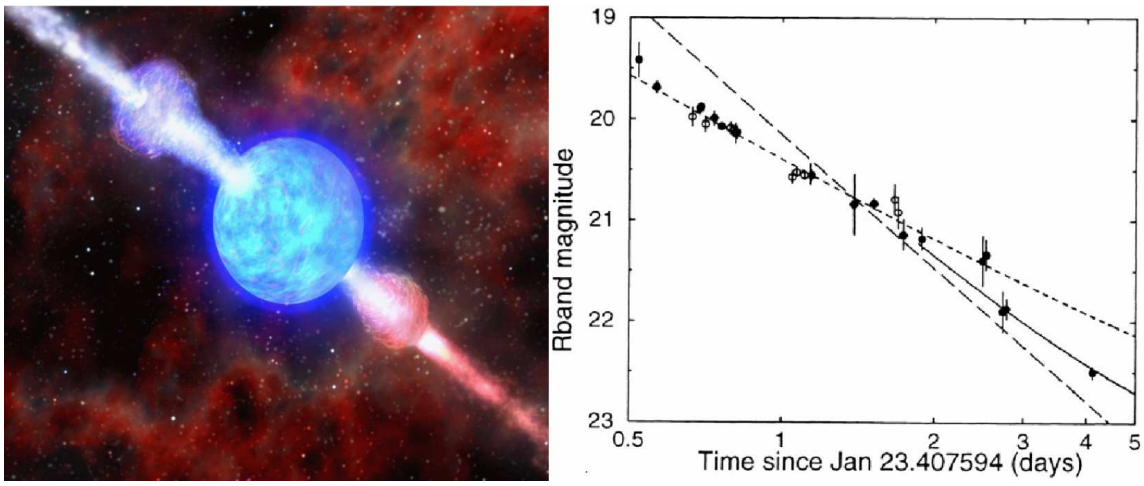

Figure 1.11: Left: Artist's conception of the explosion of a GRB with jets. Credit: Dana Berry, SkyWorks Digital. Right: The jet break of GRB 990123, adapted from Castro-Tirado et al. (1999)

This beaming not only implies a decrease in the energy needed to generate a GRB, but also that the rate of GRBs happening in the Universe is equally increased by two or three orders of magnitude. Only the small fraction that has its polar axis pointing towards us would be detected.

1.5.3 Connection with supernovae, a clue to the progenitor

An optical transient source was detected on one of the arms of a relatively nearby spiral galaxy which lied in the error box of GRB 980425 (Galama et al. 1998). It had a very unusual behaviour, its brightness was almost 1000 times greater than typical GRBs and its behaviour did not resemble previously observed bursts. Instead of showing a fast brightness decline, it increased during a fortnight, and decreased slowly afterwards, just in the way that a supernova did. It was consequently identified as SN 1998bw (Fig. 1.12).

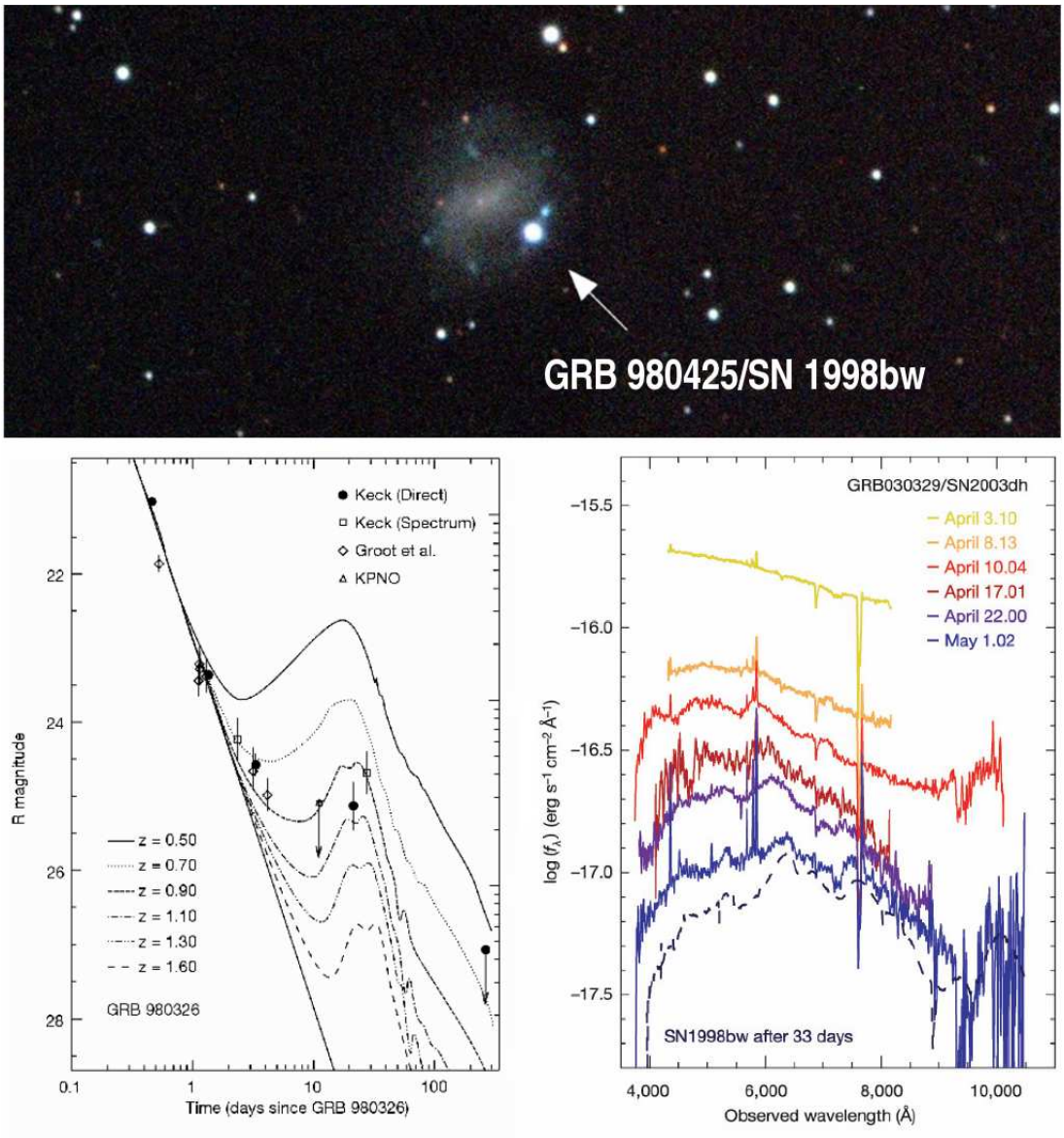

Figure 1.12: Top: Supernova 1998bw related to GRB 980425 (Galama et al. 1998). Bottom left: Supernova signature in the light curve of GRB 980326 (Bloom et al. 1999). Bottom right: Spectral evolution of GRB 030329 from synchrotron to supernova (Hjorth et al. 2003).

SN 1998bw was a peculiar supernova, with a great amount of radio emission (Kulkarni et al. 1998). Further studies demonstrated that it must have been produced between the 21^{st} and the 27^{th} April, it was thus consistent with both location and time of the GRB. Studying the radio properties of this unusual GRB/SN Iwamoto et al. (1998) estimated that the explosion had been 10 times more energetic than a typical supernova, creating what he named as a 'hypernova' (following Paczynski, 1998). The scenario that best suited the observations was the collapse of a very massive star, originally of the order of 40 $M_{\odot}$ which had lost its envelope and was about 14 $M_{\odot}$ at the moment of the explosion. The result of the burst would unavoidably be the birth of a black hole.

This would be the prove of the 'collapsar model', where a supermasive star completely implodes. But this was a peculiar burst, so the question was if this mechanism was also valid for other normal bursts. The peak emission of GRBs was reached in just a few seconds, while the supernova emission peaked a couple of weeks after. This meant that as the light from the GRB dims, the supernova brightens and at some point it could become the predominant flux contribution. This would show up as a bump in the light curve. This behaviour was first detected by Castro-Tirado & Gorosabel (1999) and later modelled by Bloom et al. (Bloom et al. 1999) and has been later detected in several other light curves. Furthermore, in GRB 030329 the relation was spectroscopically demonstrated as the GRB power law spectrum eventually evolved to a supernova spectrum (Stanek et al. 2003; Hjorth et al. 2003).

1.5.4 Early emission

At the end of the 1990's several groups had made strong efforts to be able to detect optical transients in their very early stages by the use of robotic telescopes. These telescopes would respond to the alerts distributed through the newly operating GRB Circular Network (GCN) and point within seconds to the position where the event had happened.

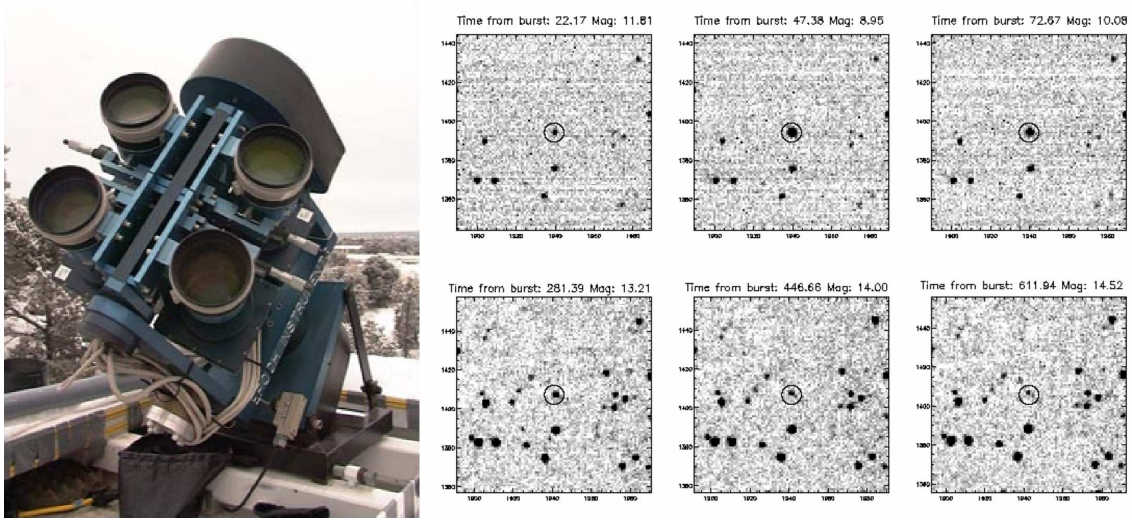

Figure 1.13: The ROTSE robotic telescope (left) and the first images of the prompt emission of a GRB (right), from Akerlof et al. (1999).

On the 23^{rd} January 1999 a burst was detected by BATSE and the wide field cameras of the ROTSE robotic telescope started imaging the field just 22 seconds after the event had begun (Akerlof et al. 1999). For the first time, the optical counterpart simultaneous to the gamma-ray emission was detected while it was still rising, reaching the peak at 50 s (Fig. 1.13). This was an unusually bright event, with a peak magnitude of 8.9. At a redshift of $z = 1.6$, it had a peak absolute magnitude of $M_V = -36$, becoming the intrinsically brightest object in the Universe. Since then, other events have been followed by other robotic telescopes such as LOTIS, TAROT, REM or BOOTES.

1.6 Short GRBs

At the beginning of the 1980s the first suggestions of a bimodality in the duration of GRBs were made (Mazets et al. 1981b; Norris et al.1984). It was not until 1993 that the idea that GRBs are most likely composed of two populations became commonly accepted. Kouveliotou et al. (1993) presented a histogram based on the observation of 222 BATSE burst which clearly showed a minimum at a duration of 2 seconds (Fig. 1.14). On average, the burst lasting less than 2 seconds are composed of harder (more energetic) photons than the longer bursts (see Chapter 2 for further details).

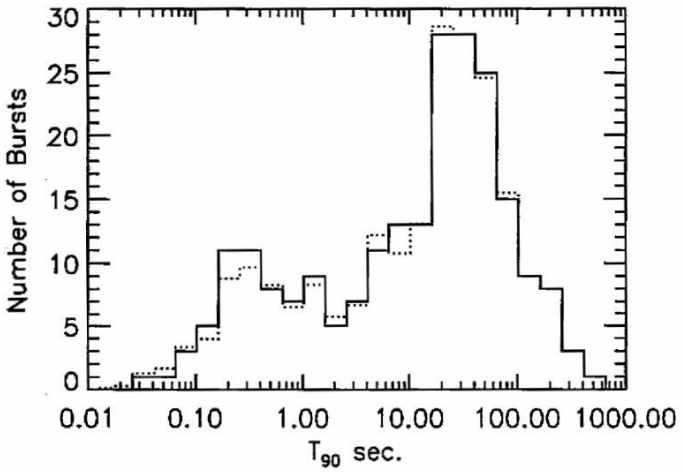

Figure 1.14: Bimodal distribution of the duration of GRBs, from Kouveliotou et al. (1993).

As we have seen in the previous sections, during the last decade great discoveries and advances have been made in the field of long GRBs thanks to the discovery of counterparts in other wavelengths. However no afterglow was detected for short burst during this time, in spite of the efforts that were made. The breakthrough in the study of short bursts had to wait until 2005, when *Swift* and *HETE-2* satellites succeeded in precisely localising the X-ray counterparts of several short bursts, leading to the detection of afterglows (Gehrels et al. 2005a; Hjorth et al. 2005b; Berger et al. 2005, see Fig. 1.15) and the indirect determination of their redshifts (Castro-Tirado et al. 2005; Gehrels et al. 2005b; Hjorth et al. 2005a; Villasenor et al. 2005; Soderberg et al. 2006). The conclusion of the first studies, was that short bursts are of cosmological origin, although not as distant as typical

long bursts. Furthermore, their luminosities are somehow lower and the progenitors of these events do not seem to be the death of massive stars, making them two different classes of phenomena. On the other hand, the afterglows of short bursts have similar properties to those of long bursts, implying similar physical processes in the explosion. The preferred scenario to explain the central engine powering short bursts is the coalescence of two neutron stars (see Chapter 3 for a discussion on the progenirtors).

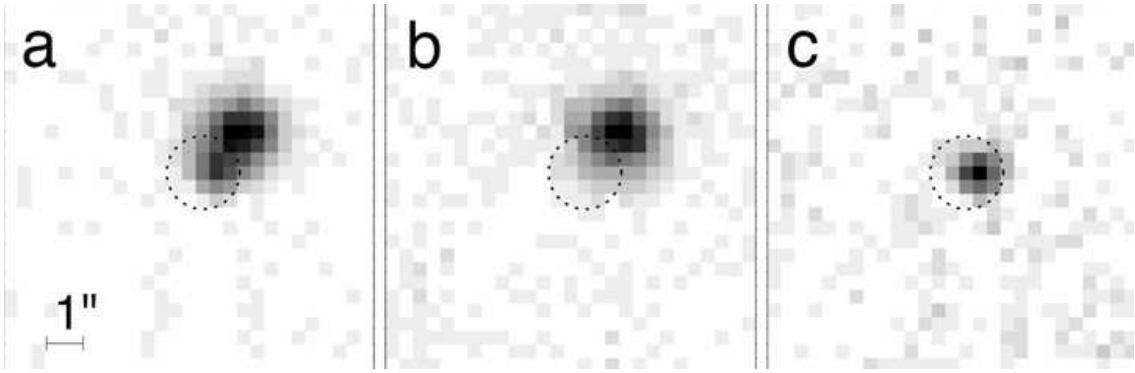

Figure 1.15: Discovery images of the afterglow of the short burst GRB 050709 (Hjorth et al. 2005).

Recent observations (Levan et al. 2006; de Ugarte Postigo et al. 2006; Berger et al. 2006) have shown that there is an emerging subpopulation of short bursts happening at redshifts similar to those of long bursts and implying similar energy releases. The era of discoveries of short bursts is just starting and there is still much to be understood.

Bibliography

Akerlof, C., et al. 1999, Nature, 398, 400

Berger, E., et al. 2005, Nature, 438, 988

Berger, E., et al. 2006, ArXiv Astrophysics e-prints, arXiv:astro-ph/0611128

Bloom, J. S., et al. 1999, Nature, 401, 453

Boella, G., Butler, R. C., Perola, G. C., Piro, L., Scarsi, L., & Bleeker, J. A. M. 1997, A&AS, 122, 299

Bremer, M., Krichbaum, T. P., Galama, T. J., Castro-Tirado, A. J., Frontera, F., van Paradijs, J., Mirabel, I. F., & Costa, E. 1998, A&A, 332, L13

Castro-Tirado, A. J., et al. 1997, IAU Circ., 6598, 2

Castro-Tirado, A. J., et al. 1999, Science, 283, 2069

Castro-Tirado, A. J., & Gorosabel, J. 1999, A&AS, 138, 449

Castro-Tirado, A. J., et al. 2005, A&A, 439, L15

Colgate, S.A. 1968, Canadian, J. Physics 46, S476.

Fenimore, E. E., et al. 1988, ApJ, 335, L71

Fishman, G. J., & Derrickson, J. H. 1975, BAAS, 7, 461

Fishman, G. J. 1981, Ap&SS, 75, 125

Frail, D. A., Kulkarni, S. R., Nicastro, S. R., Feroci, M., & Taylor, G. B. 1997, Nature, 389, 261

Galama, T. J., et al. 1998, Nature, 395, 670

Gehrels, N., et al. 2005a, Bulletin of the American Astronomical Society, 37, 1324

Gehrels, N., et al. 2005b, Nature, 437, 851

Goodman, J. 1986, ApJ, 308, L47

Groot, P. J., et al. 1997, IAU Circ., 6584, 1

Heise, J., et al. 1997, IAU Circ., 6654, 2

Higdon, J. C., & Lingenfelter, R. E. 1990, ARA&A, 28, 401

Higdon, J. C., Meegan, C. A. & Cline, T. L. 1984, AIP Conf. Proc. 141, 23

Hjorth, J., et al. 2003, Nature, 423, 847

Hjorth, J., et al. 2005, ApJ, 630, L117

Hjorth, J., et al. 2005, Nature, 437, 859

Hurley, K., Cline, T. L. & Epstein, R. 1984, AIP Conf. Proc. 141, 33

Iwamoto, K., et al. 1998, Nature, 395, 672

Jager, R., et al. 1997, A&AS, 125, 557

Klebesadel, R.W., Strong, I.B. & Olson, R.A., 1973, ApJ 182, L85.

Kommers, J. M., Lewin, W. H. G., Kouveliotou, C., van Paradijs, J., Pendleton, G. N., Meegan, C. A., & Fishman, G. J. 2000, ApJ, 533, 696

Kouveliotou, C., Meegan, C. A., Fishman, G. J., Bhat, N. P., Briggs, M. S., Koshut, T. M., Paciesas, W. S., & Pendleton, G. N. 1993, ApJ, 413, L101

Kulkarni, S. R., et al. 1998, Nature, 395, 663

Kulkarni, S. R., et al. 1999, Nature, 398, 389

Lamb, D. Q. 1995, PASP, 107, 1152

Levan, A. J., et al. 2006, ApJ, 648, L9

Mazets, E. P., Golenetskii, S. V., Aptekar, R. L., Gurian, I. A., & Ilinskii, V. N. 1981a, Nature, 290, 378

Mazets, E. P., et al. 1981b, Ap&SS, 80, 3

Meegan, C. A., Fishman, G. J., Wilson, R. B., Horack, J. M., Brock, M. N., Paciesas, W. S., Pendleton, G. N., & Kouveliotou, C. 1992, Nature, 355, 143

Mészáros, P., & Rees, M. J. 1997, ApJ, 476, 232

Metzger, M. R., Cohen, J. G., Chaffee, F. H., & Blandford, R. D. 1997a, IAU Circ., 6676, 3

Metzger, M. R., Djorgovski, S. G., Kulkarni, S. R., Steidel, C. C., Adelberger, K. L., Frail, D. A., Costa, E., & Frontera, F. 1997b, Nature, 387, 878

Murakami, T., Fujii, M., Hayashida, K., Itoh, M., & Nishimura, J. 1988, Nature, 335, 234

Nemiroff, R. J. 1994, Comments on Astrophysics, 17, 189

Norris, J. P., Cline, T. L., Desai, U. D., & Teegarden, B. J. 1984, Nature, 308, 434

Paczyński, B. 1986, ApJ, 308, L43

Paczyński, B., & Rhoads, J. E. 1993, ApJ, 418, L5

Paczyński, B. 1995, PASP, 107, 1167

Paczyński, B. 1998, ApJ, 494, L45

Piran, T. 1996, IAU Symp. 165: Compact Stars in Binaries, 165, 489

Piran, T. 1999, Phys. Rep., 314, 575

Piro, L., et al. 1996a, IAU Circ., 6467, 1

Piro, L., et al. 1996b, IAU Circ., 6480, 1

Rhoads, J. E. 1997, ApJ, 487, L1

Rhoads, J. E. 1999, A&AS, 138, 539

Ricker, G., et al. 1988, AIP Conf. Proc. 170: Nuclear Spectroscopy of Astrophysical Sources, 170, 407

Schaefer, B. E. 1992, Gamma-Ray Bursts - Observations, Analyses and Theories, 107

Schaefer, B. E. 1994, AIP Conf. Proc. 307: Gamma-Ray Bursts, 307, 382

Soderberg, A. M., et al. 2006, ApJ, 650, 261

Stanek, K. Z., et al. 2003, ApJ, 591, L17

Strong, I. B., & Klebesadel, R. W. 1976, Scientific American, 235, 66

Terekhov, O. V., et al. 1995, Astronomy Letters, 21, 217

de Ugarte Postigo, A., et al. 2006, ApJ, 648, L83

van Paradijs, J., et al. 1997, Nature, 386, 686

Villasenor, J. S., et al. 2005, Nature, 437, 855

Wilson, R. B., Fishman, G. J., & Meegan, C. A. 1982, AIP Conf. Proc. 77: Gamma Ray Transients and Related Astrophysical Phenomena, 77, 67

2

Observational characteristics of gamma-ray bursts

Gamma ray bursts are brief but very energetic events that occur at a rate of a few per day throughout the Universe. During a few seconds they outshine every other source of gamma-rays in the sky and then they disappear. However, counterparts of gamma-ray bursts are observed in all other wavelengths, from radio to X-rays and can be detected during much longer times, in the scale of days, weeks or even months (in radio wavelengths). In this chapter we describe some of the observational characteristics of gamma-ray bursts, from the prompt emission to long after the onset.

2.1 General characteristics

Gamma-ray bursts are short but very intense flashes of high energy photons ($\sim$1 keV to 10 GeV) with durations ranging from 10^{-3} s to about 10^{3} s (Meszaros 2006). The gamma-ray light curves range from smooth, fast-rise and quasi-exponential decay (FREDs), through curves with several peaks, to highly variable curves (see Fig. 2.1). GRBs are found isotropically distributed in the sky, a fact that in the early 1990's already pointed towards their cosmological origin (see Chapter 1).

Counterparts for this emission have been found in all wavelengths, from radio to X-rays. These counterparts may be detected up to several days or weeks in the near infrared (nIR), optical and X-rays, reaching peak brightness a few seconds after the gamma-ray emission (see for example Akerlof et al. 1999) and then rapidly fall, mainly following a broken powerlaw that is usually found to increase its slope some time after the burst. In radio, the peak brightness may be reached some days or even weeks after the burst and can be followed several months after the burst for the brightest events (Resmi et al. 2005; van der Horst et al. 2005). This late emission, that we detect long after the gamma-ray radiation has disappeared is what we refer to as the *afterglow*. The spectrum of gamma-ray bursts afterglows has been found to be of synchrotron nature (details will be given in Chapter 3).

Whenever a deep enough search has been carried out, an underlying host galaxy has been found in nearly all cases. For long bursts, they have been mostly found to have a very

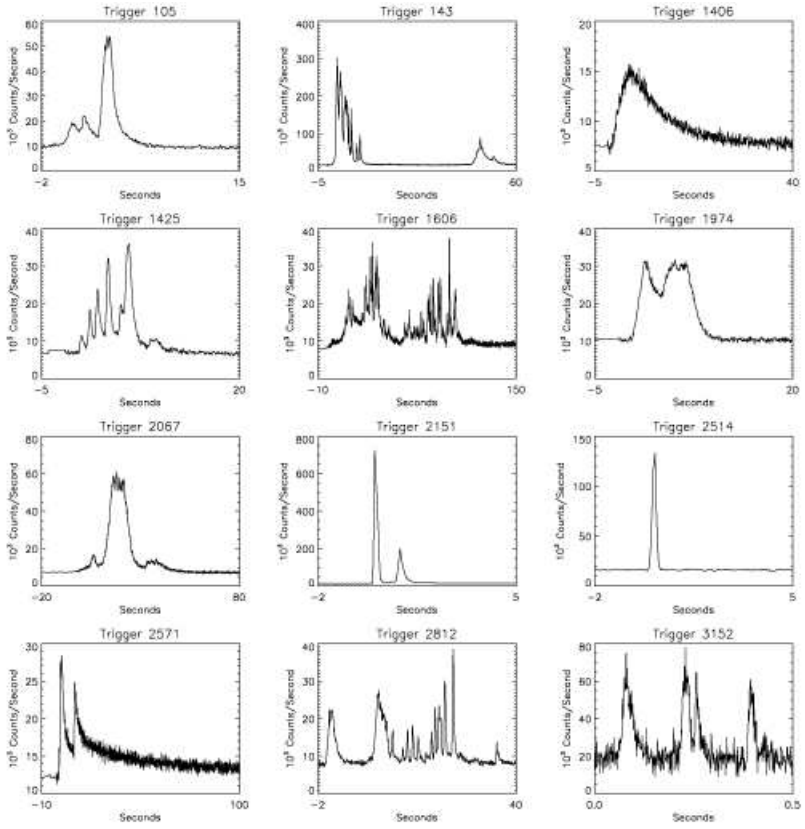

Figure 2.1: Diversity of gamma-ray light curves as observed by BATSE on *CGRO* (Fishman & Meegan 1995).

high specific star formation rate, being typically classified as starburst galaxies (Fruchter et al. 2006). However, in the case of short GRBs (see Section 2.2.1 for a definition of short and long bursts) the galactic type is much more heterogeneous.

2.2 Classes of GRBs

A fundamental question related to GRBs is the intrinsically different categories that exist and the way in which they can be classified. This gives us clues about the different progenitors, central engines and environments that can produce the differences that we observe.

2.2.1 Long versus Short

The first GRB classifications through duration were proposed in the early 1980's (Mazets et al. 1981; Norris et al.1984), but it was not until the early 1990s, using BATSE observations, that a bimodal distribution was widely accepted (Kouveliotou et al. 1993). Two criteria were used to classify these two groups: the duration and the hardness ratio. Duration is measured by the T_{90} parameter, which is the time during which the cumulative counts

increase from 5 % to 95 % above the background, thus accumulating 90 % of the counts. The hardness ratio is measured by the HR_{23} parameter, which is the ratio of total counts in the 100 - 300 keV and 50 - 100 keV energy ranges. The first group of bursts has a typical duration of 0.1 seconds and a mean hardness ratio of ∼1.5 and are referred to as short-hard bursts (or just short bursts). The group of long-soft burst have a typical duration of 20 seconds and a mean hardness ratio of ∼0.9. A separation line is usually set at 2 seconds (although a 5 seconds division might be more realistic, as indicated by Donaghy et al. 2006) to divide the two humps of the distribution. However, the dispersion in hardness ratio is such that the two populations overlap and the division between them is not so well determined (see Fig. 2.2). Based on the duration distribution, a possible third class of GRBs with intermediate duration, between 2 and 10 seconds, has been proposed (Horváth 1998; Balastegui et al. 2001). Additionally a further population of extremely short bursts, lasting less than 0.1 seconds has been proposed as distinct class (Cline et al. 1999; Cline et al. 2005). The main evidence for this group of events is that they show an anisotropic distribution in the sky and are statistically expected to be located in the near Universe ($\langle V/V_{max}\rangle \sim 0.5$, see section 2.3).

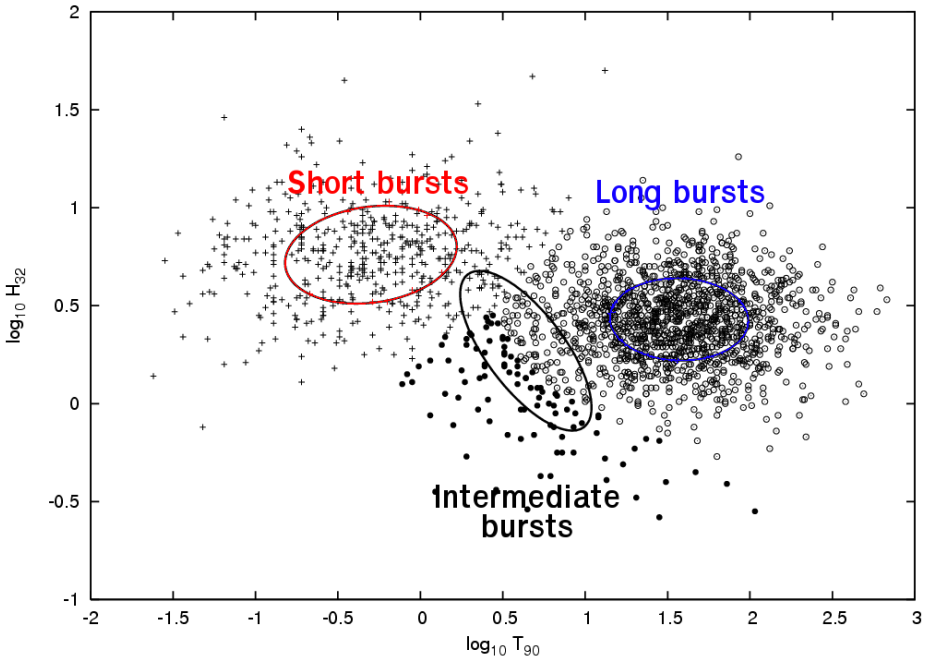

Figure 2.2: Duration versus hardness-ratio diagram, showing the difference between short-hard bursts (red) and long-soft bursts (blue). The proposed intermediate population is also marked (black). The figure is adapted from Horváth et al. (2006).

Several interesting conclusions were reached through the analysis of the prompt emission: Ghirlanda et al. (2004a) found that short GRBs are usually harder than long GRBs mainly because of a harder low-energy spectral index and not because of an intrinsically harder spectrum. Furthermore, short GRB spectra are broadly similar to those of long

GRBs if we only consider the first 2 seconds of the emission. Nakar & Piran (2002) found that temporal properties are also similar to those of long GRBs during the first 2 seconds, with highly variable temporal structures. Examination of the temporal evolution of pulses in the frequency space shows a different behaviour in the two types of bursts. This study is done by the use of *spectral lags*, which are a measurement of the spectral evolution of the pulses, an evolution from hard to soft being positive. They are quantified by the delay between the peak of the pulse in the hardest bands and its arrival to the softest ones. Norris, Scargle & Bonnel (2001) find that long bursts show a positive spectral lag that can expand up to 2 seconds, with a typical value of 50 ms, while short bursts present a symmetric distribution of lags that range between ±30 ms (see Fig. 2.3).

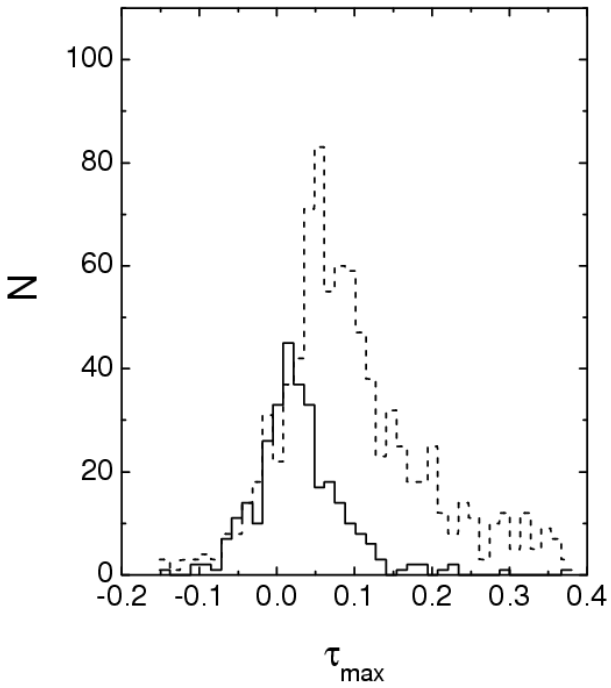

Figure 2.3: Spectral lags for short bursts (solid line) and long bursts (dashed line) (Yi et al. 2006).

Up to now over 200 afterglows have been found for long GRBs, while only a handful has been detected for short bursts (see Table 2.1). Strong associations have been found between nearby long bursts and supernovae (Galama et al. 1998; Stanek et al. 2003; Hjorth et al. 2003), while the deep supernova searches that have been carried out for short GRBs have had negative results (Castro-Tirado et al. 2005; Hjorth et al. 2005; Fox et al. 2005). On the other hand, searches for the underlying galaxies of GRBs have found that most of the hosts of long bursts have a large star formation rate, being most of them starburst, while the hosts of short bursts are of a much more varied origin. All this together indicates that most, if not all, long bursts are produced during the collapse of massive stars, the so called "collapsars", as had been suggested theoretically by several authors (Colgate 1974, Woosley 1993, Paczynski 1998, MacFayden & Woosley 1999). On the other side, the progenitors of short bursts are generally accepted to be the collapse of a binary system of compact

objects. The nature of the progenitors will be discussed in the following chapter.

Table 2.1: Properties of short bursts (or at least claimed to be so) observed since 2005. Bursts marked with * have durations of more than 5 s. From left to right: Name of the burst, duration, redshift, gamma-ray fluence, isotropic equivalent energy, X-ray luminosity 11 hours after the burst, beaming factor ($f_b = 1 - cos(\theta_j)$, being θ_j the jet opening angle), released gamma-ray energy and afterglow (X = X-ray, O = optical, R = radio).

Burst	T_{90} **(s)**	z	F_γ **(erg**$\cdot s^{-1} \cdot cm^{-2}$**)**	$E_{\gamma,iso}$ **(erg)**	L_X **(erg**$\cdot s^{-1}$**)**	f_b	E_γ **(erg)**	Aft.
050202	—	—	—	—	—	—	—	—
050509B	0.040±0.004	0.226	$(9.5 \pm 2.5) \times 10^{-9}$	4.5×10^{48}	$< 4 \times 10^{41}$	-	—	X
050709	0.070±0.010	0.1606	$(2.9 \pm 0.4) \times 10^{-7}$	6.9×10^{49}	3×10^{42}	0.03	2.1×10^{48}	XO
050724	3.0±1.0	0.257	$(3.9 \pm 1.0) \times 10^{-7}$	4.0×10^{50}	8×10^{43}	0.01	4.0×10^{48}	XOR
050813	0.6±0.1	∼1.8?	1.2×10^{-7}	6.5×10^{50}	9×10^{43}	—	—	X
050906	0.128±0.016	0.0308?	$(5.9 \pm 3.2) \times 10^{-8}$	—	—	—	—	—
050911*	∼16	0.1646	—	—	—	—	—	—
050925	—	—	—	—	—	—	—	—
051105A	—	—	—	—	—	—	—	—
051210	1.4±0.2	—	—	—	—	—	—	—
051211	4.02±1.28	—	$(8.1 \pm 1.4) \times 10^{-8}$	—	—	—	—	—
051221A	1.4±0.2	0.5465	$(1.2 \pm 0.1) \times 10^{-6}$	—	—	—	—	XOR
051227*	8.0±0.2	—	$(2.3 \pm 0.3) \times 10^{-7}$	—	—	—	—	XO
060121	1.97±0.07	∼4.6	$4.71^{+0.44}_{-0.31} \times 10^{-6}$	$2.4{\times}10^{51}$	$6.4{\times}10^{44}$	—	—	XO
060313	0.7±0.1	< 1.7	$(1.1 \pm 0.1) \times 10^{-6}$	—	—	—	—	XO
060502B	0.09±0.02	0.287	$(4.0 \pm 0.5) \times 10^{-8}$	—	—	—	—	X
060505	4.0±1.0	0.089	—	—	—	—	—	XO
060614*	102±5	0.125	—	—	—	—	—	XO
060801	∼0.50	1.1304?	$(8.1 \pm 1.0) \times 10^{-8}$	—	—	—	—	X
061006	∼0.42 ?	—	$(1.4 \pm 0.1) \times 10^{-6}$	—	—	—	—	XO
061201	∼2.0	—	—	—	—	—	—	XO
061210*	85±5	—	—	—	—	—	—	X
061217	0.3±0.05	0.827?	—	$8{\times}10^{49}$	—	—	—	X
070124	—	—	—	—	—	—	—	—
070209	0.1±0.02	—	—	—	—	—	—	—
070406	∼0.7	—	—	—	—	—	—	—
070429B	0.5±0.1	—	$(6.3 \pm 1.0) \times 10^{-8}$	—	—	—	—	X

One interesting fact that came out from recent observations is that short GRBs are not necessarily short. An extended emission following the short GRB has been seen in about 1/3 of the events (Norris & Bonnell 2006). An early hint of the existence of this component was already found by Lazzati et al. (2001), who summed the light curves of 76 BATSE short bursts and found an X-ray tail that started 30 seconds after the trigger and lasted for $\sim$ 100 seconds (see also Connaughton 2002 and Frederiks et al. 2004). This tail of the emission is clearly distinguished from the prompt component by a longer time scale, a gap that separates it from the prompt emission and a softer spectrum (see Fig. 2.4). GRB 050724 (and probably also GRB 050709) was followed by several erratic X-ray flares that have similar properties to the prompt emission and that would require to restart the central engine (Barthelmy et al. 2005, Zhang et al. 2006).

The discovery of GRB 060614 has brought the issue of the extended emission to the extreme. This burst was found to be located at a redshift of z=0.125 (Gehrels et al. 2006, Mangano et al 2007) and had a duration of ∼100 seconds. Deep searches for an underlying supernova failed, putting the limit to the emission 100 times fainter than any other previous

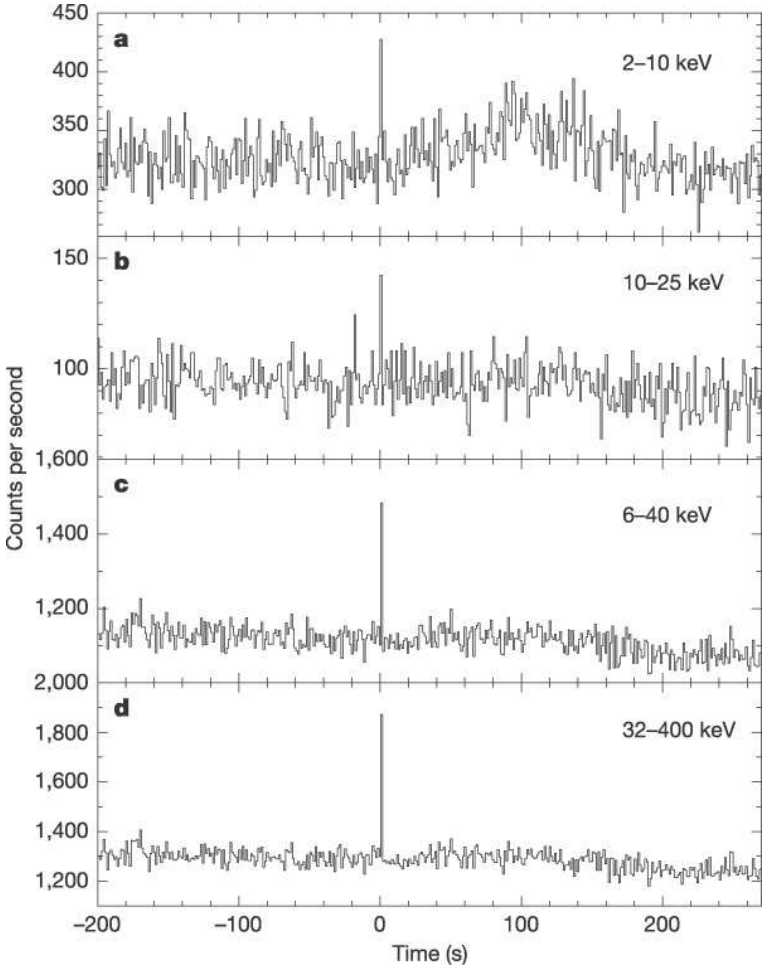

Figure 2.4: X-ray tail observed in GRB 050709 (Villasenor et al. 2005). The short GRB can be seen in all bands as a spike at 0 seconds, while the long duration tail is only present in the softest X-ray band (a, top).

supernova associated with a long GRB and fainter than any supernova ever observed (Fynbo et al. 2006, Gal-Yam et al. 2006, Della Valle et al. 2006). Furthermore the spectral lag of this burst is very short and thus consistent with what would be expected from a short burst (Gehrels et al. 2006). A similar behaviour is found in the case of GRB 060505, where a 4 second duration burst, at a probable redshift of z=0.089 does not show any supernova component down to a limit of $M_B > -12.6$ (Fynbo et al. 2006). This opens a new window of study regarding the classification of GRBs.

2.2.2 X-ray flashes, X-ray rich and gamma-ray bursts

X-ray flashes (XRFs) are transient sources, similar to long GRBs but with a softer spectrum. As normal long GRBs they have typical durations that range between several seconds to a few minutes and have a distribution in the sky that is consistent with being isotropic. They were first identified with the *BeppoSAX* satellite (Heise et al. 2001, Kippen et al. 2003) as those bursts that were detected by the X-ray Wide-Field Camera but not by the Gamma

Ray Burst Monitor. They were then extensively studied by *HETE-2*, that gave a more general classification (Sakamoto et al. 2005) and expanded the definition to include an intermediate class, the X-ray rich bursts (XRR), a class that had been previously suggested from data by *Ginga* (Yoshida & Murakami 1994) and *Granat*/WATCH (Castro-Tirado et al. 1994). This classification is based on the ratio of fluence in the X-ray band to the γ-ray band, $f_{X/\gamma} = log_{10}[S_X(2-30\ keV)/S_\gamma(30-400\ keV)]$. XRFs, XRRs and GRBs would be, respectively, those bursts with $f_{X/\gamma} < -0.5$, $-0.5 < f_{X/\gamma} < 0$ and $0 < f_{X/\gamma}$. While the three groups have a different empirical definition, they seem to form a continuum of events, with bursts varying smoothly from XRFs to XRRs to GRBs, rather than distinctive distributions. Since the identification and classification of these groups of events, many suggestions have been made in order to interpret the differences between the three groups. These differences can be extrinsical (the difference is due to the way in which we are seeing them) or intrinsical (the difference is due to the physics involved in the explosion). In the following paragraphs we give a list with some of the suggested models that would explain the origin of these bursts. The first four are "extrinsic" models and the latter five are "intrinsic" (Zhang 2007):

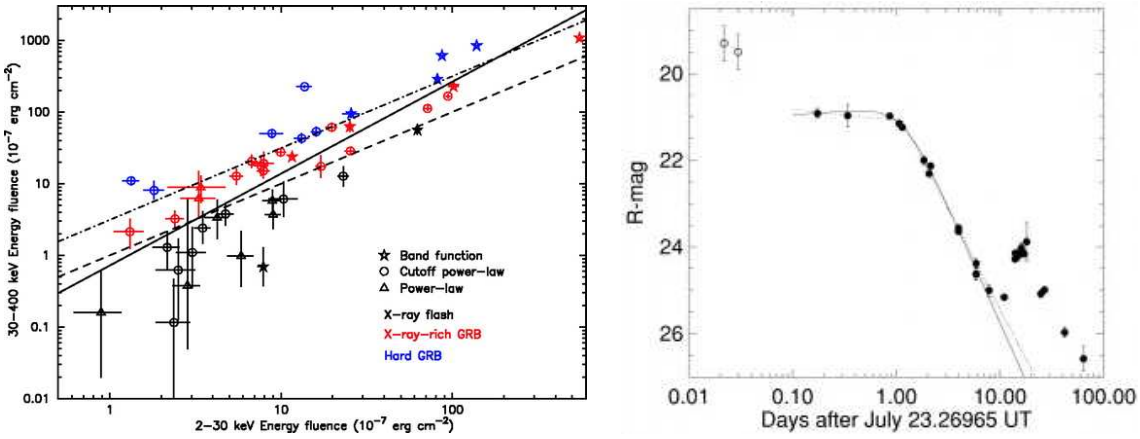

Figure 2.5: Left: Distribution of bursts in the [S_E(230 keV), S_E(30400 keV)] plane, showing a continuity between the different kinds of events that points to a common origin (Sakamoto et al. 2005). Right: Light curve of XRF 030723, the first XRF optical afterglow ever detected (Fynbo et al. 2004).

- **High redshift GRBs**. XRFs would be distant GRBs, so that the redshift effect would make them softer and fainter (Heise et al. 2001). However, redshift measurements suggest that at least some of them are nearby events: z=0.251 for XRF 020903 (Soderberg et al. 2004), z=0.21 for XRF 040701 (Soderberg et al. 2005) z=0.828 for XRF 050824 (Sollerman et al. 2007). Furthermore, analyses of the E_p (spectral peak energy) predictions in various prompt emission GRB models suggest that E_p are usually functions of many parameters (including z) and that the dependencies in other factors, such as the bulk Lorentz factor (Γ) are more sensitive than the dependency on z. A systematic study of the redshift distribution of XRFs shows that the relation XRF - high-z can be discarded (Gendre et al. 2007).

- **Off-axis seen GRB with a uniform jet**. The simplest jet model that the jet has a conical shape with sharp edges. In this scenario, a GRB would correspond to an on-beam geometry while an XRF would be seen off-axis, an XRR burst would be an intermediate case, as an analogy to the "unified" AGN model (Antonucci 1993). A direct prediction of such a scenario is that the early light curve should rise initially due to the gradual entrance of the main ultra-relativistic cone into the observers line of sight (Granot et al. 2002). In some cases of XRF and XRR bursts an early shallow decay, or even an early flat phase has been seen when early enough observations have been obtained (Fynbo et al. 2004, Granot et al. 2005, de Ugarte Postigo et al. 2007), a fact that would support this interpretation.

- **Off-axis seen GRB with a structured jet**. GRB jets can have a significant structure, with angle dependent energy per solid angle and Lorentz factors (Meszaros et al. 1998), both decreasing with the angular distance to the jet axis. At a certain viewing angle θ_v, an otherwise considered GRB would be seen as an XRF. The jet angular structure is unknown, but the normally used functions are powerlaws ($\epsilon(\theta) \propto \theta^{-k}$, usually k$\sim$2) or Gaussians ($\epsilon(\theta) \propto \epsilon_0 exp(-\theta^2/2\theta_0^2)$). Structured jets apparently over-predict the number of XRF (Lamb et al. 2005) but the Gaussian jets fit better the observational constrains (Zhang et al. 2004a, Dai & Zhang 2005).

- **Two component jet**. This is a particular type of structured jet, in which there are two uniform jets: A narrow, high-Γ jet and a wide low-Γ jet. This idea is motivated by progenitor models in which a hot cocoon is expected to surround the central relativistic jet that drills the star (Woosley et al. 1999, Zhang et al. 2003, 2004, Meszaros & Rees 2001, Ramirez-Ruiz et al 2002, Mizuta et al. 2006, Morsony et al. 2006). This cocoon would generate the second, less energetic jet component. GRBs would be detected when seen on axis while XRFs happen when the line of sight sweeps the wider beam.

- **Intrinsically faint, less collimated jet**. Lamb et al. (2005) propose a model in which GRBs are bright, narrow jets, while XRFs are much fainter wider jets. This model may account for some XRFs in which no break has been detected after long observing times. However, this behaviour has also been observed in some normal GRBs.

- **Dirty fireballs**. This model proposes that XRFs are produced by bursts with lower Lorentz factors, that would produce a softer and fainter emission (Dermer et al. 1999, Huang et al. 2002). Detailed studies of the E_p models (Zhang & Meszaros 2002) conclude that its dependence on Γ is non-trivial and that it could even increase with it.

- **Intrinsically inefficient GRB from clean fireball**. Considering that the γ-ray emission is generated by internal shocks (Barraud et al. 2005), the peak energy is $E_p \propto E_{pr,int}^4 L^{1/2} r^{-1}$, where $E_{pr,int}$ is the energy of protons in the internal shocks, L the wind luminosity and r$\sim \Gamma^2 c\delta t$ is the internal shock radius. A clean fireball (large Γ) tends to increase the shock radius and together with inefficient internal shocks (reduced $E_{pr,int}$) may give reduced enough E_p to create an XRF.

- **Photosphere dominated emission models**. Internal and external shocks, barionic and pair photospheres can be another important emission site. If this emission is dominant, under certain conditions, it could result in the soft emission that characterises the XRFs (Mészáros 2002).

- **Completely different origin with respect to GRBs**. A final possibility would be that XRFs are generated by a completely independent phenomena from GRBs, having different progenitors, central engines or radiation mechanisms. However, the smooth transition from GRBs to XRR to XRF argues against this idea.

2.2.3 High luminosity versus Low luminosity

The detection of XRF 060218 at a z=0.0331 (Mirabal et al. 2006, Pian et al. 2006, see Fig. 2.6), together with the detection of GRB 980425 at z=0.0085 (Galama et al. 1998) and GRB 031203, at z=0.1055 (Malesani et al. 2004; Thomsen et al. 2004) suggest that the rate of low-luminosity (LL-GRBs) GRBs in the local Universe is very high, much greater than the rate of conventional high-luminosity (HL-GRBs) bursts. In view that the central engine of XRF 060218 has been proposed to be a neutron star instead of a black hole (Mazzali et al. 2006; Soderberg et al. 2006b) one may speculate with the idea that this bimodal luminosity function could be related to two distinct types of central engines, HL-GRBs involving black holes and LL-GRBs involving neutron stars.

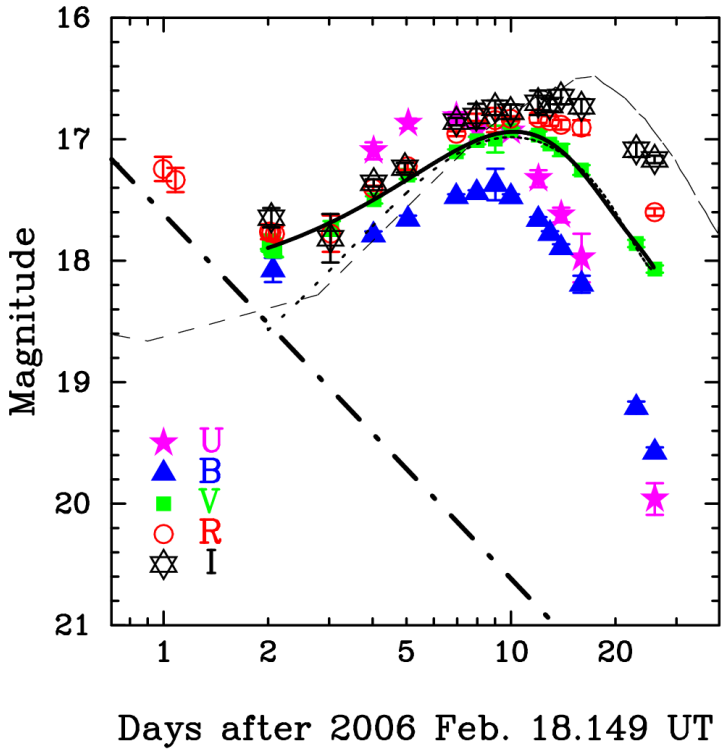

Figure 2.6: Light curve of XRF 060218, with a faint decaying afterglow that is soon dominated by a supernova component (Mirabal et al. 2006).

2.2.4 Optically bright versus optically dark

For approximately 50% of the bursts no optical afterglow is ever detected. This has led to the division between optically bright and optically dark bursts (Jakobsson et al. 2004, Rol et al. 2005). The usual criteria to distinguish between the two types refers to the relation between the X-ray flux and the optical flux (see Fig. 2.7). This is valid for late observations, when optical and X-ray emission come from the same spectral component (afterglow), but is not correct in the case of early observations, where other contributions (reverse shocks or internal shocks) may be present.

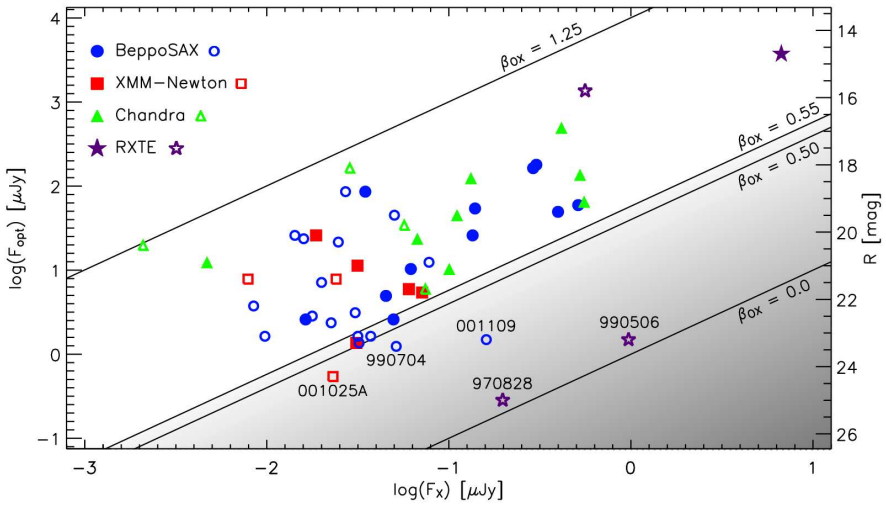

Figure 2.7: The plot shows the optical flux vs. X-ray flux 11 hours after the burst. Dark bursts would be those for which the spectral slope from optical to X-rays would be steeper than $\beta_{OX} = 0.5$ (Jakobsson et al. 2004).

2.3 Redshift distribution

As discussed in the previous Chapter, it was not until the discovery of the first afterglows of long bursts in 1997 (van Paradijs et al. 1997) that we had a clear idea of their distance scale and cosmological redshifts were accepted. After this, it was also speculated that short bursts would be found outside our Galaxy.

Indirect evidence of the cosmological origin of both families was inferred from their isotropic angular distribution in the sky (Briggs et al. 1996; Balazs et al. 1998) and in the value of $\langle V/V_{max} \rangle$ that in both cases was lower than 0.5 (Katz & Canel 1996; Schmidt 2001). $\langle V/V_{max} \rangle$ is the ratio of the volume that is enclosed within the distance at which the event is observed and the maximum volume at which it would still be detectable. Assuming an Euclidean space, a value of 0.5 implies a uniform distribution in distance, while a smaller value suggests sources at cosmological distances and the smallest $\langle V/V_{max} \rangle$ implies larger typical distances. Guetta & Piran (2005) found that for long bursts $\langle V/V_{max} \rangle = 0.29 \pm 0.01$ and for short bursts a significantly higher value of $\langle V/V_{max} \rangle = 0.39 \pm 0.02$ that indicates a smaller typical distance.

The final confirmation of the cosmological origin of short bursts came in 2005 with the secure identification of their host galaxies, thanks to the identification of the gamma-ray bursts by *Swift* and *HETE-2* and the precise localisation of the X-ray afterglows by *Swift* (Gehrels et al. 2005, Villasenor et al. 2005) and the identification of optical counterparts (Hjorth et al. 2005, Fox et al. 2005). It was immediately noted that the distance scale to short bursts was significantly shorter than to long bursts ($< z >_{short} \sim 0.26$ vs. $< z >_{long} \sim 2.8$, Jakobsson 2006, see Fig. 2.8).

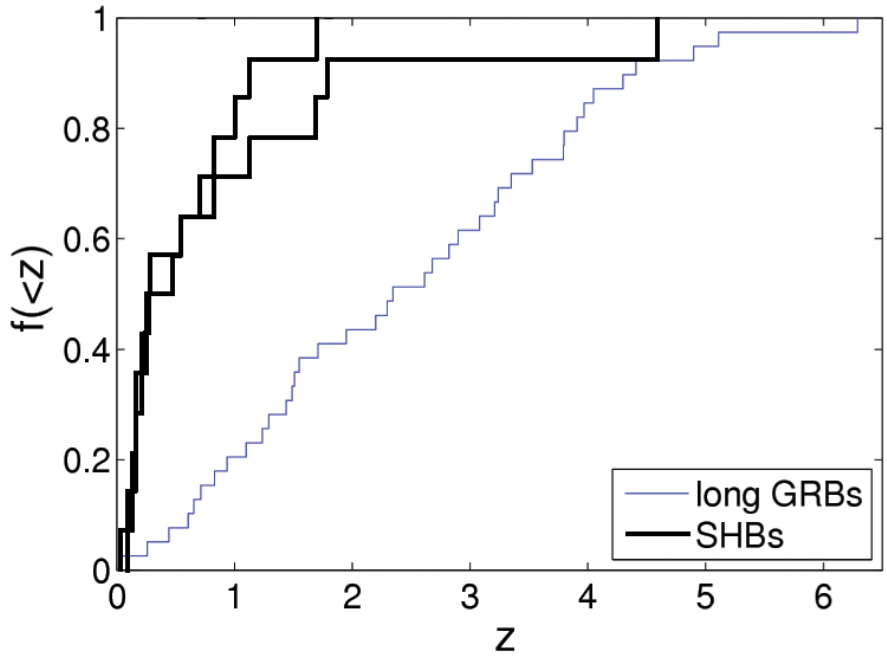

Figure 2.8: Cumulative redshift distribution of short (black thick line) and long bursts (blue thin line). For the short bursts we have drawn two distributions with the lower and upper redshift estimates for those bursts with more than one estimate. Adapted from Nakar (2007).

It must be pointed out that the mean redshift of pre-*Swift* bursts was 1.5, significantly smaller than the actual value. This is due to selection effects caused by different sensitivities in GRB triggering of the different satellites. Similarly, a strong bias is also expected in short burst studies due both to triggering and to follow-up techniques. On one side, from BATSE observations we knew that approximately 25% of the events where short while *Swift* is triggering only 10% of the times on short events. On the other, the distance to short bursts is still obtained indirectly through the redshift of the host galaxy, and only bright hosts allow spectroscopic measurements, with the resulting bias towards lower the average redshifts. Only in one case the redshift of the afterglow has been directly estimated by the use of a spectral flux distribution and the measured redshift is significantly higher than the assumed mean values (GRB 060121 was at a redshift of 1.7 or 4.6 see Chapter 7 and de Ugarte Postigo et al. 2006). Berger et al. (2007b) have systematically studied the error boxes of well localised short GRBs and have found that the faintness of the host galaxies indicate that a significant part of short bursts (between 1/3 and 2/3 of the total number)

happen at a high redshift.

On the other hand, 5 long GRBs have been detected at redshifts smaller than z $\sim$ 0.25 (Stanek et al. 2006), representing several percent. This is much larger than the 0.14 - 0.2 % expected from the predictions of the "classical" GRB population (Le & Dermer 2007) and could be representing a distinct population. This argument is also supported by a different luminosity function (Liang et al. 2006).

2.4 Energetics

Several correlations have been proposed that relate the energetic and spectral properties of the prompt emission of gamma-ray bursts with known redshifts. Amati et al. (2002) proposed that the spectral peak energy was correlated with the isotropic equivalent energy released during the prompt phase ($E_{peak} \propto E_{iso}^{1/2}$, the so called *Amati* correlation). This correlation has been later confirmed when additional bursts have been included (Ghirlanda et al. 2004b; Lamb et al. 2004; Amati 2006).

If the emission produced in GRBs is, as it seems, collimated, we can consider the opening angle in order to calculate the real energy that is released by correcting with the beaming factor ($f_b = 1 - cos(\theta_{jet})$, being θ_{jet} the jet opening angle). Frail et al. (2001) showed that by doing this, the large dispersion of E_{iso} is reduced. Then Ghirlanda et al. (2004a) discovered a tight correlation (the so called *Ghirlanda* correlation) between the GRB peak energies and the collimation corrected energy ($E_{peak} \propto E_{\gamma}^{0.7}$, where $E_{\gamma} = E_{iso} \cdot f$). Fig. 2.9 shows both the Amati and the Ghirlanda correlations.

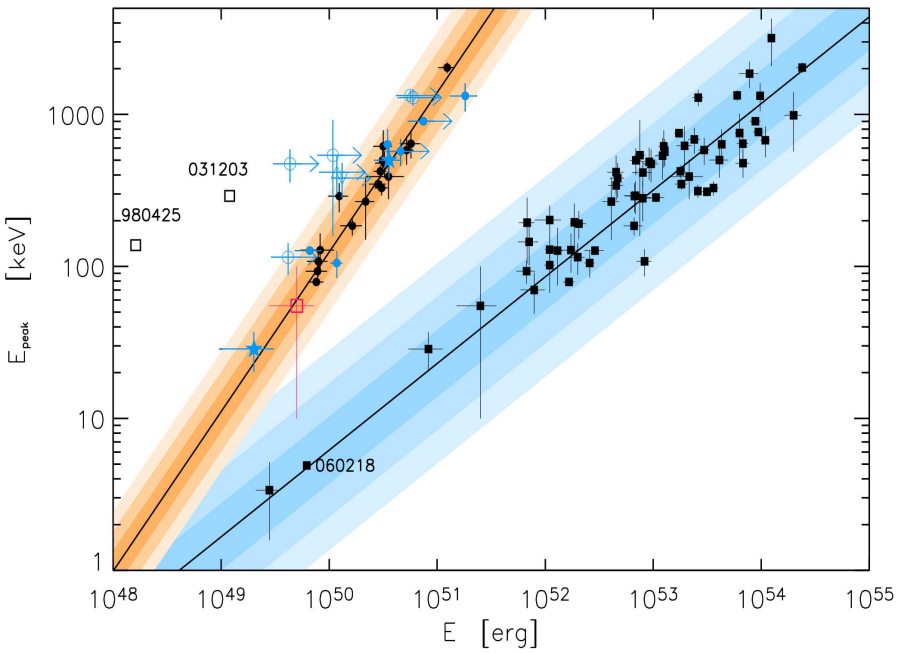

Figure 2.9: Amati and Ghirlanda correlations (Amati et al. 2002; Ghirlanda et al. 2004b; Amati 2006; Ghirlanda et al. 2007).

2.5 Anatomy of the GRB light curve

In the pre-*Swift* era, typical GRB light curves had been characterised by a powerlaw decay with a steepening several hours or days after the burst. This was interpreted as being produced by the outflow being jet-like and the break occurring when the edge of the jet becomes visible as the outflow slows down (Rhoads 1997; Rhoads 1999). Sometimes, when looking soon enough with a robotic telescope at optical wavelengths, an early flash has been detected, peaking tens of seconds after the burst and decaying more steeply than the late light curve.

Soon after the launch of *Swift*, it was realised that X-ray light curves were much more complex than expected, specially during the early hours after the burst. They showed a somehow canonical behaviour (Nousek et al. 2006; Zhang et al. 2006) with several well defined phases (see Fig 2.10): (I) A steep initial decay followed by (II) a flat phase, then by (III) a steeper decay (similar to what had been observed in pre-*Swift* afterglows) and finally, only in some cases, by (IV) a steepening like those understood in the pre-Swift era as jet-produced. The breaks that mark the transition between I and II and between II and III are usually produced at ∼500 s and between 10^3 and 10^4 s after the burst respectively. Intense (long-lasting) flaring activity (V) has been commonly found superimposed to the X-ray light curve. This behaviour has its correspondence in optical afterglows, although sometimes the breaks are not observed simultaneously in both bands, so that the optical and X-ray light curves depart. These deviations have not been yet satisfactorily explained.

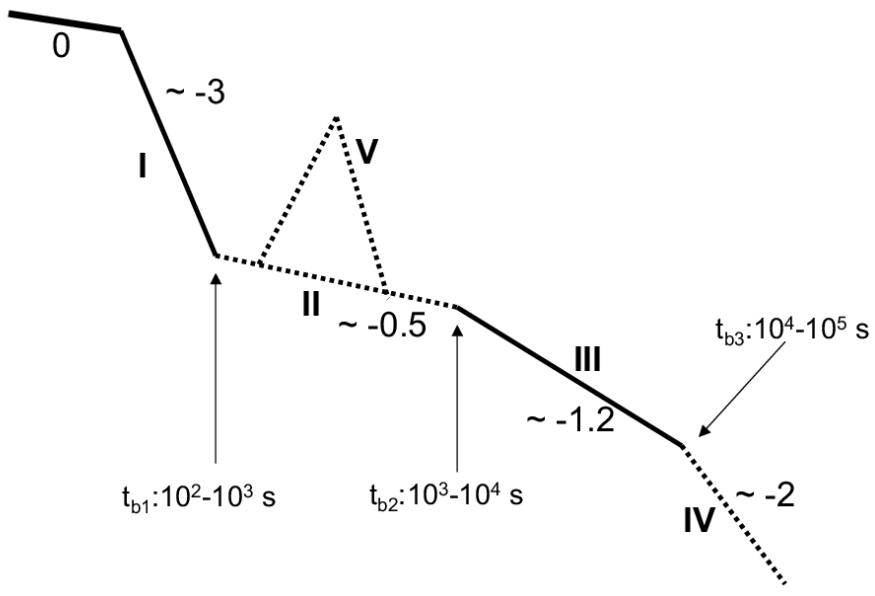

Figure 2.10: GRB X-ray light curves show a canonical shape (Nousek et al. 2006; Zhang et al. 2006). The figure indicates the average power law index α and the break times.

In many cases, when light curves are sampled in detail, significant departures from the powerlaw decay have been observed in the form of bumps, wiggles and spikes. The physics

behind these deviations is discussed in the next chapter.

2.6 Host galaxies

Host galaxies give important clues about the environment in which GRBs are originated, which indirectly point to the progenitors of the explosions. Significantly different host galaxies have been found for short and long gamma-ray bursts, indicating that we are looking at independent phenomena. We will treat them separately in this section.

2.6.1 Long GRBs

Long gamma-ray bursts are generally found in extremely blue, sub-luminous host galaxies (Christensen et al. 2004; Fruchter et al. 2006; Bloom & Prochaska 2006; Savaglio et al. 2006; Stanek et al. 2006), not especially located in dense galaxy fields (clusters). They present strong emission lines and a very high specific star formation rate ($\mathrm{SSFR}_{long} \simeq 10\, M_{\odot} yr^{-1}(L/L_*)^{-1}$, Christensen et al. 2004), suggesting a significant abundance of young massive stars. This supports the generally accepted idea that long GRBs arise from the death of young massive stars similarly to what happens with core-collapse supernovae. However, significant differences have been found in the environments of long GRBs and core-collapse supernovae. In a sample of 42 host galaxies observed by *Hubble Space Telescope*, Fruchter et al. (2006) found that only one host was a grand-design spiral, being the rest irregular galaxies (see Fig. 2.11), while supernovae non associated with GRBs are equally distributed in irregulars and spirals. Furthermore GRBs are concentrated on the brightest regions of their hosts, in the most prolific star forming regions, while supernovae are more uniformly distributed on the galaxies. This is best understood if we assume that GRBs are formed from the core collapse of extremely massive, low metallicity, very short-living stars.

2.6.2 Short GRBs

Host galaxies of short bursts include both early and late type galaxies, as well as field and cluster galaxies, in contrast to the very uniform sample of long burst hosts (see Fig. 2.12). Furthermore, specific star formation rates of short bursts host galaxies have been found to be generally smaller than $1\, M_{\odot} yr^{-1}(L/L_*)^{-1}$. A comparison between the dominant stellar age of long and short hosts rejects that the two populations come from the same parent distribution with a 99.75% significance (Gorosabel et al. 2006). GRB 050709 and GRB 051221 show a dominant population of ~ 1 Gyr (Covino et al. 2006; Soderberg et al. 2006a) and GRB 050724 ~ 2.6 Gyr (Gorosabel et al. 2006).

Berger et al. (2007a) have explored the association of short GRBs with clusters. Through a systematic search in the error box of 15 *Swift* short bursts for the diffuse X-ray emission that characterises the presence of a cluster they find that except for the case of GRB 050509B, there is no evidence of other associations of *Swift* short GRBs with clusters brighter than $3 \times 10^{-14} erg\, s^{-1}\, cm^{-2}$ in X-rays or with mass $M > 5 \times 10^{13} M_{\odot}$. This suggests that ~ 20 % of short bursts are associated with massive clusters. Association of GRB 050911 and GRB 050906 with clusters have been also proposed (Berger 2005a; Levan et al. 2007), but the non detection of any afterglow prevents a clear correlation.

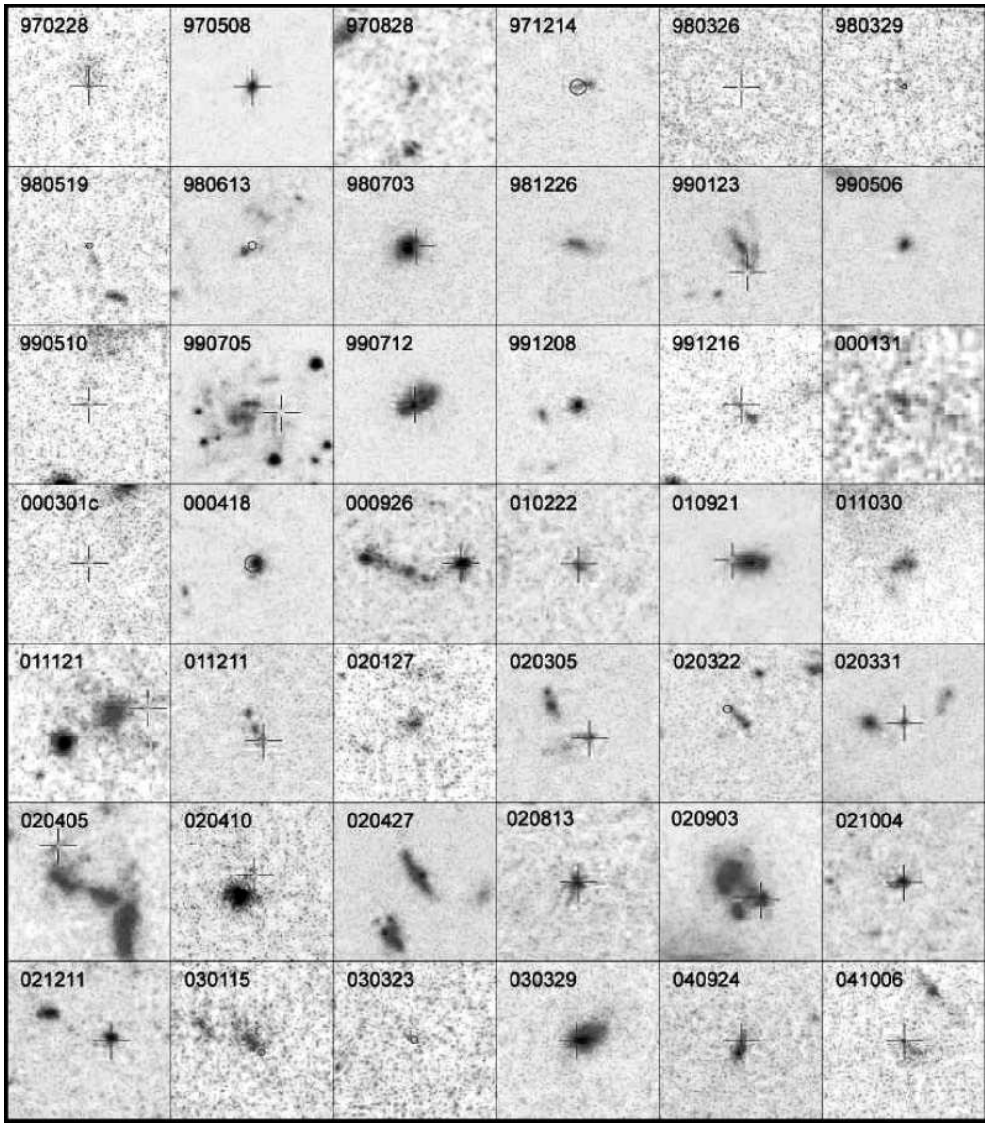

Figure 2.11: Sample of 42 GRB host galaxies observed by the *Hubble Space Telescope* (Fruchter et al. 2006). The boxes have a size of $3.75'' \times 3.75''$.

It is important to note that the host galaxy studies that have been made until now with short bursts generally refer to the nearby population of bright galaxies and the number is still small, so selection effects can be still significant. Additionally, the most popular progenitor models (compact binary mergers, see chapter 3) predict that some of the events will take place far away from their birth places ($\geqslant$ 100 kpc) so afterglow - host galaxy associations can be imprecise.

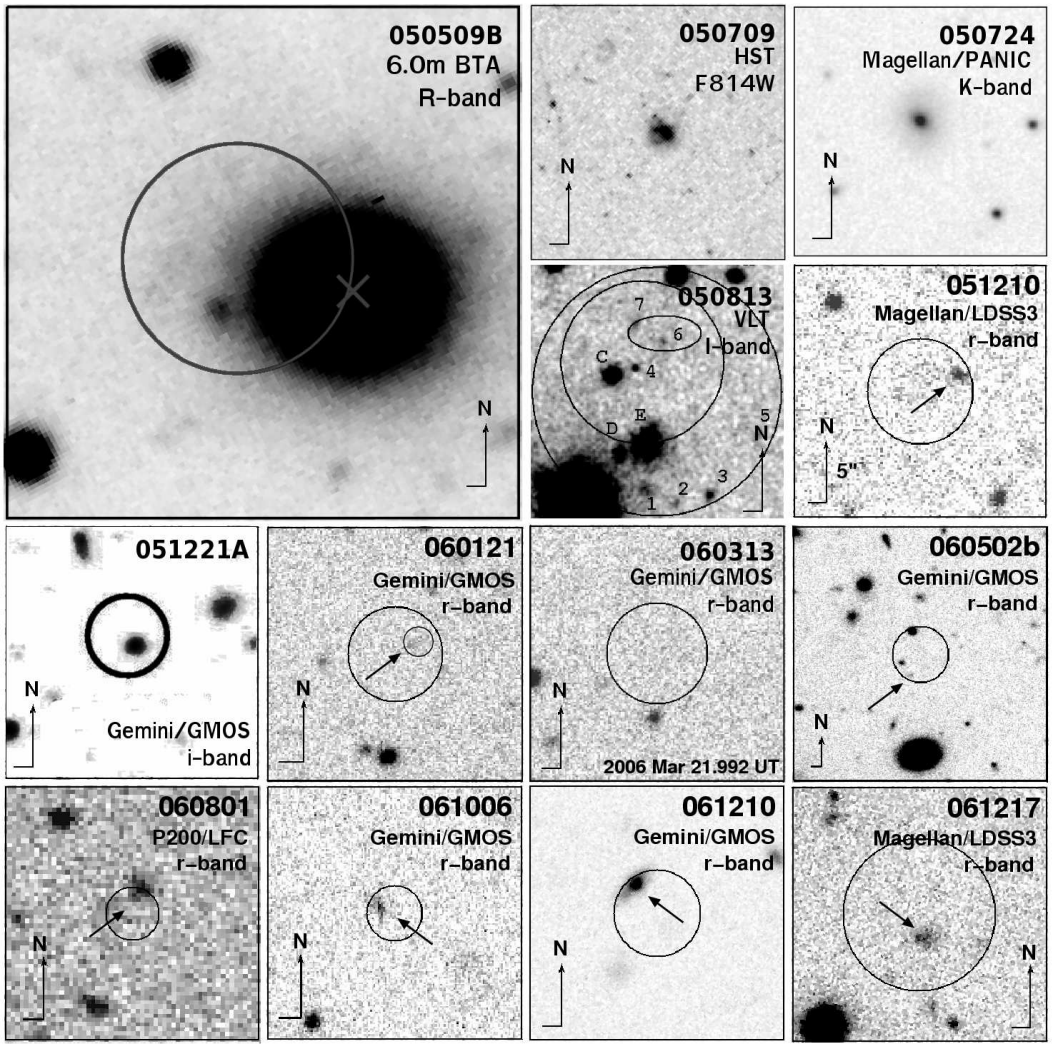

Figure 2.12: Short GRB host galaxies, adapted from Castro-Tirado et al. (2005), Fox et al. (2005), Berger et al. (2005b), Ferrero et al. (2006), Berger et al. (2007b). The boxes have a size of $20'' \times 20''$ except for GRB 050509B (with $40'' \times 40''$).

Bibliography

Akerlof, C., et al. 1999, Nature, 398, 400

Amati, L., et al. 2002, A&A, 390, 81

Amati, L. 2006, MNRAS, 372, 233

Antonucci, R. 1993, ARA&A, 31, 473

Balastegui, A., Ruiz-Lapuente, P., & Canal, R. 2001, MNRAS, 328, 283

Balazs, L. G., Meszaros, A., & Horvath, I. 1998, A&A, 339, 1

Barraud, C., Daigne, F., Mochkovitch, R., & Atteia, J. L. 2005, A&A, 440, 809

Barthelmy, S. D., et al. 2005, Nature, 438, 994

Berger, E. 2005a, GRB Coordinates Network, 3962, 1

Berger, E., et al. 2005b, Nature, 438, 988

Berger, E., Shin, M.-S., Mulchaey, J. S., & Jeltema, T. E. 2007a, ApJ, 660, 496

Berger, E., et al. 2007b, ArXiv Astrophysics e-prints, arXiv:astro-ph/0611128

Bloom, J. S., & Prochaska, J. X. 2006, Gamma-Ray Bursts in the Swift Era, 836, 473

Briggs, M. S., et al. 1996, ApJ, 459, 40

Castro-Tirado, A. J., Brandt, S., Lund, N., Lapshov, I. Y., Terekhov, O., & Sunyaev, R. A. 1994, AIP Conf. Proc. 307: Gamma-Ray Bursts, 307, 17

Castro-Tirado, A. J., et al. 2005, A&A, 439, L15

Christensen, L., Hjorth, J., & Gorosabel, J. 2004, A&A, 425, 913

Cline, D. B., Matthey, C., & Otwinowski, S. 1999, ApJ, 527, 827

Cline, D. B., Czerny, B., Matthey, C., Janiuk, A., & Otwinowski, S. 2005, ApJ, 633, L73

Colgate, S. A. 1974, ApJ, 187, 333

Connaughton, V. 2002, ApJ, 567, 1028

Covino, S., et al. 2006, A&A, 447, L5

Dai, X., & Zhang, B. 2005, ApJ, 621, 875

Della Valle, M., et al. 2006, Nature, 444, 1050

Dermer, C. D., Chiang, J., Böttcher, M. 1999, ApJ, 513, 656

Donaghy, T. Q., et al. 2006, ArXiv Astrophysics e-prints, arXiv:astro-ph/0605570

Ferrero, P., et al. 2006, ArXiv Astrophysics e-prints, arXiv:astro-ph/0610255

Fishman, G. J., & Meegan, C. A. 1995, ARA&A, 33, 415

Fox, D. B., et al. 2005, Nature, 437, 845

Frail, D. A., et al. 2001, ApJ, 562, L55

Frederiks, D. D., Aptekar, R. L., Golenetskii, S. V., Il'Inskii, V. N., Mazets, E. P., Palshin, V. D., & Cline, T. L. 2004, Astronomical Society of the Pacific Conference Series, 312, 197

Fruchter, A. S., et al. 2006, Nature, 441, 463

Fynbo, J. P. U., et al. 2004, ApJ, 609, 962

Fynbo, J. P. U., et al. 2006, Nature, 444, 1047

Galama, T. J., et al. 1998, Nature, 395, 670

Gal-Yam, A., et al. 2006, Nature, 444, 1053

Gehrels, N., et al. 2006, Nature, 444, 1044

Gendre, B., Galli, A., & Piro, L. 2007, A&A, 465, L13

Ghirlanda, G., Ghisellini, G., & Celotti, A. 2004a, A&A, 422, L55

Ghirlanda, G., Ghisellini, G., & Lazzati, D. 2004b, ApJ, 616, 331

Ghirlanda, G., Nava, L., Ghisellini, G., & Firmani, C. 2007, A&A, 466, 127

Gorosabel, J., et al. 2006, A&A, 450, 87

Granot, J., Panaitescu, A., Kumar, P., & Woosley, S. E. 2002, ApJ, 570, L61

Granot, J., Ramirez-Ruiz, E., & Perna, R. 2005, ApJ, 630, 1003

Guetta, D., & Piran, T. 2005, A&A, 435, 421

Heise, J., in't Zand, J., Kippen, R. M., & Woods, P. M. 2001, Gamma-ray Bursts in the Afterglow Era, 16

Hjorth, J., et al. 2003, Nature, 423, 847

Hjorth, J., et al. 2005, Nature, 437, 859

Horváth, I. 1998, ApJ, 508, 757

Horváth, I., Balázs, L. G., Bagoly, Z., Ryde, F., & Mészáros, A. 2006, A&A, 447, 23

Huang, Y. F., Dai, Z. G., & Lu, T. 2002, MNRAS, 332, 735

Jakobsson, P., Hjorth, J., Fynbo, J. P. U., Watson, D., Pedersen, K., Björnsson, G., & Gorosabel, J. 2004, ApJ, 617, L21

Jakobsson, P., et al. 2006, A&A, 447, 897

Katz, J. I., & Canel, L. M. 1996, ApJ, 471, 915

Kippen, R. M., Woods, P. M., Heise, J., in't Zand, J. J. M., Briggs, M. S., & Preece, R. D. 2003, Gamma-Ray Burst and Afterglow Astronomy 2001: A Workshop Celebrating the First Year of the HETE Mission, 662, 244

Kouveliotou, C., Meegan, C. A., Fishman, G. J., Bhat, N. P., Briggs, M. S., Koshut, T. M., Paciesas, W. S., & Pendleton, G. N. 1993, ApJ, 413, L101

Lamb, D. Q., et al. 2004, New Astronomy Review, 48, 423

Lamb, D. Q., Donaghy, T. Q., & Graziani, C. 2005, ApJ, 620, 355

Lazzati, D., Ramirez-Ruiz, E., & Ghisellini, G. 2001, A&A, 379, L39

Le, T., & Dermer, C. D. 2006, ArXiv Astrophysics e-prints, arXiv:astro-ph/0610043

Levan, A. J., et al. 2007, ArXiv e-prints, 705, arXiv:0705.1705

Liang, E., Zhang, B., Virgili, F., & Dai, Z. G. 2006, ArXiv Astrophysics e-prints, arXiv:astro-ph/0605200

MacFadyen, A. I., & Woosley, S. E. 1999, ApJ, 524, 262

Malesani, D., et al. 2004, ApJ, 609, L5

Mangano, V., et al. 2007, ArXiv e-prints, 704, arXiv:0704.2235

Mazzali, P. A., et al. 2006, Nature, 442, 1018

Mazets, E. P., et al. 1981, Ap&SS, 80, 3

Mészáros, P., Rees, M. J., & Wijers, R. A. M. J. 1998, ApJ, 499, 301

Mészáros, P., & Rees, M. J. 2001, ApJ, 556, L37

Mészáros, P. 2002, ARA&A, 40, 137

Mészáros, P. 2006, Reports of Progress in Physics, 69, 2259

Mirabal, N., Halpern, J. P., An, D., Thorstensen, J. R., & Terndrup, D. M. 2006, ApJ, 643, L99

Mizuta, A., Yamasaki, T., Nagataki, S., & Mineshige, S. 2006, ApJ, 651, 960

Morsony, B. J., Lazzati, D., & Begelman, M. C. 2006, ArXiv Astrophysics e-prints, arXiv:astro-ph/0609254

Nakar, E., & Piran, T. 2002, MNRAS, 330, 920

Nakar, E. 2007, Phys. Rep., 442, 166

Norris, J. P., Cline, T. L., Desai, U. D., & Teegarden, B. J. 1984, Nature, 308, 434

Norris, J. P., Scargle, J. D., & Bonnell, J. T. 2001, Gamma-ray Bursts in the Afterglow Era, 40

Norris, J. P., & Bonnell, J. T. 2006, ApJ, 643, 266

Nousek, J. A., et al. 2006, ApJ, 642, 389

Paczynski, B. 1998, ApJ, 494, L45

Pian, E., et al. 2006, Nature, 442, 1011

Ramirez-Ruiz, E., Celotti, A., & Rees, M. J. 2002, MNRAS, 337, 1349

Resmi, L., et al. 2005, A&A, 440, 477

Rhoads, J. E. 1997, ApJ, 487, L1

Rhoads, J. E. 1999, A&AS, 138, 539

Rol, E., Wijers, R. A. M. J., Kouveliotou, C., Kaper, L., & Kaneko, Y. 2005, ApJ, 624, 868

Sakamoto, T., et al. 2005, ApJ, 629, 311

Savaglio, S., Glazebrook, K., & Le Borgne, D. 2006, Gamma-Ray Bursts in the Swift Era, 836, 540

Schmidt, M. 2001, ApJ, 559, L79

Soderberg, A. M., et al. 2004, ApJ, 606, 994

Soderberg, A. M., et al. 2005, ApJ, 627, 877

Soderberg, A. M., et al. 2006a, ApJ, 650, 261

Soderberg, A. M., et al. 2006b, Nature, 442, 1014

Sollerman, J., et al. 2007, A&A, 466, 839

Stanek, K. Z., et al. 2003, ApJ, 591, L17

Stanek, K. Z., et al. 2006, Acta Astronomica, 56, 333

Thomsen, B., et al. 2004, A&A, 419, L21

de Ugarte Postigo, A., et al. 2006, ApJ, 648, L83

de Ugarte Postigo, A., et al. 2007, A&A, 462, L57

van der Horst, A. J., Rol, E., Wijers, R. A. M. J., Strom, R., Kaper, L., & Kouveliotou, C. 2005, ApJ, 634, 1166

van Paradijs, J., et al. 1997, Nature, 386, 686

Vestrand, W. T., et al. 2005, Nature, 435, 178

Villasenor, J. S., et al. 2005, Nature, 437, 855

Woosley, S. E. 1993, ApJ, 405, 273

Woosley, S. E., Eastman, R. G., & Schmidt, B. P. 1999, ApJ, 516, 788

Yi, T., Liang, E., Qin, Y., & Lu, R. 2006, MNRAS, 367, 1751

Yoshida, A., & Murakami, T. 1994, AIP Conf. Proc. 307: Gamma-Ray Bursts, 307, 333

Zhang, B., & Mészáros, P. 2002, ApJ, 581, 1236

Zhang, W., Woosley, S. E., & MacFadyen, A. I. 2003, ApJ, 586, 356

Zhang, B., & Mészáros, P. 2004a, International Journal of Modern Physics A, 19, 2385

Zhang, W., Woosley, S. E., & Heger, A. 2004b, ApJ, 608, 365

Zhang, B., Fan, Y. Z., Dyks, J., Kobayashi, S., Mészáros, P., Burrows, D. N., Nousek, J. A., & Gehrels, N. 2006, ApJ, 642, 354

Zhang, B. 2007, Chinese Journal of Astronomy and Astrophysics, 7, 1

3

Physics of gamma-ray bursts

The underlying physics that generates gamma-ray bursts and their counterparts at shorter wavelengths is discussed throughout this chapter. The emission is explained by adopting the fireball model, which is the most widely accepted and has been used during our research work to model GRB light curves. This model has proved to be equally valid for long and short bursts, although the central engine that powers the fireball is probably very different in each case.

3.1 Introduction

It is widely believed that the highly variable emission of GRBs is produced in an ultrarelativistic outflow, which explains the optical thinness to pair formation and electron scattering and at the same time the non thermal spectrum that extends over 1 Mev and sometimes even above 1 GeV. In this scenario, the dissipation of the kinetic energy (and subsequent particle acceleration and emission of synchrotron/inverse Compton radiation) is caused by large fluctuations in the Lorentz factor that produce *internal shocks* (Rees & Meszaros 1994). The afterglow emission that can be detected from radio to X-rays following the burst is attributed to the interaction between the GRB ejecta and the circumburst medium. This leads to a long-lived *foward shock* that energises the ambient medium and a much shorter *reverse shock* that returns towards the central engine, crossing the GRB ejecta (external shock model - i.e. Paczynski & Rhoads 1993; Meszaros & Rees 1997; Sari & Piran 1999).

The energy source that powers this kind of events is most probably associated with a catastrophic energy release in a stellar mass object. For long bursts this is almost certainly associated with the final stages of a very massive star, when its core collapses (Woosley 1993; Paczynski 1998) which is, at least in some cases, associated with a detectable supernova (Galama et al. 1998; Bloom et al. 1999; Stanek et al. 2003; Hjorth et al. 2003). For short bursts, it has long been assumed (Paczynski 1986; Eichler et al. 1989) that they are related with compact binary mergers (NS-NS or NS-BH) and although there are a number of observations that support this idea (Castro-Tirado et al. 2005; Hjorth et al. 2005; Berger et al. 2005) the matter can not be considered yet settled.

3.2 The compactness problem and relativistic effects

One of the keys to understand the emission mechanisms of GRBs lies in learning how the compactness problem is solved. The issue arises when we try to council the very fast variability (of the order of milliseconds) observed in GRB light curves and the observed energy release. The variability would imply compact sources of the order of ~ 1000 km, while if placed at cosmological distances we would be observing a gamma-ray emission of the order of 10^{51} erg. Such a high energy in such a reduced space would produce an extremely high opacity, as the gamma-ray photons would interact with lower energy photons and produce electron-positron pairs with an enormous optical depth. However, the observed non-thermal spectrum indicates that the sources must be optically thin. This problem was soon realised (Ruderman 1975; Schmidt 1978) and used to argue against the cosmological origin of GRBs.

The compactness problem stems from the assumption that the size of the sources that emit the observed radiation is determined by the observed variability time scale. The puzzle is solved naturally by assuming ultrarelativistic expansions, which strongly affect the observational properties of the radiation. In this section we describe some of the effects caused by this ultrarelativistic motion.

3.2.1 Reference frames and time distortions

In order to explain the effects that are affecting the observations we will consider three reference frames:

- **Observer-frame K**. Located on the Earth, from which we observe the GRB.
- **GRB-frame K$_*$**. Located at the origin of the explosion.
- **Comoving-frame K$'$**. Located on the expanding gas rest frame.

To simplify the explanation, we will initially consider no cosmological effects (that will only affect our result by factors $(1+z)$, of the order of unity) by placing the observer in the vicinity of the burst, so that K and K_* are relatively motionless and just have a different point of view of the ongoing phenomena.

The emitting material moves relativistically with velocity defined by $v/c = (1-1/\Gamma^2)^{1/2}$ (with Γ being the Lorentz factor) relative to K_* (moving towards K). A proper length dr' has a GRB-frame length $dr_* = dr'/\Gamma$ (the usual Fitz-Gerald contraction) and a proper time interval dt' has a GRB-frame duration of $dt_* = dt'\Gamma$ (the usual time dilation effect). Considering an ejecta which expands radially in a direction at an angle $cos\,\theta = \mu$ with respect to the observer line of sight, if a first photon is emitted when the gas is at the radius $r_{*1} = r_1$ (which is at a distance d from the observer) at t_{*1}, this photon arrives at the observer at an observer time $t_1 = t_{*1} + d/c$. A second photon emitted from a radius $r_{*2} = r_2$ at a time t_{*2} will arrive at an observer time $t_2 = t_{*2} + (d/c - v/c\mu dt_*)$, where $dt_* = t_{*2} - t_{*1}$. This is ilustrated in Fig. 3.1. For an observer close to the line of sight, the observed lapse between the arrival of two photons is:

$$dt = dt_*(1 - v/c\mu) \simeq dt_*(1/2\Gamma^2 + \theta^2/2) \simeq dr/(2\Gamma^2 c)(1 + \Gamma^2\theta^2) \simeq dr/(2\Gamma^2 c) \qquad (3.1)$$

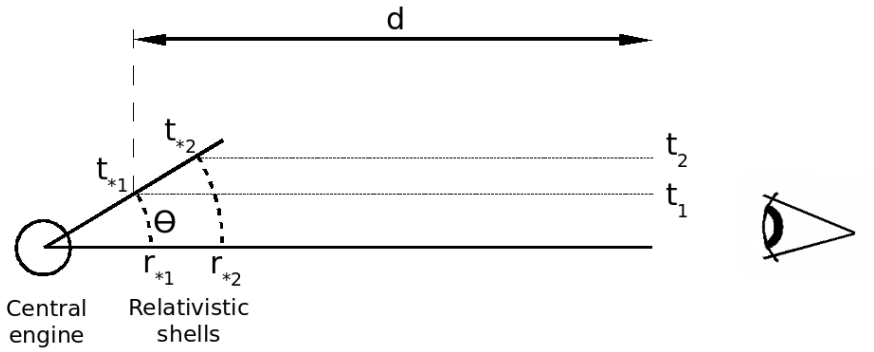

Figure 3.1: Emission and observation of two photons from a relativistic expanding shell (adapted from Mészáros 2006).

Where we have assumed that $\Gamma \gg 1$ for an approaching material ($\mu = cos\theta > 0$) along a radial direction well inside the light cone $\theta \ll \Gamma^{-1}$.

While both dt and dt_* are in the same reference frame $K = K_*$, the difference is that dt_* is the time interval between the emission of two photons and dt the lapse between their arrival to the observer.

In this context, if we assume that we are viewing an on-axis expansion, the variability of milliseconds that is observed in GRB light curves would imply sizes of $\sim 10^7$ km if we assume $\Gamma = 100$, in contrast to the $\sim 10^3$ km of the static emitter. Additionally, a large Γ also reduces the energy of the photons in the emitter rest frame as $h\nu' \approx h\nu/\Gamma$. All this together naturally solves the compactness problem.

3.2.2 Causal connection and quasi-sphericity

Let us now consider a spherical shell expanding at $\Gamma \gg 1$ and a signal that is propagating on its surface at a velocity v_s (in the local rest frame). While the shell expands from R to $R + dR$ the signal will have travelled $d\theta_s = v_s/cdR/(\Gamma R)$, and during the expansion time (time needed to double the radius) the signal propagates $\theta_s \approx v_s/c/\Gamma$ (neglecting second order logarithmic terms). Since $v_s/c \leq 1$, the angular size of a casually connected patch of the shell is $\sim 1/\Gamma$. Therefore, an observer will not observe anything that is outside the $1/\Gamma$ angular region.

This effect greatly simplifies the analysis of the early stages of the GRB, as we can assume spherical symmetry as long as the angular structure does not vary over angles greater than $1/\Gamma$. This is what we refer to as *quasi-sphericity*.

3.2.3 High latitude emission

If the expanding shell emits a short pulse at a radius R, it would arrive as a distorted signal to the observer. The first photons to arrive would be those on the line of sight (t_{los}) and at

later time photons would be arriving from larger angles (t_{ang}). Additionally, the relativistic blueshift decreases with increasing latitude, resulting in a decay of the energy flux. In the case of a power-law spectrum ($F_\nu \propto \nu^\beta$), the observed flux depends on the Lorentz boost as $F_\nu = \mathcal{D}^{\beta-2}$, where $\mathcal{D} = [\Gamma(1 - v/ccos\,\theta)]^{-1}$ is the Doppler factor. In the limit of $\Gamma \gg 1$ we obtain (Kumar & Panaitescu 2000; Nakar & Piran 2003):

$$F_\nu \propto \left(1 + \frac{t - t_{los}}{t_{ang}}\right)^{\beta-2} \tag{3.2}$$

At late times, ($t \gg t_{los}$ and $t \gg t_{ang}$) the light curve decays as $t^{-(2+\beta)}$. This imposes limits to the decay slopes expected in the light curves of GRBs and is what we also refer to as the *curvature effect*.

3.2.4 Equal arrival time surface and limb brightening

Due to the relativistic distortions that we have shown, at a given observer time T, the photons that the observer will be receiving will have been generated at a non spherical surface. From eq. 3.1 and taking into account that $dt_* = dr_*/v$ we find that the radius from which the photons come is described by:

$$R = \frac{vT}{1 - v/c\mu} \tag{3.3}$$

which defines an ellipsoid. However, in GRBs, the emission is concentrated in a thin shell that decelerates as it interacts with the interstellar medium. When this deceleration is accounted for the ellipsoid is distorted (see Fig. 3.2). Assuming a deceleration in which $\Gamma \propto R^{-3/2}$ as derived from an adiabatic ultrarelativistic hydrodynamic solution the eq. 3.3 is generalised as (Granot et al. 1999):

$$R = \frac{cT}{1 - \mu + 1/(8\Gamma^2)} \tag{3.4}$$

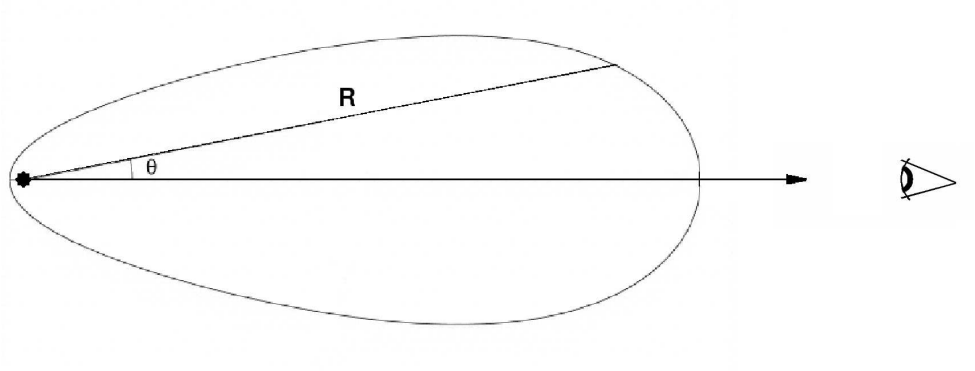

Figure 3.2: Equal arrival time surface. Shape of the surface from which photons reach the observer at a given time T. The observer is located at the right of the figure and the symmetry axis is the line of sight to the centre of the GRB. In order to arrive simultaneously, the photons coming from different locations have to be emitted at different times, according to eq. 3.1 (Granot et al. 1999).

The shape of the equal arrival time surface (EATS) described by eq. 3.4 is shown in Fig. 3.2. An interesting effect is that the effective emitting region seen by the observer resembles a ring (Goodman 1997; Waxman 1997; Panaitescu & Meszaros 1998; Sari 1998b; Granot et al. 1999). This limb brightening varies with time and frequency. See Fig. 3.3.

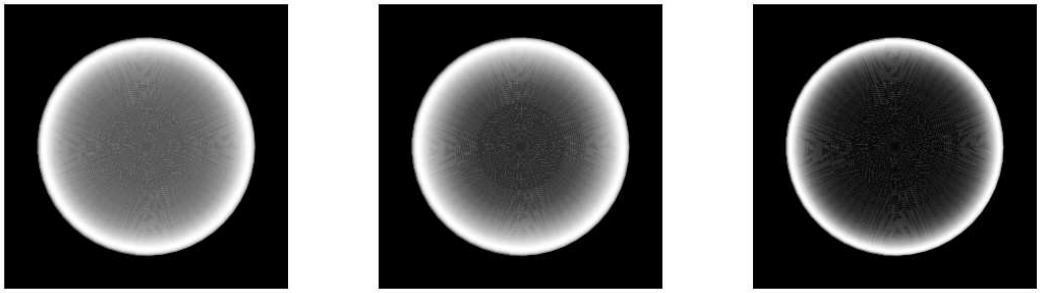

Figure 3.3: Limb brightening effect. Image of a GRB afterglow as it would be observed if the resolution was good enough. The different images can represent either the afterglow at different frequencies at the same observer time or the image at the same frequency at different times (Granot et al. 1999).

3.3 The prompt emission

The observed prompt emission of a GRB has most of its energy concentrated in the 0.1-2 MeV energy range. The spectrum is described by a broken power law (Band et al. 1993) with a break energy in the above range and power law extensions down into the X-rays and up into the 100 MeV to GeV ranges. This radiation is generated at a radius in which the optical depth of the relativistic flow is low, otherwise the energy would be only dissipated through expansion. Depending on the composition of the flow, the dissipation mechanism will differ and can result either from strong shocks (baryonic or weakly-magnetised plasma) or from dissipation of the magnetic field (Poynting-flux dominated flows). Following the most widely accepted model we will assume the first scenario.

The dissipation that produces the gamma-ray emission can be internal to the flow (*internal shocks*) or by interaction to the external medium (*external shocks*). In internal dissipation models, the duration of the burst is related to the duration of the engine activity, as the light-crossing time of the engine is shorter than the burst duration. In the external shock model, the duration of the burst is determined by the radius at which the interaction takes place and the variability is limited by the angular smoothing (see sect. 3.2.3). Due to the high variability observed in prompt GRB light curves (amplitudes of $\sim 100\%$ on time scales $\delta t \ll t$) the internal shock model is generally accepted for the prompt emission (Narayan et al. 1992; Rees & Meszaros 1994; Paczynski & Xu 1994). The external shocks will still happen but produce the afterglow, which we will describe in the following section.

The internal shocks that produce the dissipation are generated when shells of plasma with different velocities collide. Each observed pulse of light would correspond to a single episode of collision (see Fig. 3.4). This events are naturally expected to arise in the baryonic outflow and can easily reproduce the observed light curve. The simplest interpretation of the emission as synchrotron radiation roughly predicts the correct observed frequencies and

spectral behaviour.

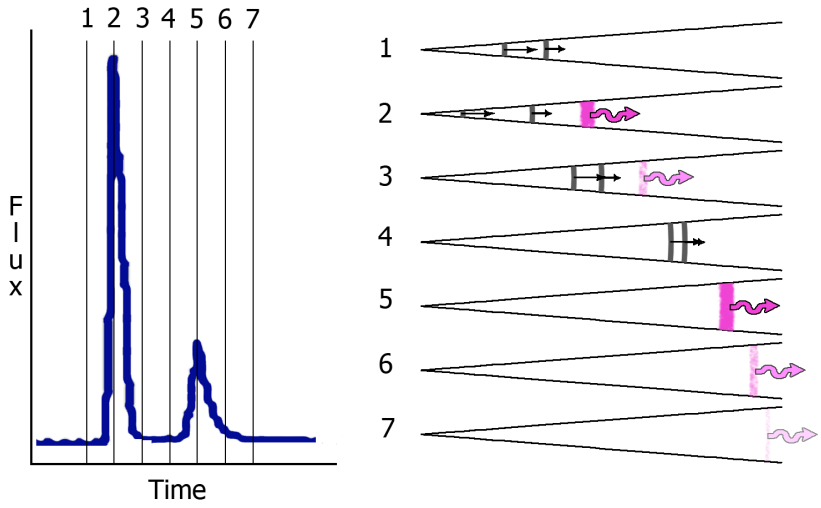

Figure 3.4: Schematic picture showing how a prompt light curve (left) of a GRB is produced by internal shocks (right). We have divided the evolution in 7 phases in which several shells are generated with different Lorentz factors (grey). As they catch up with each other they collide producing gamma ray emission (violet).

3.4 The afterglow

It is generally accepted that the observed afterglow results from slowing down of a relativistic shell on the external interstellar medium. The afterglow is produced, in this case, by an external shock. Another alternative is a continuous emission, where the inner engine that powers the GRB continues to emit energy for longer duration with a lower amplitude (Katz et al. 1998) and that may produce the earliest part of the afterglow. The most likely explanation is that both processes are taking part up to some extent, a solution that could help to explain the early plateau phase seen in many of the *Swift* afterglows (see sect. 2.5). In this section we will focus our attention on the external shock model and then consider some of the possible deviations from this simplified solution.

3.4.1 Standard model of the forward shock

The relativistic energy flow that remains from the prompt emission is transferred to the external medium by driving a shock wave into it. At early times the content of energy in the ejecta is comparable to the one in the shocked material. At this time, the ejecta composition has strong effects in the dynamics and in the emission, as is later discussed in sect. 3.4.2. Once all the energy is dissipated into the external medium, of the initial conditions, only the total amount of energy and its angular distribution will affect the dynamical evolution. This is the phase that we discuss here.

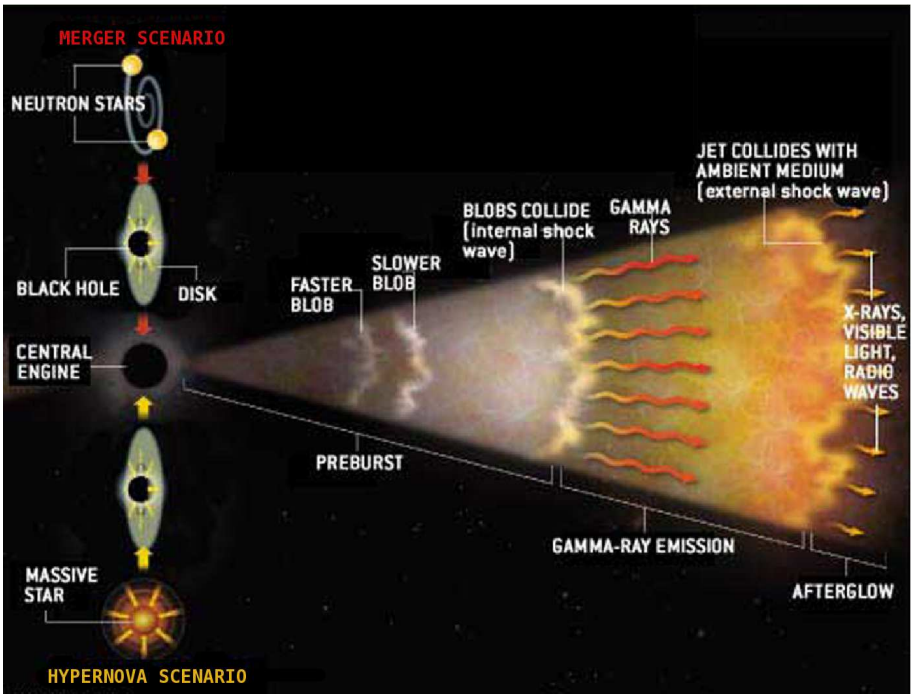

Figure 3.5: Schematic view of the different phases of the model, including the prompt and the afterglow emission. Adapted from Gehrels et al. (2002).

We consider an adiabatically-expanding, spherical[1], collisionless blast wave (Blandford & McKee 1976) with an isotropical equivalent energy E_{iso} that propagates with a Lorentz factor Γ into an external medium composed of proton-electron plasma with density n. During this evolution, the energy conservation dictates the following evolution relations for the Lorentz factor and the Radius of the front shock (Sari et al. 1998):

$$\Gamma \propto \left(\frac{t}{1+z}\right)^{-3/8} \tag{3.5}$$

$$R \approx 4 \cdot 10^{17} cm \left(\frac{E_{52}}{n}\right)^{1/4} \left(\frac{t}{1+z}\right)^{1/4} \tag{3.6}$$

where t is the time in the observer frame and $E_{52} = E_{iso}/(10^{52} erg)$, being E_{iso} measured in erg. The model is characterised by five free parameters: E, n, p, ϵ_e and ϵ_B. As we said, E is the equivalent isotropic energy and n the density, which can take values that range $10^{-2} - 10^{-1} cm^{-3}$ (interstellar medium, ISM), $10^{-3} - 10^{-2} cm^{-3}$ (intercluster medium, ICM) or $\sim 10^{-6} cm^{-3}$ (intergalactic medium, IGM). For long bursts only ISM is relevant, as they are expected to have short lives and happen near their birth places, but short bursts could be happening in any of the three environments, as they are expected to have much longer life-times. The simplest model assumes that the shock accelerates all the electrons to

[1]The spherical approximation is valid as long as the blast wave properties do not vary over angles that are smaller than $1/\Gamma$ (see sect. 3.2.2). Deviations from this behaviour are later discussed in sect. 3.7.

a power law $dN/dE \propto E^{-p}$ starting at a minimal Lorentz factor $\Gamma_{e,m}$ where the electron index $p > 2$ to keep the energy of the photons finite (typical values are expected in the range $2 < p < 3$). ϵ_e is the fraction of internal energy that is carried by the electrons and ϵ_B is the fraction that is carried by magnetic fields in the shocked plasma (by definition $\epsilon_e + \epsilon_B < 1$). The emission can be considered mainly synchrotron, ignoring inverse Compton scattering in most cases. Typical values range $0.05 < \epsilon_e < 0.5$ and $10^{-3} < \epsilon_B < 0.1$ (Panaitescu & Kumar 2001; Yost et al. 2003).

The synchrotron spectrum that dominates the emission is characterised by three frequencies: ν_m is the typical synchrotron frequency that corresponds to $\Gamma_{e,m}$ and is the maximum of the emission; ν_c is the cooling frequency, above which radiative cooling is significant; ν_a is the synchrotron self-absorption frequency. The observed spectrum is usually a four-segment broken power law with breaks at the characteristic frequencies. The power law indexes between the breaks depend on the order in which they are found. There are two main cases: Fast cooling, where $\nu_c < \nu_m$, happening at very early times and slow cooling, where $\nu_m < \nu_c$ which is normally observed during the afterglow phase. The spectral slope and temporal evolution of each of the spectral segments are parametrised in eq. 3.7 and eq. 3.9. The spectral breaks have a temporal evolution themselves, as shown in eq. 3.8 and eq. 3.10 for the fast and slow cooling respectively. The spectral behaviour is schematised in Fig. 3.6.

Fast cooling:

$$F_\nu \propto \begin{cases} \nu^2 t^{1/2} & \nu < \nu_a \\ \nu^{1/3} t^{1/6} & \nu_a < \nu < \nu_c \\ \nu^{-1/2} t^{-1/4} & \nu_c < \nu < \nu_m \\ \nu^{-p/2} t^{-\frac{3p-2}{4}} & \nu_m < \nu \end{cases} \tag{3.7}$$

$$\begin{aligned} \nu_a &\propto t^{-1/2} \\ \nu_c &\propto t^{-1/2} \\ \nu_m &\propto t^{-3/2} \end{aligned} \tag{3.8}$$

Slow cooling:

$$F_\nu \propto \begin{cases} \nu^2 t^{1/2} & \nu < \nu_a \\ \nu^{1/3} t^{1/2} & \nu_a < \nu < \nu_m \\ \nu^{-(p-1)/2} t^{-\frac{3}{4}(p-1)} & \nu_m < \nu < \nu_c \\ \nu^{-p/2} t^{-\frac{3p-2}{4}} & \nu_c < \nu \end{cases} \tag{3.9}$$

$$\begin{aligned} \nu_a &\propto t^{0} \\ \nu_m &\propto t^{-3/2} \\ \nu_c &\propto t^{-1/2} \end{aligned} \tag{3.10}$$

By observing the spectral slope of each of the segments and the location of the spectral breaks we are able to extract the parameters that determine the model, as has been done for several afterglows in Part II of this thesis.

Once the blast wave accumulates enough mass it decelerates to non-relativistic velocities and makes a transition between the self-similar Blandford-McKee solution (Blandford & McKee 1976) to the Newtonian self-similar Sedov-von Neumann-Taylor solution (Sedov 1946; von Neumann 1947; Taylor 1950). This late time behaviour is normally seen only in

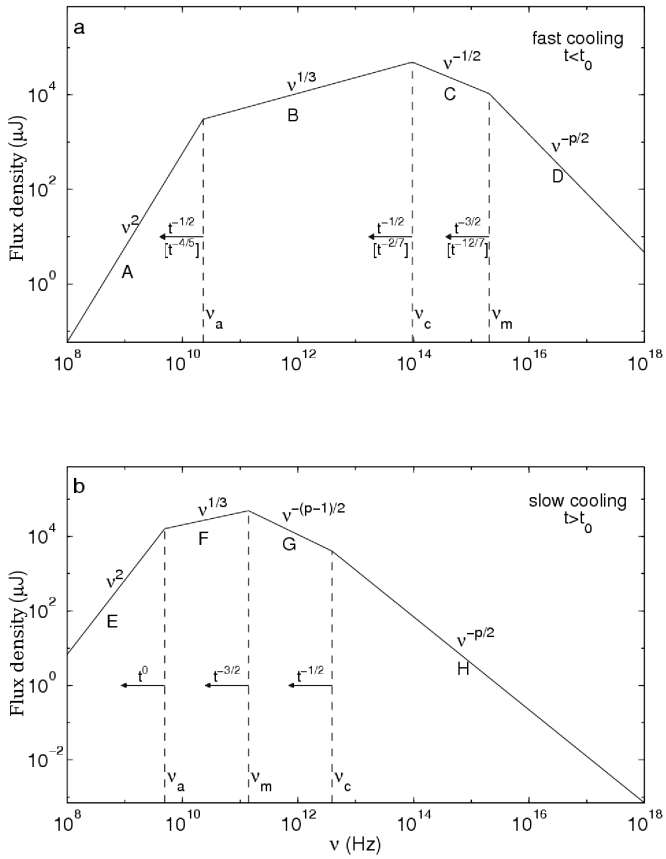

Figure 3.6: Synchrotron spectrum of the afterglow of a GRB. Top: Fast cooling, which is expected at early times, characterised by having $\nu_c < \nu_m$. Bottom: Slow cooling, with $\nu_m < \nu_c$ is the spectrum typically observed in GRB afterglows (Sari et al. 1998).

radio frequencies. The transition that is gradual and can take about one decade in time happens, in the observer frame, at:

$$t_{NR} \sim 0.5yr \left(\frac{E_{52}}{n}\right)^{1/3} (1+z) \tag{3.11}$$

3.4.2 The reverse shock and the early afterglow

Between the prompt emission and the late afterglow there is an intermediate phase, during which the energy of the ejecta is dissipated into the external medium and the composition of the ejecta plays an important role. If the GRB is dominated by a baryonic flow, there is a reverse shock which can show a characteristic optical flash and radio flare that would not be expected in a Poynting flux dominated flow.

The interaction of the baryonic ejecta with the external medium generates two shocks, one propagating into the external medium (forward shock, see previous section) and another that propagates back into the ejecta (reverse shock). These two shocks are separated by a

contact discontinuity. The reverse shock is generally expected to be mildly relativistic. In this case, both shocks carry a similar total energy but the reverse electrons radiate a much softer spectrum ($\nu_m^r = \nu_m^f/\Gamma^2$), while the peak flux is larger a factor Γ than the forward shock. This reverse shock peaks soon after or during the prompt GRB emission and then decays as t^{-2} (Sari & Piran 1999). An accompanying radio flare is expected to peak hours to days later (Kulkarni et al. 1999b; Nakar & Piran 2004).

3.4.3 "Naked" afterglow

When the relativistic outflow that produces the prompt emission is quasi-spherical, an afterglow is expected even if no emission from the external shock is observable (i.e. due to a very low density environment). This afterglow would be produced by the high latitude emission (see sect. 3.2.3) of the prompt emission that decays at late times as $F_\nu \propto \nu^\beta t^{\beta-2}$. This type of "naked" afterglow (Kumar & Panaitescu 2000; Dermer 2004; Page et al. 2006) could be responsible of the fast decay phase observed in *Swift* GRB afterglows (Nousek et al. 2006; Zhang et al. 2006) and could also be the only observable afterglow for short GRBs, where the environment density is expected to be very low.

3.4.4 Jets

The spherical assumption that we have been considering in the last sections is valid even if the relativistic flow is collimated as long as the observer line of sight is inside the collimation cone and the edges are casually disconnected (the Lorentz factor is greater than the inverse of the jet half opening angle, $\Gamma > 1/\theta_j$, sect. 3.2.2). However, as the ejecta decelerates the Lorentz factor drops below this value changing the dynamics and the light curves (Rhoads 1997; Rhoads 1999). The most remarkable signature of this transition is an achromatic break in the light curve of the afterglow (Castro-Tirado et al. 1999; Kulkarni et al. 1999a; Frail et al. 2001). From the time at which this break is observed (t_j) the half opening angle (θ_j) can be derived (for a constant density environment) through:

$$\theta_j \sim 0.057 \left(\frac{t_j}{1\,day}\right)^{-3/8} \left(\frac{1+z}{2}\right)^{-3/8} \left(\frac{E_{iso}}{10^{53}\,erg}\right)^{-1/8} \left(\frac{\eta_\gamma}{0.2}\right)^{1/8} \left(\frac{n}{0.1\,cm^{-3}}\right) \tag{3.12}$$

Where η is the efficiency of the fireball in converting energy of the ejecta into gamma-rays. The equation is adapted from Frail et al. (2001).

After this jet break we begin to observe the edges of the jet and the light curve decays more steeply (see Fig. 3.7). The evolution of the light curve then behaves as follows (from Nakar 2007):

$$F_\nu \propto \begin{cases} \nu^2 t^0 & \nu < \nu_a \\ \nu^{1/3} t^{-1/3} & \nu_a < \nu < \nu_m \\ \nu^{-(p-1)/2} t^{-p} & \nu_m < \nu < \nu_c \\ \nu^{-p/2} t^{-p} & \nu_c < \nu \end{cases} \tag{3.13}$$

Up to now we have assumed a uniform external medium, which has been found to reproduce most afterglows, however, in some cases, a wind-like external medium (with a

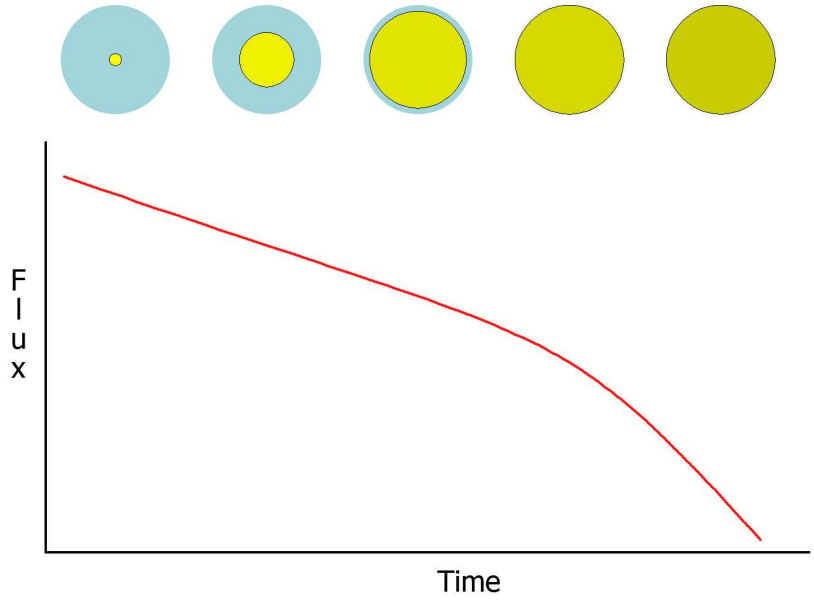

Figure 3.7: Ultrarelativistic expansion in an on axis viewed jet. While the casually connected area (yellow) is smaller than the jet (blue), the evolution is quasi-spherical. Once Γ becomes smaller than the inverse of the jet opening angle we begin to se the edges of the jet and the power law decline of the light curve steepens (see bottom graph). Both axis are in logarithmic scale.

density profile that follows $n = Ar^{-2}$) is preferred (Panaitescu & Kumar 2000; Chevalier & Li 2000; Li & Chevalier 2001). This would be expected if the progenitor of the GRB has been expelling a stellar wind during the last phases of its evolution. In this case, eq. 3.12 would be written as:

$$\theta_j \propto \left(\frac{E}{A}\right)^{-1/4} \left(\frac{t_j}{1+z}\right)^{1/4} \tag{3.14}$$

If the density profile was wind-like, it would also affect the pre-break evolution of the light curve. In Table 3.1 we show the values that are expected for the light curve decay slope and the spectral indexes for the wind profile and the uniform density profile in both pre-break and post-break phases. These observables allow us to rapidly distinguish between the two environments.

3.4.5 Fluctuations in the light curves

The models that we have been considering up to now result in smooth and regular light curves, the models are simplified by assuming that the outflow is uniform and so is the environment surrounding the burst. However, from the detailed observations of some GRB afterglow light curves and spectra we know that this is not normally the case and that light curves present fluctuations that depart from this smooth behaviour. In this section we consider some of the phenomena that would result in a deviation from the simple power law and give some clues on the way in which the different effects can be distinguished.

Table 3.1: Temporal (α, $F_\nu \propto t^\alpha$) and spectral (β, $F_\nu \propto \nu^\beta$) indexes as a funcion of the electron index in constant density and stellar wind environments for the slow cooling phase.

	$\nu < \nu_\mathbf{a}$		$\nu_\mathbf{a} < \nu < \nu_\mathbf{m}$		$\nu_\mathbf{m} < \nu < \nu_\mathbf{c}$		$\nu_\mathbf{c} < \nu$	
MEDIUM	α	β	α	β	α	β	α	β
Pre-jet break (isotropic):								
Constant density ($\mathbf{n = constant}$)	1/2	2	1/2	1/3	3(1-p)/4	(1-p)/2	(2-3p)/4	-p/2
Stellar wind ($\mathbf{n \propto r^{-2}}$)	1	2	0	1/3	(1-3p)/4	(1-p)/2	(2-3p)/4	-p/2
Post-jet break (collimated):								
Constant density ($\mathbf{n = constant}$)	0	2	-1/3	1/3	-p	(1-p)/2	-p	-p/2
Stellar wind ($\mathbf{n \propto r^{-2}}$)	0	2	-1/3	1/3	-p	(1-p)/2	-p	-p/2

Density fluctuations

Stellar winds or turbulent interstellar media will affect the behaviour of the light curve as the blast wave impacts a varying environment (Wang & Loeb 2000; Ramirez-Ruiz et al. 2001; Dai & Lu 2002; Lazzati et al. 2002; Dai & Wu 2003; Nakar & Piran 2003; Nakar et al. 2003). This will result in either bumps or dips relative to the undistorted light curve. The main distinction of density induced variability is that it is chromatic. The light curve will vary both bellow and above ν_c but these variations will be uncorrelated (Nakar et al. 2006).

Patchy shell

If the outflow energy distribution has an intrinsic angular structure (patches) it will produce a variable afterglow light curve (Meszaros et al. 1998; Kumar & Piran 2000). As the blast wave decelerates, the angular size of the observed region ($\sim 1/\Gamma$) increases and as it covers different energy regions, the observed flux fluctuates. The gradual change in the visibility of the patches determines that the variability time scale is $\Delta t \sim t$ (Nakar & Piran 2004). A peculiarity of the patchy shell is that it breaks the axial symmetry and can thus produce linear polarisation. Both the angle and the amplitude of the polarisation are correlated with the light curve variations (Granot et al. 2003; Nakar & Piran 2004).

Energy injections

Energy injections or refreshed shocks are produced when energy is injected into the blast wave by late-arriving shells (Rees & Meszaros 1998; Kumar & Panaitescu 2000; Sari & Mészáros 2000; Granot et al. 2003; Fox et al. 2003; Björnsson et al. 2004; de Ugarte Postigo et al. 2005; Jóhannesson et al. 2006; Nousek et al. 2006; Zhang et al. 2006; Granot & Kumar 2006). These shells can be produced either by late energy releases or during the initial burst as a slow shell that catches up with the initially faster blast wave as it decelerates against the ambient medium. In both cases, the blast wave energy increases and the observed flux is expected to rise above the unperturbed light curve in all wavelengths during the injection. When the injection stops the initial decay is resumed. The light curve of an afterglow with a discrete episode of energy injection shows a step-like structure. Time scales are expected to be $\Delta t \sim t$ before the jet break and can be $\Delta t < t$ after the break.

In any case the fluctuation time is limited by the time associated with the width of the shell behind the afterglow shock, implying $\Delta t \gtrsim t/10$. A variant of this model is the two component jet (Berger et al. 2003; Königl 2004; Granot 2005; Peng et al. 2005; Resmi et al. 2005; Wu et al. 2005; Jin et al. 2007), where a fast narrow jet may be found to be superposed to a slower wider jet.

Late engine activity

In some cases we have observed flares that are too fast and too broad to be explainable by external shock fluctuations. In this case we may consider a reignition of the central engine (Dai & Lu 1998; Rees & Mészáros 2000; Zhang & Mészáros 2002; Ramirez-Ruiz 2004). In this case the fluctuations would be produced by internal dissipation of flow ejected during late engine activity. The radiation would be most probably produced by collisions between shells injected at late times, in a similar way as those that produce the prompt emission. Liang et al. (2006) tested the validity of this model by assuming that the decay of the X-ray flares is controlled by the curvature effect after the abrupt cessation of the internal dissipation, so that $\alpha = \beta - 2$ is assumed to be valid (see Sect. 3.2.3). They subtracted the underlying forward shock light curve and searched the valid ignition time for each flare, which should be before the rising of the flares. The results show that most of the flares do indeed behave as expected, implying that the model is robust for most of the flares.

This fluctuations have the advantage of being very economical, as they require only a small fraction of the prompt emission energy to produce noticeable features, while external shock models require energies of at least the order of the energy already deposited in the blast wave.

Microlensing

The apparent radius of an afterglow increases with time (see sect. 3.2.4) and, at cosmological distances, can reach angular sizes of $\sim \mu as$, comparable to the Einstein radius of solar mass gravitational lens at these distance. Microlensing events are therefore expected to happen although their probability is low and can only explain a few of the observed light curve fluctuations (Loeb & Perna 1998; Garnavich et al. 2000; Ioka & Nakamura 2001; Granot & Loeb 2001; Mao & Loeb 2001; Gaudi & Loeb 2001; Gaudi et al. 2001; Koopmans & Wambsganss 2001; Baltz & Hui 2005). In such an event we expect a brightening that would be simultaneous in all wavelengths, although some colour dependence would be expected due to the colour dependent afterglow surface brightness (Granot et al. 1999).

Dust echoes

Another alternative explanation that has been proposed (Esin & Blandford 2000; Mészáros & Gruzinov 2000; Reichart 2001) for some late bumps seen in GRB light curves is based on the scattering of a prompt optical burst by dust located beyond the sublimation radius of the burst. The properties of the emission will be dependant on the luminosity of the optical transient. These bumps would be expected to peak at the thermal emission of the hot subliming dust, in the near infrared. A further prediction of the dust echo model is

that, unless the dust and the burst are both located axisymmetrically with respect to the line of sight, we expect to see linear polarisation associated with the dust echo.

Supernova bumps

Late bumps observed in nearby long GRBs are normally attributed to a supernova component. The paradigm of these supernova component is SN 1998 bw, which was associated with GRB 980425 (Galama et al. 1998). This was the first long GRB/SN association ever postulated, where a very bright, peculiar supernova was observed but not an afterglow. The light curves and spectra that where obtained for this burst are usually used as a template for fitting other events. These bumps are expected to peak at $\sim 15(1+z)$ days after the GRBs. They are normally redder than the afterglow and the supernova signatures can be clearly distinguished through spectroscopy (Stanek et al. 2003; Hjorth et al. 2003).

3.5 Progenitors

In both long and short gamma-ray bursts, the most commonly discussed central engine invokes a black hole and a surrounding torus, either produced by the collapse of a massive star (long bursts) or by the merger of neutron star - neutron star (NS-NS) or neutron star - black hole binaries (NS-BH) (short bursts).

3.5.1 Long bursts

As explained in sect. 2.6 almost all the hosts of long GRBs have been early-type, blue, star-forming galaxies (Christensen et al. 2004; Fruchter et al. 2006; Bloom & Prochaska 2006; Savaglio et al. 2006; Stanek et al. 2006). Furthermore, their metallicity is generally lower than the average massive star forming galaxies (Le Floc'h et al. 2003; Le Floc'h et al. 2006; Stanek et al. 2006). This has implications on the expected redshift distribution of GRBs, indicating that $\sim 40\%$ of long GRBs may originate at $z \gtrsim 4$ and being, in principle, detectable up to $z \gtrsim 25-30$ (Ciardi & Loeb 2000; Lamb & Reichart 2000; Gou et al. 2004; Natarajan et al. 2005). The high population of massive, short-lived stars in those galaxies, together with the established correlation between long GRBs and core-collapse supernovae has provided strong support to a massive stellar collapse origin for long GRBs (Woosley 1993; Paczynski 1998; Woosley & Heger 2006).

The relatively long duration of the gamma-ray emission of these bursts ($2 \lesssim t_\gamma \lesssim 10^3 s$) is generally attributed to the duration of the accretion of the debris falling into the central black hole that is generated when the star collapses. Initial masses greater than $28-30\,M_\odot$ are expected to collapse into a black hole (Fryer & Kalogera 2001), while smaller initial masses of $10\,M_\odot \lesssim M_* \lesssim 28\,M_\odot$ would lead to a neutron star. This accretion onto the black hole would feed a relativistic jet, which breaks through the collapsing core and the stellar envelope along the direction of the rotation axis.

3.5.2 Short bursts

On the contrary to long events, short bursts happen in a much more wide distribution of galaxies with an average older dominant stellar population. This alone is a strong proof

that the two kind of bursts are generated by different kind of progenitors and is relevant for the most frequently discussed progenitor for short GRBs, the merger of neutron star binaries (Paczynski 1986; Eichler et al. 1989; Barthelmy et al. 2005; Lee et al. 2005), which should be more abundant in old galaxies. This argument is based on the long binary merger times, which through early population synthesis and merger simulations (Bloom et al. 1999) was estimated to be of $\sim 10^8$ years. More recent population synthesis calculations (Belczynski et al. 2002) have reduced the merger time to the point where they could be expected in substantial numbers also in young star-forming galaxies, although statistically, they would be expected to occur more often in old galaxies.

The lack of supernova component weeks after the burst (Castro-Tirado et al. 2005; Hjorth et al. 2005; Fox et al. 2005) argue against models of massive stellar collapse (where a Ib/c supernova would be expected) and against a those that invoke a gravitational collapse of white dwarfs to neutron stars leading to a supernova Ia (Dado et al. 2005).

An alternative explanation is that short bursts could be the initial spike that has been detected in giant flares from soft gamma repeaters or SGR (Hurley et al. 2005; Palmer 2005). SGR should be young objects and the total energy associated with these flares is at least two orders of magnitude smaller than needed to explain the short GRB fluxes detected at $z \gtrsim 0.2$. The lack of star formation in some of the ellipticals that have been associated with short GRBs indicate that at least some of the short GRBs can not be associated with SGR. A statistical analysis indicates that the fraction of short bursts which could be due to SGRs is less than 15% (Nakar et al. 2006). A correlation between short bursts and X-ray selected galaxy clusters has been observed (Ghirlanda et al. 2006), giving a better than 2-σ correspondence with clusters at less than $z = 0.1$, implying that a large number of short bursts would be originated within ~ 270 Mpc.

Another interesting fact that can give good information about the nature of the progenitors is the location of the bursts with respect to the host galaxy. The location will depend on the natal kick of the progenitor and the time between the kick and the merger as well as on the gravitational potential. In the case of compact binaries, the natal kick is expected to be from several tens to hundreds of km/s (Hobbs et al. 2005). A binary with an inspiral time of several Gyr born with a kick of several hundred km/s can merge after travelling $\sim$ 1 Mpc, while a binary that merges within 1 Myr will always end up near its birth place. The typical offset that would be expected for a small (giant) elliptical would be of 100 (10) kpc. The circumburst gas density will depend on this offset and will be determinant for the brightness of the afterglow. Belczynski et al. (2006) present a distribution of densities as predicted by models with different kind of hosts. They find that the lowest densities are expected for binaries that are born in small elliptical galaxies, while those in large, star forming galaxies will have the highest densities.

3.6 Very high energy photons and non-electromagnetic emission

The high Lorentz factors involved in GRBs result in a synchrotron spectrum, which in observer frame extends beyond 100 MeV and inverse Compton scattering of such synchrotron photons, which would predict GeV and TeV spectral components (Meszaros et al. 1994). Detection of GeV photons has been already claimed for GRBs (Hurley et al. 1994), but TeV are likely to be converted into electron-positron pairs via interaction with the extragalactic

infrared radiation fields (Coppi & Aharonian 1997; de Jager & Stecker 2002).

GRBs are expected to be luminous in other channels, such as neutrinos, gravitational waves and cosmic rays. The nucleons involved in the fireball will have $\gtrsim 100$ GeV bulk kinetic energies in the observer frame, which can lead to the production of pions, muons, neutrinos and electrons (and corresponding antiparticles) through inelastic collisions. Massive progenitors offer denser targets for nuclear collisions and larger photon density for $p\gamma$ and $\gamma\gamma$ interactions, leading to a modification of the photon spectra. On the other hand, NS-NS mergers would be characterised by neutron-rich outflows, leading to stronger 5-10 GeV neutrinos and photons from neutron-proton collisions (Bahcall & Mészáros 2000; Beloborodov 2003; Rossi et al. 2006). Photo-pion signatures of $\gtrsim 100$ Gev photons and 10^{14-18} eV neutrinos may be expected to be relatively stronger in massive progenitors.

Compact binary mergers are one of the most promising sources for gravity waves. Knowing the fraction of GRBs (if any) are produced in such kind of event is crucial for gravitational wave detectors. These detectors are expected to give important clues (and may be the only definitive proof) as to whether short bursts are indeed produced by NS-NS (or NS-BH) mergers. They could also indicate if massive stellar collapses are asymmetric enough to produce substantial gravitational waves and serve as a further test for the relationship between long GRBs and supernovae.

In a compact binary merger there are three different phases that would produce gravitational waves: the chirp inspiral signal, the coalescence signal and the signal from the ringdown of the remaining black hole (Cutler & Thorne 2002). The frequency of the typical signal during the final inspiral stages of NS-NS and NS-BH mergers passes through the most sensitive range of gravitational wave detectors ($\sim$ 100 - 500 Hz) such as LIGO[2] or VIRGO[3]. The current estimates give a detection rate by current observatories of $1(10) \times 10^{-4} \lesssim \mathcal{R}_{GW} \lesssim 0.1(1) yr^{-1}$ for NS-NS (NS-10 $M_\odot$ BH) mergers. Therefore, in the most optimistic scenario (short bursts being narrowly beamed with many dim undetected bursts) LIGO-I might get to detect gravitational waves from a short burst. With the new generation of observatories, planned to become opperational around the half of the next decade, the sensitivity is expected to improve by one order of magnitude. If, as it seems, short bursts are compact binary mergers and assuming that an efficient GRB detector is available simultaneously with LIGO-II, a coincident electromagnetic and gravitational wave detection is almost guaranteed.

[2] http://www.ligo.caltech.edu/

[3] wwwcascina.virgo.infn.it

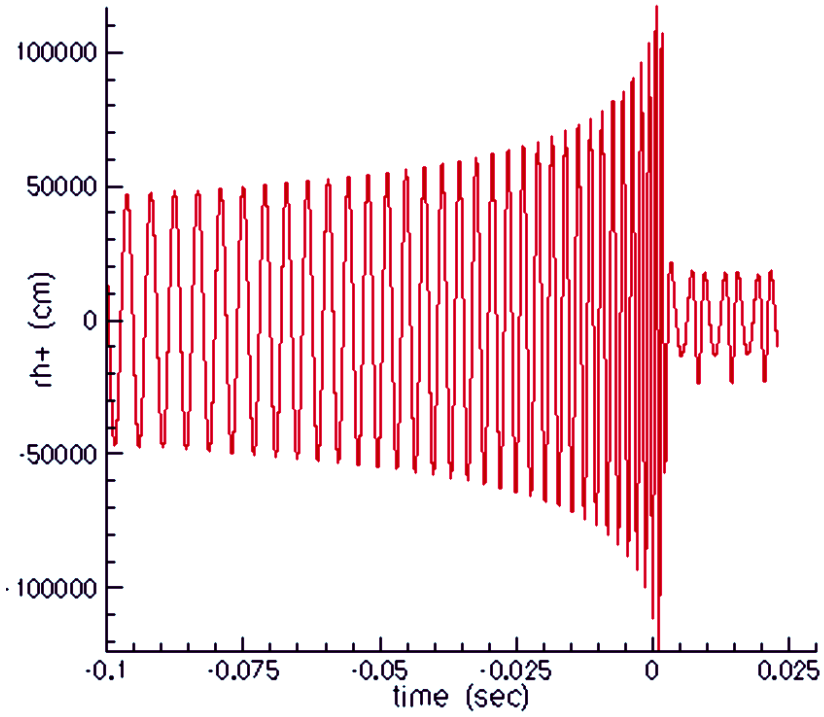

Figure 3.8: Shape of the expected gravitational waves from the final stages of a NS-BH merger (Lee 2000).

Bibliography

Bahcall, J. N., & Mészáros, P. 2000, Physical Review Letters, 85, 1362

Baltz, E. A., & Hui, L. 2005, ApJ, 618, 403

Band, D., et al. 1993, ApJ, 413, 281

Barthelmy, S. D., et al. 2005, Nature, 438, 994

Belczynski, K., Bulik, T., & Rudak, B. 2002, ApJ, 571, 394

Belczynski, K., Perna, R., Bulik, T., Kalogera, V., Ivanova, N., & Lamb, D. Q. 2006, ApJ, 648, 1110

Beloborodov, A. M. 2003, ApJ, 588, 931

Berger, E., et al. 2003, Nature, 426, 154

Berger, E., et al. 2005, Nature, 438, 988

Björnsson, G., Gudmundsson, E. H., & Jóhannesson, G. 2004, ApJ, 615, L77

Blandford, R. D., & McKee, C. F. 1976, Physics of Fluids, 19, 1130

Bloom, J. S., et al. 1999, Nature, 401, 453

Bloom, J. S., & Prochaska, J. X. 2006, Gamma-Ray Bursts in the Swift Era, 836, 473

Castro-Tirado, A. J., et al. 1999, Science, 283, 2069

Castro-Tirado, A. J., et al. 2005, A&A, 439, L15

Chevalier, R. A., & Li, Z.-Y. 2000, ApJ, 536, 195

Christensen, L., Hjorth, J., & Gorosabel, J. 2004, A&A, 425, 913

Ciardi, B., & Loeb, A. 2000, ApJ, 540, 687

Coppi, P. S., & Aharonian, F. A. 1997, ApJ, 487, L9

Cutler, C., & Thorne, K. S. 2002, ArXiv General Relativity and Quantum Cosmology e-prints, arXiv:gr-qc/0204090

Dado, S., Dar, A., & de Rujula, A. 2005, GRB Coordinates Network, 3424, 1

Dai, Z. G., & Lu, T. 1998, A&A, 333, L87

Dai, Z. G., & Lu, T. 2002, ApJ, 565, L87

Dai, Z. G., & Wu, X. F. 2003, ApJ, 591, L21

Dermer, C. D. 2004, ApJ, 614, 284
Eichler, D., Livio, M., Piran, T., & Schramm, D. N. 1989, Nature, 340, 126
Esin, A. A., & Blandford, R. 2000, ApJ, 534, L151
Fox, D. W., et al. 2003, Nature, 422, 284
Fox, D. B., et al. 2005, Nature, 437, 845
Frail, D. A., et al. 2001, ApJ, 562, L55
Fryer, C. L., & Kalogera, V. 2001, ApJ, 554, 548
Fruchter, A. S., et al. 2006, Nature, 441, 463
Galama, T. J., et al. 1998, Nature, 395, 670
Garnavich, P. M., Loeb, A., & Stanek, K. Z. 2000, ApJ, 544, L11
Gaudi, B. S., & Loeb, A. 2001, ApJ, 558, 643
Gaudi, B. S., Granot, J., & Loeb, A. 2001, ApJ, 561, 178
Gehrels, N., Piro, L., & Leonard, P. J. T. 2002, Scientific American, 287, 52
Ghirlanda, G., Magliocchetti, M., Ghisellini, G., & Guzzo, L. 2006, MNRAS, 368, L20
Granot, J., Piran, T., & Sari, R. 1999, ApJ, 513, 679
Granot, J., & Loeb, A. 2001, ApJ, 551, L63
Granot, J., Nakar, E., & Piran, T. 2003, Nature, 426, 138
Granot, J. 2005, ApJ, 631, 1022
Granot, J., & Kumar, P. 2006, MNRAS, 366, L13
Goodman, J. 1997, New Astronomy, 2, 449
Gou, L. J., Mészáros, P., Abel, T., & Zhang, B. 2004, ApJ, 604, 508
Hjorth, J., et al. 2003, Nature, 423, 847
Hjorth, J., et al. 2005, Nature, 437, 859
Hobbs, G., Lorimer, D. R., Lyne, A. G., & Kramer, M. 2005, MNRAS, 360, 974
Hurley, K., et al. 1994, Nature, 372, 652
Hurley, K., et al. 2005, Nature, 434, 1098
Ioka, K., & Nakamura, T. 2001, ApJ, 561, 703
de Jager, O. C., & Stecker, F. W. 2002, ApJ, 566, 738
Jin, Z. P., Yan, T., Fan, Y. Z., & Wei, D. M. 2007, ApJ, 656, L57
Jóhannesson, G., Björnsson, G., & Gudmundsson, E. H. 2006, ApJ, 647, 1238
Katz, J. I., Piran, T., & Sari, R. 1998, Physical Review Letters, 80, 1580
Königl, A. 2004, Gamma-Ray Bursts: 30 Years of Discovery, 727, 257
Koopmans, L. V. E., & Wambsganss, J. 2001, MNRAS, 325, 1317
Kulkarni, S. R., et al. 1999a, Nature, 398, 389

Kulkarni, S. R., et al. 1999b, ApJ, 522, L97

Kumar, P., & Panaitescu, A. 2000, ApJ, 541, L51

Kumar, P., & Piran, T. 2000, ApJ, 535, 152

Lamb, D. Q., & Reichart, D. E. 2000, ApJ, 536, 1

Lazzati, D., Rossi, E., Covino, S., Ghisellini, G., & Malesani, D. 2002, A&A, 396, L5

Lee, W. H. 2000, MNRAS, 318, 606

Lee, W. H., Ramirez-Ruiz, E., & Granot, J. 2005, ApJ, 630, L165

Le Floc'h, E., et al. 2003, A&A, 400, 499

Le Floc'h, E., Charmandaris, V., Forrest, B., Mirabel, F., Armus, L., & Devost, D. 2006, Gamma-Ray Bursts in the Swift Era, 836, 528

Li, Z.-Y., & Chevalier, R. A. 2001, ApJ, 551, 940

Liang, E. W., et al. 2006, ApJ, 646, 351

Loeb, A., & Perna, R. 1998, ApJ, 495, 597

Mao, S., & Loeb, A. 2001, ApJ, 547, L97

Meszaros, P., Rees, M. J., & Papathanassiou, H. 1994, ApJ, 432, 181

Meszaros, P., & Rees, M. J. 1997, ApJ, 476, 232

Meszaros, P., Rees, M. J., & Wijers, R. A. M. J. 1998, ApJ, 499, 301

Mészáros, P., & Gruzinov, A. 2000, ApJ, 543, L35

Meszaros, P. 2006, Reports of Progress in Physics, 69, 2259

Nakar, E., & Piran, T. 2003, ApJ, 598, 400

Nakar, E., Piran, T., & Granot, J. 2003, New Astronomy, 8, 495

Nakar, E., & Piran, T. 2004, MNRAS, 353, 647

Nakar, E., Gal-Yam, A., Piran, T., & Fox, D. B. 2006, ApJ, 640, 849

Nakar, E. 2007, ArXiv Astrophysics e-prints, arXiv:astro-ph/0701748

Narayan, R., Paczynski, B., & Piran, T. 1992, ApJ, 395, L83

Natarajan, P., Albanna, B., Hjorth, J., Ramirez-Ruiz, E., Tanvir, N., & Wijers, R. 2005, MNRAS, 364, L8

Nousek, J. A., et al. 2006, ApJ, 642, 389

Paczynski, B. 1986, ApJ, 308, L43

Paczynski, B., & Rhoads, J. E. 1993, ApJ, 418, L5

Paczynski, B., & Xu, G. 1994, ApJ, 427, 708

Paczynski, B. 1998, ApJ, 494, L45

Page, K. L., et al. 2006, ApJ, 637, L13

Palmer, D. M., et al. 2005, Nature, 434, 1107

Panaitescu, A., & Meszaros, P. 1998, ApJ, 493, L31

Panaitescu, A., & Kumar, P. 2000, ApJ, 543, 66

Panaitescu, A., & Kumar, P. 2001, ApJ, 560, L49

Peng, F., Königl, A., & Granot, J. 2005, ApJ, 626, 966

Piran, T. 1999, Phys. Rep., 314, 575

Ramirez-Ruiz, E., Dray, L. M., Madau, P., & Tout, C. A. 2001, MNRAS, 327, 829

Ramirez-Ruiz, E. 2004, MNRAS, 349, L38

Rees, M. J., & Meszaros, P. 1994, ApJ, 430, L93

Rees, M. J., & Meszaros, P. 1998, ApJ, 496, L1

Rees, M. J., & Mészáros, P. 2000, ApJ, 545, L73

Reichart, D. E. 2001, ApJ, 554, 643

Resmi, L., et al. 2005, A&A, 440, 477

Rhoads, J. E. 1997, ApJ, 487, L1

Rhoads, J. E. 1999, ApJ, 525, 737

Rossi, E. M., Beloborodov, A. M., & Rees, M. J. 2006, MNRAS, 369, 1797

Ruderman, M. 1975, New York Academy Sciences Annals, 262, 164

Sari, R., Piran, T., & Narayan, R. 1998, ApJ, 497, L17

Sari, R. 1998b, ApJ, 494, L49

Sari, R., Piran, T., & Halpern, J. P. 1999, ApJ, 519, L17

Sari, R., & Piran, T. 1999, ApJ, 520, 641

Sari, R., & Mészáros, P. 2000, ApJ, 535, L33

Savaglio, S., Glazebrook, K., & Le Borgne, D. 2006, Gamma-Ray Bursts in the Swift Era, 836, 540

Schmidt, W. K. H. 1978, Nature, 271, 525

Sedov, L. I. 1946, Prikl. Mat. i Mekh., 10, 241

Stanek, K. Z., et al. 2003, ApJ, 591, L17

Stanek, K. Z., et al. 2006, Acta Astronomica, 56, 333

Taylor, G. 1950, Royal Society of London Proceedings Series A, 201, 175

de Ugarte Postigo, A., et al. 2005, A&A, 443, 841

von Neumann, J. 1947, Los Alamos Sci. Lab. Tech. Series, 7

Wang, X., & Loeb, A. 2000, ApJ, 535, 788

Waxman, E. 1997, ApJ, 489, L33

Woosley, S. E. 1993, ApJ, 405, 273

Woosley, S. E., & Heger, A. 2006, ApJ, 637, 914

Wu, X. F., Dai, Z. G., Huang, Y. F., & Lu, T. 2005, MNRAS, 357, 1197

Yost, S. A., Harrison, F. A., Sari, R., & Frail, D. A. 2003, ApJ, 597, 459

Zhang, B., & Mészáros, P. 2002, ApJ, 566, 712

Zhang, B., Fan, Y. Z., Dyks, J., Kobayashi, S., Mészáros, P., Burrows, D. N., Nousek, J. A., & Gehrels, N. 2006, ApJ, 642, 354

Part II

Study of a representative sample of gamma-ray burst afterglows

4

GRB 021004 modelled by multiple energy injections

The work presented in this Chapter is based on:

de Ugarte Postigo, A., Castro-Tirado, A. J., Gorosabel, J., Jóhannesson, G., Björnsson, G., Gudmundsson, E. H., Bremer, M., Pak, S., Tanvir, N., Castro Cerón, J. M., Guzyi, S., Jelínek, M., Klose, S., Pérez-Ramírez, D., Aceituno, J., Campo Bagatín, A., Covino, S., Cardiel, N., Fathkullin, T., Henden, A. A., Huferath, S., Kurata, Y., Malesani, D., Mannucci, F., Ruiz-Lapuente, P., Sokolov, V., Thiele, U., Wisotzki, L., Antonelli, L. A., Bartolini, C., Boattini, A., Guarnieri, A., Piccioni, A., Pizzichini, G., del Principe, M., di Paola, A., Fugazza, D., Ghisellini, G., Hunt, L., Konstantinova, T., Masetti, N., Palazzi, E., Pian, E., Stefanon, M., Testa, V. & Tristram, P. J.
Astronomy & Astrophysics, 443, 841 (2005)

GRB 021004 is one of the best sampled gamma-ray bursts to date yet the nature of its light curve is still being debated. Here we present 107 optical, near-infrared (NIR) and millimetre observations, ranging from 2 hours to more than a year after the burst that we combine with the previously published data to produce a comprehensive dataset. Fitting the multiband data to a model based on multiple energy injections suggests that at least 7 refreshed shocks took place during the evolution of the afterglow, implying a total energy release (collimated within an angle of 1°.8) of $\sim 8 \times 10^{51}$ erg. Analysis of the late photometry reveals that the GRB 021004 host is a low extinction ($A_V \sim 0.1$) starburst galaxy with $M_B \simeq -22.0$.

4.1 Introduction

At 12:06:13.57 UT of the 4^{th} October 2002 a long-duration GRB triggered the FREGATE, WXM and SXC instruments aboard the *HETE-2* satellite (see Fig. 4.1). The detection was immediately transmitted to observatories around the globe that began observing a few

minutes after the burst. A fast identification of the optical afterglow 9.5 minutes after the burst (Fox 2002) allowed observations of the event from the first stages, producing one of the best multiwavelength coverage of a GRB obtained to date.

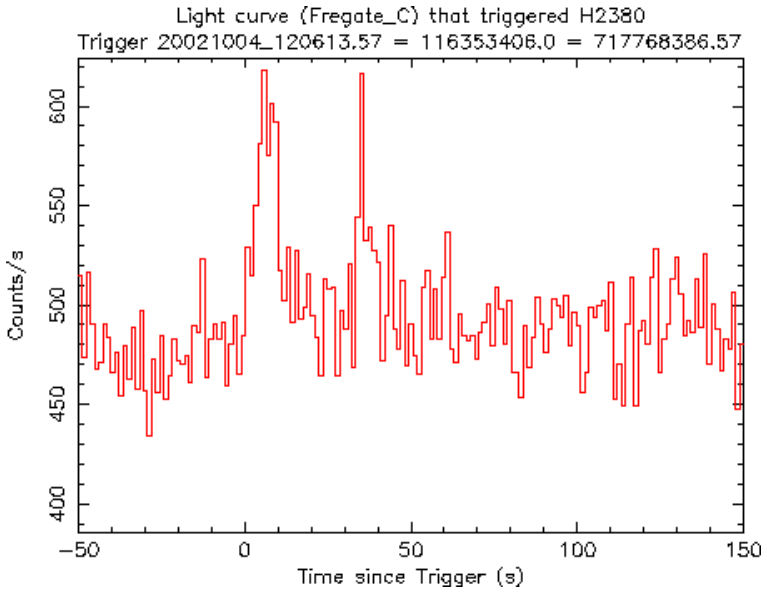

Figure 4.1: Gamma-ray light curve of GRB 021004 with a duration of ∼100 s, as recorded by FREGATE instrument aboard *HETE-2* satellite (Shirasaki et al. 2002).

Here we present a compilation of observations covering optical, NIR and millimetre wavelengths. We revisit the light curve of GRB 021004 using the new data together with what had been previously published. Our study covers almost the complete history of the event, from a few minutes after the trigger to more than a year later, when the afterglow light disappeared into the underlying galaxy. We pay special attention to the bumpy nature of the light curve which we explain by using the multiple energy injection model described by Björnsson et al. (2004) and Jóhannesson et al. (2006).

In Sect. 4.2 we present the observations and the methods that were used for the data reduction. Sect. 4.3 gives an introduction to the model we used for fitting the data. Sect. 4.4 presents a study of the extinction derived from the spectral flux distribution, the modeling of the afterglow and the properties of the host galaxy. Sect. 4.5 discusses the implications of the modelling proposed here. In Sect. 4.6 we present our conclusions.

Throughout, we assume a cosmology where $\Omega_\Lambda = 0.7$, $\Omega_M = 0.3$ and $H_0 = 72$ km s^{-1} Mpc^{-1}. Under these assumptions, and using a redshift of $z = 2.3293$ (Castro-Tirado et al. 2007) the luminosity distance of GRB 021004 is $d_l = 18.2$ Gpc and the look-back time is 10.4 Gyr (79.5 % of the present Universe age).

4.2 Observations and data reduction

4.2.1 Optical and nIR observations

For this data set we have made use of 11 telescopes, 9 in optical bands and 2 in nIR bands. The observations started 2 hours after the burst and extended to more than a year later. The images where reduced with standard procedures based on IRAF[1] and JIBARO (see Chapter 9).

Photometric calibration of the optical images is based on the secondary standards given by Henden (2002), while the NIR calibration was carried out observing NIR standards (Persson et al. 1998) at a similar airmass as the GRB field. The instrumental magnitudes obtained were based on aperture photometry running under DAOPHOT. Table 4.1 displays the magnitudes of the secondary standards shown in Fig. 4.2. The magnitude errors were calculated by adding in quadrature the zero point error (obtained from the dispersion of the secondary standards) and the afterglow statistical error given by DAOPHOT. Table 4.2 displays the complete optical/nIR list of observations performed by our collaboration on this event.

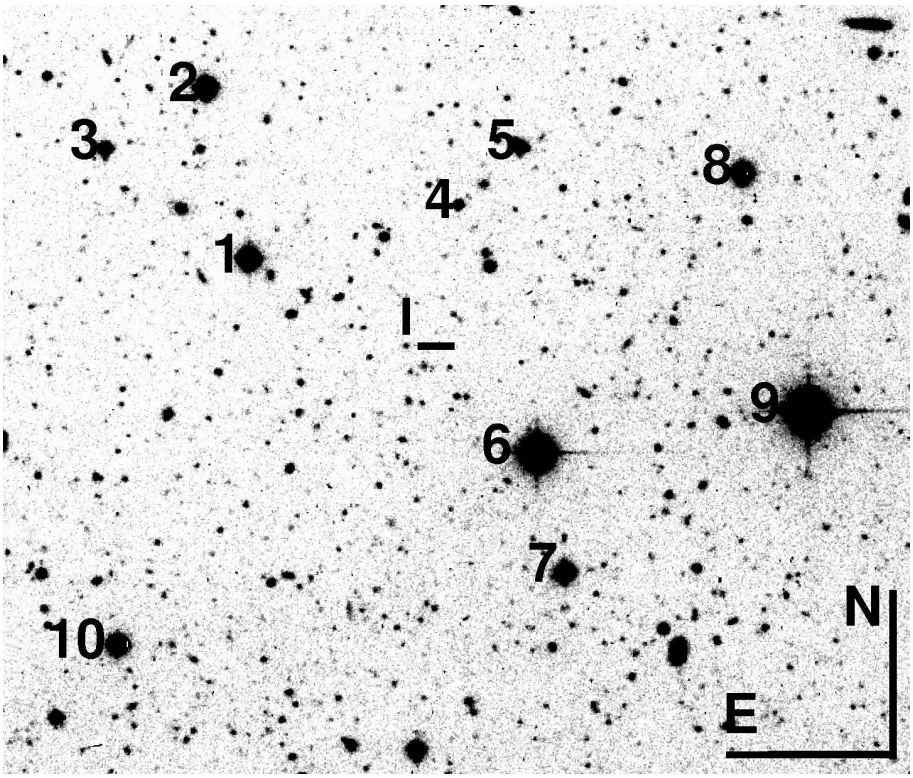

Figure 4.2: Reference stars in the surroundings of the GRB 021004 location (bracketed by tick marks). The depicted field of view is 4.3′ x 4.0′.

[1]IRAF is distributed by the National Optical Astronomy Observatories, which is operated by the Association of Universities for Research in Astronomy, Inc. (AURA) under cooperative agreement with the National Science Foundation.

Table 4.1: Calibration stars in the GRB 021004 field, marked in Fig. 4.2.

	U	B	V	R
1	17.37±0.03	17.34±0.03	16.70±0.01	16.33±0.01
2	18.54±0.04	17.43±0.03	16.26±0.01	15.54±0.02
3	20.70±0.04	19.48±0.02	17.90±0.02	17.06±0.02
4	—	21.12±0.11	19.74±0.04	18.78±0.06
5	—	19.76±0.03	18.29±0.02	17.36±0.03
6	16.49±0.05	15.51±0.03	14.44±0.05	13.88±0.06
7	18.10±0.02	18.09±0.01	17.49±0.01	17.14±0.01
8	17.83±0.16	17.61±0.02	16.71±0.01	16.20±0.02
9	14.71±0.09	14.62±0.08	13.97±0.05	13.62±0.08
10	17.62±0.06	17.84±0.03	17.32±0.01	17.00±0.01
	I	J	H	K
1	15.95±0.02	15.48±0.07	15.16±0.10	14.90±0.14
2	14.90±0.03	14.06±0.03	13.47±0.03	13.36±0.05
3	16.08±0.05	15.01±0.04	14.46±0.06	14.18±0.08
4	17.83±0.06	—	—	—
5	16.46±0.03	15.41±0.06	14.72±0.06	14.44±0.10
6	13.39±0.07	12.56±0.02	12.07±0.02	11.95±0.02
7	16.79±0.03	16.33±0.13	15.84±0.16	—
8	15.70±0.03	14.96±0.04	14.43±0.05	14.61±0.11
9	13.25±0.09	12.61±0.02	12.23±0.02	12.18±0.02
10	16.64±0.02	16.20±0.11	15.75±0.14	—

Table 4.2. Optical and nIR observations carried out for the GRB 021004 afterglow. The magnitudes are in the Vega system and not corrected for Galactic reddening.

Date UT	Telescope	Filter	Exp time (s)	Mag	Mag error
2002 Oct 4.9792	2.2CAHA	U	900	19.15	0.07
2002 Oct 5.0986	2.2CAHA	U	900	19.59	0.08
2002 Oct 5.1785	2.2CAHA	U	900	19.83	0.09
2002 Oct 5.9653	2.2CAHA	U	1,200	20.48	0.08
2002 Oct 6.9284	2.2CAHA	U	1,800	20.89	0.08
2002 Oct 7.9767	2.2CAHA	U	600	21.16	0.17
2002 Oct 9.2990	1.0USNO	U	5×1,800	21.70	0.14
2002 Oct 10.244	1.0USNO	U	1,800	21.73	0.25
2002 Oct 11.269	1.0USNO	U	4×1,800	21.76	0.17
2002 Oct 5.4890	1.0USNO	B	1,200	20.30	0.05
2002 Oct 5.9844	2.2CAHA	B	600	20.86	0.05
2002 Oct 6.0300	1.52Loiano	B	1,800	20.73	0.11
2002 Oct 6.9537	2.2CAHA	B	1,800	21.17	0.04
2002 Oct 6.9965	1.52Loiano	B	2×2,400	21.42	0.09
2002 Oct 7.9522	2.2CAHA	B	1,200	21.41	0.06
2002 Oct 9.3160	1.0USNO	B	5×900	21.74	0.06
2002 Oct 10.115	3.5TNG	B	2×300	22.12	0.05
2002 Oct 11.287	1.0USNO	B	4×1,200	22.20	0.11
2002 Oct 26.050	4.2WHT	B	7×300	24.28	0.13
2002 Nov 27.003	2.5INT	B	10×600	24.54	0.05
2002 Dec 5.762	6.0SAO	B	3,600	24.65	0.13
2002 Oct 4.5857	0.6MOA	Blue(V)	180	16.90	0.05
2002 Oct 4.5934	0.6MOA	Blue(V)	180	16.91	0.04
2002 Oct 4.6002	0.6MOA	Blue(V)	180	17.01	0.03
2002 Oct 4.9896	2.2CAHA	V	300	18.93	0.05
2002 Oct 5.1090	2.2CAHA	V	300	19.32	0.05
2002 Oct 5.1882	2.2CAHA	V	300	19.54	0.05
2002 Oct 5.4780	1.0USNO	V	600	19.71	0.04
2002 Oct 5.5232	0.6MOA	Blue(V)	2×600	19.77	0.09
2002 Oct 5.5330	0.6MOA	Blue(V)	600	19.76	0.13
2002 Oct 5.5593	0.6MOA	Blue(V)	2×600	19.71	0.07
2002 Oct 5.6060	0.6MOA	Blue(V)	3×600	19.74	0.07
2002 Oct 5.9920	2.2CAHA	V	300	19.74	0.07
2002 Oct 6.0110	1.52Loiano	V	1,200	20.18	0.06
2002 Oct 6.1240	1.52Loiano	V	900	20.15	0.31
2002 Oct 6.8650	1.52Loiano	V	1,800	20.52	0.13
2002 Oct 6.9410	1.52Loiano	V	2×1,800	20.75	0.08
2002 Oct 6.9595	2.2CAHA	V	600	20.55	0.05
2002 Oct 7.9668	2.2CAHA	V	600	20.85	0.06
2002 Oct 9.3250	1.0USNO	V	5×600	21.20	0.05

Table 4.2. continued.

Date UT	Telescope	Filter	Texp (s)	Mag	ErMag
2002 Oct 10.348	1.0USNO	V	5×600	21.60	0.08
2002 Oct 11.298	1.0USNO	V	4×600	21.75	0.10
2002 Nov 29.811	6.0SAO	V	2,250	24.43	0.17
2002 Dec 5.698	6.0SAO	V	3,600	24.13	0.09
2003 Sep 17.073	4.2WHT	V	5×900	24.45	0.04
2002 Oct 4.9965	2.2CAHA	Rc	300	18.55	0.03
2002 Oct 5.1146	2.2CAHA	Rc	300	18.96	0.02
2002 Oct 5.1938	2.2CAHA	Rc	300	19.12	0.03
2002 Oct 5.4700	1.0USNO	Rc	600	19.35	0.04
2002 Oct 5.5000	1.0USNO	Rc	600	19.31	0.04
2002 Oct 5.9790	1.52Loiano	Rc	1,200	19.67	0.06
2002 Oct 5.9976	2.2CAHA	Rc	300	19.73	0.03
2002 Oct 6.0500	1.52Loiano	Rc	1,200	19.87	0.06
2002 Oct 6.0620	3.5TNG	Rc	2×120	19.72	0.04
2002 Oct 6.8140	1.52Loiano	Rc	3×1,800	20.20	0.08
2002 Oct 6.9687	2.2CAHA	Rc	600	20.13	0.03
2002 Oct 7.9906	2.2CAHA	Rc	600	20.39	0.06
2002 Oct 9.3060	1.0USNO	Rc	4×600	20.87	0.06
2002 Oct 10.105	3.5TNG	Rc	2×180	21.05	0.05
2002 Oct 10.356	1.0USNO	Rc	5×600	21.14	0.07
2002 Oct 11.305	1.0USNO	Rc	4×600	21.35	0.10
2002 Nov 29.693	6.0SAO	Rc	2,700	24.29	0.18
2002 Oct 4.5823	0.6MOA	Red(Ic)	180	16.19	0.08
2002 Oct 4.5900	0.6MOA	Red(Ic)	180	16.09	0.08
2002 Oct 4.5968	0.6MOA	Red(Ic)	180	16.13	0.12
2002 Oct 5.0035	2.2CAHA	Ic	600	18.09	0.08
2002 Oct 5.1215	2.2CAHA	Ic	600	18.45	0.08
2002 Oct 5.2017	2.2CAHA	Ic	600	18.62	0.08
2002 Oct 5.2750	1.55USNO	Ic	900	18.68	0.02
2002 Oct 5.3970	1.55USNO	Ic	900	18.71	0.01
2002 Oct 5.4620	1.0USNO	Ic	600	18.79	0.06
2002 Oct 5.5149	0.6MOA	Red(Ic)	2×600	18.90	0.13
2002 Oct 5.5247	0.6MOA	Red(Ic)	600	18.85	0.17
2002 Oct 5.5510	0.6MOA	Red(Ic)	2×600	18.61	0.11
2002 Oct 5.6067	0.6MOA	Red(Ic)	3×600	18.98	0.13
2002 Oct 5.9940	1.52Loiano	Ic	900	19.32	0.08
2002 Oct 6.0069	2.2CAHA	Ic	900	19.24	0.08
2002 Oct 6.0580	3.5TNG	Ic	2×120	19.22	0.04
2002 Oct 6.9120	1.52Loiano	Ic	1,200	19.70	0.10
2002 Oct 6.9811	2.2CAHA	Ic	900	19.60	0.07
2002 Oct 8.3310	1.55USNO	Ic	2×900	20.09	0.02
2002 Oct 9.3120	1.0USNO	Ic	4×480	20.29	0.08

Table 4.2. continued.

Date UT	Telescope	Filter	Texp (s)	Mag	ErMag
2002 Oct 10.363	1.0USNO	Ic	5×600	20.78	0.13
2002 Oct 11.313	1.0USNO	Ic	4×600	21.05	0.13
2002 Dec 3.000	6.0SAO	Ic	2,640	23.77	0.19
2003 Dec 28.888	2.5NOT	Ic	14×300	23.82	0.17
2002 Oct 4.8847	1.5Tirgo	J	1,680	16.74	0.10
2002 Oct 5.1167	1.5Tirgo	J	1,920	17.90	0.23
2002 Oct 5.8514	1.5Tirgo	J	1,680	18.06	0.39
2004 Jan 5.805	3.5CAHA	J	7,260	23.15	0.38
2004 Jan 7.2775	3.5CAHA	H	6,120	> 21.5	—
2002 Oct 4.8622	1.5Tirgo	Ks	1,740	15.30	0.14
2002 Oct 5.0882	1.5Tirgo	Ks	2,040	15.95	0.17
2002 Oct 5.8743	1.5Tirgo	Ks	1,920	16.12	0.24
2002 Oct 6.0014	1.5Tirgo	Ks	3,480	16.71	0.21

4.2.2 Millimetre observations

The dataset is completed with observations obtained in 230 GHz and 90 GHz bands (see Table 4.3) at the 6-antenna Plateau de Bure Interferometer (PdB, Guilloteau et al. 1992). Data calibration was done with CLIC and the UV plane fitting and analysis with MAPPING, which are part of the GILDAS software package[2]. MWC349 was used as primary flux calibrator and 0109+224 as phase calibrator.

Table 4.3: Millimetre observations of the GRB 021004 afterglow at PdB.

Date 2002 (UT)	Frequency (GHz)	Flux density (mJy)	Flux density error (mJy)
Oct 5.9844	86.293	2.47	0.29
Oct 5.9844	231.700	2.15	1.22
Oct 6.1458	115.261	1.62	1.44
Oct 6.1458	231.700	0.22	3.65
Oct 7.1438	87.717	2.57	0.56
Oct 7.1438	232.034	3.26	1.54
Oct 10.981	86.235	1.67	0.34
Oct 10.981	208.475	4.71	1.96
Oct 19.919	92.016	0.97	0.25
Oct 19.919	231.972	1.60	1.00
Nov 5.9813	97.991	0.15	0.27
Nov 5.9813	239.551	-0.33	0.71

[2]GILDAS is the software package distributed by the IRAM Grenoble GILDAS group.

4.3 Brief description of the modelling

Our starting point is the standard fireball model (see e.g. Piran 2005). To account for the observed light curve rebrightenings, we modify the model by adding multiple energy injection episodes (see Björnsson et al. 2004 and in particular Jóhannesson et al. 2006 for a detailed discussion of the expressions and formulae that were used). We assume that the central engine releases, essentially simultaneously, several shells with different Lorentz factors. The evolution of the fireball is then derived, as in Rhoads (1999), from the conservation of energy and momentum. The fastest moving shell drives the initial evolution of the afterglow, but as it decelerates, the slower moving shells catch up with the shock front, producing an energy injection (see Fig. 4.3 for a schematic description of the process). Each shell collision is assumed to be instantaneous and the dynamics of the interaction is neglected, as well as any reverse shock contribution (these are expected to contribute mostly at early stages in the fireball evolution).

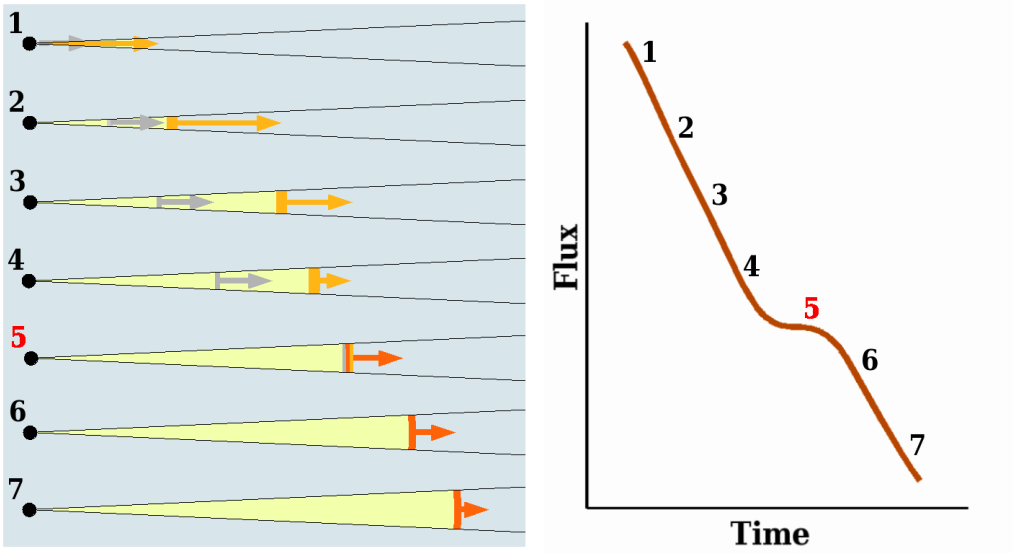

Figure 4.3: Energy injection: Two shells are released with different velocities (left). The fastest one (yellow) drives the initial afterglow (1). As it decelerates (2, 3, 4) it is caught by the slower one (gray) producing an energy injection (5) to the front shock and a bump in the light curve (right). The afterglow is then (6, 7) driven by the shell resulting from the collision (red).

As in the standard fireball model, the afterglow radiation is assumed to be of synchrotron origin and the local spectrum at each point in the radiating shell is approximated by smoothly joined power law segments (similar to Granot & Sari 2002). Assuming that the shell is homogeneous in the co-moving frame, its thickness is obtained from the shock conditions (Blandford & McKee 1976) and from the conservation of swept up particles. The total flux at a given frequency and observer time is then obtained by integrating over the equal arrival time surface (Granot et al. 1999 and references therein). The polarisation light curve and position angle can be calculated adapting the model of Ghisellini & Lazzati (1999) to the fireball model (see Björnsson et al. 2004 for details on how the modelling adapts to the polarisation measurements).

4.4 Results

4.4.1 Multiwavelength light curves

Fig. 4.4 shows the light curves in the visible, NIR and millimetre bands for GRB 021004. The optical/nIR data points are plotted together with other published data (Fox et al. 2003; Uemura et al. 2003; Pandey et al. 2003; Bersier et al. 2003; Holland et al. 2003; Mirabal et al. 2003; Pak et al. 2007) in order to show the complexity of the light curves.

4.4.2 The optical and nIR SFD

As a starting point all the optical/nIR magnitudes are corrected for foreground Galactic extinction ($E(B-V) = 0.06$; Schlegel et al. 1998). Then, we estimate the restframe extinction (A_V) and the favoured extinction law based on the afterglow optical/nIR spectral flux distribution (SFD) constructed for several epochs. The selected epochs are those for which a quasi-simultaneous wide optical/nIR coverage is available. The SFDs are clustered around 9 epochs displayed in Table 4.4. For each subset of photometric measurements we subtract the underlying host galaxy (see Sect. 4.4.4). This contribution is significant only after the first week. Finally, we fit each SFD by using a power law dimmed with different extinction laws (Pei 1992): Milky Way (MW), Large Magellanic Cloud (LMC) and Small Magellanic Cloud (SMC).

We obtain the best $\chi^2/d.o.f.$ (degrees of freedom) with the SMC extinction law (see Table 4.5), as has been previously observed for other GRB afterglows (Jensen et al. 2001; Fynbo et al. 2001; Holland et al. 2003). For each epoch the both spectral slope (β; the flux being $F_\nu \propto \nu^\beta$) and A_V are calculated. We can adopt the averaged SMC values for A_V and β since there is no evolution of the SFD on the considered time interval. The mean value inferred for the extinction and spectral index are, $\langle A_V \rangle = 0.20 \pm 0.08$, and $\langle \beta \rangle = -0.5 \pm 0.2$, respectively.

We note that the unextinguished SFD in the optical/nIR range might not be well represented by a perfect power law spectrum, showing some degree of intrinsic convex curvature (see the shape of the spectra in Fig. 4.6). Thus, the A_V values displayed in Table 4.4 have to be considered a formal upper limit, likely close to the real ones. The inferred $\langle A_V \rangle$ is used as the starting point for correcting the intrinsic extinction of the object when applying the model.

4.4.3 Afterglow model

A number of attempts have been made to explain the nature of the bumps seen in this GRB's light curve (Lazzati et al. 2002; Schaefer et al. 2003; Nakar et al. 2003; Heyl & Perna 2003).

In the present Chapter we show that the light curve can also be described by multiple energy injections, using the model of Björnsson et al. (2004). Our multiwavelength data is fitted along with other measurements reported in the literature, optical and nIR data cited in Sect. 4.2 together with X-ray data from Sako & Harrison (2002a; 2002b) and radio data from Berger et al. (2002) and Frail & Berger (2002). The model only reproduces the afterglow, hence the contribution of the host galaxy has been subtracted (see Sect. 4.4.4).

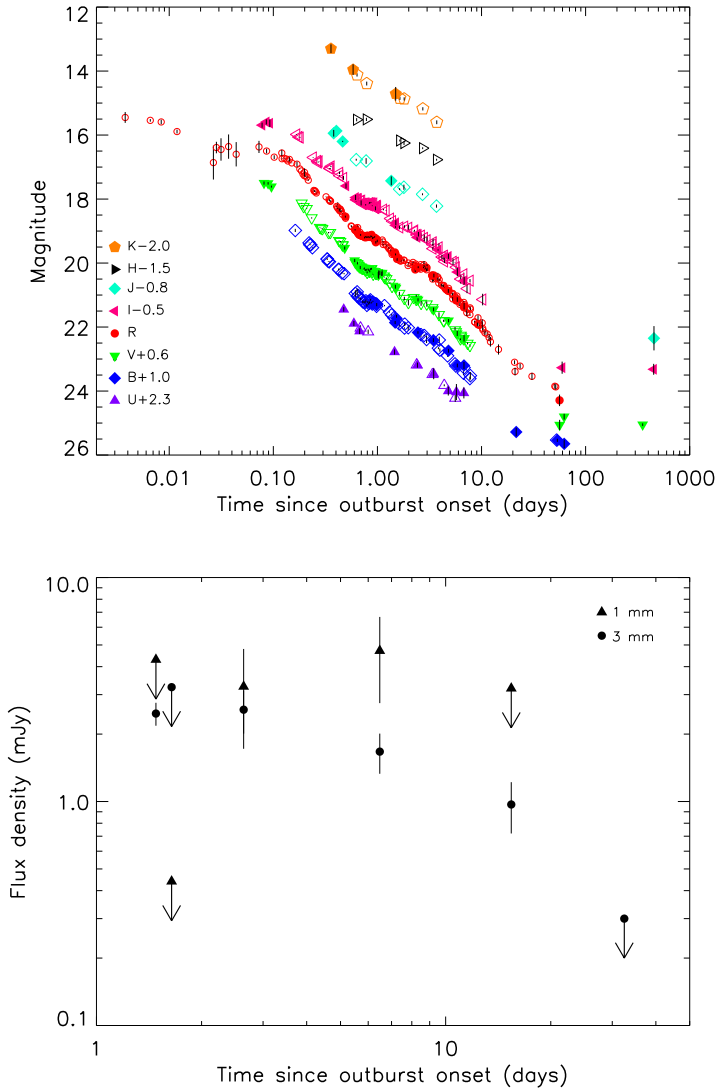

Figure 4.4: Top: Optical and NIR light curves of GRB 021004 for the first $\sim$ 500 days after the event. The different bands have been intentionally separated for clarity. Our observations are marked with filled symbols while published data are represented with void ones (see text for references). Bottom: Millimetre light curves for the first $\sim$ 35 days, obtained at PdB in the $\sim$ 90 GHz band. The arrows indicate the 2-σ limits.

This GRB is located at a redshift of z=2.3293 (Castro-Tirado et al. 2007) which shifts the Lyman break to the range of the U-band. Thus, we must consider a correction for the Lyman-α blanketing that appears at shorter wavelengths. We use the model described by Madau (1995) at this redshift and convolve it with the Johnson U-band. This yields a reduction of the measured flux to 82% of the original one. Due to the uncertainty of this approximation we do not use the corrected U-band for fitting the model, but only for the

Table 4.4: The GRB 021004 SFD at 9 epochs. An SMC extinction law has been assumed.

SFD #	Time since outburst onset (days)	β	A_V	$\chi^2/d.o.f.$
1	0.3609	-0.43±0.18	0.17±0.04	0.8
2	0.6380	-0.30±0.07	0.24±0.02	3.1
3	0.7851	-0.20±0.10	0.29±0.04	1.5
4	1.4216	-0.47±0.24	0.17±0.06	1.7
5	1.6304	-0.82±0.14	0.08±0.06	0.3
6	1.8090	-0.47±0.09	0.24±0.03	1.3
7	2.7018	-0.39±0.08	0.26±0.03	0.6
8	3.6520	-0.78±0.10	0.09±0.04	2.6
9	5.7388	-0.47±0.20	0.25±0.06	0.4

Table 4.5: Mean $\chi^2/d.o.f.$ obtained by fitting each extinction law on the 9 available SFDs.

Extinction Law	$\langle\chi^2/d.o.f.\rangle$
NE	11±7
MW	11±9
LMC	3.2±1.9
SMC	2.0±1.4

verification of it. The uncertainty of this approximation is due to the complexity of the spectra between 912 Å(Lyman break) and 1216 Å(Lyman-α) in the rest frame.

From the analysis of the SFD done in the optical/nIR range (Sect. 4.4.2), an SMC extinction law with of $A_V \lesssim 0.2$ is favoured. The multiband fitting has been tested using a grid of extinctions ranging from zero to $A_V = 0.4$ (within 2.5 sigma of the best fit value obtained from the optical/nIR SFD fitting). After several iterations we find that the best fit of the whole multirange data set is achieved with $A_V \sim 0.1$.

The parameters that result from the best fit of our model are displayed in Table 4.6. The fitted model is characterised by an initial shock followed by 7 subsequent refreshed shocks, the last injection being the most energetic. The number of injection episodes is higher than in Björnsson et al. (2004), as a result of a more complete dataset. Two injections are needed to account for late time radio data, and one (E_2) is added to better model an optical bump at ≈ 0.35 days. In addition, the electron energy index p is a free parameter here, but was fixed in Björnsson et al. (2004).

Fig. 4.5 shows all the observational data along with the light curves predicted by the model for each band. Fig. 4.6 shows the evolution of the afterglow multiband SFD at three epochs. As predicted by the model, we observe an evolution of the peak frequency (ν_m) from infrared to radio as the afterglow decays. We note the excellent U-band light curve prediction (not used for the fit) once the Lyman-α blanketing correction is a posteriori introduced.

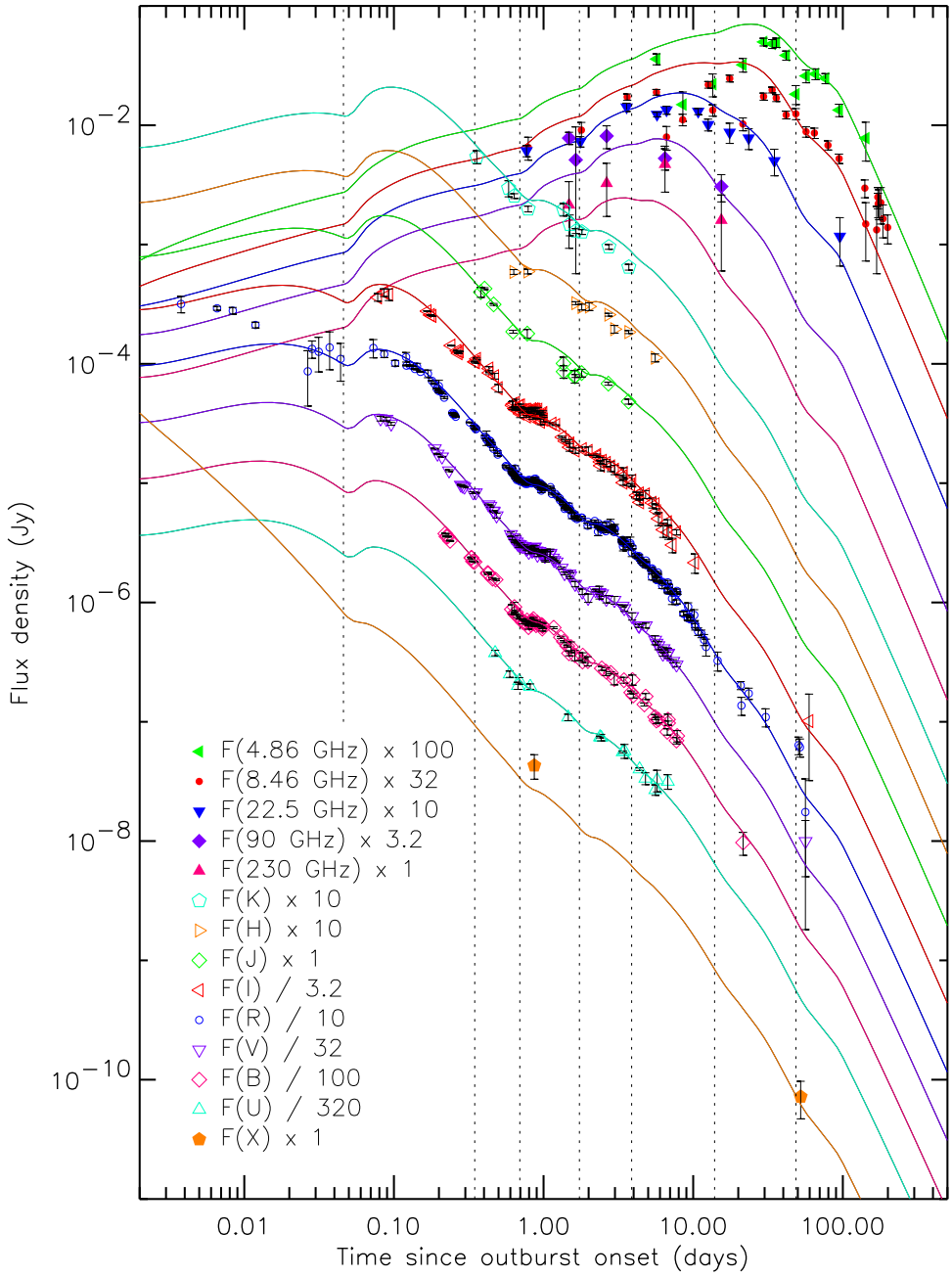

Figure 4.5: Multiband light curves from radio to X-rays (for the time interval 0.01 - 250 days after the burst onset) fitted with the multiple energy injection model. Seven energy injection episodes (see Table 4.6), indicated by vertical lines, can account for the observed behaviour. The visible and nIR observations are corrected for extinction and the U-band also for Lyman-α blanketing.

Table 4.6: The 7-injection episodes model parameters. The injection energies E_1 to E_7 are in units of E_0, the initial energy. Other model parameters are: the initial Lorentz factor Γ_0, the ambient density n_0, the initial half opening angle θ_0, the line of sight angle θ_ν, the electron energy index p, the fraction of internal energy stored in electrons after acceleration ϵ_e and the fraction of internal energy stored in the form of magnetic field ϵ_B.

Parameter	Value
E_0 (10^{50}erg)	1.5
E_1 (0.046 days)	2.2
E_2 (0.347 days)	0.7
E_3 (0.694 days)	4.6
E_4 (1.736 days)	10.0
E_5 (3.877 days)	8.6
E_6 (13.89 days)	10.0
E_7 (48.61 days)	15.0
Γ_0	770
$n_0(cm^{-3})$	60.0
θ_0	$1\overset{\circ}{.}8$
θ_ν	$0.8\theta_0$
p	2.2
ϵ_e	0.35
ϵ_B	1.7×10^{-4}

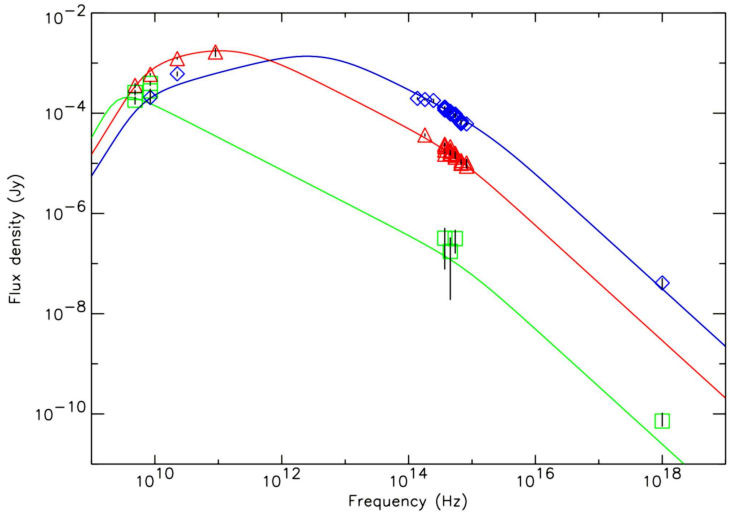

Figure 4.6: Evolution of the GRB 021004 afterglow SFDs at 0.8 (diamonds), 6 (triangles) and 60 days (squares) after the burst.

4.4.4 The host galaxy

In order to study the SFDs and constrain the model of the afterglow we need to isolate the flux produced by the afterglow from that of the underlying host galaxy. For the study of the host galaxy we use the $BVIJ$-band magnitudes measured when the contribution of the afterglow was negligible, between $\sim 62(B)$ and $\sim 454(J)$ days after the burst.

The fit of the host galaxy SFD is based on HyperZ (Bolzonella et al. 2000). The fitting assumes Solar metallicity, a Miller & Scalo (1979) initial mass function (IMF), and an SMC extinction law (Prévot et al. 1984). The best fit is obtained with a $\sim$ 15 Myr starburst galaxy with an absolute magnitude of $M_B = -22.0 \pm 0.3$ and an intrinsic extinction of $A_V = 0.06 \pm 0.08$ (see Fig. 4.7).

For the subtraction of the host galaxy colours in all the optical/NIR bands, it is necessary to predict its magnitudes in the $URHK$-bands, for which no photometric information is available. Convolving the spectra of the fitted galaxy with standard optical and infrared filters, a prediction of those magnitudes is possible (see Table 4.7), assuming the transformations given by Fukugita et al. (1995). The U-band must be corrected for Lyman-α blanketing as described in Sect. 4.4.3. In order to calculate the errors of the estimated magnitudes, a Monte Carlo method is used, in which the fitting of the galaxy is repeated with randomly modified input $BVIJ$ magnitudes (Gaussianly weighted) in the measured error range.

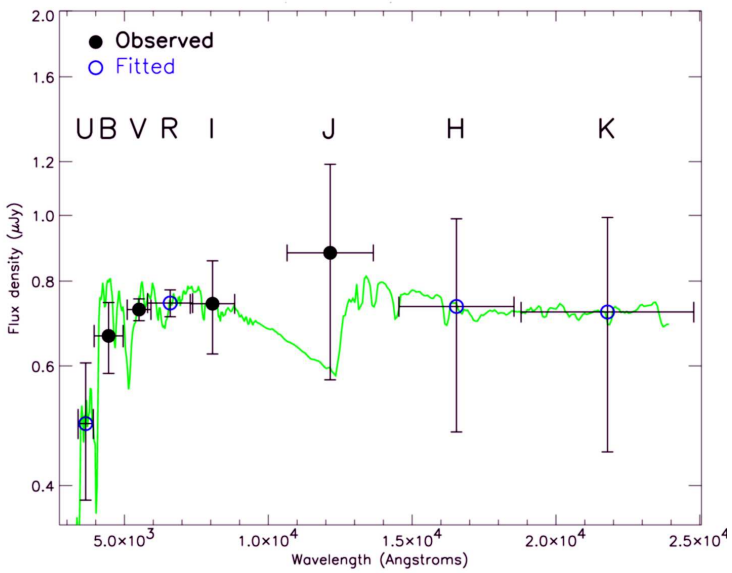

Figure 4.7: A fit to the photometric points of the GRB 021004 host galaxy yielding a starburst galaxy template. The H-band limit of 21.5 magnitude ($\sim$ 2.7μ Jy) is not plotted. The filled points are our observations while the open ones are obtained from the fit of the galaxy. The flux density is represented in logarithmic scale.

4.5 Discussion

We show that the multiwavelength observations can be satisfactorily reproduced in the context of the refreshed shock model. It is capable of reproducing the "bumpy" behaviour of the entire light curve of this event, not only the visible bands, but in a spectral range that spans from radio to X-rays. In addition, the variations in the polarisation of the afterglow are naturally explained in the framework of the energy injections (Björnsson et al. 2004).

Table 4.7: Magnitudes for the GRB 021004 host galaxy. The values marked with * are measured values, while the rest are predictions obtained from the fitted template. The magnitudes are given in the Vega system and are not corrected for Galactic reddening.

Band	Magnitude
U	24.49 ± 0.28
B	$24.65 \pm 0.13^\star$
V	$24.45 \pm 0.04^\star$
R	24.21 ± 0.05
I	$23.82 \pm 0.17^\star$
J	$23.15 \pm 0.38^\star$
H	22.92 ± 0.31
K	22.42 ± 0.37

* Measured values.

The number of required model parameters can be quite large, and depends on the structure of the light curve and modelling detail required.

The bumpy light curve behaviour may also be explained by the patchy shell model (Nakar et al. 2003), or by density variations in the surrounding medium (Lazzati et al. 2002), although in the latter case, simultaneously accounting for the polarisation measurements appears to be problematic. As in the refreshed shock model, the number of required parameters in these models also increases with the amount of structure in the light curve.

The afterglow model assumes an adiabatic expansion, so the proposed scenario might not be valid at very early times, when this assumption may not be accurate enough. Additionally, at early time, there can also be a strong contribution from the early reverse shock to the light curve. This might explain the excess of R-band flux observed during the first minutes that followed the burst. The very last points of our dataset for GRB 021004 may indicate a transition to a non-relativistic expansion regime. We have not included all of the relevant modifications required to capture such a transition in detail and our model results may therefore be inaccurate at very late times.

Although the X-ray observations are very limited (only two measurements), there seems to be an excess in the observed flux as compared to the model. This could be due to inverse Compton effect as seen in other GRBs (Harrison et al. 2001; in´t Zand et al. 2001; Castro-Tirado et al. 2003), an effect not considered in our modelling. The correction for the Lyman-α blanketing in the U-band that we introduced in Sect. 4.3 shifts the photometric points consistently with the prediction of the GRB model.

The inferred host galaxy extinction (A_V), dominant stellar age (~ 15 Myr) and galaxy type (starburst) are consistent with the findings reported by Fynbo et al. (2005) for GRB 021004. The age and the extinction are also consistent with the ones derived for GRB hosts in general, being similar to young starburst galaxies present in the *Hubble* Deep Field sample (Christensen et al. 2004). However, the B-band absolute magnitude of the host galaxy of GRB 021004 ($M_B \simeq -22.0$) is brighter than the 10 hosts present in the above mentioned sample.

4.6 Conclusions

Due to the early detection and rapid follow-up of GRB 021004 we have had the opportunity of obtaining a very complete dataset concerning temporal range, wavelength coverage and sample density. This has allowed us to introduce important constrains on the models capable to explain the bumps present in the afterglow light curve.

In our analysis we assume several energy injection episodes to explain the light curve. A reasonable scenario includes an initial burst followed by 7 refreshed shocks. These add up to a total burst energy of 7.8×10^{51} ergs, that were emitted through a collimated jet with an initial half-opening angle of $1\overset{\circ}{.}8$, pointing almost directly towards us.

A study of the photometric data of the host galaxy of GRB 021004 reveals a bright ($M_B = -22.0 \pm 0.3$) starburst galaxy with low extinction ($A_V = 0.06 \pm 0.08$).

Further tests of afterglow models with this multiwavelength dataset are encouraged. Future efforts should be aimed towards obtaining multiwavelength photometry and polarimetric observations of other events in order to be able to discriminate between the different models.

Bibliography

Berger, E., Frail, D. A., & Kulkarni, S. R. 2002, GCN Circ. 1613.

Bersier, D., Stanek, K. Z., Winn, J. N. et al. 2003, ApJ 584, L43.

Björnsson, G., Gudmundsson, E. H., & Jóhannesson, G. 2004, ApJ 615, L77.

Blandford, R. D. & McKee, C. F. 1976, PhFl 19, 1130.

Bolzonella, M., Miralles, J.-M., & Pelló, R. 2000, A&A 363, 476.

Castro-Tirado, A. J., Gorosabel, J., Guziy, S. et al. 2003, A&A 411, L315.

Castro-Tirado, A. J., Møller, P., García-Segura, G. et al. 2007, in preparation.

Christensen, L., Hjorth, J., & Gorosabel, J. 2004, A&A 425, 913.

Fox, D.W. 2002, GCN 1564.

Fox, D.W., Yost, S., Kulkarni, S.R. et al. 2003, Nature 422, 284.

Frail, D. A., & Berger, E. 2002, GCN Circ. 1574.

Fukugita, M., Shimasaku, K., & Ichikawa, T. 1995, PASP 107, 945.

Fynbo, J.P.U., Jensen, B.L., Dall, T.H. et al. 2001, A&A 373, 796.

Fynbo, J. P. U., et al. 2005, ApJ, 633, 317

Ghisellini, G. & Lazzati, D. 1999, MNRAS 309, L7.

Granot, J., Piran, T. & Sari, R. 1999, ApJ 513, 679.

Granot, J. & Sari, R. 2002, ApJ 568, 820.

Guilloteau S., Delannoy, J., Downes, D. et al. 1992, A&A 262, 624.

Jensen, B.L., Fynbo, J.P.U., Gorosabel, J. et al. 2001, A&A 370, 909.

Jóhannesson, G., Björnsson, G., & Gudmundsson, E. H. 2006, ApJ, 647, 1238

Harrison, F.A., Yost, S. A., Sari, R. et al. 2001, ApJ 559, 123.

Henden, A.A. 2002, GCN Circ. 1583.

Heyl, J. S. & Perna, R. 2003, ApJ 586, 13.

Holland, S.T., Weidinger, M., Fynbo, J.P.U. et al. 2003, AJ 125, 2291.

Lazzati, D., Rossi, E., Covino, S., Ghisellini, G. & Malesani, D. 2002, A&A 396, L5.

Madau, P. 1995, ApJ 441, 18.

Miller, G. E., & Scalo, J. M. 1979, ApJS, 41, 513.

Mirabal N., Halpern, J. P., Chornock, R. et al. 2003, ApJ 595, 935.

Nakar, E., Piran, T. & Granot, J. 2003, NewA 8, 495.

Pak, S. et al. 2007, A&A, in preparation.

Pandey, S. B., Sahu, D. K., Resmi, L. et al. 2003, BASI 31, 19.

Pei, Y.C. 1992, ApJ 395, 130.

Piran, T. 2005, Rev. Mod. Phys. 76, 1143

Persson, S.E., Murphy, D.C., Krzeminski, W. et al. 1998, AJ 116, 2475.

Prévot, M. L., Lequeux, J., Prévot, L., Maurice, E., & Rocca-Volmerange, B. 1984, A&A 132, 389.

Rhoads, J. E. 1999, ApJ 525, 737.

Sako, M., & Harrison, F. A. 2002a, GCN Circ. 1624.

Sako, M., & Harrison, F. A. 2002b, GCN Circ. 1716.

Schaefer, B.E., Gerardy, C.L., Höflich, P. et al. 2003, ApJ 588, 387.

Schlegel, D.J., Finkbeiner, D.P. & Davis, M. 1998, ApJ 500, 525.

Shirasaki, Y., et al. 2002, GRB Coordinates Network, 1565, 1

Uemura, M.,Kato, T., Ishioka, R. et al. 2003, PASJ 55, L31.

in´t Zand, J. J. M., Kuiper, L., Amati, L. et al. 2001, ApJ 559, 710.

5

Extensive multiband study of the X-ray rich GRB 050408. A likely off-axis event with an intense energy injection

The work presented in this Chapter is based on:

de Ugarte Postigo, A., Fatkhullin, T.A., Jóhannesson, G., Gorosabel, J., Sokolov, V.V., Castro-Tirado, A.J., Balega, Yu.Yu., Spiridonova, O.I., Jelínek, M., Guziy, S., Pérez-Ramírez, D., Hjorth, J., Laursen, P., Bersier, D., Pandey, S.B., Bremer, M., Monfardini, A., Huang, K.Y., Urata, Y, Ip, W.H., Tamagawa, T., Kinoshita, D., Mizuno, T., Arai, Y., Yamagishi, H., Soyano, T., Usui, F., Tashiro, M., Abe, K., Onda, K., Aslan, Z., Khamitov, I. & Ozisik, T.
Astronomy & Astrophysics, 462, L57 (2007)

GRB 050408 was detected by *HETE-2* and identified as an X-ray rich (XRR) burst, the intermediate class between the hard spectrum gamma-ray bursts (GRB) and the softer X-ray flashes (XRF). Here we present a comprehensive multiband optical light curve, covering the time from the onset of the gamma-ray event to several months after, when we only detect the host galaxy. Together with X-ray, millimetre and radio observations we compile what, to our knowledge, is the most complete multiband coverage of an XRR burst afterglow to date.

The optical and X-ray light curve is characterised by an early flattening and an intense bump peaking around 6 days after the burst onset. We explain the former through an off-axis viewed jet, in agreement with the predictions made for XRR by some models, and the latter with an energy injection equivalent in intensity to the initial shock. The analysis of the spectral flux distribution reveals an extinction compatible with a low chemical enrichment surrounding the burst. Together with the detection of an underlying starburst host galaxy,

typical of long GRBs, these observations strengthen the link between XRR and classical long-duration bursts.

5.1 Introduction

XRFs where first identified by *Beppo-SAX* (Heise et al. 2001) as those bursts detected by the X-ray camera but not the gamma-ray monitor. Later studies based on the larger sample gathered by *HETE-2* (Sakamoto et al. 2005b) gave a more general (and instrument-independent) classification and confirmed the intermediate group of events, the XRR class, previously detected by *Ginga* (Yoshida & Murakami 1994) and *Granat*/WATCH (Castro-Tirado et al. 1994). It is now known that long-duration GRBs (LGRBs), XRR bursts and XRFs share the same isotropic distribution in the sky, the same duration range and similar spectrum, with the main difference of having respectively lower observed spectral peak energy E^{obs}_{peak} in the νF_ν spectrum. They seem to form a continuum and thereby, most of the proposed models have tried to explain them as a unified phenomena (see a summary of the different models in Granot et al. 2005).

GRB 050408 was detected by WXM, SXC, and FREGATE aboard *HETE-2* (Sakamoto et al. 2005a) at 16:22:50.93 UT on the 8^{th} of April 2005 (t_0 hereafter). With an observed peak energy of ∼20 keV it was classified as an XRR event (see Fig. 5.1). The 1.0m Zeiss and 6.0m BTA telescopes at the Special Astrophysical Observatory (SAO) in Russia pointed at the position delivered by *HETE-2* through the GCN (GRB Circular Network) and detected the optical afterglow (de Ugarte Postigo et al. 2005a) coincident with the position of the X-ray afterglow detected by *Swift*/XRT (Wells et al. 2005). Spectroscopic observations from 6.5m Magellan/Clay and 8m Gemini telescopes determined a redshift of z=1.236 (Berger et al. 2005; Prochaska et al. 2005).

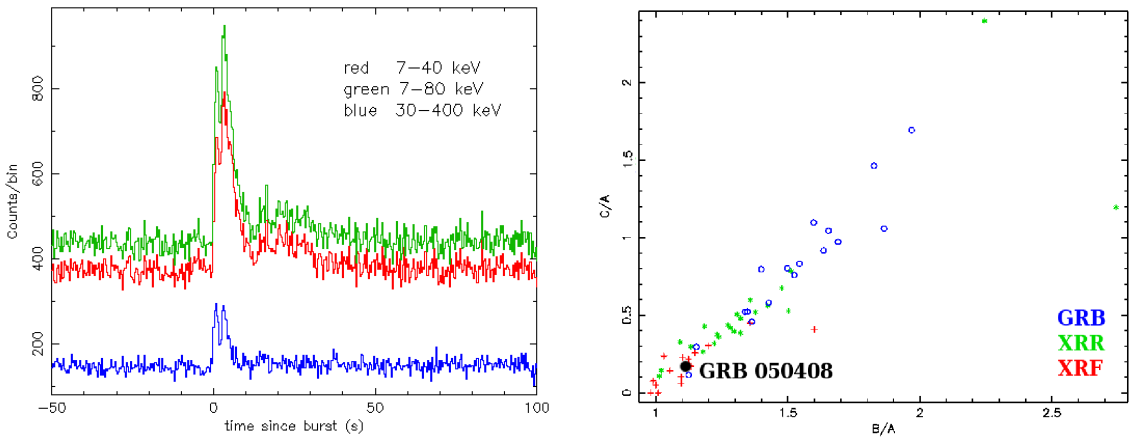

Figure 5.1: Left: Gamma-ray light curve of GRB 050408 in three different bands with a duration (T_90) of 14.6 seconds. Being an XRR burst, most of the counts are detected in the softest bands. Right: A colour-colour diagram showing the ratio of total counts in FREGATE band C (30-400 keV) to band A (7-40 keV) vs. band B (7-80 keV) to band A. All the *HETE-2* bursts are overlaid, showing a clear separation between GRBs, XRFs and XRR bursts. Both graphs have been adapted from http://space.mit.edu/HETE/Bursts/GRB050408/.

In Sect. 5.2 we present the observations and reduction methods that have been used for the analysis of the data. Sect. 5.3 describes the results that have been obtained, including observations of the host galaxy and modelling of the light curve. Sect. 5.4 discusses the implications of the analysis of the light curve. In Sect. 5.5 we present our conclusions.

5.2 Observations and data reduction

For this work we have compiled over 60 photometric measurements in *U, B, V, Rc* and *Ic* bands from 12 telescopes. The images where reduced using standard techniques based on IRAF and JIBARO (this Thesis, Chapter 9).

The burst happened during night time in Japan, where a fast follow up was carried out. The very wide field camera, WIDGET was monitoring the field of view of *HETE-2* when the event was reported but detected no optical emission before, during or after the gamma-ray emission down to an unfiltered limiting magnitude of 9.7 (all limits given throughout the Chapter are 3-σ). The 1.05m KISO Schmidt telescope pointed to the error box 20 minutes after the burst but failed to detect the afterglow. Finally, the 1m LOT telescope observed the field 55 minutes after the burst, images that later served to confirm the afterglow (Huang et al. 2005).

The discovery of the afterglow was made by our team with the data of the 1.0m Zeiss and 6.0m BTA telescopes in Russia (de Ugarte Postigo et al. 2005a), starting 115 minutes after the burst, when observations became possible from that site.

Further observations were performed from the 1.5m Russian-Turkish telescope, located in TÜBITAK National Observatory, the 4.0m Blanco telescope in Cerro Tololo, the 4.0m Mayall telescope in Kitt Peak, the 2.0m Faulkes Telescope North (FTN) in Haleakala and the 3.5m Telescopio Nazionale Galileo (TNG) in la Palma. A specially intense multiband campaign was carried out from the 1.54m Danish telescope in La Silla, where daily observations were obtained during the first 8 nights that followed the burst onset.

Finally, 8 months after the burst, deep observations were made from the 3.5m telescope at Calar Alto. In these images we detect the host galaxy of the burst in *B* and *Rc* bands and impose a limit in *Ic* band.

Optical photometric calibration is based on the observation of several standard fields (Landolt 1992) using the 1.54m Danish telescope at La Silla and the 1.5m telescope at Sierra Nevada Observatory. From these observations we derive 12 secondary standards of different brightnesses. Identification of these stars is shown on Fig. 5.2, while their photometric values are displayed on Table. 5.1. A log of the observations is given in Table 5.2.

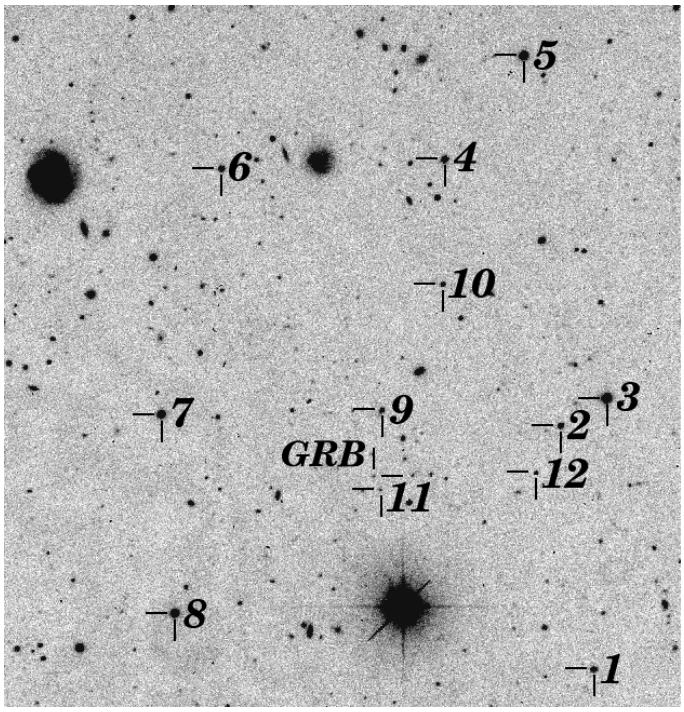

Figure 5.2: Identification chart of GRB 050408. The calibration stars and the afterglow location have been marked. The field of view is $6.0' \times 6.5'$, North is to the top and East to the left.

Table 5.1: Calibration stars in the field of GRB 050408, as marked in Fig. 5.2.

#	RA (J2000)	Dec (J2000)	U	B	V	R	I
1	12:02:09.16	+10:49:24.1	19.114±0.053	19.174±0.024	18.601±0.009	18.213±0.008	17.835±0.024
2	12:02:10.38	+10:51:37.3	18.982±0.053	19.241±0.024	18.776±0.009	18.438±0.008	18.062±0.025
3	12:02:08.70	+10:51:52.4	19.743±0.054	18.759±0.023	17.167±0.008	16.125±0.007	14.776±0.022
4	12:02:14.68	+10:54.02.8	18.200±0.051	18.508±0.023	18.028±0.008	17.671±0.007	17.292±0.023
5	12:02:11.76	+10:54:59.6	18.204±0.051	17.855±0.023	17.089±0.008	16.627±0.007	16.218±0.022
6	12:02:22.95	+10:53:57.8	18.896±0.051	19.098±0.023	18.638±0.009	18.300±0.008	17.980±0.024
7	12:02:25.20	+10:51:43.6	20.034±0.058	19.143±0.023	17.681±0.008	16.742±0.007	15.695±0.022
8	12:02:24.70	+10:49:54.7	17.237±0.051	17.406±0.023	17.020±0.008	16.652±0.007	16.324±0.022
9	12:02:17.02	+10:51:45.5	20.510±0.064	20.805±0.030	20.216±0.018	19.673±0.020	18.951±0.041
10	12:02:14.76	+10:52:54.6	—	21.885±0.058	20.528±0.019	19.617±0.014	18.631±0.028
11	12:02:17.10	+10:51:02.5	—	23.674±0.051	22.376±0.098	21.823±0.092	20.947±0.137
12	12:02:11.32	+10:51:11.3	21.129±0.089	21.249±0.034	20.810±0.023	20.507±0.029	20.025±0.066

Table 5.2. Optical observations carried out for GRB 050408, with t_0 at 16:22:50.93 UT on the 8^{th} of April 2005. The magnitudes are in the Vega system and are not corrected for Galactic reddening.

(t-t_0) (days)	Tel. + Inst.	Filter	Exp. time (s)	Mag.	Mag. error
0.4780	Dk1.54m+DFOSC	*U*	9,000	23.09	0.18
1.5939	4.0mKPNO	*U*	1,600	23.75	0.26
0.1297	6.0mBTA+SCORPIO	*B*	600	22.37	0.05
0.1385	6.0mBTA+SCORPIO	*B*	500	22.44	0.05
0.1467	6.0mBTA+SCORPIO	*B*	600	22.46	0.05
0.1554	6.0mBTA+SCORPIO	*B*	600	22.55	0.05
0.2301	6.0mBTA+SCORPIO	*B*	500	22.79	0.07
0.3712	Dk1.54m+DFOSC	*B*	1,200	23.05	0.10
0.5681	Dk1.54m+DFOSC	*B*	1,200	23.54	0.17
1.5001	Dk1.54m+DFOSC	*B*	9,000	24.26	0.10
242.5213	3.5mCAHA	*B*	1,800	25.32[1]	0.22
0.2245	6.0mBTA+SCORPIO	*V*	300	22.11	0.06
0.3599	Dk1.54m+DFOSC	*V*	600	22.24	0.09
1.6206	4.0mKPNO	*V*	1,200	23.98	0.22
2.4394	4.0mCTIO	*V*	1,500	24.10	0.17
0.0155	Kiso 1.05 Schmidt	*Rc*	300	>19.50	—
0.0388	1.0mLOT	*Rc*[2]	180	20.34	0.10
0.0859	1.0mZeiss	*Rc*	900	20.99	0.09
0.0919	1.0mLOT	*Rc*[2]	180	20.80	0.18
0.0956	1.0mLOT	*Rc*[2]	300	20.98	0.14
0.1029	6.0mBTA+SCORPIO	*Rc*	180	20.92	0.03
0.1068	6.0mBTA+SCORPIO	*Rc*	180	20.94	0.03
0.1104	6.0mBTA+SCORPIO	*Rc*	180	20.92	0.03
0.1139	6.0mBTA+SCORPIO	*Rc*	180	20.92	0.02
0.1172	6.0mBTA+SCORPIO	*Rc*	180	20.95	0.02
0.1207	6.0mBTA+SCORPIO	*Rc*	180	21.03	0.03
0.1240	6.0mBTA+SCORPIO	*Rc*	180	21.05	0.03
0.1471	RTT150+TFOSC	*Rc*	450	21.13	0.08
0.1629	RTT150+TFOSC	*Rc*	450	21.05	0.06
0.1771	RTT150+TFOSC	*Rc*	540	21.10	0.06
0.1863	RTT150+TFOSC	*Rc*	540	21.19	0.06
0.1984	RTT150+TFOSC	*Rc*	480	21.42	0.08
0.2080	RTT150+TFOSC	*Rc*	480	21.40	0.08
0.2175	RTT150+TFOSC	*Rc*	480	21.39	0.09
0.2204	6.0mBTA+SCORPIO	*Rc*	180	21.32	0.04
0.2296	RTT150+TFOSC	*Rc*	480	21.19	0.06
0.2380	RTT150+TFOSC	*Rc*	480	21.52	0.09

[1] Host galaxy magnitude

[2] *VR* broad band filter was transformed to *Rc*.

Table 5.2. Continued.

(t-t_0) (days)	Tel. + Inst.	Filter	Exp. time (s)	Mag.	Mag. error
0.2463	RTT150+TFOSC	*Rc*	480	21.56	0.08
0.2742	RTT150+TFOSC	*Rc*	720	21.52	0.06
0.2867	RTT150+TFOSC	*Rc*	720	21.58	0.06
0.3392	RTT150+TFOSC	*Rc*	600	21.80	0.12
0.3496	RTT150+TFOSC	*Rc*	600	21.50	0.09
0.3540	Dk1.54m+DFOSC	*Rc*	300	21.81	0.13
0.3600	RTT150+TFOSC	*Rc*	600	21.84	0.14
0.3705	RTT150+TFOSC	*Rc*	600	21.95	0.15
0.4362	Dk1.54m+DFOSC	*Rc*	600	21.91	0.08
0.5366	Dk1.54m+DFOSC	*Rc*	900	22.00	0.07
0.5963	Dk1.54m+DFOSC	*Rc*	1,200	22.02	0.08
0.7166	2.0mFTN	*Rc*	2,400	22.50	0.11
1.4024	Dk1.54m+DFOSC	*Rc*	5,700	23.08	0.09
1.5864	Dk1.54m+DFOSC	*Rc*	3,600	23.31	0.14
2.4911	Dk1.54m+DFOSC	*Rc*	14,700	23.86	0.17
3.4506	Dk1.54m+DFOSC	*Rc*	14,000	23.85	0.13
5.1575	RTT150+ANDOR CCD	*Rc*	9,000	23.70	0.20
5.5124	Dk1.54m+DFOSC	*Rc*	7,200	23.72	0.18
7.4663	Dk1.54m+DFOSC	*Rc*	15,600	23.97	0.11
30.2567	3.5mTNG	*Rc*	3,600	24.64	0.17
242.4885	3.5mCAHA	*Rc*	2,500	24.60[1]	0.15
0.3871	Dk1.54m+DFOSC	*Ic*	1,200	21.25	0.07
0.6137	Dk1.54m+DFOSC	*Ic*	1,500	22.52	0.11
6.4766	Dk1.54m+DFOSC	*Ic*	13,800	23.50	0.18
242.5446	3.5mCAHA	*Ic*	1,500	>24.0	—
-0.00340	WIDGET	Unfiltered	95	>9.7	—
-0.00224	WIDGET	Unfiltered	95	>9.7	—
-0.00108	WIDGET	Unfiltered	95	>9.7	—
0.00007	WIDGET	Unfiltered	95	>9.8	—
0.00123	WIDGET	Unfiltered	95	>9.7	—

Our dataset is completed with several millimetre and radio limits. 6 epochs of millimetre observations were carried out with the 6-antenna Plateau de Bure interferometer (PdB, Guilloteau et al. 1992). No detection was obtained in either of the 1 mm or 3 mm bands, although a 3-σ signal was found on the phase centre in both observing bands on the 18^{th} April. Careful re-analysis of the data did not reveal these signals as instrumental artifacts. Based on the extreme spectral slope and the non-detection on the 19^{th} April, we conclude that this result is either due to a statistical fluctuation or an unusual event of interstellar scattering at high galactic latitude, and not due to a source-intrinsic variation. Data calibration was done with the GILDAS software package using MWC349 as primary flux calibrator and 3C273 as amplitude and phase calibrator. Further observations were obtained 13 days after the burst at 1.28 GHz from GMRT and at 8.4 GHz from RATAN-600.

The result of the observations is displayed on Table 5.3 and Table 5.4 respectively.

Table 5.3: Observations in millimetre wavelengths from the Plateau du Bure interferometer (compact 6-antenna configuration on all dates). The errors are based on point-source fits in the UV plane to the phase centre.

(t-t_0) (days)	Band (GHz)	Flux density (mJy)	3-σ limit (mJy)
3.23	86.789	0.0±0.3	0.9
3.23	229.068	1.0±1.6	4.8
5.19	115.477	0.5±0.8	2.5
5.19	232.295	3.3±1.8	5.4
10.34	86.251	0.9±0.3	0.9[a]
10.34	232.171	8.4±2.3	6.9[a]
11.19	108.995	-1.7±1.7	5.2
11.19	228.534	-9.9±6.5	19.5
12.40	108.995	-0.9±0.7	2.2
12.40	228.534	3.6±2.7	8.2
14.29	111.619	-0.8±0.4	1.3
14.29	224.680	1.4±2.1	6.3

[a]The faint detections found on this epoch are considered to be due to a statistical fluctuation or to an unusual event of interstellar scattering at high Galactic latitude, taking into account the non detection the next night and the extreme spectral slope

Table 5.4: Observations in radio wavelengths from the Giant Metrewave Radio Telescope (GMRT) and Radio Astronomical Telescope Academy Nauk (RATAN-600). Only limits to the flux density are reported.

(t-t_0) (days)	Telescope	Band (GHz)	3-σ limit (mJy)
13.0	GMRT	1.28	0.45
13.0	RATAN-600	8.4	5.0

5.3 Results

5.3.1 Light curve

In order to put together all the radio, millimetre, near infrared (nIR), optical and X-ray data available (including data from Foley et al. 2006, Soderberg 2005a and Soderberg 2005b), we have determined the corresponding flux density values for all observations. X-ray afterglow counts, obtained from Foley et al. (2006) have been converted to flux density and corrected for hydrogen column extinction using WEBPIMMS[3]. The optical data has been corrected for galactic reddening (using an E(B-V)=0.026, Schlegel et al. 1998) and intrinsic extinction (see Sect. 5.3.2). The measured/estimated host galaxy flux has been subtracted from the data to obtain the clean afterglow flux (see Sect. 5.3.3). The conversion of the optical data to flux density was done using the transformations given by Fukugita et al. (1995) for the optical and by Allen et al. (2000) for the nIR. The resulting light curves are shown in Fig. 5.3. Note the intense bump, rising at ∼3 days and peaking at ∼6 days,

[3]http://heasarc.nasa.gov/Tools/w3pimms.html

both in optical and X-rays. These kind of fluctuations have already been detected in the light curves of LGRBs and short-duration bursts (SGRBs) (see Chapters 4 and 7 of this Thesis).

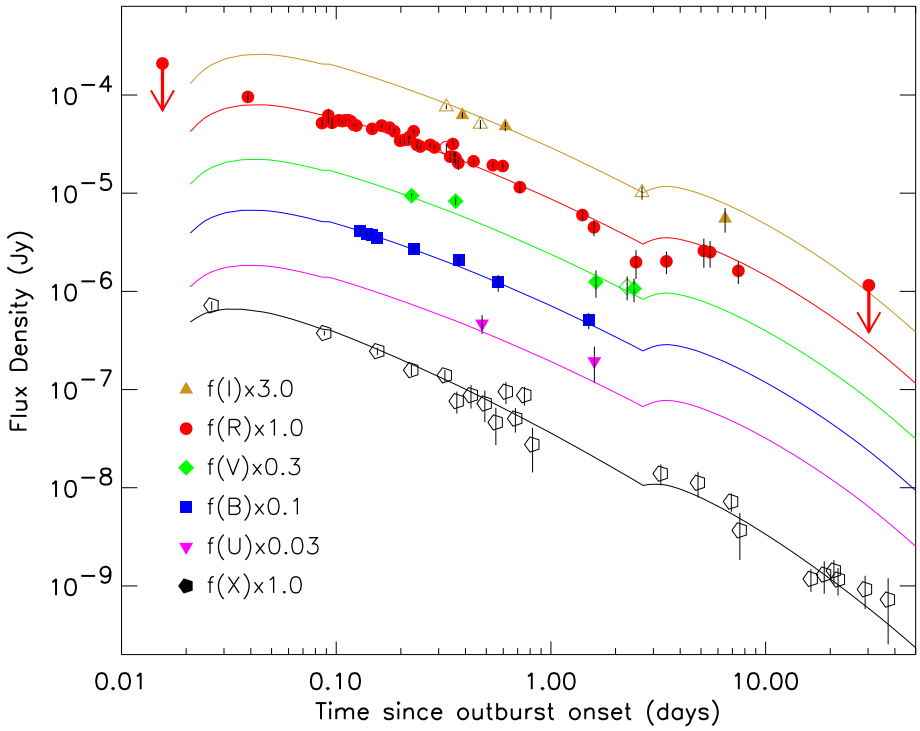

Figure 5.3: Multiwavelength light curve of the GRB 050408 afterglow. The lines show the best fit of a fireball model with one energy injection (at 2.9 days) seen off-axis (see text for details). Our observations are plotted with filled symbols, while the ones obtained from the literature are represented by empty ones. This convention is used for all the figures in this Chapter.

5.3.2 Study of the optical-nIR SFD

We have constructed the $UBVRcIcJHK$-band Spectral Flux distribution (SFD) of the afterglow 0.6 days after the burst, when near simultaneous optical and nIR observations were available. The $UBVRcIc$-band magnitudes from this work were complemented with the JHK-band values reported by Foley et al. (2006). Synchronisation to a unique timing is done by assuming a powerlaw with an index of α = -0.7 (F $\propto t^{\alpha}$), as derived from a fit of the nearby multiband data of the afterglow.

The fluxes are used for fitting an extincted powerlaw ($F_{\nu} \propto 10^{-0.4A_{\nu}}\nu^{\beta}$) with 3 different extinction laws: Milky Way (MW), Large Magellanic Cloud (LMC) and Small Magellanic Cloud (SMC) as described by Pei (1992). This allows us to obtain A_V and β simultaneously. The results of these 3 fits are complemented with an unextincted powerlaw case (NE), see Fig. 5.4 and Table 5.5. The best fit to the SFD of the afterglow is obtained when considering

a SMC extinction law ($\chi^2/d.o.f. = 1.0$). This is consistent with what has been previously found for other LGRB afterglows (Kann et al. 2006).

Table 5.5: Results of the SFD fitting at 0.6 days for different extinction laws.

Extinction Law	β	A_V	$\chi^2/d.o.f.$
MW	-1.85±0.30	-0.18±0.22	4.9
LMC	+0.12±0.48	1.19±0.32	2.3
SMC	-0.28±0.33	0.73±0.18	1.0
NE	-1.62±0.07	0	4.2

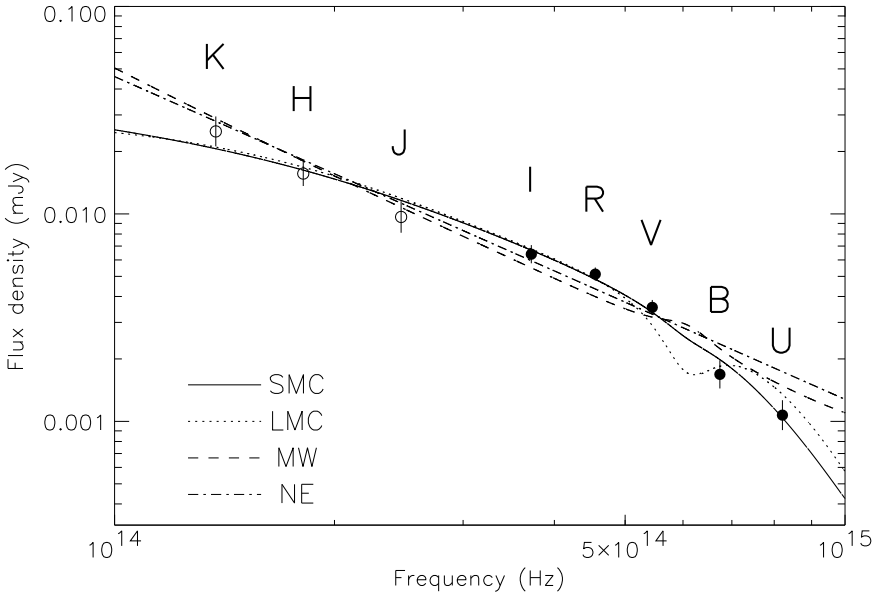

Figure 5.4: Spectral flux distribution of the afterglow 0.6 days after the burst onset. The different lines represent results from fitting the data to various extinction laws: Small Magellanic Cloud (SMC), Large Magellanic Cloud (LMC), Milky Way (MW) and No Extinction (NE).

5.3.3 The host galaxy

Several months after the gamma-ray event we revisited the GRB field with the 3.5m telescope at Calar Alto Observatory in order to search for the host galaxy. Images were obtained in B, Rc and Ic bands, yielding a faint detection in B and Rc and imposing a limit on Ic (see Fig. 5.5). We derive galaxy colour indexes of $(B-Rc) = 0.7\pm0.5$ and $(Rc-Ic) \leq 0.73$. These values are corrected for Galactic extinction. We have compared these values to the ones derived from the templates computed by Kinney et al. (1996) for a wide variety of galaxy types. We may conclude that only starburst galaxy templates are consistent with them. The best correlation is obtained with the so named "starburst 2" template, with an intrinsic extinction of E(B-V) = 0.16.

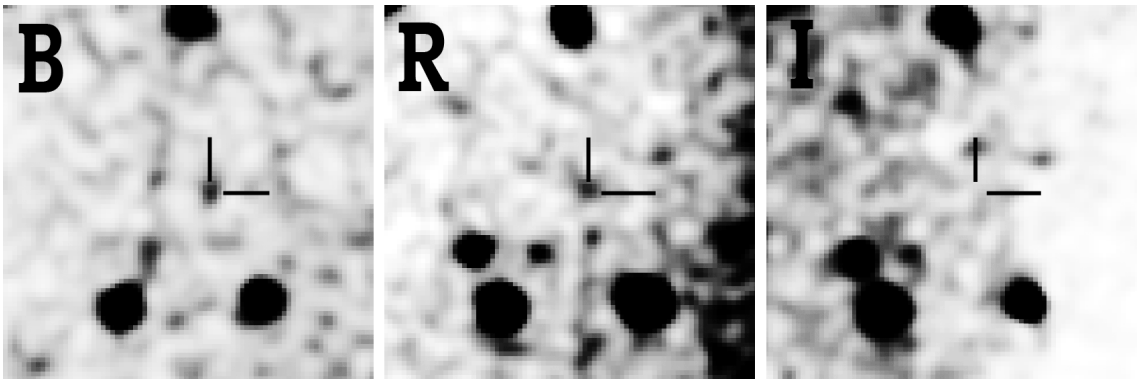

Figure 5.5: The host galaxy of GRB 050408 as imaged from the 3.5m telescope at Calar Alto observatory. There is detection in B and R bands and a limit in I band. The field of view is $25'' \times 25''$, with North to the top and East to the left.

5.3.4 Modelling of the multiband data

Using the model and methods described by Jóhannesson et al. (2006) we fitted the multiband observations of the afterglow (galaxy subtracted) to a fireball model with energy injections, viewed both on-axis and off-axis (with varying viewing angles). At least one injection is needed in order to account for the bump seen at 6 days which would carry as much energy as the initial shock. Another characteristic of the light curve is a flattening of the early light curve, seen in Rc and X-rays during the first hours of the burst, which has already been reported by Foley et al. (2006). This can be explained either by an early energy injection, an outflow with a low initial Lorentz factor, or as the result of an off-axis viewed burst.

Our preferred scenario (giving the best fit) describes the burst as a collimated ($\theta_0 = 2.7°$) fireball seen off axis ($\theta_v = 1.45\theta_0$) expanding into a uniform low density environment ($n_0 = 0.01$ cm^{-3}) with an electron index $p = 2.03$ and having an additional energy injection after 2.9 days with 1.2 times the initial energy. No further injections are needed to explain the light curve with the available amount of data. From the fit we obtain a $\chi^2/d.o.f. = 1.7$. Fig. 5.6 shows the radio to X-ray SFD predicted by our model for 3 epochs, together with observational data. The flux density that is being plotted as been corrected for extinction in our galaxy and in the host galaxy. The contribution of the host has been also removed, leaving only the afterglow.

5.4 Discussion

The optical-nIR SFD shows a clear curvature, implying a need for extinction along the afterglow line of sight in the host galaxy. The only reliable fit ($\chi^2/d.o.f. = 1.0$) is based on a SMC extinction law. This result points towards a low stage of chemical enrichment in the region of the progenitor, as is usually found for LGRBs (Kann et al. 2006). The detection of a starburst host galaxy is also a common feature with most LGRBs (Fruchter et al. 2006), facts that once again favour the hypothesis of shared nature between XRR bursts and LGRBs.

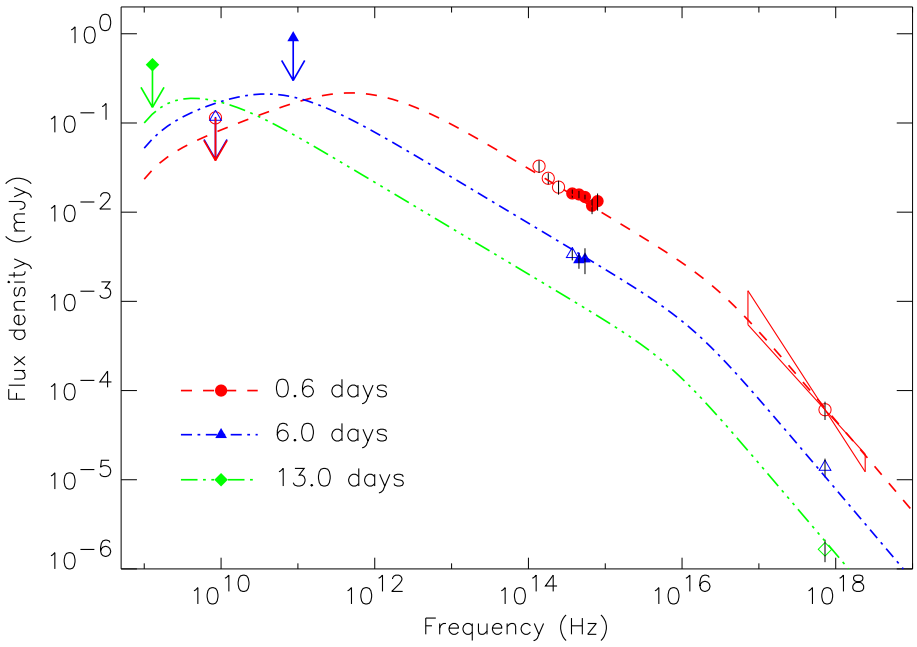

Figure 5.6: Spectral Flux Distribution of the afterglow from radio to X-rays 0.6, 6.0 and 13.0 days after the burst. Several 3-σ upper limits from radio and millimetre observations are plotted.

The optical spectral index obtained from this fit ($\beta_o = -0.28 \pm 0.33$) and the X-ray one ($\beta_X = -1.14 \pm 0.19$, Nousek et al. 2006) are consistent with a synchrotron spectra in which the cooling break frequency (ν_c) is located between optical and X-rays. A linear fit of the optical (Rc) and X-ray data between 0.1 and 1.0 days (where there is more data available and the light curve seems more stable) returns temporal slope values of $\alpha_o = -0.69 \pm 0.04$ and $\alpha_X = -0.99 \pm 0.21$. These numbers, together with the optical and X-ray spectral slopes, are consistent with a standard fireball model (Sari et al. 1999) in which a relativistic outflow is expanding in a uniform density environment in the slow cooling regime with an electron power law distribution index of $p \sim 2.0$.

A more complex multirange model, confirms these results and is used to account for the bump that has been found to peak at ~ 6 days by allowing for refreshed shocks. This fluctuation is simultaneously observed in optical and X-rays and can be explained by an energy injection of the order of the initial shock. This achromaticity and the simultaneity at both sides of ν_c rules out other explanations such as a density fluctuation, a dust echo or a supernova bump (which could also be ruled out by amplitude and peak time). Other explanations involving an additional energy release through a double jet (Berger et al. 2003) or a patchy shell (Meszaros et al. 1998) can not be discarded.

To explain the flattening seen in the earliest points of the light curve we have studied the case of a collimated fireball seen off-axis, as predicted by some unified models (Yamazaki et al. 2002) that simultaneously intend to explain LGRBs, XRR bursts and XRFs by only varying the viewing angle. Our fit accounts reasonably well for the multiband and long

scale behaviour of the light curve. However, the fits obtained with an on-axis model with an additional early injection or a low initial gamma factor (dirty fireball) can also interpret the data (although returning worse fits) and can not be ruled out (see Fig. 5.7).

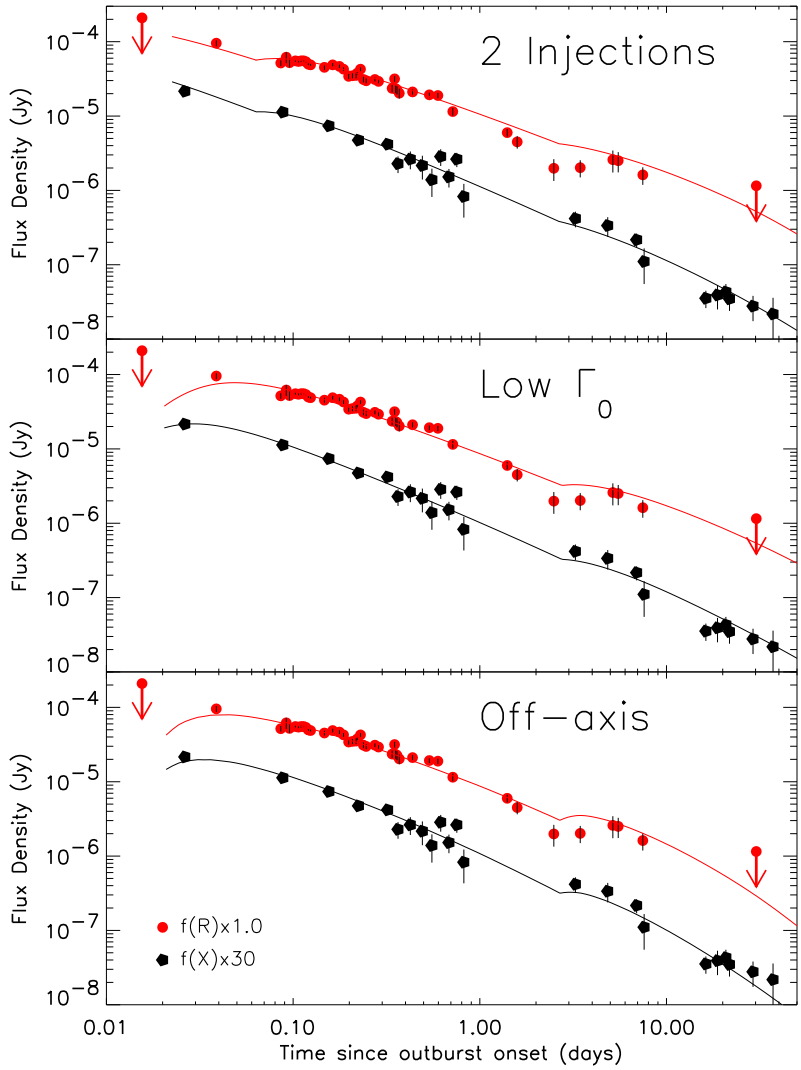

Figure 5.7: We tested several models on the data and, although the best fit was obtained with an off-axis viewed jet plus an energy injection (bottom), a low initial gamma factor plus an injection (centre) or a model with two injections (top) can also produce reasonable results.

Regarding the energetics of the afterglow we find that, with an observed peak energy of ∼20 keV and a fluence of $\sim\ 3.3 \times 10^{-6}$erg cm^{-2} (2-400 keV) it has an isotropic equivalent energy release in gamma-rays $E_{\gamma,iso} \gtrsim 1.3 \times 10^{52}$ erg, at least 6 times greater than the predicted by E_{peak}-E_{iso} relation (Amati 2006).

5.5 Conclusions

1. GRB 050408 is, to our knowledge, the first X-ray rich burst for which an extensive photometric follow up has been carried out in optical and X-rays. Additional data points in nIR and some limits in radio and millimetre wavelengths complete the dataset.

2. It is a bright burst for which $E_{\gamma,iso}$ is at least 6 times greater than predicted by the Amati relation for its E_{peak}.

3. A SFD study shows that the afterglow spectra can be modelled by a powerlaw with a slope of -0.28±0.33 and a SMC extinction of $A_V = 0.73 \pm 0.18$ favouring a low metallicity in the surroundings of the progenitor. Late time observations show an underlying starburst host galaxy. Both SMC extinction and a starburst host galaxy are typically found in LGRBs, favouring unification models.

4. We have performed a complete modelling of the afterglow in the context of a collimated fireball model. This model includes an energy injection of the order of the initial shock energy, explaining the achromatic bump peaking at $\sim$ 6 days. The flattening during the first hours of the burst, reported by Foley et al. (2006) is explained through the off-axis view of the jet. This is expected from some theories that unify the nature of LGRBs, XRFs and XRR bursts by only changing the viewing angle (Yamazaki et al. 2002).

We encourage polarimetric observations of XRR bursts and XRF events as they will be extremely useful to better understand the physics and geometry of the emission (i.e. Gorosabel et al. 2006) and to discriminate between energy models when explaining the fluctuations seen in the light curves.

Bibliography

Allen, C.W. 2000, Astrophysical Quantities (4th ed.; London: Athlone)

Amati, L. 2006, MNRAS, 372, 233

Berger, E., et al. 2003, Nature, 426, 154

Berger, E., Gladders, M., & Oemler, G. 2005, GRB Coordinates Network, 3201

Castro-Tirado, A. J., Brandt, S., Lund, N., Lapshov, I. Y., Terekhov, O., & Sunyaev, R. A. 1994, AIP Conf. Proc. 307: Gamma-Ray Bursts, 307, 17

Foley, R. J., et al. 2006, ApJ, 645, 450

Fruchter, A. S., et al. 2006, Nature, 441, 463

Fukugita, M., Shimasaku, K., & Ichikawa, T. 1995, PASP, 107, 945

Gorosabel, J., et al. 2006, ArXiv Astrophysics e-prints, arXiv:astro-ph/0609761

Guilloteau, S., et al. 1992, A&A, 262, 624

Granot, J., Ramirez-Ruiz, E., & Perna, R. 2005, ApJ, 630, 1003

Huang, K. Y., Ip, W. H., Kinoshita, D., Urata, Y., Tamagawa, T., Qiu, Y., & Lou, Y. Q. 2005, GRB Coordinates Network, 3196

Heise, J., in't Zand, J., Kippen, R. M., & Woods, P. M. 2001, Gamma-ray Bursts in the Afterglow Era, 16

Jóhannesson, G., Björnsson, G., & Gudmundsson, E. H. 2006, ApJ, 647, 1238

Kann, D. A., Klose, S., & Zeh, A. 2006, ApJ, 641, 993

Kinney, A.L., Calzetti, D., Bohlin, R.C. et al. 1996, ApJ, 467, 38

Landolt, A. U. 1992, AJ, 104, 340

Meszaros, P., Rees, M. J., & Wijers, R. A. M. J. 1998, ApJ, 499, 301

Nousek, J. A., et al. 2006, ApJ, 642, 389

Pei, Y.C., 1992, ApJ 395, 130

Prochaska, J. X., Bloom, J. S., Chen, H.-W., Foley, R. J., & Roth, K. 2005, GRB Coordinates Network, 3204

Sakamoto, T., et al. 2005a, GRB Coordinates Network, 3189

Sakamoto, T., et al. 2005b, ApJ, 629, 311

Sari, R., Piran, T., & Halpern, J. P. 1999, ApJ, 519, L17

Schlegel, D.J., Finkbeiner, D.P., & Davis, M., 1998, ApJ, 500, 525

Soderberg, A. M. 2005a, GRB Coordinates Network, 3210

Soderberg, A. M. 2005b, GRB Coordinates Network, 3234

de Ugarte Postigo, A., et al. 2005a, GRB Coordinates Network, 3192

Wells, A. A., et al. 2005, GRB Coordinates Network, 3191

Yamazaki, R., Ioka, K., & Nakamura, T. 2002, ApJ, 571, L31

Yoshida, A., & Murakami, T. 1994, AIP Conf. Proc. 307: Gamma-Ray Bursts, 307, 333

6

GRB 050509B: The elusive afterglow of a short burst

The work presented in this Chapter is based on:

Castro-Tirado, A. J., de Ugarte Postigo, A., Gorosabel, J., Fathkullin, T., Sokolov, V., Bremer, M., Márquez, I., Marín, A. J., Guziy, S., Jelínek, M., Kubánek, P., Hudec, R., Vitek, S., Mateo Sanguino, T. J., Eigenbrod, A., Pérez-Ramírez, M. D., Sota, A., Masegosa, J., Prada, F. & Moles, M.
Astronomy & Astrophysics, 439, L15 (2005)

We present multiwavelength (optical, near-infrared and millimetre) observations of GRB 050509B, the first short duration gamma-ray burst detected and precisely localised through X-rays by *Swift*. The data was collected between 0 seconds and $\sim$ 18.8 days after the event. However, no optical, near infrared or millimetre counterpart was detected in spite of the fast response and deep follow-up campaign, confirming the elusiveness of the short duration events. The distance scale at which the burst was produced is also discussed. We consider the possibility of happening in the outskirts of a bright elliptical galaxy which is part of a cluster at $z = 0.225$ or of being part of a much more distant population. In the former case, the spectral energy distribution of the neighbour, potential host galaxy, favours a system harbouring an evolved dominant stellar population (age $\sim$ 720 Myr), unlike most long duration GRB host galaxies observed so far, thus giving support to a compact binary merger origin. Any underlying supernova that could be associated with this particular event should have been at least 3 magnitudes fainter than the type Ib/c SN 1998bw and 2.3 magnitudes fainter than a typical type Ia SN.

6.1 Introduction

The detection of counterparts of gamma-ray bursts (GRBs) at wavelengths other than gamma for long duration GRBs, revealed their cosmological origin (see van Paradijs et al.

Table 6.1: Journal of optical and nIR observations of the GRB 050509B field.

Date of 2005 UT (mid exposure)	Telescope/Instrument	Filter	Exposure (s)	Seeing (arcsec)	Limiting Magnitude (3σ)
May 09, 04:00.25	BOOTES-1 (ASCCD)	*R*	30	3.0	6.0
May 09, 04:40	1.2Mer (MEROPE)	*R*	600	2.5	21.0
May 09, 23:40	1.2Mer (MEROPE)	*R*	600	1.3	22.1
May 11, 20:00	6.0BTA (SCORPIO)	*R*	7 020	2.0	26.0
May 18, 23:00	1.5OSN (CCD)	*I*	3 600	1.4	21.9
May 27, 22:57	2.2CAHA (BUSCA)	*R*	2 500	1.4	23.9
May 09, 21:21	3.5CAHA (OMEGA2000)	*H*	3 378	2.1	20.2
May 09, 23:22	3.5CAHA (OMEGA2000)	*K*	2 730	1.6	18.8
May 10, 00:05	3.5CAHA (OMEGA2000)	*J*	3 656	2.1	21.2
May 10, 02:29	3.5CAHA (OMEGA2000)	*H*	3 563	2.4	20.5
May 10, 21:50	3.5CAHA (OMEGA2000)	*J*	1 897	1.9	20.3
May 12, 21:55	3.5CAHA (OMEGA2000)	*H*	2 314	1.7	20.3
May 15, 22:29	3.5CAHA (OMEGA2000)	*J*	1 620	1.4	21.7
May 17, 23:00	3.5CAHA (OMEGA2000)	*J*	3 656	2.0	22.2

2000 for a review) and it is accepted nowadays that they are associated with the death of massive stars. On the other hand, the nature of short duration GRBs, a class that comprises about 25% of all events (Mazets et al. 1981; Kouveliotou et al. 1993), still remains a puzzle. At the time of GRB 050509B no counterparts had been discovered, in spite of intense follow-up campaigns in optical, infrared and radio wavelengths (Kehoe et al. 2001; Gorosabel et al. 2002; Hurley et al. 2002; Klotz et al. 2003). A possible optical transient, related to GRB 000313 was proposed by Castro-Tirado et al. (2002) but a firm conclusion could not be established.

The *Swift* satellite (Gehrels et al. 2004) offers unique capabilities for the detection of GRBs thanks to its high sensitivity and imaging capabilities at γ-rays, X-rays and optical wavelengths. The short GRB 050509B was discovered by *Swift*/BAT detector on 9 May 2005. The burst started at 04:00:19.23 UT and lasted for $\approx$ 40 ms, putting it in the "short-duration" class of GRBs (see Fig. 6.1). It had a fluence of $(0.95 \pm 0.25)\times10^{-8}$ erg cm^{-2} in the 15-150 keV range (Gehrels et al. 2005). The prompt dissemination (13.7 s) of the GRB position (Hurkett et al. 2005) enabled prompt responses of automated and robotic telescopes on ground, like ROTSE-III (Rykoff et al. 2005), RAPTOR (Wozniak et al. 2005) and BOOTES-1 (shown in this paper), although no prompt afterglow emission was detected. By the time when *Swift* slewed and started data acquisition (about 60 s after the event onset), a fading X-ray emission was detected by the *Swift*/XRT; this can be considered as the first clear detection of an afterglow in a short duration GRB (Kennea et al. 2005). This triggered a multiwavelength campaign at many observatories aimed at detecting the afterglow at other wavelengths, as in the case of the long duration GRB class. Here we report the results of the multiwavelength observations carried out by our group,

Table 6.2: Journal of mm observations of the GRB 050509B field.

Date of 2005 UT	Configuration	Detection level (mJy, 1σ)	Frequency (GHz)	Beam (arcsec)	Position angle (deg)
May 11, 02:56-03:38	6Dp	1.9	80.327	32.2 x 4.44	-136
		12.0	242.842	9.89 x 1.62	-137
May 11, 21:38-23:49	6Dp	0.8	80.467	9.56 x 4.51	+ 66
		5.9	242.842	3.24 x 1.73	+ 64
May 13, 00:26-02:44	6Dp	1.0	80.467	25.30 x 4.54	+ 48
		4.4	221.501	6.05 x 1.70	-128
May 16, 17:33-22:28	5Dp	0.3	92.682	6.55 x 5.44	+ 93

from millimetre (mm) wavelengths to the optical bands.

6.2 Observations and data reduction

The BOOTES-1 all-sky camera (see Chapter 8), located at Estación de Sondeos Atmosféricos (INTA-CEDEA) in Huelva (Spain), observed the region of the sky containing the *Swift*/BAT error box of GRB 050509B as part of its routine observing schedule (Castro-Tirado et al. 2004). A 30 s exposure started at 04:00:00 UT (19 s prior to the onset of the 40 ms short burst), with the following frame starting at 04:01:00 UT. A limiting (unfiltered, airmass 4.0) magnitude of 6.0 is derived for any prompt optical flash arising from this event.

Target of opportunity observations in the optical were triggered starting 32 minutes after the event at the 1.2 m Mercator telescope (+ MEROPE CCD camera) at Observatorio del Roque de los Muchachos in La Palma (Spain). Subsequently, target of opportunity observations were made at the 1.5 m telescope at Observatorio de Sierra Nevada in Granada (Spain) and at the 6.0 m BTA telescope (+ SCORPIO) at the Special Astrophysical Observatory (SAO-RAS) in Nizhnij-Arkhyz (Russia), and at the 2.2 m telescope (+BUSCA) at Calar Alto (Spain). Near infrared (nIR) observations were obtained at the 3.5 m telescope (+ OMEGA2000) at Calar Alto as part of the ALHAMBRA[1] back-up programme. Table 6.1 displays the observing log. Additionally, mm observations were obtained at the Plateau de Bure Interferometer (PdBI) as part of our target of opportunity programme. The PdBI observed the source on May 11 and May 13 (6 antennas compact D configuration) and May 16 (5 antennas compact D configuration). The data reduction was done with the standard CLIC and MAPPING software distributed by the Grenoble GILDAS group[2]; the flux calibration is relative to the carbon star MWC349. Table 6.2 displays the millimetre observing log.

In order to subtract in all of our optical and nIR images the contribution of the bright elliptical galaxy $9\farcs5$ away from the XRT error box, we modeled it using the ELLIPSE

[1]http://www.iaa.es/alhambra
[2]http://www.iram.es/IRAMFR/GS/gildas/gildas.html

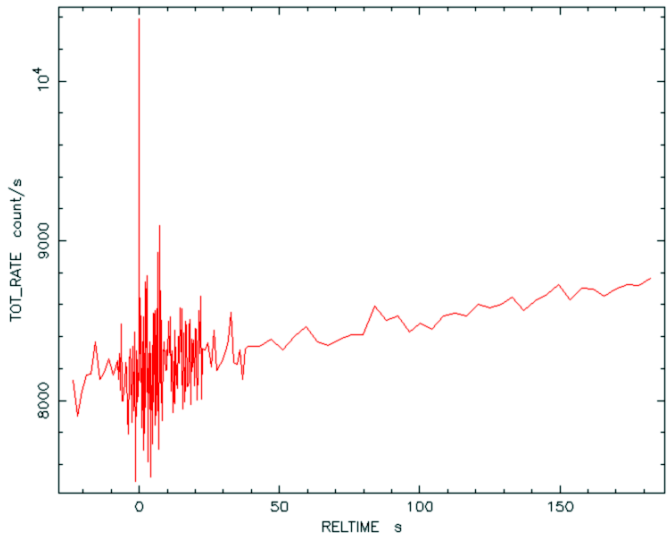

Figure 6.1: The gamma-ray light curve showing a $\approx$ 40 ms spike that classifies GRB 050509B into the short duration class.

routine under IRAF[3]. We used the residual to perform further analysis in the optical and nIR images. The optical field was calibrated using the field photometry provided by Henden (2005). The nIR images were calibrated using the 2MASS Catalogue.

6.3 Results and discussion

The main observational result is the lack of any variable optical/nIR/mm counterpart in our images, within the refined *Swift/XRT* error box (Gehrels et al. 2005), in spite of the intensive searches, in agreement with the upper limits reported by ROTSE-III and RAPTOR and *Swift*/UVOT (Gehrels et al. 2005) for the prompt optical emission and by PAIRITEL (Bloom et al. 2005) for the prompt nIR emission. Similarly, the deep upper limits reported at the Keck (Bloom et al. 2005; Cenko et al. 2005) and at the VLT (Hjorth et al. 2005a; Covino et al. 2005) are in agreement with our conclusions drawn from the deep 6.0m BTA observations.

6.3.1 No optical/nIR/mm afterglow at all ?

The fact that the detected X-ray afterglow for GRB 050509b (Gehrels et al. 2005) is the faintest of all afterglows detected by the *Swift*/XRT so far may indicate that the density of the surrounding medium where the progenitor took place is much lower than the typical value of $\approx$ 1 cm^{-3} derived for several long-duration GRBs. Assuming that the X-ray afterglow is caused by synchrotron emission, as in the case of the long-duration family, one should also expect some contribution at nIR and optical wavelengths, but a simple

[3]IRAF is distributed by the NOAO, which are operated by USRA, under cooperative agreement with the US NSF.

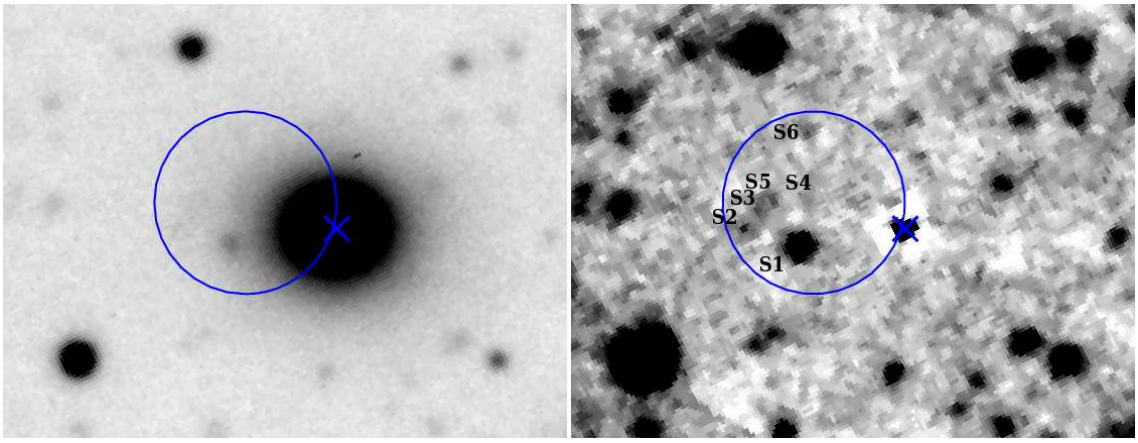

Figure 6.2: The deep R band image of the GRB 050509B field taken at the 6.0BTA on the 11^{th} May 2005. The contribution of the elliptical galaxy, marked with a cross (left) has been removed in order to better show the content of the *Swift*/XRT error box (right). The six sources S1-S4 (Cenko et al. 2005) and S5-S6 (Hjorth et al. 2005b) within the *Swift*/XRT error box are indicated. The field is $55'' \times 42''$ with North up and East to the left.

$S_{X-ray}/S_{optical}$ scaling would predict prompt optical fluxes $\sim 10^2$ (i.e. ~ 5 magnitudes) fainter than the optical afterglows observed so far for the long-duration events. Moreover, the combined *Swift*/XRT and *Chandra* X-ray Observatory (*CXO*) observations (Patel et al. 2005) imply that the decay exponent α is -1.1 (Gehrels et al. 2005), i.e., an optical afterglow might have rapidly decayed in brightness with a similar power-law decay index for $\nu_{opt} < \nu_X < \nu_c$ (Sari et al. 1998).

6.3.2 Is GRB 050509b at $z = 0.225$?

GRB 050509b is located in the direction of the NSC J123610+285901 cluster of galaxies (Gal et al. 2003) at $z = 0.225$ (see also Bloom et al. 2005). In fact, during the prompt search for the X-ray afterglow detected by *Swift*/XRT, *CXO* has detected the diffuse X-ray emission from the intracluster gas rather than the point source itself (Patel et al. 2005). If this would be the case, taking into account the proximity ($9\farcs5$) of the X-ray error box to the elliptical galaxy 2MASX J12361286+2858580 (Fig. 6.2), the relationship to it cannot be discarded. It would be only ~ 33 kpc in projection (3.563 kpc/$''$), as the angular size distance $D_A = 735$ Mpc, considering a Hubble constant of $H_0 = 71$ km s^{-1} Mpc^{-1}, a matter density $\Omega_m = 0.3$, and a cosmological constant $\Omega_\Lambda = 0.7$. Assuming this, the progenitor would have been originated in the halo of the elliptical galaxy and could favour a neutron-star merger origin (Goodman et al. 1987; Eichler et al. 1989; Narayan et al. 1992), a physical scenario that can explain a short-duration burst like GRB 050509B. We note that past searches for correlations between clusters of galaxies and GRBs did not reveal positive results (Hurley et al. 1997; Gorosabel & Castro-Tirado 1997).

Radio emission in (or close to) the center of this galaxy has been detected at the WSRT (van der Horst et al. 2005) although no emission lines are seen in the optical spectrum (Bloom et al. 2005). The restframe colours (and therefore the associated K-corrections)

Table 6.3: AB magnitudes of the possible elliptical host galaxy 2MASX J12361286+2858580 used for the fit.

Band	AB Magnitude
u	20.38±0.13
g	18.60±0.03
r	17.18±0.02
i	16.66±0.02
z	16.31±0.03
J	15.25±0.10
H	14.46±0.10
K	14.09±0.10

have been obtained based on the HyperZ code (Bolzonella et al. 2000). We have used the *ugri* & *z* magnitudes of the nearby galaxy from the Sloan Digital Sky Survey and the nIR ones from the 2 Micron All Sky Survey (correcting all for the Galactic reddening E($B-V$) = 0.019; Schlegel et al. 1998) to create a spectral flux distribution (SFD) that was fitted to galactic templates using HyperZ. The best fit favours (χ^2/d.o.f = 0.8) a moderately extincted ($A_{\rm v} \sim 0.8$ mag) galaxy harbouring an evolved dominant stellar population (age $\sim$ 720 Myr). Figure 6.3 shows the SFD of the elliptical galaxy.

In this scenario, an intriguing possibility arises if the event would be the result of a stellar collapse, similarly to the long duration GRBs. At such a redshift, an underlying type Ib/c SN similar to SN 1998bw/GRB 980425 (Galama et al. 1998) should have peaked at $R \sim 21$, about 20 days since the burst onset. An underlying Type Ia SN is also expected if the event is the result of the gravitational collapse of a C/O white dwarf into a neutron star (Dar & De Rújula 2004). Our optical limits in the R-band 18.5 days after the event onset imply that the peak flux of any underlying supernova should have been $\sim$ 3 magnitudes fainter than the one observed for the type Ib/c SN 1998bw/GRB 980425 (Galama et al. 1998), and 2.3 magnitudes fainter than a typical type Ia SN (Filippenko 1997 and references therein), in agreement with the VLT results (Hjorth et al. 2005a).

6.3.3 Is GRB 050509b at high redshift ?

It is also plausible that GRB 050509B was originated at a redshift considerably higher than 0.225, if it were hosted by one of the faint sources detected in the XRT error box (see Bloom et al. 2005) or even at an extremely high redshift that prevented us from detecting the host. In the former case, extinction could have played a considerable role in order to hide optical variability in the first hours/days following the event. However, the lack of detection of a nIR transient in the observations presented here disfavours this argument. On the other hand, if GRB 050509b arose from a high-redshift host galaxy, it would have easily been beyond the limit of the optical/nIR telescopes, because of the Lyman α blanketing affecting the optical band.

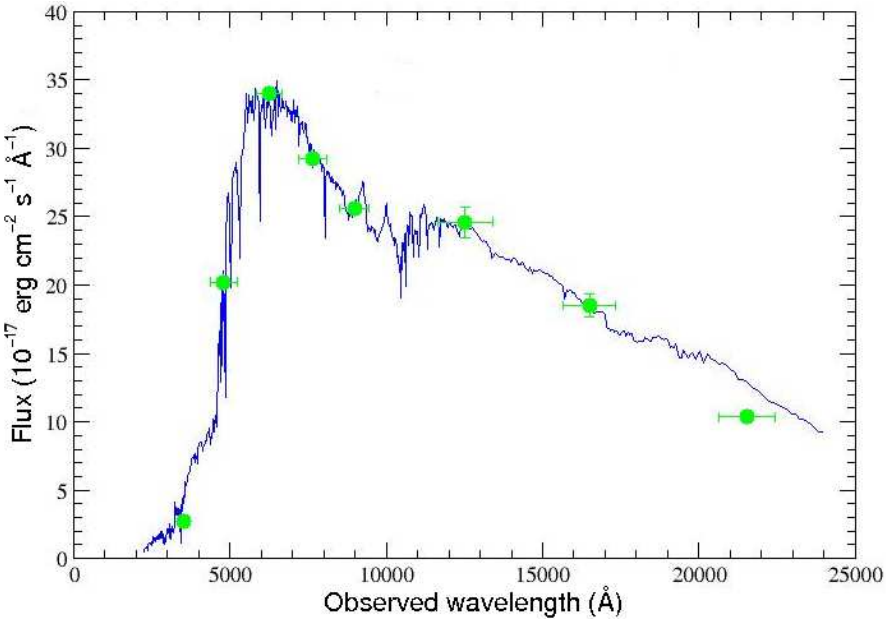

Figure 6.3: Synthetic fit to the *ugrizJHK* band photometric points of the elliptical galaxy. The best fist is achieved with a moderately extincted ($A_v = 0.8$ mag) galaxy harbouring an evolved stellar population (age ∼720 Myr). The SFD fit assumed a Salpeter (1955) IMF and a Calzetti et al. (2000) extinction law. It supersedes to Fig. 2 of Castro-Tirado et al. (2005).

6.4 Conclusions

We have shown multiwavelength observations of the short duration gamma-ray burst detected by *Swift* (GRB 050509B) between 0 s and ∼ 18.8 days after the event. No optical/nIR/mm afterglow emission has been detected, in spite of the reported X–ray afterglow detection by *Swift* few minutes after the event, confirming the elusiveness of the afterglow of the short duration events. The spectral flux distribution of the neighbouring, potential host galaxy, favours a system harbouring an evolved dominant stellar population (age ∼ 720 Myr), unlike most long duration GRB host galaxies observed so far, i.e. thus giving support to a compact binary merger origin. Any underlying supernova that could be associated with this particular event should have been at least 3 magnitudes fainter than SN 1998bw and 2.3 magnitudes fainter than a type Ia SN.

GRB 050509B is the second short duration GRB which is detected by *Swift*/BAT after GRB 050202 (which occurred too close to the Sun and could not be properly followed-up), and the first one localised with high accuracy by *Swift*/XRT. In spite of *CGRO*/BATSE detecting about 1/4 of events belonging to the short duration class, *Swift* had only detected 2 (out of ∼ 40 events) at the time of this burst, most likely due to its softer threshold energy. However, thanks to its extraordinary repointing capabilities, the accurate localisations for future events and the corresponding multiwavelength follow-up, will shed more light on the origin of the short-duration GRBs.

Bibliography

Bloom, J.S., Prochaska, J.X., Pooley, D., et al. 2005, ApJ, submitted (astro-ph/0505480)

Bolzonella, M., Miralles, J.-M. & Pelló, R. 2000, A&A 363, 476

Calzetti, D., Armus, L., Bohlin, R.C., et al. 2000, ApJ 533, 682

Castro-Tirado, A.J., Castro Cerón, J.M., Gorosabel, J., et al. 2002, A&A 393, L55

Castro-Tirado, A.J., Jelínek, M., Mateo Sanguino, T.J., et al. 2004, AN 325, 679

Castro-Tirado, A. J., et al. 2005, A&A, 439, L15

Cenko, S.B., Soifer, B.T., Bian, C., et al. 2005, GCN Circ. 3401

Covino, S., Israel, G.L., Antonelli, L.A., et al. 2005, GCN Circ. 3413

Dar, A. & De Rújula, A. 2004, Physics Reports, 405, 203

Eichler, D., Livio, M., Piran, T. & Schramm, D.N. 1989, Nature 340, 126

Filippenko, A.V. 1997, ARA&A, 35, 309

Gal, R.R., de Carvalho, R.R., Lopes, P.A.A., et al. 2003, AJ 125, 2064

Galama, T.J., Vreeswijk, P.M., van Paradijs, J., et al. 1998, Nature 395, 670

Gehrels, N., Chincarini, G., Giommi, P., et al. 2004, ApJ 611, 1005

Gehrels, N., et al. 2005, Nature, 437, 851

Goodman, J., Dar, A. & Nussinov, S. 1987, ApJ 314, L7

Gorosabel, J. & Castro-Tirado, A.J. 1997, ApJ 483, L83

Gorosabel, J., Andersen, M.I., Hjorth, J., et al. 2002, A&A 383, 112

Henden, A. A. 2005, GCN Circ. 3454

Hjorth, J., Sollerman, J., Gorosabel, J., et al. 2005a, ApJ, submitted (astro-ph/0506123)

Hjorth, J., Sollerman, J., Jensen, B.L., et al. 2005b, GCN Circ. 3410

Hurkett, C., Rol, E., Barbier, L., et al. 2005, GCN Circ. 3381

Hurley, K., Hartmann, D., Kouveliotou, C., et al. 1997, ApJ 479, L113

Hurley, K., Berger, E., Castro-Tirado, A.J., et al. 2002, ApJ 567, 447

Kehoe, R., Akerlof, C., Balsano, R., et al. 2001, ApJ 554, L159

Kennea, J.A., Burrows, D.N., Housek, J., et al. 2005, GCN Circ. 3383

Klotz, A., Böer, M. & Atteia, J.-L. 2003, A&A 404, 815

Kouveliotou, C., Meegan, C.A., Fishman, G.J., et al. 1993, ApJ, 413, 101

Mazets, E.P., Golenetskii, S.V., Ilyinskii, V.N., et al. 1981, A&SS, 80, 119

Narayan, R., Paczyński, B. & Piran, T., 1992, ApJ 395, L83

Patel, S., Kouveliotou, C., Burrows, D.N., et al. 2005, GCN Circ. 3419

Rykoff, E.S., Swan, H., Schaefer, B., et al. 2005, GCN Circ. 3382

Salpeter, E.E., 1955, ApJ 121, 161.

Sari, R., Piran, T. & Narayan, R. 1998, ApJ 497, L17

Schelgel, D. J., Finkbeiner, D. P. & Davis, M. 1998, ApJ 500, 525

van der Horst, A.J., Wiersema, K., Wijers, R.A.M.J., et al. 2005, GCN Circ. 3405

van Paradijs, J., Kouveliotou, C. & Wijers, R.A.M.J. 2000, ARA&A, 38, 379.

Wozniak, P., Vestrand, W.T., Wren, J., et al. 2005, GCN Circ. 3414

7

GRB 060121: Implications of a short/intermediate duration gamma-ray burst at high redshift

The work presented in this Chapter is based on:

de Ugarte Postigo, A., Castro-Tirado, A. J., Guziy, S., Gorosabel, J., Jóhannesson, G., Aloy, M. A., McBreen, S., Lamb, D. Q., Benitez, N., Jelínek, M., Pandey, S. B., Coe, D., Pérez-Ramírez, M. D., Aceituno, F. J., Alises, M., Acosta-Pulido, J. A., Gómez, G., López, R., Donaghy, T. Q., Nakagawa, Y. E., Sakamoto, T., Ricker, G. R., Hearty, F. R., Bayliss, M., Gyuk, G. & York, D. G.
Astrophysical Journal, 648, L83 (2006)

Since the discovery of the first short-duration gamma-ray burst afterglows in 2005, the handful of observed events have been found to be embedded in nearby ($z < 1$), bright underlying galaxies. Here we present multiwavelength observations of GRB 060121, the first short burst observed to clearly outshine its host galaxy (by a factor $> 10^2$). A photometric redshift for this event places the progenitor at a most probable redshift of $z = 4.6$, with a less probable scenario of $z = 1.7$. In either case, GRB 060121 is the farthermost short-duration GRB detected to date and implies an isotropic-equivalent energy release in gamma-rays comparable to the ones seen in long-duration bursts. We discuss the implications of the released energy on the nature of the progenitor. These results suggest that GRB 060121 may belong to a family of energetic short-population events, lying at $z > 1$ and whose optical afterglows would outshine their host galaxies, unlike the first short GRBs observed in 2005. The possibility of GRB 060121 being an intermediate-duration burst is also discussed.

7.1 Introduction

Since 1993 GRBs have been classified into two subgroups according to the observed duration and hardness-ratio derived from their gamma-ray spectra: short-hard and long-soft events (Kouveliotou et al. 1993). Recent studies have shown that there may be no difference in the hardness distribution between the two (Sakamoto et al. 2006), so we will refer to them just as short-duration bursts and long-duration bursts.

The detection of the first X-ray afterglows (Gehrels et al. 2005; Fox et al. 2005; Barthelmy et al. 2005) – and particularly the first optical afterglows (Hjorth et al. 2005; Fox et al. 2005; Covino et al. 2006; Berger et al. 2005a) of short bursts – led to identification of the probable host galaxy of GRB 050509B (Gehrels et al. 2005; Castro-Tirado et al. 2005) and the secure identification of the host galaxies of GRB 050709 (Villasenor et al. 2005) and GRB 050724 (Barthelmy et al. 2005; Gorosabel et al. 2006), and therefore the redshifts of these bursts. These results suggest that short bursts release less energy than do long bursts (Fox et al. 2005; Soderberg et al. 2006): $E_\gamma(\mathrm{short}) \sim 10^{49}$ erg vs. $E_\gamma(\mathrm{long}) \sim 10^{51}$ erg and that they may originate from the merger of neutron star-neutron star (NS-NS) or neutron star-black hole (NS-BH) binaries at cosmological distances.

Until GRB 060121, the detected optical afterglows of short bursts have been comparable in brightness to their host galaxies or dimmer, unlike the case of long burst that may outshine their hosts by a factor of up to $\sim 10^6$ (van Paradijs et al. 2000). The distance scale is also considered to be different, having all short bursts with definite redshifts been $z_{\mathrm{short}} < 0.6$[1] while long bursts show a broader range, mainly between 0.5 and 5, with a mean redshift $< z_{\mathrm{long}} > \sim 2.8$ (Jakobsson et al. 2006; Berger et al. 2005b).

7.2 Observations and Data Reduction

GRB 060121 was detected at 22:24:54.50 UT on the 21^{st} January 2006 by FREGATE, WXM and SXC instruments aboard the *HETE-2* mission (Arimoto et al. 2006). The position of the gamma-ray event was distributed using the GRB Coordinates Network (GCN) 13 s later. The spectral peak energy $Ep = 120 \pm 7$ keV (Boer et al. 2006), together with a duration of 1.97 ± 0.06 s classified it in the short burst group of events (see Fig. 7.1). It was also observed by Konus/ *WIND* (Golenetskii et al. 2006a) and followed up in X rays by *Swift*/XRT (Mangano et al. 2006), whose observations substantially improved the initial $28'$ *HETE-2* error box radius and helped to identify the optical counterpart (Malesani et al. 2006).

On receipt of the initial alert by *HETE-2*, a mosaic of images was triggered at the 1.5 m telescope of Observatorio de Sierra Nevada (OSN) in order to map the entire error box. The first detection of the afterglow was obtained 22 minutes after the gamma-ray event. Complementary observations were requested with the 2.2 m telescope of Calar Alto Observatory (CAHA), the 4.2 m William Herschel telescope (WHT) at Roque de los Muchachos Observatory and the 3.5 m Astrophysical Research Consortium (ARC) telescope at Apache Point Observatory. Equatorial coordinates of the optical near-infrared (nIR)

[1] We point out that there is still an ongoing debate about the redshift of GRB 050813, which could lie at a redshift of $z \sim 1.8$ (Berger 2006), although no optical or radio counterpart was found to support this scenario.

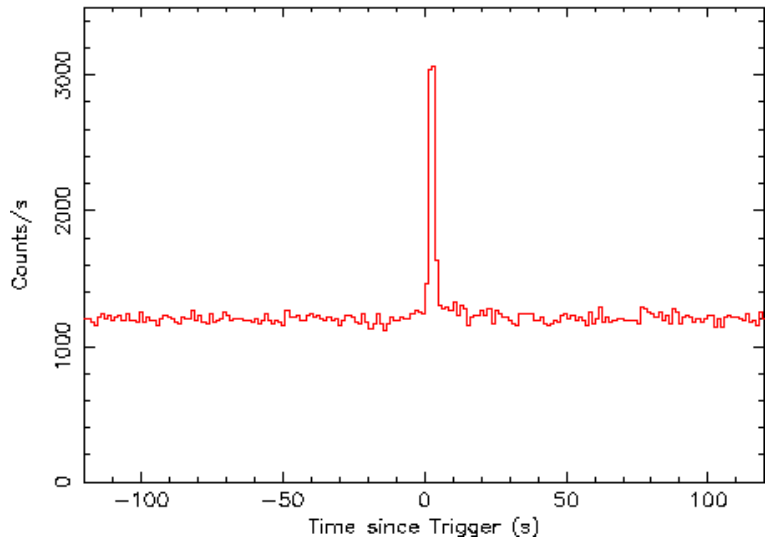

Figure 7.1: Gamma-ray light curve of GRB 060121 as detected by *HETE-2*.

afterglow yielded: R.A.(J2000)=$09^h09^m52\overset{s}{.}02$, Dec.(J2000)=$+45°39'45\overset{''}{.}9$ ($0\overset{''}{.}5$ uncertainty at 1σ level). The reduction of all the optical and nIR data was done using JIBARO (see Chapter 9).

Optical images have been photometrically calibrated against the Sloan Digital Sky Survey (Adelman-McCarthy et al. 2006) applying the corresponding transformations (Jester et al. 2005) for our photometric system. For nIR images we have used field stars from the 2 Micron All Sky Survey catalogue (Skrutskie et al. 2006). See Fig. 7.2 and Table 7.1 for the calibration stars that were used. A Galactic extinction (Schlegel et al. 1998) correction of E(B-V)=0.014 is applied and magnitudes have been converted to flux density units (Jy) for clarity (Fukugita et al. 1995; Cox 2000). The photometric data are displayed in Table 7.2.

Table 7.1: Calibration stars in the field of GRB 060121, as marked in Fig. 7.2.

#	U	B	V	R	I	K
1	20.131±0.128	20.475±0.046	20.134±0.039	19.836±0.065	19.554±0.081	—
2	17.690±0.067	18.045±0.031	17.835±0.014	17.396±0.035	16.985±0.038	—
3	20.661±0.404	19.708±0.036	18.535±0.024	17.723±0.040	16.917±0.044	15.396±0.224
4	20.290±0.291	19.349±0.033	18.179±0.019	17.252±0.037	16.393±0.039	15.025±0.168
5	20.594±0.352	20.299±0.044	19.454±0.037	18.800±0.054	18.192±0.060	—
6	—	—	—	—	—	13.739±0.055
7	—	—	—	—	—	14.074±0.074

The X-ray light curve and spectrum were obtained from the *Swift*/XRT data. The spectrum was fitted with a power-law plus a fixed Galactic hydrogen column density ($N_{\rm H(Gal)} = 1.7 \times 10^{20}$ cm^{-2}) and an intrinsic column density $N_{\rm H(int)}$ at a varying redshift in the range $0.1 \leq z \leq 6.0$ (Dickey & Lockman 1990). A spectral index ($F \sim \nu^{\beta}$) of $\beta = -1.10^{+0.17}_{-0.16}$ ($\chi^2/d.o.f. = 36/29$) was derived from the fit with an intrinsic column density that, depending on the selected redshift scenario, ranges from $N_{\rm H(}z{=}1.7{\rm)}} = 0.46^{+0.23}_{-0.21} \times 10^{22}$

Table 7.2: Observations of the afterglow of GRB 060121

Mean Date (Jan 2006 U.T.)	Band	Tel.	Exp. time (s)	Flux density (μJy)
22.2443	K	4.2mWHT	750	17.1±1.4
23.2402	K	4.2mWHT	1,000	6.3±1.6
23.3308	K	3.5mARC	3,600	7.48±0.65
27.2588	K	3.5mARC	3,600	<2.13
21.9495	I	1.5mOSN	120	19.3±4.4
21.9633	I	1.5mOSN	120	10.0±2.8
22.0458	I	1.5mOSN	300	10.8±2.5
22.1162	I	1.5mOSN	6×300	4.55±0.83
22.2539	I	1.5mOSN	5×300	<2.5
22.0493	R	2.2mCAHA	600	3.70±0.97
22.0963	R	2.2mCAHA	2×600	1.14±0.33
22.1590	R	2.2mCAHA	2×600	1.23±0.49
22.2385	R	2.2mCAHA	3×600	1.35±0.37
23.1828	R	1.5mOSN	12×900	<0.8
24.0804	R	2.2mCAHA	6×900	0.55±0.14
22.0885	V	2.2mCAHA	2×600	<1.1
22.1952	V	2.2mCAHA	5×600	<0.7
22.0336	B	2.2mCAHA	600	<1.7
22.1560	B	2.2mCAHA	7×600	<0.9
22.0258	U	2.2mCAHA	600	<3.3
22.1200	U	2.2mCAHA	5×600	<2.1

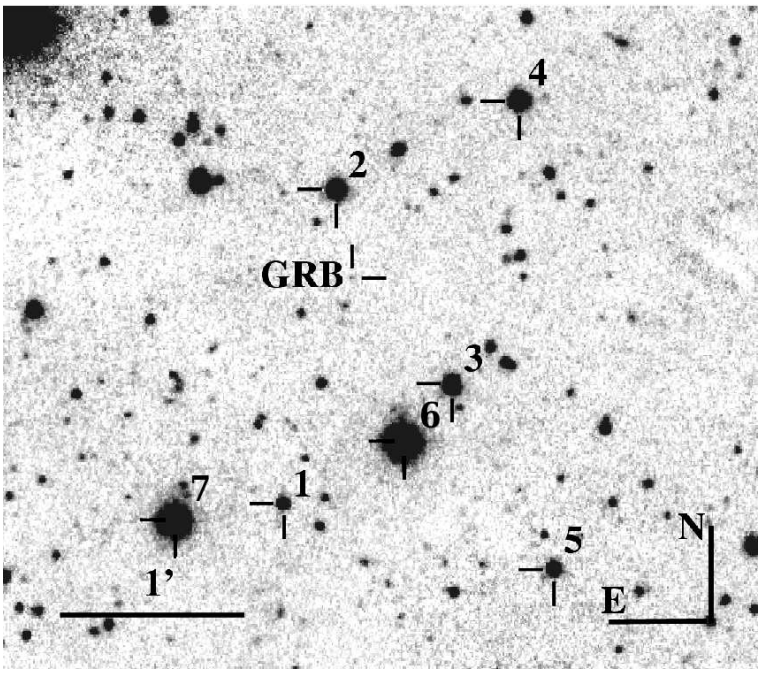

Figure 7.2: Finding chart showing the position of the GRB together with the reference stars used for the optical and nIR photometry.

cm^{-2} to $N_{\mathrm{H}(z=4.6)} = 2.9^{+1.3}_{-1.5} \times 10^{22}\mathrm{cm}^{-2}$ (see Fig. 7.3).

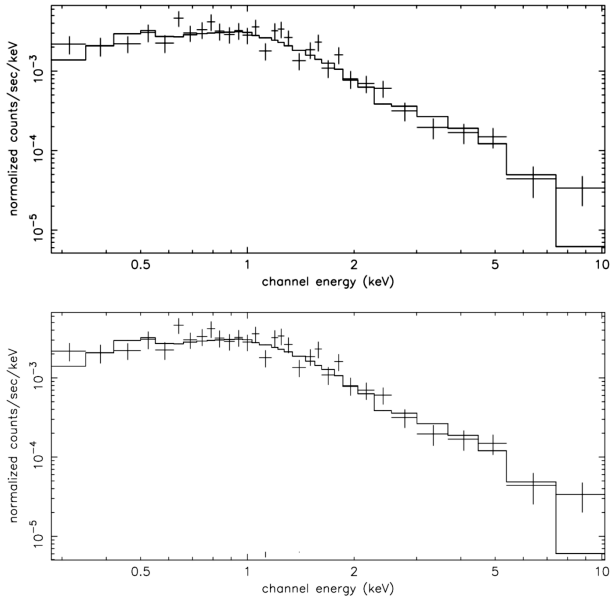

Figure 7.3: X-ray spectra of GRB 060121 obtained with *Swift*/XRT fitted with a power law plus a fixed Galactic hydrogen column and an intrinsic column density at redshift 4.6 (top) and 1.7 (bottom).

Table 7.3: Physical properties of the short gamma-ray bursts detected at the time of this work. The table displays, in columns: Name of the burst, redshift, duration of the gamma ray emission, measured gamma-ray fluence, isotropic-equivalent gamma-ray energy, isotropic-equivalent luminosity observed in X-rays 10 hours after the burst and the optical fluxes ratio between the afterglow 12 hours after the burst and the host galaxy (both in R band). The compilation is based on this work, Fox et al. (2005), Schady & Pagani (2006), Golenetskii et al. (2006b), Soderberg et al. (2006) and references therein.

GRB	Redshift	T_{90} (s)	Fluence (erg cm^{-2})	$E_{\gamma,\mathrm{iso}}$ (erg)	L_X (erg s^{-1})	$F_{A/G}$
050509B	0.225	0.04	9.5×10^{-9}	4.5×10^{48}	$< 7 \times 10^{41}$	< 0.005
050709	0.160	0.07	2.9×10^{-7}	6.9×10^{49}	3×10^{42}	~ 1.0
050724	0.258	3.00	6.3×10^{-7}	4.0×10^{50}	8×10^{43}	~ 0.2
050813[†]	0.722	0.60	1.2×10^{-7}	6.5×10^{50}	9×10^{43}	< 0.15
	1.8			3.9×10^{51}	5×10^{44}	
051221A	0.546	1.40	3.2×10^{-6}	2.4×10^{51}	6×10^{44}	~ 1.0
060121	1.7	1.97	4.8×10^{-6}	3.7×10^{52}	1.1×10^{46}	~ 20.0
	4.6			2.4×10^{53}	6×10^{46}	
060313	≤ 1.7	0.70	1.4×10^{-5}	$\leq 1 \times 10^{53}$	-	> 3.0

7.3 Results

The detections in I, R and K bands and the upper limits imposed for the U, B and V bands, allowed us to construct a spectral flux distribution (SFD) at a mean epoch of 2.5 hours after the burst (Fig. 7.4). The nIR K band point is extrapolated from a near epoch using as reference a quasi-simultaneous R passband detection and assuming constant (R-K). The data were fit with a power law spectrum, a superposed intrinsic extinction (Pei 1992) and a Lyman-α blanketing model (Madau 1995) at a varying redshift. The slope of the powerlaw was chosen to be $\beta_{\mathrm{opt}} = -0.60 \pm 0.09$, as derived from the X-ray spectra, assuming $\nu_{\mathrm{opt}} < \nu_{\mathrm{c}} < \nu_{\mathrm{X}}$ at a pre-break epoch in the standard fireball model (Sari et al. 1999). This is confirmed by the modelling described below. We obtained two probability peaks in our redshift study. The main one (with a 63% likelihood) places the burst at $z = 4.6 \pm 0.5$ with an intrinsic extinction of $A_{\mathrm{V}} = 0.5 \pm 0.2$ magnitudes. A secondary peak (with a 35% likelihood) would imply that the afterglow lies at a $z = 1.7 \pm 0.4$ and $A_{\mathrm{V}} = 1.1 \pm 0.2$ magnitudes. In either case, GRB 060121 is the farthermost short duration GRB detected to date. A redshift of $z < 0.5$ has a likelihood $\leq 0.5\%$ and implies extinctions $A_{\mathrm{V}} > 1.8$. Adopting a flat cosmology with $\Omega_\Lambda = 0.73$, $\Omega_{\mathrm{M}} = 0.27$ and $H_0 = 71$ km s^{-1} Mpc^{-1} and considering a gamma-ray fluence of $(4.77 \pm 0.28) \times 10^{-6}$ erg cm^{-2}, we obtain an isotropic-equivalent energy release in gamma-rays of $E_{\gamma,\mathrm{iso}} = 2.4^{+0.6}_{-0.3} \times 10^{53}$ erg ($E_{\gamma,\mathrm{iso}} = 3.7^{+1.2}_{-0.6} \times 10^{52}$ erg) for a redshift of $z = 4.6$ (1.7), 2(1) orders of magnitude higher than other $E_{\gamma,\mathrm{iso}}$ values determined for previous short bursts (Table 7.3). This is comparable to the values measured for long bursts (Frail et al. 2001).

We have modelled the GRB 060121 afterglow following the prescription of Jóhanesson et al. (2006) on the basis of the standard fireball model with 2 energy injections 0.035 and

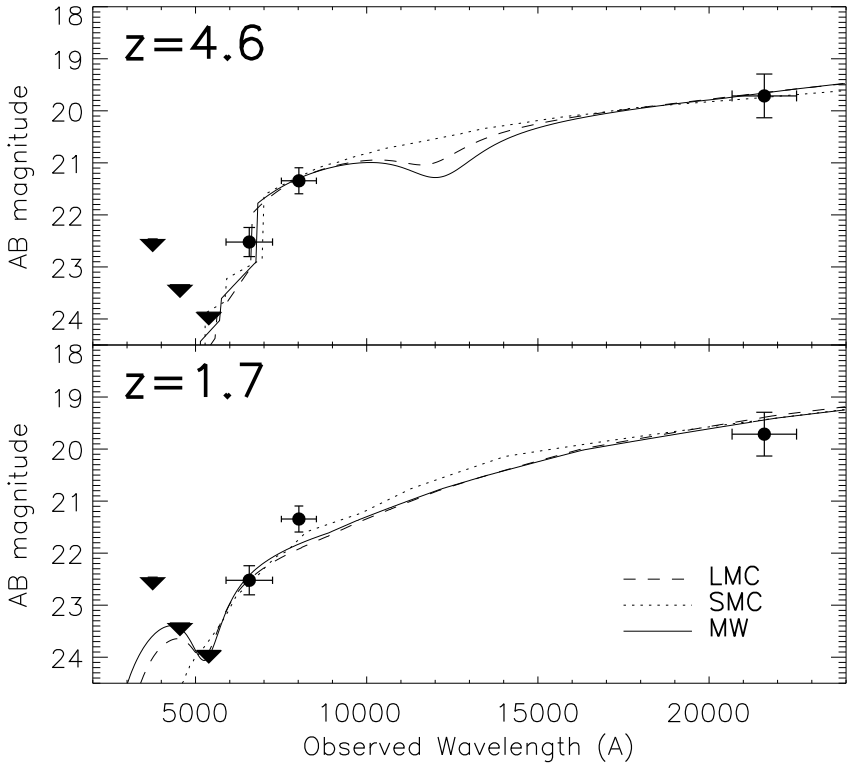

Figure 7.4: Spectral flux distribution. A fit of the data points with an extincted simple power law and a Lyman-α break returns two peaks of probability. The main one, covering a probability of 63% is centred at $z = 4.6$ with rest frame extinction of $A_{\rm V} = 0.5 \pm 0.2$ (top) and the secondary with a 35% likelihood is centred at $z = 1.7$ with $A_{\rm V} = 1.1 \pm 0.2$ (bottom).

0.23 days after the onset of the burst. These energy injections are required in order to explain the bumpy behaviour seen during the first hours (Fig. 7.5); similar features have been seen in long burst light curves (Castro-Tirado et al. 2006) at $z \sim 4$. The model has been fitted for both $z = 4.6$ and $z = 1.7$ scenarios with slightly better results for the high-z case ($\chi^2/d.o.f._{z=4.6} = 1.9$ versus $\chi^2/d.o.f._{z=1.7} = 2.8$). We localise the cooling frequency between optical and X-ray, just below the X-ray measurements and the maximum frequency below the nIR. Together with the multiwavelength spectral slopes, the model parameters are constrained and independently on the redshift, point to a narrow jet with half opening angle $\theta_0 < 10^\circ$ in a low density environment (10^{-3} cm$^{-3} \leq n \leq 0.1$ cm^{-3}; the lower density limit fits the observations better for the case where the GRB took place at $z = 4.6$ while the upper density value accommodates better the data at $z = 1.7$), with efficiencies of conversion of kinetic to gamma-ray energy $\eta_\gamma < 0.05$ (found when we maximise the opening angle in the fit, while minimising the initial energy). Although the jet break time cannot be accurately calculated from the available data, we find a steepening around 4 days after the burst in the best fit of the model.

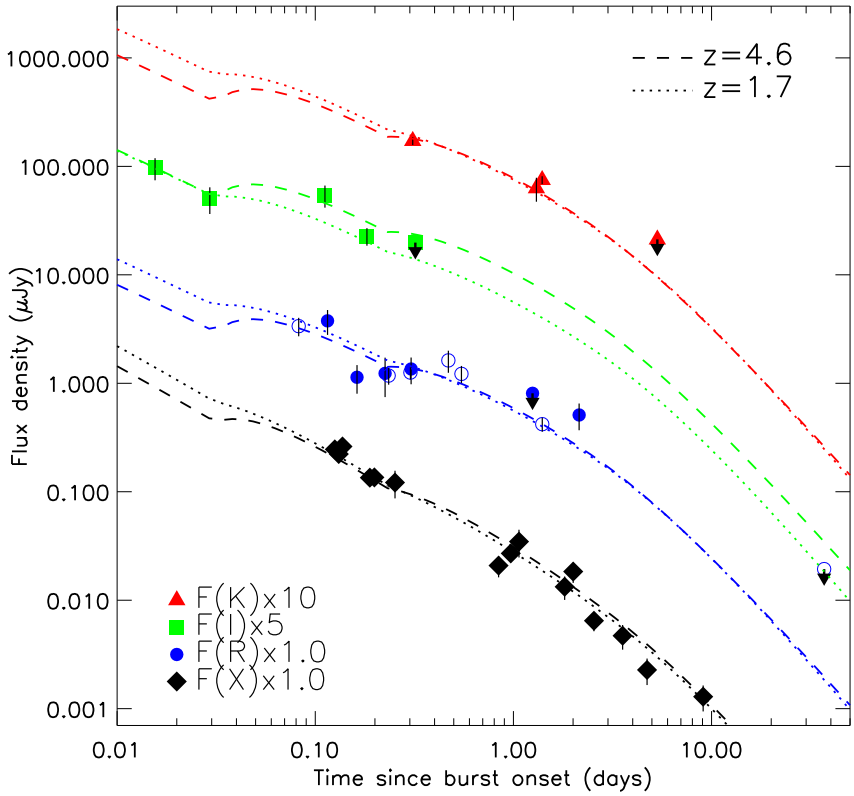

Figure 7.5: Light curve of the afterglow in the near infrared (K), visible (R & I) and X-ray bands. The figure shows the result of the best fit of the model in the most probable high-z (4.6) case which has been optimised with values of $p = 2.06$, $\theta_0 = 0.^\circ 6$ and $n = 0.1$ cm^{-3} and in the low-z (1.7) case, which gives a slightly worse fit with $p = 2.05$, $\theta_0 = 2.^\circ 3$ and $n = 0.04$ cm^{-3}, as discussed in the text. Filled symbols are data presented in this article whereas empty ones are data from the literature.

7.4 Discussion

GRB 060121 has a T_{90} duration of 1.97 ± 0.06 s in the 85-400 keV energy band and a hardness ratio (HR) $S_E(100-300\ \mathrm{keV})/S_E(50-100\ \mathrm{keV}) = 1.48 \pm 0.18$. We note that the intrinsic duration of GRB 060121 would be 1.1 s with a HR of 3.0 if $z = 1.7$, or 0.7 s with a HR of 3.9 if $z = 4.6$, where in transforming T_{90} to the rest frame we have taken into account both cosmological time dilation and the fact that burst duration decreases with increasing energy. Both sets of values place GRB 060121 near the centre of the cluster of BATSE short bursts in the (T_{90}, HR)-plane (see Fig. 7.6). We have studied the classification of GRB 060121 (as either a short burst or a long burst), using nine criteria: (1) duration, (2) pulse widths, (3) spectral hardness, (4) spectral lag, (5) energy radiated in gamma-rays, (6) existence of a long, soft bump following the burst, (7) location of the burst in the host galaxy, (8) lack of detection of a supernova component to deep limits, and (9) type of host galaxy. Four criteria (1, 5, 6, and 7) provide strong evidence that GRB 060121 is a short burst if $z = 1.7$ and two other criteria (2 and 4) provide additional strong evidence

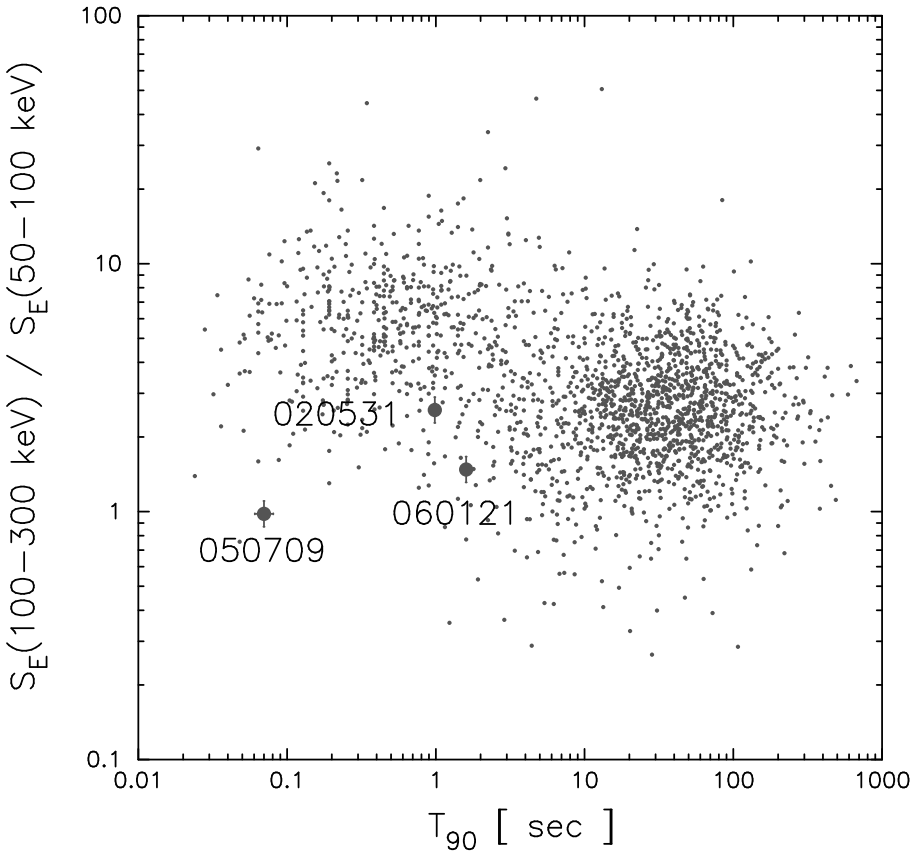

Figure 7.6: Burst duration vs. spectral hardness diagram. Large black circles are the locations of the three currently established *HETE-2* short GRBs superimposed on the distribution of 1973 BATSE short and long GRBs (small grey dots).

that GRB 060121 is a short burst if $z = 4.6$. None of the criteria provide evidence that GRB 060121 is a long burst. Thus, we can make a strong, although not conclusive, claim that GRB 060121 is a short burst. Further details about this analysis are given by Donaghy et al. (2006).

If we consider the progenitor to be a merger of compact objects (Eichler et al. 1989; Aloy et al. 2005), the released energy needs either a large conversion efficiency of the accreted mass into neutrino emission ($\gtrsim 0.05$), a large accretion disk mass ($\gtrsim 0.1 M_{\odot}$) or an appropriate combination of both factors (Oechslin & Janka 2006). Considering a merger at a redshift $z > 1.5$, there is a higher consistency with the theoretical models where the rate of NS+NS or NS+BH mergers follows the star formation rate with delays of $\sim$ 1 Gyr (Janka et al. 2006) than with those of very old populations of NS+NS progenitor systems (Nakar et al. 2005). Furthermore, the high extinction derived from the SFD fit indicates that the merger probably took place within the galaxy rather than in the outer halo or intergalactic medium and thus, the system received a small natal kick, although the density of the local event environment is relatively low ($n \sim 0.1$ cm^{-3}) as indicated by the afterglow fits discussed here. Alternatively, if the energy was extracted via a Blandford-Znajek process (Blandford & Znajek 1977), either the value of the dimensionless angular

momentum of the central BH is $a > 0.3$, the magnetic field surrounding the BH is $B \gtrsim 10^{16}$ G or the BH has a mass larger than $3M_{\odot}$ (or a combination of these parameters).

Late observations by the *Hubble Space Telescope* (*HST*) have shown no trace of the afterglow down to magnitude $R \sim 28$ about 37 days after the burst but do show an underlying galaxy (Levan et al. 2006). We have reanalysed the photometry of the galaxy using ColorPro (Coe et al. 2006) obtaining $F606W_{\rm AB} = 27.35 \pm 0.16$ (*HST* wide band filter centred at 606 nm) and $F160W_{\rm AB} = 24.05 \pm 0.38$ (*HST* wide band filter centred at 1600 nm). Although the information is very limited we have used this photometry to study the probability distribution for the redshift of the galaxy using a Bayesian photometric redshift as described by Benítez (2000) and Benítez et al. (2004). We obtain two peaks of probabiliy at $z = 1.0$ and $z = 5.2$, the latter being more probable. By multiplying this probability by the one obtained for the afterglow we can assign a probability of 70% to the higher redshift case and a 28% to the lower redshift scenario (see Fig. 7.7). Applying a prior based on well determined extinctions for long bursts (Kann et al. 2006) the likelihood of a high redshift event would rise to 98% as no bursts are usually found with high extinction. This is a soft constrain as it favours low extinctions, like it could be expected from the low density derived from our model, significantly lower than the one found for long bursts.

7.5 Conclusion

These results suggest that assuming that GRB 060121 were a short burst, there exists an emerging population of short events located at high redshifts and with energies comparable to those of long events. In this group we may also include GRB 060313 (Schady & Pagani 2006) or GRB 000301C (Jensen et al. 2001). This population would produce afterglows which significantly outshine their host galaxies, with isotropic energy releases of $E_{\gamma,\rm iso} \sim 10^{52-53}$ erg similar to the values observed in long events. Furthermore, following the classification by Horváth et al. (2006) GRB 060121 could be classified in the "intermediate group" (Horváth 1998; Balastegui et al. 2001) of events with a 68% probability (28% for short-burst and 4% for long-burst). The relationship between this second population of short bursts and the intermediate population of GRBs will be determined or excluded by future observations of similar events.

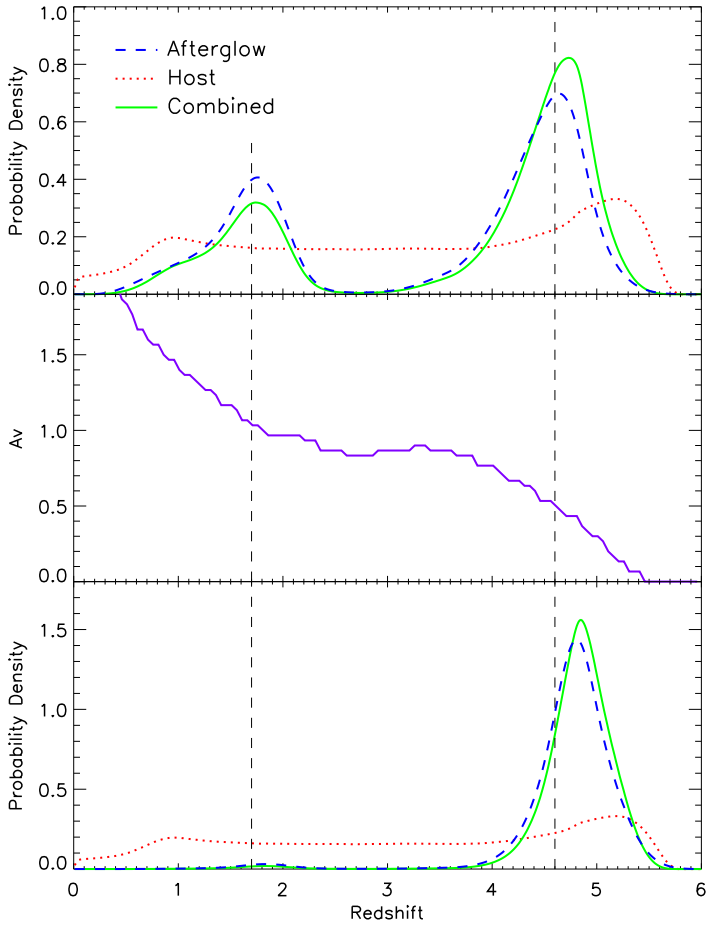

Figure 7.7: Probability distribution and extinction vs. redshift. The top panel shows the probability distribution for the GRB afterglow, the host galaxy and a combination of both which favours the high redshift scenario. In the central panel the extinction distribution shows a lower A_V for the high redshift, in the range of what has been observed for long bursts. Using an extinction based prior, that gives more credibility to the extinctions observed in long bursts we find a new redshift distribution which favours the high redshift scenario (lower panel).

Bibliography

Adelman-McCarthy, J. K. et al. 2006, ApJS, 162, 38

Aloy, M. A., Janka, H.-T. & Müller, E. 2005, A&A, 436, 273

Arimoto, M. et al. 2006, GCN Circ. 4550

Balastegui, A., Ruiz-Lapuente, P. & Canal, R. 2001, MNRAS, 328, 283

Barthelmy, S. et al. 2005, Nature, 438, 994

Blandford, R. D. & Znajek, R. L. 1977, MNRAS, 179, 433

Benítez, N. 2000, ApJ, 536, 571

Benítez, N. et al. 2004, ApJS, 150, 1

Berger, E. et al. 2005a, Nature, 438, 988

Berger, E. et al. 2005b, ApJ, 634, 501

Berger, E. 2006, astro-ph/0602004

Boer, M. et al. 2006, GCN Circ. 4552

Castro-Tirado, A. J., et al. 2005, A&A, 439, L15

Castro-Tirado, A. J., et al. 2006, A&A, 459, 763

Coe, D. et al. 2006, astro-ph/0605262

Covino, S. et al. 2006, A&A, 447, L5

Cox, A. N. 2000, Allen's astrophysical quantities, 4th ed. Publisher: New York: AIP Press; Springer, 2000. Editedy by Arthur N. Cox. ISBN: 0387987460

Dickey, J. M. & Lockman, F. J. 1990, ARA&A, 28, 215

Donaghy, T. Q. et al. 2006, astro-ph/0605570

Eichler, D., Livio, M., Piran, T. & Schramm, D. N. 1989, Nature, 340, 126

Fox, D. B. et al. 2005, Nature, 437, 845

Frail, D. A. et al. 2001, ApJ, 562, L55

Fukugita, M., Shimasaku, K. & Ichikawa, T. 1995, PASP, 107, 945

Gehrels, N. et al. 2005, Nature, 437, 851

Golenetskii, S. et al. 2006a, GCN Circ. 4564

Golenetskii, S. et al. 2006b, GCN Circ. 4881

Gorosabel, J., et al. 2006, A&A, 450, 87

Hjorth, J. et al. 2005, Nature, 437, 859

Horváth, I. 1998, ApJ, 508, 757

Horváth, I., Balázs, L. G., Bagoly, Z., Ryde, F. & Mészáros, A. 2006, A&A, 447, 23

Jakobsson, P. et al. 2006, A&A, 447, 897

Janka, H.-T., Aloy, M.-A., Mazzali, P. A., & Pian, E. 2006, ApJ, 645, 1305

Jensen, B. L. et al. 2001, A&A, 370, 909

Jester, S. et al. 2005, AJ, 130, 873

Jóhannesson, G., Björnsson, G., & Gudmundsson, E. H. 2006, ApJ, 647, 1238

Kann, D. A., Klose, S. & Zeh, A. 2006, ApJ, 641, 993

Kouveliotou, C. et al. 1993, ApJ, 413, L101

Levan, A. J., et al. 2006, ApJ, 648, L9

Madau, P. 1995, ApJ, 441, 18

Malesani, D. et al. 2006, GCN Circ. 4561

Mangano, V. et al. 2006, GCN Circ. 4560

Nakar, E., Gal-Yam, A. & Fox, D. B. 2005, astro-ph/0511254

Oechslin, R. & Janka, H.-T. 2006, MNRAS, 368, 1489

Pei, Y. C. 1992, ApJ, 395, 130

Sari, R., Piran, T. & Halpern, J. P. 1999, ApJ, 519, L17

Sakamoto, T. et al. 2006, American Institute of Physics Conference Series, 838, 43

Schady, P. & Pagani, C. 2006, GCN Circ. 4877

Schlegel, D. J., Finkbeiner, D. P. & Davis, M. 1998, ApJ, 500, 525

Skrutskie, M. F. et al. 2006, AJ, 131, 1163

Soderberg, A. M., et al. 2006, ApJ, 650, 261

van Paradijs, J., Kouveliotou, C. & Wijers, R. A. M. J. 2000, ARA&A, 38, 379

Villasenor, J. S. et al. 2005, Nature, 437, 855

Part III

Instrumentation

8

BOOTES robotic observatories

Gamma-ray burst are astronomical phenomena which evolve in very short temporal scales. Thus, traditional instrumentation turns out to be inefficient and new observational techniques, based in robotic instrumentation become necessary. In view of this circumstances BOOTES (the **B**urst **O**bserver and **O**ptical **T**ransient **E**xploring **S**ystem) was developed in the framework of an Spanish-Czech collaboration at the end of the 1990's. BOOTES is composed of three observatories located in Andalusia, in the provinces of Huelva, Málaga and Granada respectively, with a baseline of 300 km. First light was obtained at BOOTES-1 (Huelva station) during the summer of 1998, becoming the first fully functional intelligent robotic observatory in Spain shortly after. Since then, BOOTES has responded to more than 100 GRB alerts and collaborates with observing campaigns of many astronomical phenomena (meteors, comets, variable stars, etc.).

Our participation in BOOTES project began in 1999 and has covered all the fields and subsequent development phases, from instrumentation design and construction, through software programming to the scientific analysis of the data. Among the diverse advances that have been accomplished during this time, we emphasise in the reduction and analysis software (JIBARO, treated in the next Chapter) and the design and construction of a wide field spectrograph that was installed on one of the BOOTES telescopes.

8.1 Introduction

During the decade of the 1990s significant advances were finally beginning to be made in the field of GRBs. New observatories such as *CGRO* or *BeppoSAX* were being launched, opening new windows to observe the high energy Universe. We would soon have accurate localisations in a short enough time to point telescopes with the hope of observing an optical counterpart. It was in this context that BOOTES (Castro-Tirado et al. 1996) was conceived by Alberto J. Castro-Tirado in 1993. The idea was to create an observatory, with cameras of different fields of view and sensitivities, that would do daily sky surveys searching for transient sources and being capable of interrupting these observations to respond to a GRB alert in fast, autonomous way.

BOOTES found its space as part of the ground base preparation for *INTEGRAL* space

mission, lead by the European Space Agency (Castro-Tirado et al. 1999; Hudec et al. 1999). After obtaining funding for the project an appropriate site was searched, looking for a place with an appropriate infrastructure, reasonable sky quality and the best possible meteorology. The first BOOTES station was finally chosen to be placed in the *Estación de Sondeos Atmosféricos* at the *Centro de Experimentación de El Arenosillo* (ESAt-INTA-CEDEA), in Huelva, Spain (see Fig. 8.1). It was there that BOOTES saw its first light in the Summer of 1998, with one 0.3 m telescope and two wide field cameras.

Figure 8.1: Images of BOOTES-1 during 1999, in its original location.

A year later, in July 2001, BOOTES-2 was inaugurated in the *Estación Experimental de La Mayora* (EELM-CSIC), in Málaga (see Fig. 8.2), 240 km east from the first station with a 0.3 m telescope and a wide field camera. This second observatory supports the first station by giving a stereoscopic view that allows to distinguish between atmospheric phenomena and astronomical sources through triangulation (Castro-Tirado et al. 2004). By using the 0.3 m telescopes we are able to distinguish local sources up to a distance of $\sim 10^6$ km, from astronomical ones.

Figure 8.2: Offitial opening ceremony of BOOTES-2 in 2001.

A third observatory, BOOTES-IR (Castro-Tirado et al. 2006), which saw first ligh at the beginning of 2005, is now working in Sierra Nevada (see Fig. 8.3), with a very fast slewing mount and 0.6 m optics. The aim of this new telescope is to explore the infrared emission of GRBs during the first seconds after the explosion with a high temporal resolution. The near infrared camera will be installed shortly and in the mean time an optical camera is already producing the first results (Pérez-Torres et al. 2005; de Ugarte Postigo et al. 2005a; Jelínek et al. 2005; de Ugarte Postigo & Gorosabel 2006a; de Ugarte Postigo et al. 2006b; de Ugarte Postigo et al. 2006c).

Figure 8.3: Images of BOOTES-IR during the construction of the housing during August 2003 (left) and the installation of the telescope in November 2004 (right).

8.2 Scientific aims

The main scientific aim of the BOOTES projects is the simultaneous and quasi-simultaneous observation of the error boxes of GRBs. Wide field cameras are routinely pointing to the observing fields of gamma-ray satellites in order to provide data prior, during and after the gamma ray event. This was initially done by following the pointings of the X-ray cameras aboard *BeppoSAX* and later by following the antisolar pointings of *HETE-2* mission. This is more complicated in the *Swift* era as the wider field of BAT is only covered by all-sky cameras, also developed in the context of the BOOTES project. Deeper follow-up is carried out after a GRB alert is received by using the narrow field instrumentation of the observatories.

As secondary science, BOOTES is monitoring the sky in different bands, accumulating photometric data of as many objects as possible in order to create a long term database that will be useful for other astronomical studies, such as star variability, asteroids, comets and other transient phenomena. During this monitoring of the sky, the automatic detection software looks through the images searching for emerging astronomical sources such as novae, supernovae or even for orphan gamma-ray burst afterglows; those that have not been previously detected by gamma-ray satellites.

From BOOTES we also support and collaborate in observing campaigns of other transient astronomical phenomena such as comets, variable stars or meteors.

8.3 Location and equipment

At the beginning of 2007 BOOTES is composed of 3 observatories: The first of them, BOOTES-1, is located at the *Estación de Sondeos Atmosféricos* (ESAt) of the *Centro de Experimentación De El Arenosillo* (CEDEA-INTA), Huelva. The second station is placed 240 km East of this, at the *Estación Experimental de La Mayora* from the Consejo Superior de Investigaciones Científicas (EELM-CSIC) in Algarrobo Costa, Málaga. Finally, BOOTES-IR is located in Sierra Nevada mountains in the *Observatorio de Sierra Nevada* (OSN-CSIC), at a height of 2 896 m in the province of Granada. The location of the observatories is marked in Fig. 8.4.

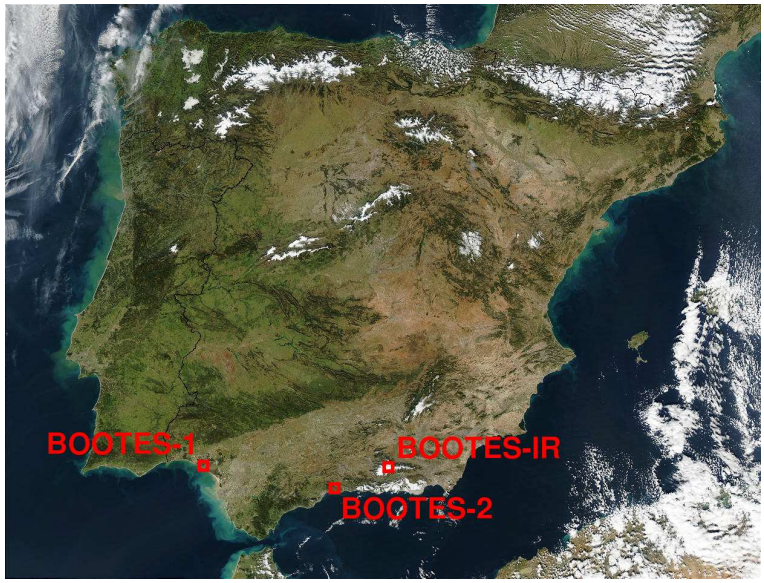

Figure 8.4: Location of the different BOOTES observatories.

All the observatories have an independent and autonomous weather station (see Fig. 8.5) with wind, rain, and humidity sensors that decides if the conditions are appropriate for observing and that has the capability of opening and closing the domes when needed. This weather station system was initially developed by T.J. Mateo Sanguino (Mateo Sanguino et al. 2004a; Mateo Sanguino et al. 2004b) and has been updated an maintained by S. Vítek. A GPS (Global Positioning System) in each of the observatories acts as a time server that tells the weather station when it is time to open or close the dome. This time server also provides the camera software the precision that is necessary to keep track of the time when each exposure is obtained and helps the telescope to keep its pointing accuracy over long periods of time. High sensitivity video cameras provide images during day and night off all three observatories through Internet so that the observer can have an idea of the current conditions of each site and detect any problem in real time (see Fig. 8.5). The observatories

are controlled by RTS-2 (Kubánek et al. 2006), a robotic observatory manager that takes care of the communications and priorities between the different parts of the observatory.

Figure 8.5: Image of the weather station in BOOTES-1 (left) and capture of the web-page where the observatories can be seen in real time (right).

8.3.1 BOOTES-1

BOOTES-1 was the first observatory of the BOOTES experiment, working since 1998. The site has one of the best weather conditions in Spain, with an average of 300 clear nights per year. During these 9 years, BOOTES-1 has suffered significant updates (see for example de Ugarte Postigo et al. 2003). In the summer of 2000 a second dome was added to BOOTES-1 dividing the observatory into BOOTES-1A containing the wide field cameras and BOOTES-1B which houses the telescopes. Latter on, two 0.2m telescopes where added to the initial 0.3m telescope, all driven in parallel a unique mount that allowes simultaneous imaging in 2 bands plus spectroscopy (or a third band) in the other telescope (see Fig. 8.6). The current configuration, schematised in Table 8.1 has been working since 2005.

Table 8.1: Equipment of BOOTES-1. Columns display the name of the instrument, optics + detector and field of view.

	BOOTES-1A	
Wide Field Camera	50mm lens + 1k×1.5k CCD	$16° \times 11°$
Very Wide Field Camera	18mm lens + 1k×1.5k CCD	$40° \times 28°$
All Sky Camera	16mm fish eye lens + 4k×4k CCD	180° diameter
	BOOTES-1B	
Wide Field Spectrograph	0.3m telescope + Spectrograph + 1k×1.5k CCD	$43' \times 28'$
Narrow Field Camera	0.2m telescope + 0.5k×0.5k CCD	$30' \times 30'$
Narrow Field Camera	0.2m telescope + 0.5k×0.5k CCD	$30' \times 30'$

During the spring of 2006 a lightning stroke on one of the antennas that are connected to the building that hosts BOOTES-1 observatory. Most of the electronics in BOOTES-1

Figure 8.6: Picture of the current telescope assembly of BOOTES-1B.

were affected, including the computers, electronic boards of the telescope mounts, cameras and weather sensors and consequently the operations had to be stopped. Since then an important human and economic effort has been made to bring back the observatory to operation, and a new, updated BOOTES-1 will start to work again during the summer of 2007. New lightning sensors are now installed in all the BOOTES observatories in order to alert of an upcoming storm with enough time to allow a complete disconnection of the observatory anr to avoid similar damage in the future.

8.3.2 BOOTES-2

BOOTES-2 (see Fig. 8.7) is a simplified version of BOOTES-1 that supports it by giving a stereoscopic view that allows to distinguish between atmospheric and astronomical events with a base line of 240 km. This is also very interesting in the case of meteor observations as it allows to construct entrance trajectories. The equipment is described in Table 8.2.

Table 8.2: Equipment of BOOTES-2. Columns display the name of the instrument, optics + detector and field of view.

BOOTES-2		
Very Wide Field Camera	18mm lens + 1k×1.5k CCD	$40° \times 28°$
All Sky Camera	16mm fish eye lens + 4k×4k CCD	$180°$ diameter
Narrow Field Camera	0.3m telescope + 0.5k×0.5k CCD	$20' \times 20'$

Figure 8.7: Images of BOOTES-2 observatory, in Málaga.

8.3.3 BOOTES-IR

BOOTES-IR is the natural evolution of BOOTES towards the near-infrared. It is based on a fast slewing 0.6 m f/8.0 Richtey-Chrètien telescope, capable of reaching speeds of 20°/s, that make it one of the fastest telescopes of the World in its category. This allows to reach any part of the sky in less than 20 seconds, with a typical slew time of about 5 seconds. It has two Nashmyth foci, one for the near-infrared and optical cameras and the other one idle, although future instrumentation is foreseen. BOOTES-IR was built with the collaboration and experience of the team that built REM (Chincarini et al. 2003), a similar telescope that was installed in the southern hemisphere at La Silla Observatory, in Chile during 2003.

Figure 8.8: Picture of BOOTES-IR during nigh time operation illuminated by the full Moon.

The site of this observatory is Sierra Nevada Mountains (see Fig. 8.8), near the city of Granada. Its high altitude and dry climate make it ideal for near-infrared observations. The observatory is in the middle of a sky resort, so access and support is granted all through the year, even after heavy snow storms.

Table 8.3: Equipment of BOOTES-IR. Columns display the name of the instrument, optics + detector and field of view.

BOOTES-IR		
Fast optical camera	0.6m telescope + 0.5k×0.5k EMCCD camera	$6' \times 6'$
Near infrared camera	0.6m telescope + 1k×1k nIR detector	$12' \times 12'$

The main instrument of the observatory (see Table. 8.3) is a near infrared camera with a HgCdTe Hawaii detector sensitive from 0.9 to 2.5 μm with 1024×1024 pixels at a scale of $0.7''$/pixel, providing a field of view of $12'\times12'$ (see Fig. 8.9). The dithering of the images is achieved by using a rotating tilted window (dithering wedge) that displaces the images in a circular pattern. This allows to latter correct the sky background (see chapter 10 for details on the procedure). The camera is now undergoing final tests and is expected to be installed on the telescope before the end of the Summer of 2007. BOOTES-IR will simultaneously work with an optical camera through the use of a dichroic that divides the light beam at around 900 nm with a minimum light loss. The optical camera is already working at the telescope and producing the first scientific results. This simultaneous observation in two bands will allow to more reliably identify the optical counterparts of gamma-ray bursts as they have proved to be significantly redder than typical field objects such as stars or galaxies (Gorosabel et al. 2002).

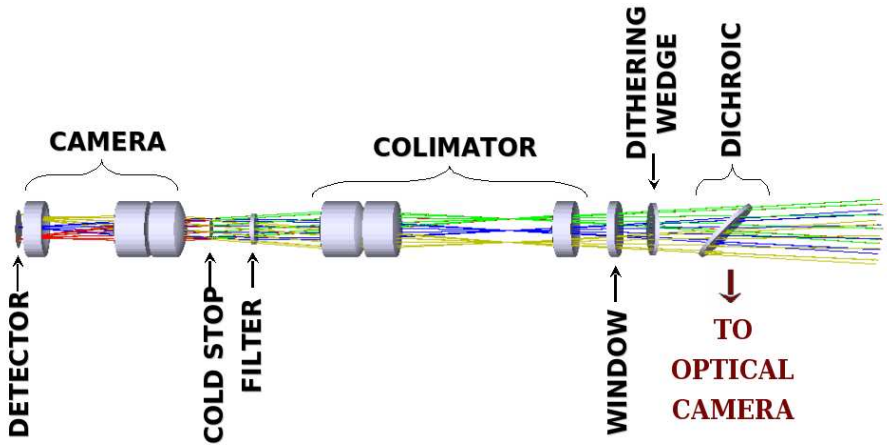

Figure 8.9: Scheme showing the optical arrangement of the near infrared camera.

8.4 Technological developments

During the lifetime of the BOOTES project, many scientific developments have been undertaken in order to overcome problems that were not solved by commercial devices. Among them we have the automatic dome system based in the data provided by a weather station (T.J. Mateo Sanguino & S. Vitek) or RTS-2, the observatory control software (P. Kubankek) which manages the different devices of the observatory. In this section we will concentrate on the technological developments in which the author has had an active participation.

8.4.1 Wide field spectrograph

During the Autumn of 1999 we designed a wide field spectrograph that, installed in the Cassegrain focus of the 0.3 m telescope allows to obtain spectra of all the point sources located in a field of $43' \times 28'$ down to a limiting magnitude of R$\sim$13. This system can cover the initial error boxes of gamma-ray bursts and can quickly change from spectroscopic to imaging mode if needed. The spectrograph was built by Ondřejov observatory (Czech Republic) and saw first light in November 2000. The spectrograph is shown in Fig. 8.10.

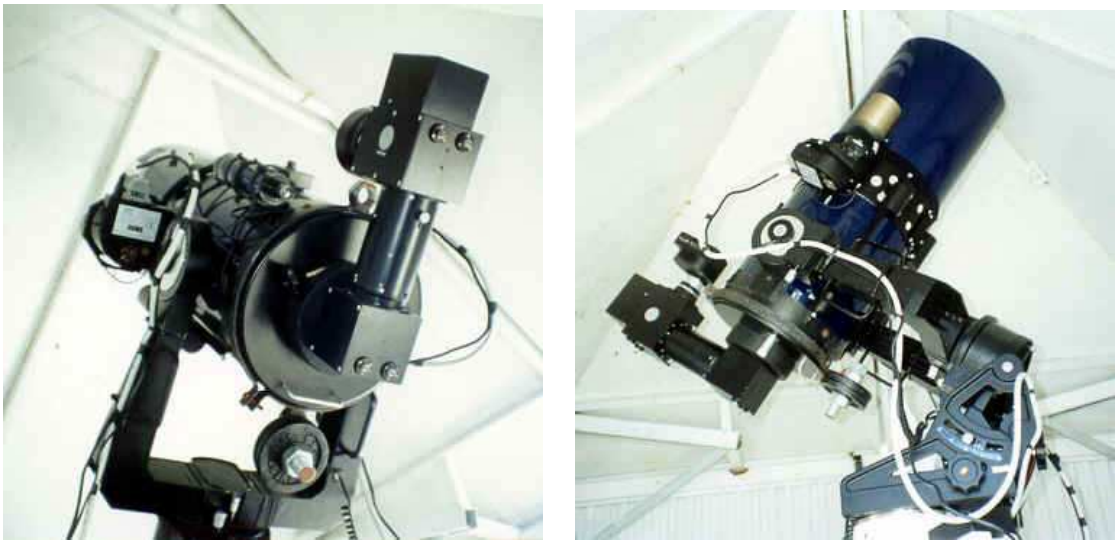

Figure 8.10: Pictures of the wide field spectrograph with its original assembly on the 0.3m Schmidt Cassegrain telescope in BOOTES-1.

The light that is collected by the telescope is collimated, then dispersed by a direct vision prism and finally concentrated by an additional lens that focuses the light onto a CCD. The prism is mounted with a mechanism that allows it to be removed from the optical path to produce a direct image of the field. As collimator we are using a 135 mm focal length photographic lens and a 50 mm one as camera. The difference in focal lengths works as a focal reducer that allows to cover a wider field of view. An example of the images produced by the spectrograph is shown in Fig. 8.11, while some technical details are given in Table 8.4.

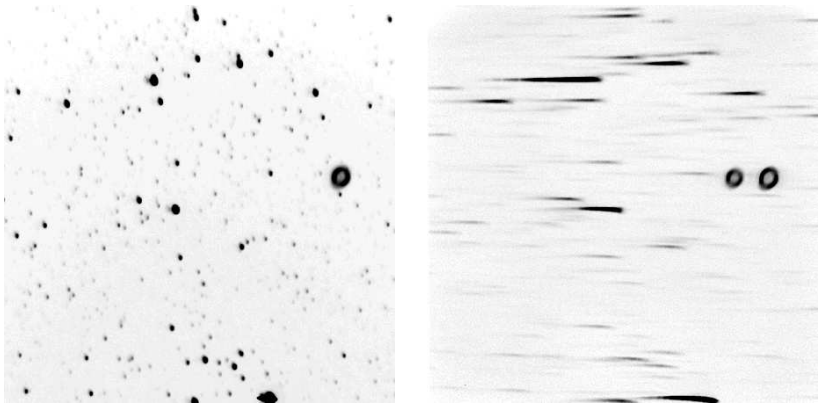

Figure 8.11: Images of field of M57, the ring planetary nebula through the spectrograph, without the prism (left) in the optical path and with the prism inserted (right). Prominent emission of Hα 6 563 λ and [OIII] 5 007 λ is noticeable.

Table 8.4: Technical specifications of the wide field spectrograph mounted on a 0.3m f/10 telescope

Wide field spectrograph	
Field of view	$43' \times 28'$
Dispersing element	Direct vision prism (SK16 + F2)
Dispersion	4 Å/pixel at 4 000 Å
	30 Å/pixel at 5 500 Å
	100 Å/pixel at 8 000 Å
Limiting magnitude	13.5 in 30s (spectrograph mode, 3-sigma)

The design of the spectrograph is registered for Spain in the *Oficina Española de Patentes y Marcas* as Utility Patent number **U 200201303**. At the time in which the spectrograph was designed, the afterglows of gamma-ray bursts were expected to be commonly reaching peak magnitudes brighter than R$\sim$12, as was the case of GRB 990123 which peaked at R$\sim$9. However, experience has shown that this was a very exceptional case, and afterglow searches using the spectrograph have shown to be unfruitful. An upgrade of the spectrograph with a lower, more uniform dispersion for a larger telescope which will reach dimmer magnitudes is foreseen.

8.4.2 Image reduction and analysis software

A robotic observatory such as BOOTES generates large amounts of data, as there are numerous instruments working simultaneously in an efficient way. These data can not be handled manually and due to the lack of appropriate automatised pipelines we decided to develop our own utilities. The result was the JIBARO package (see Chapter 9), which is described in the following chapter. This software automatically reduces and analyses all the data produced by the observatory searching for transient sources like the afterglows of gamma-ray bursts.

8.5 Scientific results

Since its very beginning BOOTES observatories began to produce scientific results (Castro-Tirado et al. 2000a; Castro Cerón et al. 2001a; Castro Cerón et al. 2001b; Castro Cerón et al. 2001c). Although the main scientific interest has been gamma-ray bursts, BOOTES has been very productive in other fields, specially in the study of meteors, resulting in several refereed publications. Throughout this section we present some examples of results obtained with the BOOTES observatories. We will concentrate on some of the scientific achievements in which the author has had and active participation.

8.5.1 Gamma-ray bursts

More than 100 gamma-ray burst alerts have been followed by BOOTES observatories since the first light of BOOTES-1. Here we present some examples of the work that has been done with these observations

GRB 000313: Detection of an optical transient in the error box of a short GRB

On the 13^{th} March 2000 BATSE was triggered by a short (0.5 s) hard burst. The alert was received by BOOTES-1 which immediately started to cover the error box with a mosaic using a wide field camera, due to the large size of the error box. On an image obtained 4 minutes after the gamma-ray event, a point-like source was detected with an I-band magnitude of 9.4±0.1 (see Fig. 8.12). The next image was obtained 53 minutes after the burst and the object was no longer visible. This would have been the first ever detection of the counterpart of a short hard burst, but further deep searches with bigger telescopes failed to detect the decaying afterglow, so the association with the GRB could not be confirmed. The results of these observations where reported in a GRB circular and later published in a paper (Castro-Tirado et al. 2000b; Castro-Tirado et al. 2002).

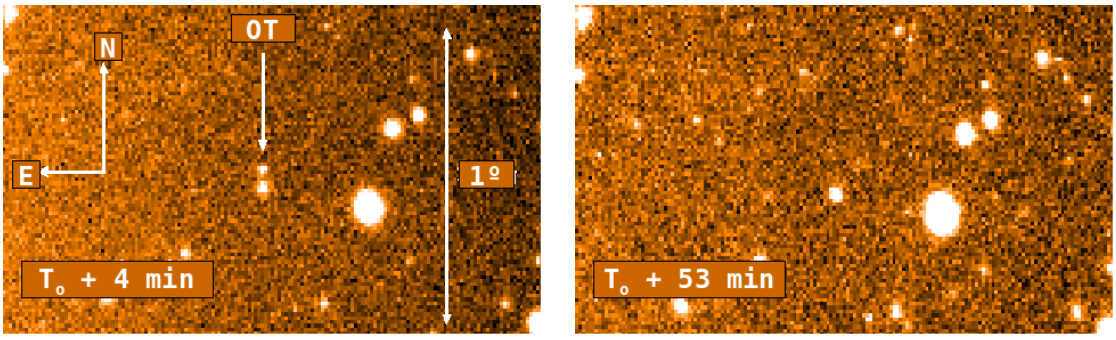

Figure 8.12: BOOTES responded to the BATSE trigger generated for GRB 000313, a short burst and detected a point-like source inside the error box. The object is no longer detectable on an image obtained 53 minutes after the burst.

GRB 030226: Observation of the error box before, during and after the burst

GRB 030226 was detected by *HETE-2* while the wide field cameras of BOOTES-1 were observing the field. Although an optical counterpart was discovered (Fox et al. 2003), we did not detect any bright optical flash before, during or after the event, showing that the flash recorded for GRB 990123 had been an exceptional event. The result of this observation, shown in Fig. 8.13, was reported by Castro-Tirado et al. (2003).

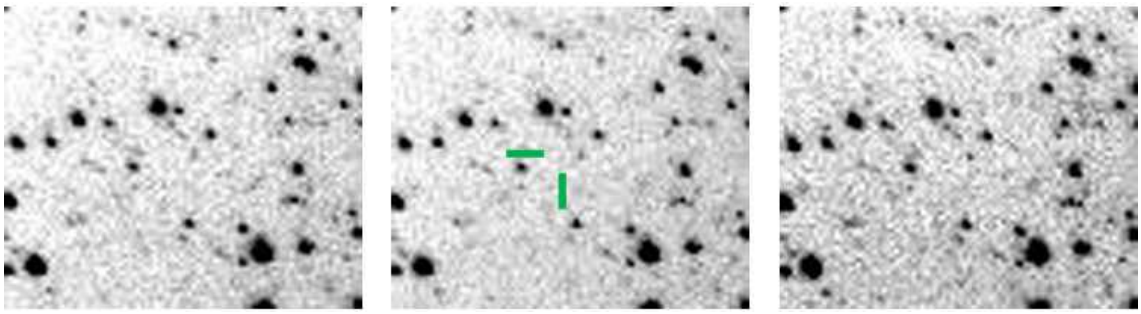

Figure 8.13: During GRB 030226 BOOTES was covering the field of *HETE-2* with the wide field cameras and observed before, during and after the burst, imposing limits to the pre-GRB and prompt emission. The images shown here range in time from -335 to -155 (left), from -87 to +133 (centre) and from +201 to +381 seconds (right) considering the onset of the burst as 0 seconds.

GRB 050525: Simultaneous observations from BOOTES-1 and BOOTES-2 contemporaneous to the gamma-ray event

GRB 050525 was an intense gamma-ray burst with a bright counterpart (Rykoff et al. 2005) detected by *Swift*. We observed it simultaneously from BOOTES-1 and BOOTES-2 using the all-sky cameras (Castro-Tirado et al. 2007) and imposed a limit to the prompt optical flash of 9 magnitudes (see Fig. 8.14). The result was reported in a GRB circular (de Ugarte Postigo et al. 2005a).

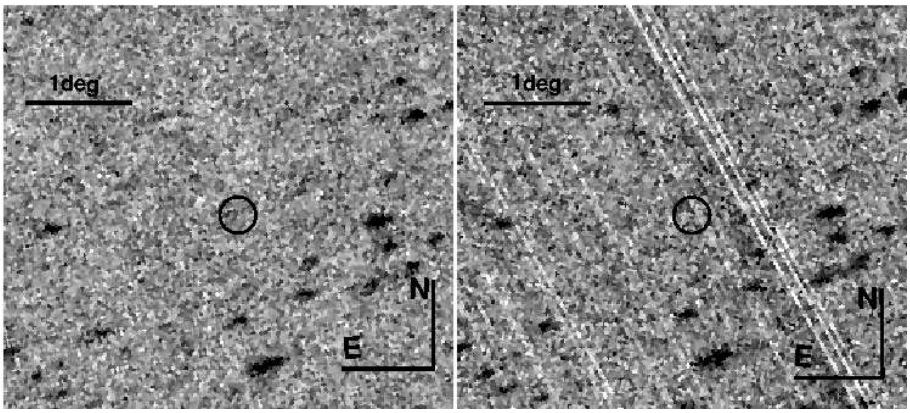

Figure 8.14: GRB 050525 was observed by the all-sky cameras at BOOTES-1A (left) and BOOTES-2 (right) while the gamma-ray emission was still ongoing.

GRB 050904: Observation of the furthermost gamma-ray burst

GRB 050904 is to date the furthermost burst ever detected, with a redshift of 6.29 (Kawai et al. 2005). BOOTES-1 responded automatically to this alert and started imaging 124 s after the alert. Our observations were obtained with an R-band filter and no detection was achieved in spite of the deep images, as shown in Fig. 8.15. This was an indication that the Lyman break was lying at longer wavelengths, implying an extremely high redshift. Further observations obtained by our team from Calar Alto did show the object when using longer wavelength filters. The results are published by Haislip et al. (2006).

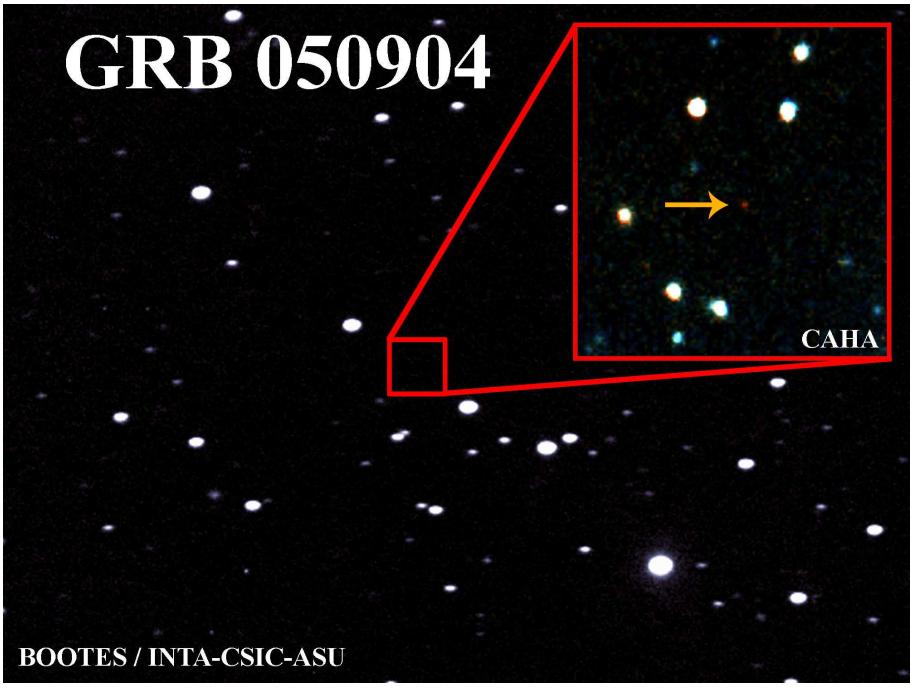

Figure 8.15: Image of the field of GRB 050904, the furthermost gamma-ray burst detected to date, at a redshift of z=6.3. The observations of BOOTES failed to detect the counterpart because the Ly break fell at higher wavelengths. The inset shows a detection obtained at Calar Alto using longer wavelength filters.

GRB 060707: The first afterglow discovered by BOOTES-IR

GRB 060707 was the first optical counterpart of a GRB discovered from BOOTES-IR. The observations began 3.83 hours after the event due to observability constrains. In the preliminary analysis no source was detected (de Ugarte Postigo & Gorosabel 2006a), however a more careful reduction showed an object at an R-band magnitude of around 20.2 (de Ugarte Postigo et al. 2006b), which is marked in Fig. 8.16. After the alert we triggered the VLT at Paranal Observatory to obtain spectroscopy and measured a redshift of 3.43 (Jakobsson et al. 2006a; Jakobsson et al. 2006b).

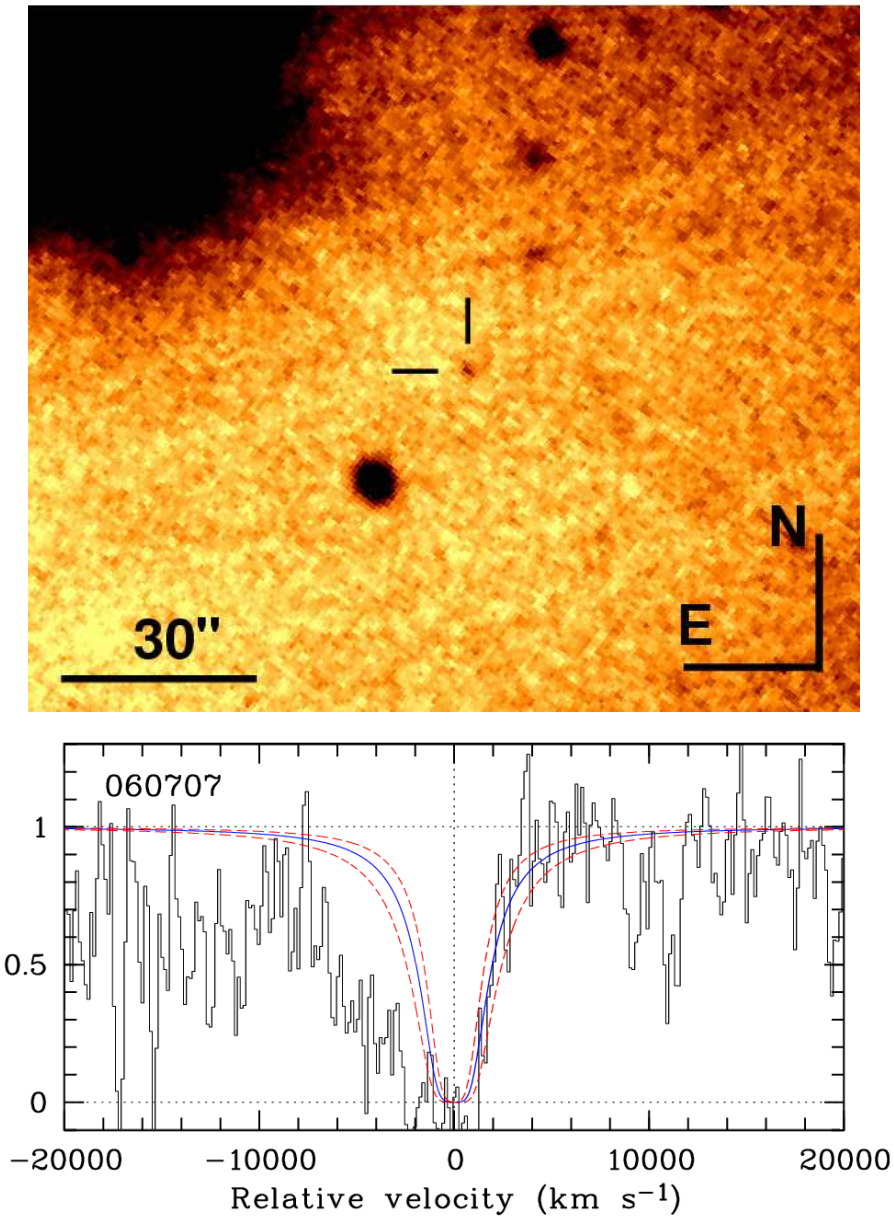

Figure 8.16: Top: Image showing the location of the afterglow of GRB 060707, discovered by BOOTES-IR. Bottom: Detail of the spectra of GRB 060707 obtained with VLT showing the Lyman-α absorption (Jakobsson et al. 2006b).

8.5.2 Secondary science and meteors

Apart of gamma-ray bursts, BOOTES is being used for other branches of Astronomy. Variable star studies and supernova searches and studies are a common issue. A very prolific topic for BOOTES has been the study of meteors, through a collaboration with Dr. Josep María Trigo Rodriguez, which has resulted in several publications (Trigo-Rodríguez et al. 2001; Trigo-Rodríguez et al. 2003; Trigo-Rodríguez et al. 2004; Trigo-Rodríguez et al.

2005a; Trigo-Rodríguez et al. 2005b). In Fig. 8.17 and Fig. 8.18 we have an example of some spectacular results in meteor studies. First, we show a bright meteor that was recorded during the Leonid storm of 2000 that left a track that could be followed as it evolved in the atmosphere for more than 10 minutes. The following figure shows an extremely bright fireball that was registered the 27^{th} January 2003 that reached an amazing magnitude of -17. Thanks to the data gathered by BOOTES-1, both in the all-sky and in wide field cameras the trajectory of the fireball be computed.

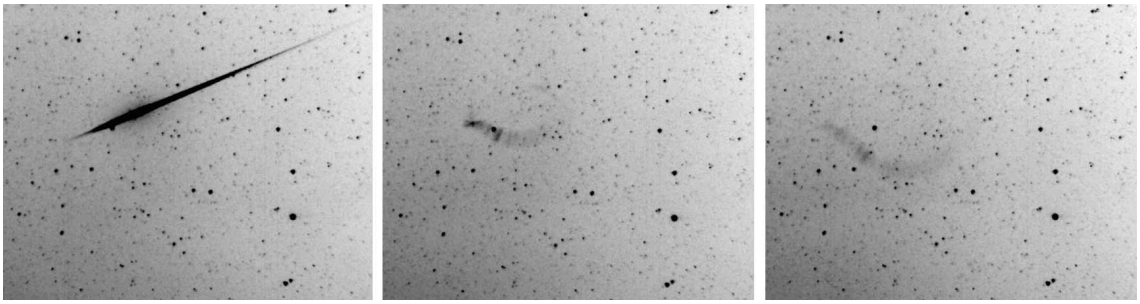

Figure 8.17: During the Leonid shower of November 2000 BOOTES recorded a meteor that left a trace that could be followed for more than 10 minutes as it evolved in the atmosphere.

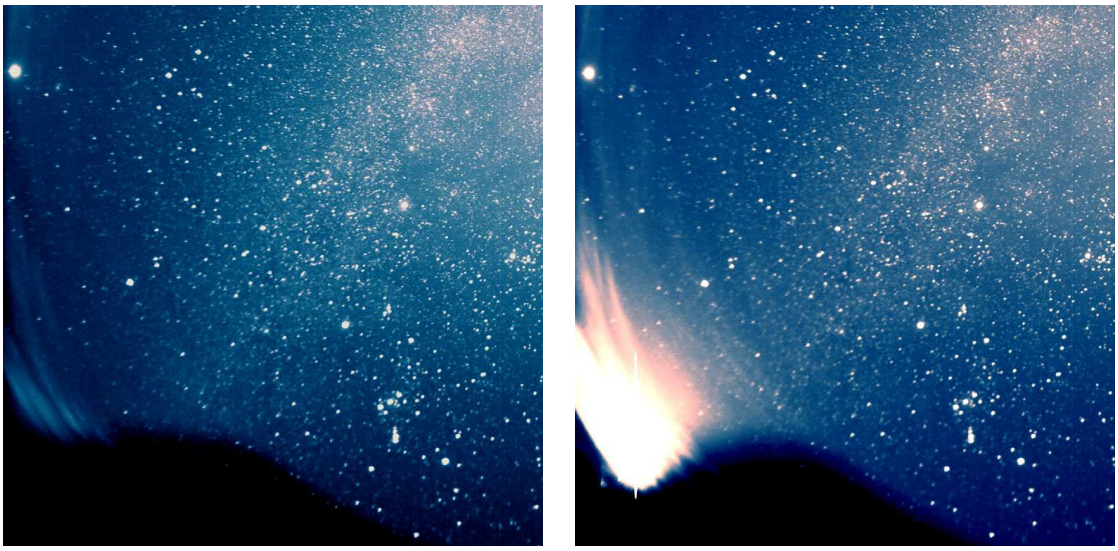

Figure 8.18: Images of a very bright meteor recorded by the all sky camera of BOOTES-1A. At the left we see an image of the sky obtained a few seconds before the occurence of the meteor and at the right the image with the meteor, which saturates the detector at its brightest moments, when it reached a magnitude of -17. The event was also recorded by one of the Wide Field Cameras.

8.6 Conclusions

After almost nine years since the first light of a BOOTES telescope, the project is now composed of 3 observatories separated by a baseline of 300 km, which are equipped with 5 telescopes and 9 cameras. The author has collaborated in most of the phases and technological developments of the project, of which we emphasise on the development of a wide field spectrograph and an image reduction and analysis software package.

The observatories have been providing scientific results since the very beginning. BOOTES has followed more than 100 GRBs, resulting in many GCN circulars, proceedings and refereed papers. Secondary science has also been accomplished, with special productivity in the study of meteors.

The development of the observatories is still ongoing and a nIR camera will soon be installed on BOOTES-IR telescope. An upgrade is also foreseen that will provide the different observatories with new 0.6 m telescopes that will make the observations more efficient by allowing the detection of fainter GRB afterglows.

Bibliography

Castro Cerón, J. M., et al. 2001a, Gamma-ray Bursts in the Afterglow Era, 53

Castro Cerón, J. M., et al. 2001b, Highlights of Spanish astrophysics II, 37

Castro Cerón, J. M., et al. 2001c, ESA SP-459: Exploring the Gamma-Ray Universe, 407

Castro-Tirado, A. J., Hudec, R., & Soldán, J. 1996, American Institute of Physics Conference Series, 384, 814

Castro-Tirado, A. J., et al. 1999, A&AS, 138, 583

Castro-Tirado, A. J., et al. 2000a, Gamma-ray Bursts, 5th Huntsville Symposium, 526, 260

Castro-Tirado, A., et al. 2000b, GRB Coordinates Network, 612, 1

Castro-Tirado, A. J., et al. 2002, A&A, 393, L55

Castro-Tirado, A. J., et al. 2003, GRB Coordinates Network, 1887, 1

Castro-Tirado, A. J., et al. 2004, ESA SP-552: 5th INTEGRAL Workshop on the INTEGRAL Universe, 637

Castro-Tirado, A. J., et al. 2006, Proc. SPIE, 6267

Castro-Tirado, A. J., et al. 2007, in preparation

Chincarini, G., et al. 2003, The Messenger, 113, 40

Fox, D. W., Chen, H. W., & Price, P. A. 2003, GRB Coordinates Network, 1879, 1

Gorosabel, J., et al. 2002, A&A, 384, 11

Haislip, J. B., et al. 2006, Nature, 440, 181

Hudec, R., et al. 1999, Blazar Monitoring towards the Third Millennium, 131

Jakobsson, P., Tanvir, N., Jensen, B. L., Fynbo, J. P. U., de Ugarte Postigo, A., Gorosabel, J., Klose, S., & Vreeswijk, P. 2006a, GRB Coordinates Network, 5298, 1

Jakobsson, P., et al. 2006b, A&A, 460, L13

Jelinek, M., de Ugarte Postigo, A., Kubanek, P., Sanguino, T. J. M., Castillo, S., Gorosabel, J., Guziy, S., & Castro-Tirado, A. J. 2005, GRB Coordinates Network, 3285, 1

Kawai, N., Yamada, T., Kosugi, G., Hattori, T., & Aoki, K. 2005, GRB Coordinates Network, 3937, 1

Kubánek, P., Jelínek, M., Vítek, S., de Ugarte Postigo, A., Nekola, M., & French, J. 2006, Proc. SPIE, 6274

Mateo Sanguino, T. J., et al. 2004a, Astronomical Society of the Pacific Conference Series, 312, 536

Mateo Sanguino, T. D. J., et al. 2004b, Gamma-Ray Bursts: 30 Years of Discovery, 727, 761

Perez-Torres, M. A., Jelinek, M., Gorosabel, J., de Ugarte Postigo, A., Castro-Tirado, A. J., Sota, A., & Alberdi, A. 2005, IAU Circ., 8546, 2

Rykoff, E. S., Yost, S. A., & Swan, H. 2005, GRB Coordinates Network, 3465, 1

Trigo-Rodríguez, J. M., et al. 2001, WGN, Journal of the International Meteor Organization, 29, 139

Trigo-Rodríguez, J. M., Castro-Tirado, A., Llorca, J., de Ugarte Postigo, A., Sanguino, T. M., & Galvez, F. 2003, WGN, Journal of the International Meteor Organization, 31, 49

Trigo-Rodríguez, J. M., et al. 2004, Earth Moon and Planets, 95, 553

Trigo-Rodríguez, J. M., et al. 2005a, Earth Moon and Planets, 97, 269

Trigo-Rodríguez, J. M., et al. 2005b, WGN, Journal of the International Meteor Organization, 33, 5

de Ugarte Postigo, A., et al. 2003, Gamma-Ray Burst and Afterglow Astronomy 2001: A Workshop Celebrating the First Year of the HETE Mission, 662, 553

de Ugarte Postigo, A., et al. 2005a, GRB Coordinates Network, 3376, 1

de Ugarte Postigo, A., et al. 2005b, GRB Coordinates Network, 3480, 1

de Ugarte Postigo, A., & Gorosabel, J. 2006a, GRB Coordinates Network, 5288, 1

de Ugarte Postigo, A., Gorosabel, J., Jelinek, M., Cunniffe, R., Kubanek, P., Vitek, S., Castro-Tirado, A. J., & Sabau-Graziati, M. D. 2006b, GRB Coordinates Network, 5290, 1

de Ugarte Postigo, A., et al. 2006c, GRB Coordinates Network, 5968, 1

9

JIBARO: Tools for automatic image analysis

A robotic observatory must not only be able to do autonomous observations, but also to handle the data that is generated and make use of it. The last step is to give the observatory the ability to use the data obtained in the observations to modify the observing plan without human intervention.

JIBARO (**J**oined ut**I**lities in **B**OOTES for the **A**nalysis and **R**eduction of **O**bservations) is a group of programs created in the context of the BOOTES project to reduce and analyse astronomical images in real time. The results of this analysis are used to interact with the observatory itself and to generate external alerts that communicate a relevant astronomical event to the scientists.

9.1 Introduction

JIBARO (de Ugarte Postigo et al. 2005) was conceived in the context of BOOTES (see Chapter 8) in 2000, when the rate of data that was being produced by the observatory became greater than the time needed to analyse it manually. The aim of JIBARO is the reduction and analysis of optical and infrared images without human intervention. It analyses the objects in the field in real-time, searching for new sources and variability by comparing with deep catalogues and archive images. Among the possible uncatalogued objects that are detected, our main interest are the optical and near infrared counterparts of GRBs. The analysis of the images obtained by the observatory can be used to modify the subsequent observations and to alert the astronomer about potentially interesting discoveries.

JIBARO is composed of a group of programs written in C that are linked through shell scripts under a Linux environment, so they can be used in many different ways. The codes that are described here were initially based on the OPERA package created by C.E. García Dabó (García-Dabó & Gallego 1998), from which we extracted the basic routines that evolved to create JIBARO. Additional libraries used here are FITSIO (Pence 1999), WCSTOOLS (Mink 2002) and LIBNOVA [1].

[1] http://libnova.sourceforge.net/

9.2 Image reduction

The image reduction codes receive the scientific raw image as an input, together with the corresponding calibration images. The programs calculate the processed image and an estimate of the error balance for each pixel.

9.2.1 Bias correction

In order to have a correct readout of the chip, each pixel is charged to a certain zero-level that must be later subtracted by software during reduction. In order to correct for this effect we use an image with an exposure time of 0 seconds, so that all the counts that are registered correspond to the bias and not to incident photons (see Fig. 9.1). We generally use several images (at least 3 but preferably 5 or more) in order to be able to average, discarding spurious signals and reducing the noise. This bias image (I_b) is subtracted from the raw scientific image (I_S) to create the bias corrected scientific image (I_{Sb}).

$$I_{Sb} = I_S - I_b \tag{9.1}$$

The error of this operation is, in the simplest case, the one of the raw image plus the one of the bias image, that can be obtained, pixel by pixel, from the standard deviation of all the images that were averaged to create the final bias.

$$\delta I_{Sb} = \delta I_S + \delta I_b \tag{9.2}$$

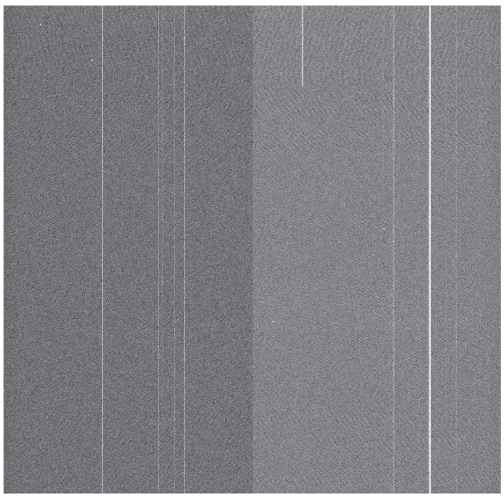

Figure 9.1: BIAS image.

9.2.2 Dark frame correction

In addition to the charge that gets generated due to incident photons, the detector accumulates thermal noise that grows with exposure time and temperature. This is the reason

why astronomical cameras, which necessarily use long exposure times, need to be cooled to very low temperatures. Professional astronomical detectors, usually cooled by liquid Nitrogen or Helium, have very small dark current and this correction is not normally necessary. However, in lower segment cameras in which refrigeration is not so efficient (normally thermoelectric) this contribution must be removed. An example is shown in see Fig. 9.2

The dark current image, usually referred to as *dark frame* (I_d), is an image of equal exposure time to the scientific image, obtained with the detector cooled to the same temperature as it is during the scientific image, but with the shutter closed. The image should be obtained as shortly before or after the scientific image as possible in order to avoid long term variability in the properties of the chip. The dark corrected image (I_{Sd}) is:

$$I_{Sd} = I_S - I_d \tag{9.3}$$

As the dark frame includes the bias the previous correction is not necessary, thus saving computation time. The errors are calculated in the same way as before. In order to reduce the uncertainty of the dark frame it is useful to use an average of several images as in the case of bias. This combination is even more important in this case because long exposure can be easily affected by cosmic rays.

$$\delta I_{Sd} = \delta I_S + \delta I_d \tag{9.4}$$

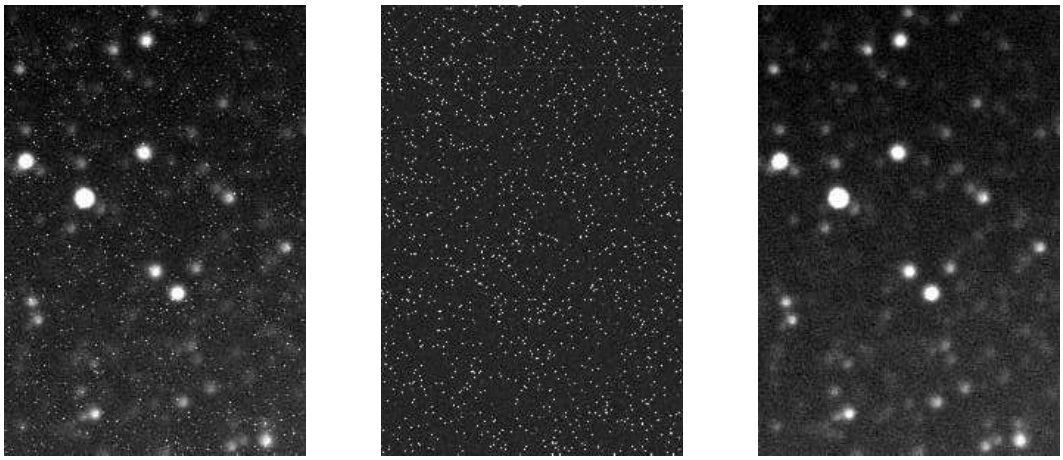

Figure 9.2: Left: Image obtained with one of the BOOTES-1 cameras showing the effect of dark current. Centre: Dark frame obtained with the same exposure time. Right: The same image corrected with the dark frame.

9.2.3 Flat field correction

Each pixel of a camera acts as an individual detector, with a unique efficiency. This differential response is due to both the individual sensitivity of each pixel to the incident photons and to the different transmission of the intervening optical system (because of vignetting, dust, differential transmisivity of the optics, etc.).

In order to correct for this effect we must obtain an image for which we can assume a uniform illumination, a *flat field*. There are two common methods of obtaining this image: The first is done by pointing the telescope to the sky during the twilight before dawn of after dusk, when the sky brightness hides most stars but does not saturate the detector, we call these *sky flats*. The second method is to observe with the dome closed, pointing the telescope to a uniformly illuminated region of the dome (a flat fielding screen is commonly used), these are normally named *dome flats*. Sky flats are preferred, as their illumination is more similar to the one that astronomical images will have. In any of the two methods, a series of images is obtained. The raw images (I_{fr}) are bias or dark corrected, normalised and combined in order to get the best possible flat field. Although any normalisation can be used we normally assign unity to the mode of the image.

$$I_{fdn} = (I_{fr} - I_d)/mode(I_f r - I_d) \tag{9.5}$$

The final dark-(or bias-)corrected-normalised image (I_{fdn}) is used to divide the scientific image(see Fig. 9.3), so that the final signal obtained at each pixel is proportional to the incident photon flux, a flat-fielded dark-(or bias-)corrected image (I_{Sfd}). If we assume that we are correcting of dark frame, the result would be:

$$I_{Sfd} = I_{Sd}/I_{fdn} \tag{9.6}$$

The error of the corrected image is:

$$\delta I_{Sfd} = I_{Sfd}(\delta I_{Sd}/I_{Sd} + \delta I_{fdn}/I_{fdn}) \tag{9.7}$$

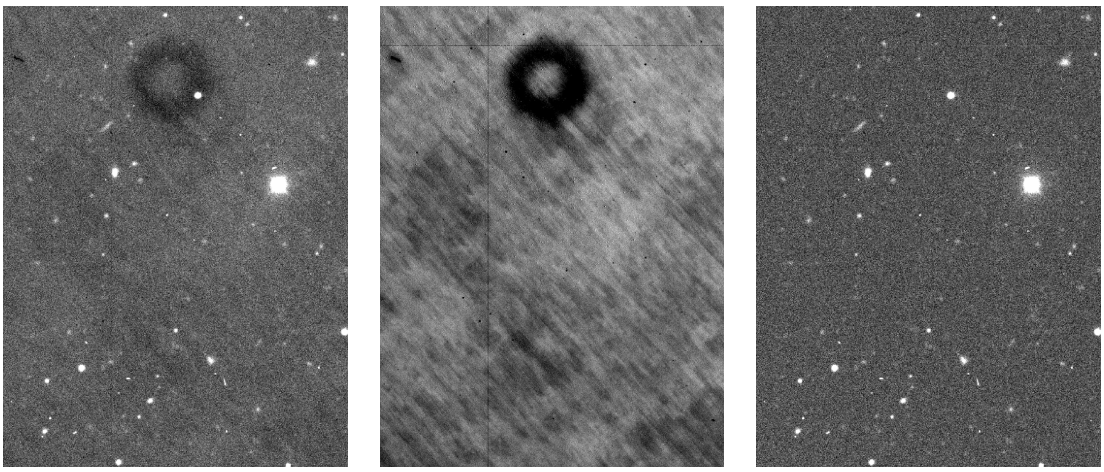

Figure 9.3: Left: Scientific image before flat field calibration. Centre: Flat field image. Right: Flat fielded image.

9.2.4 Sky subtraction

When we observe an object in the sky we have to consider that we are not only receiving the photons that arrive from the object itself, but that we are observing through a medium

that is affecting the received signal by adding, blocking, or dispersing photons. Of all the matter that the light has to travel through, the most important effect is normally produced in the Earth's atmosphere. It is specially important in the case of infrared wavelengths, where there is an important atmospheric emission that can be more significant than signal of the studied object.

The contribution to the image background can be summarised in three effects: Airglow, fringing and dispersed light (due to human produced light pollution or by natural effects like the presence of the Moon). The *airglow* is an emission of light produced by chemical processes that take place in the upper atmosphere, such as the recombination of ions which were photoionised by solar light during the day or the chemiluminescence of the reaction of oxygen and nitrogen with hydroxide ions at a height of a few hundred kilometres. In an astronomical image, the effect of airglow shows as an increase of the background with large scale fluctuations, mainly affecting the near infrared (see Fig. 9.4). This emission is variable with time, and the scale of variance depends on the wavelength, being typically more variable in longer wavelengths. A side effect of airglow appears in very thin detectors with a thickness that is comparable to the wavelength of an airglow emission line. This is what we know as *fringing* and appears as a structure of interference fringes supperposed to the image (see Fig. 9.5) with a slow temporal evolution. This usually affects observations in the reddest optical bands and with near-infrared chips. Finally we find a contribution to the images that is due to the effect of *dispersed light* which can be produced by natural effects, such as the Moon or by human produced light pollution. This effect normally shows as a gradient in the background of the image.

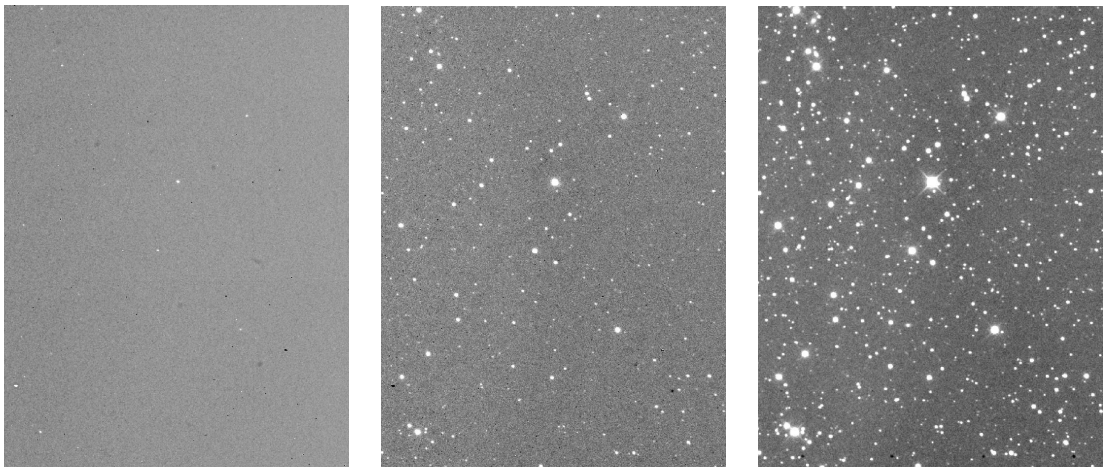

Figure 9.4: The effect of background light is very spectacular in near infrared images, where the sky background can be stronger than the object signal. In order to not saturate the detector with the airglow flux we must obtain short exposures. Here we show the raw image (left), where objects are difficult to detect. When we subtract the sky image the astronomical sources begin to appear (centre). If we then combine several short exposures we can obtain a deep image (right).

All of these contributions to the image background can be corrected simultaneously using a single reduction procedure but should be foreseen when planning the observations

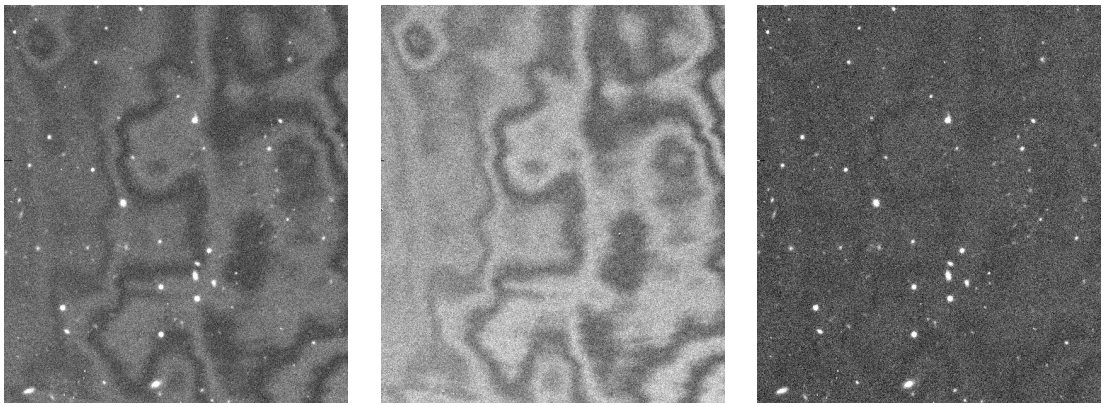

Figure 9.5: Left: I-band image affected of fringing. Centre: Background image obtained as described in the text. Right: Final corrected image.

in order to obtain the data in the appropriate way. The observations must be prepared to produce a good sky image that will be subtracted from the scientific image. While doing the observations we use a technique known as *dithering*, where we obtain several short exposures with slight displacements so that our region of study is still covered by the intersection while the objects are moved enough to not overlap from one image to the other (see Fig. 9.6).

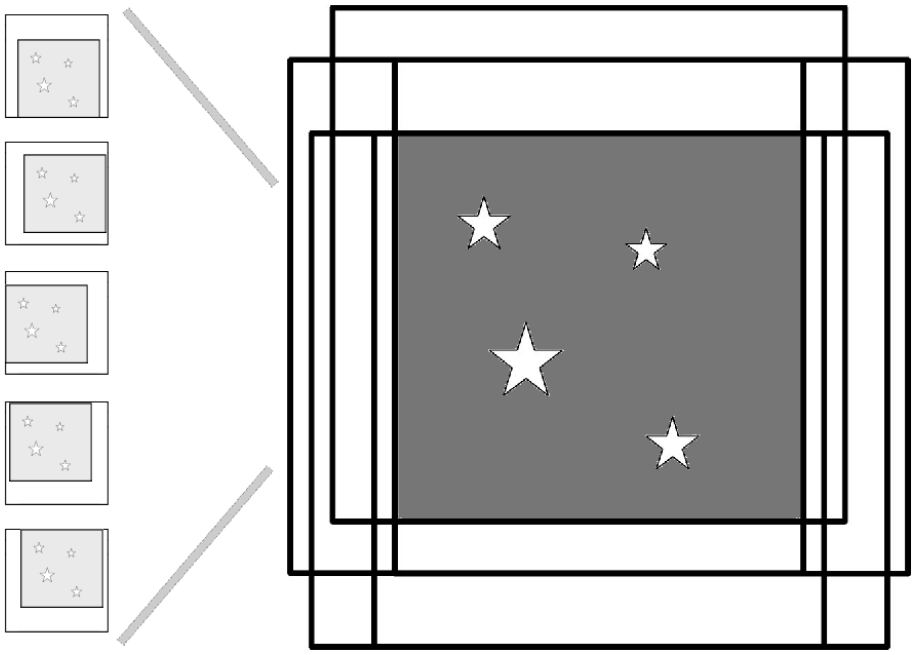

Figure 9.6: Dithering technique: In this figure we see how 5 individual images (left) are obtained using dithering in order to combine them to a single, corrected image (right).

If we obtain the median of the non aligned images, the objects of the field will not overlap

and their contribution will disappear, leaving only the background sky level that reaches the detector. Due to the temporal variability of the background it is best to calculate a unique sky frame (I_s) for each scientific (I_{Sf}) image using the exposures obtained shortly before and after it. It is good to exclude the actual scientific image from the set that will make its own sky image in order to avoid any effect in the place where objects lay in the final frame. The sky image is then subtracted from the scientific image, that should be already flat fielded. The sky corrected scientific images (I_{Ss}) can be then aligned and combined in order to create the final image.

$$I_{Ss} = I_{Sf} - I_s \tag{9.8}$$

$$\delta I_{Ss} = \delta I_{Sf} + \delta I_s \tag{9.9}$$

A more sophisticated approach to sky subtraction is to do it in two cycles. In the first step the reduction of the data is done as described above. From the reduced image, we would locate all the objects in the field. In the second cycle, at the point of creating the sky image, we exclude the regions in which objects are located by masking those pixels. This is useful for deep imaging in which we want to detect very faint objects as it will be creating a cleaner sky image.

The dithering technique explained above is only valid in the case of point-like objects. If we are studying an extended source we must move the telescope to an alternative field close to our observing region in order to create the sky images. In this case we usually alternate one sky frame and one scientific frame until we complete the desired exposure time and then process as explained above.

9.2.5 Linearity correction

Astronomical detectors normally have a linear response to light so that if we double the amount of incoming light we will measure twice as much signal for most of their dynamical range. However, some detectors suffer deviance from this linear regime and must be corrected before we attempt to obtain photometry. Obtaining the response curve of the detector is generally provided in their webpage (see Fig 9.7).

If not provided this response curve can be obtained by acquiring exposures of increasing exposure times with a stable illumination. Through this we obtain a curve that can be fitted by a polynomial. This function is latter used to correct all the observations obtained with the camera.

9.3 Object detection

Once we have the corrected scientific image we proceed to the analysis phase where we will study the information available in the image. The first step would be to detect the sources that are present in the image. There are several ready made tools that help us in this step and most of them are based in a similar structure.

The first step is to establish a background level (which should be near zero if we have done the background subtraction), that should be calculated locally, with its correspondent

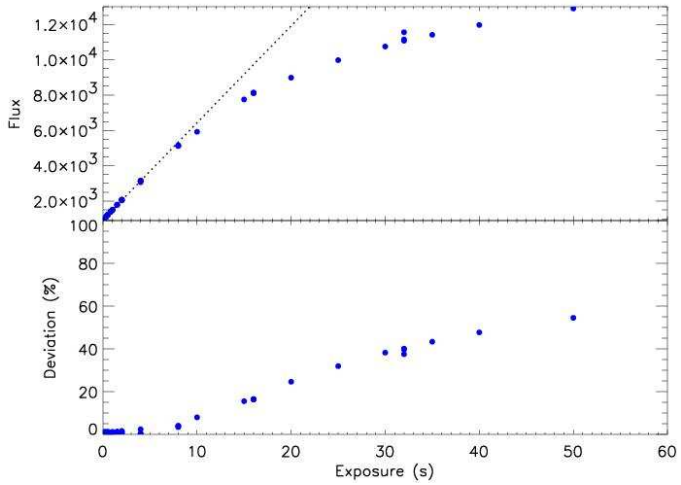

Figure 9.7: Measure of the linearity of an EMCCD camera mounted on BOOTES-IR. A large, but correctable deviation can be seen in these observations obtained with a fixed gain value.

standard deviance or noise level. The software then considers as active pixels those that have a signal that is a certain number of times the noise level above the background (this is a factor that can be tuned by the user depending on the kind of observations that are being made). This is, however, not enough to consider it a detection, as an object in an image is composed of several adjacent pixels. The minimum number of pixels needed to consider that an object has been detected will depend on the plate scale and on the seeing. This will normally allow us to distinguish a real object from a cosmic ray or a hot pixel.

In crowded fields we can have an additional problem to properly detect objects due to overlapping or blending of nearby objects. In order to deblend these objects, the most common method is to progressively increase the detection level, so that at a certain level the peaks of the different objects are separated (see Fig. 9.8).

Once the object pixels are determined, the code calculates the centroid and the total number of counts that make the object (with correspondent errors) which will be useful for obtaining astrometry and photometry respectively. Additional data such as the size and shape of the objects are typical provided by this kind of codes. The output is usually given as a list with one object per line containing the measured properties.

During the development of JIBARO we have tested different detection codes, from which two of them stand out:

- *Createsky and Buhofits*: They are two codes of OPERA package that work together. Createsky determines the sky level for each pixel of the image with its correspondent error by calculating the mode of boxes in the image. Buhofits uses this sky and error images to detect objects. Our experience with this code is quite good specially for detecting objects near the noise limit of the image. However, it is too slow for the real time reduction of images.

- *Sextractor* (Bertin & Arnouts 1996): Is the most widely used tool for the extraction of object catalogues from astronomical images. This code is well optimised and very

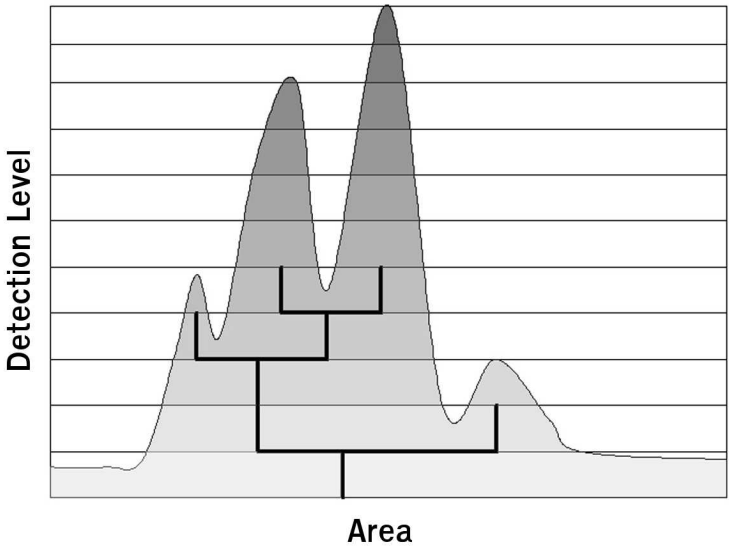

Figure 9.8: Object deblending in the detection software. Adapted from Bertin & Arnouts (1996).

fast, making it suitable for real time reduction of data in robotic observatories. Due to this, sextractor is the code that we have selected to be used in the latest versions of JIBARO.

These detection routines are also used to create the masks that are used for the two step background subtraction.

9.4 Astrometry

The astrometry will calculate the sky coordinates of every pixel in the image. It is one of the most complicated steps in the astronomical data reduction as it requires to take decisions on how to correlate objects in the image with objects in an astrometrical catalogue. If we plan to generalise this to any type of telescope, the task turns out to be even more complex.

Our code accepts as input both the processed image and the list of objects that has been extracted through the detection program. By evaluating the field of view of the image (from the information that is stored in the image header) and the deepness of the image (which can be estimated from the amount of objects detected in the field) the code is capable of deciding which catalogue to use and what range of magnitudes should be used to obtain optimal results. Depending on the band and the needed deepness of the catalogue we may use Tycho-2 (Høg et al. 2000), GSC 1.1 (Jenkner et al. 1990) USNO-A2.0 (Monet 1998) or 2MASS (Skrutskie et al. 2006). Once this decision has been made, the corresponding catalogue is searched and the required objects are extracted. These catalogue objects are compared to the detected ones from the image.

The comparison between detected and catalogue objects is the crucial part of the astrometrical fit. Although the information that we have from the header will give us an estimation of the position in which the stars should be found, depending on the optical

distortion and the quality of the telescope pointing, the offset can be significantly large. Our code is based on several routines extracted from the WCSTOOLS library that are used iteratively and that can take into account the distortion of the image and a considerable pointing error (we have been able to compute correct astrometric solutions for images for which the predicted centre of the image was out of the field). However, and in order to compute faster solutions, we have built a database with the results of the astrometry for each instrument that has been previously used in order to accurately predict the expected distortion.

Once the stars have been correlated with the catalogue, the code applies a polynomial fit that relates each pixel of the image with a sky position. The degree of the polynomial should be chosen depending on the distortion of the image that we are using. Once again we can use the database in order to select the polynomial degree that should be used in each case. The solution that we obtained, known as WCS (World Coordinate System) solution is written into the header using standard keywords so that it may be used by any other astronomical software. Additionally our program returns a list of the detected objects with the corresponding sky coordinates, keeping the information that came from the detection procedure. The precision of the final result depends mainly on the precision of the astrometric catalogue that is used. With USNO-A2.0 the astrometric solutions can have precisions down to $0.2''$

9.5 Photometry

The photometry is made by comparing the measured flux for the objects in the field with the magnitudes of a photometric catalogue. We search for correspondence of each object of our list with those of the catalogue by choosing the nearest object with a maximum acceptable displacement. Once we have gone through the list of detections, we use the correlations to obtain an analytic law that is used to derive the magnitude of each of the objects in the field. In order to eliminate the effect of objects which have been wrongly correlated, we do a sigma clipping of the data and recalculate the analytic law. As the number of bright objects is more scarce than that of dim ones we weight with the flux in order to obtain better results.

Sometimes the flux calculated by Sextractor is not precise enough for our purposes and we prefer to obtain aperture or PSF (Point Spread Function) photometry before going through the photometric routine. For these cases we have prepared several scripts that use DAOPHOT (Stetson 1987) to create the flux files.

9.6 Object detection

When searching for a GRB afterglow, we normally look at a reasonably large field in which we expect to find an uncatalogued object. We have created a routine that helps us to do this work. For this we must try to identify each of the objects in a deep catalogue: USNO-B1.0 (Monet et al. 2003) or SDSS (Adelman-McCarthy et al. 2006) if available. In some cases the deepness of the survey will be limited by the image itself, but in the case of data obtained from a large telescope, the limit will be usually given by the catalogue. The limits of both image and catalogue are calculated by the software in order to provide a correct

matching and to avoid false detections of transient sources. As we are normally searching for point-like objects we will eliminate those with a great ellipticity.

The transient sources can be, however, due to very different causes. Among them we can find detector defects, cosmic rays, meteors that come at approximately the line of sight, flashes from artificial satellites and, of course, real astronomical sources.

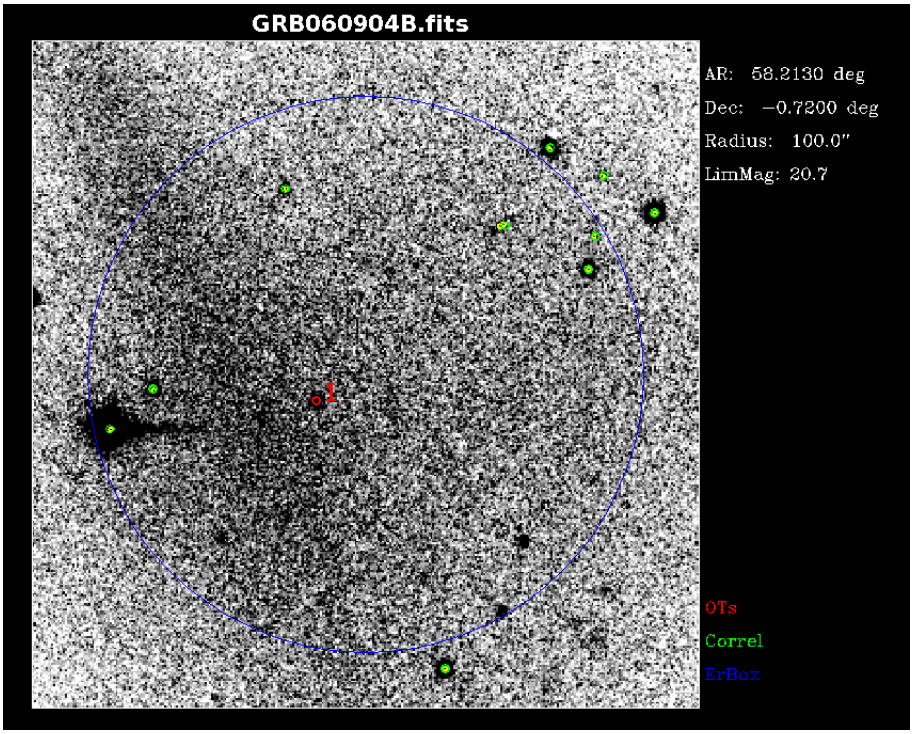

Figure 9.9: Afterglow of GRB 060904B automatically detected by JIBARO in a BOOTES-IR image.

Once a transient object has been detected the information can be transmitted in several ways. On one side, the data is sent to the planner software of the observatory to adjust forecoming observations to the optimal sequence of exposure and filters considering the brightness of the source and can even correct the pointing if necessary. On the other side, the information is communicated to the observer through an email which can contain an image showing the newly detected source, as shown in Fig. 9.9.

9.7 Other utilities

In parallel to the creation of image reduction codes for BOOTES, we developed other utilities come out that allow us to use JIBARO in a more general way or even for other purposes. In the following section we present some of them.

9.7.1 Header correction

A great amount of the information needed to do the image analysis is found in the image header. Although the structure of these headers is standardised through the FITS[2] (Flexible Image Transport System) format, the way in which they are used is not. Different observatories use different keywords to store the same information in their image headers. Consequently, these headers must be homogenised to the JIBARO format in order to be correctly interpreted by our programs.

This code has information of the way in which different observatories create their headers, so that it is capable of identifying which instrument created the images and reconstruct them accordingly. A compilation of the instruments recognised by the header correction software is given in Table 9.1. An additional manual option allows the user to introduce the approximate image information if it is not contained in the header using one of the available instrument profiles.

Table 9.1: Instruments recognised by the header correction software

INSTRUMENT	TELESCOPE	OBSERVATORY
ROPER	1.5m	OSN
OMEGA-2000	3.5m	CAHA
OMEGA-CASS	3.5m	CAHA
LAICA	3.5m	CAHA
CAFOS	2.2m	CAHA
BUSCA	2.2m	CAHA
MAGIC	1.5/2.2m	CAHA
PFIC	4.2mWHT	ORM
LIRIS	4.2mWHT	ORM
NICS	3.5mTNG	ORM
WCF	2.5mINT	ORM
ALFOSC	2.5mNOT	ORM
SCORPIO	6.0mBTA	SAO
FORS	8.1mVLT	Paranal
MOA	0.6m	Mt. John

9.7.2 Image combination

Using the astrometrical solution, we can combine images of a unique field with great precision, taking into account, displacements, rotations and different scales. For this we have created a shell script that calls several IRAF (Tody 1986) routines that account for the coordinate transformation and combine the images.

9.7.3 Colour combination

Once more, through the use of the astrometrical solution that we have calculated we can align images obtained with different filters to create colour compositions. We then adjust the background levels and the signal in order to combine them assigning a consistent value for each band. In order to achieve a more realistic effect in the combined image we have

[2]http://fits.gsfc.nasa.gov/fits_home.html

used a code that assigns each image the real colour of the central wavelength of the observed band[3]. In Fig. 9.10 we show an example of one of these compositions.

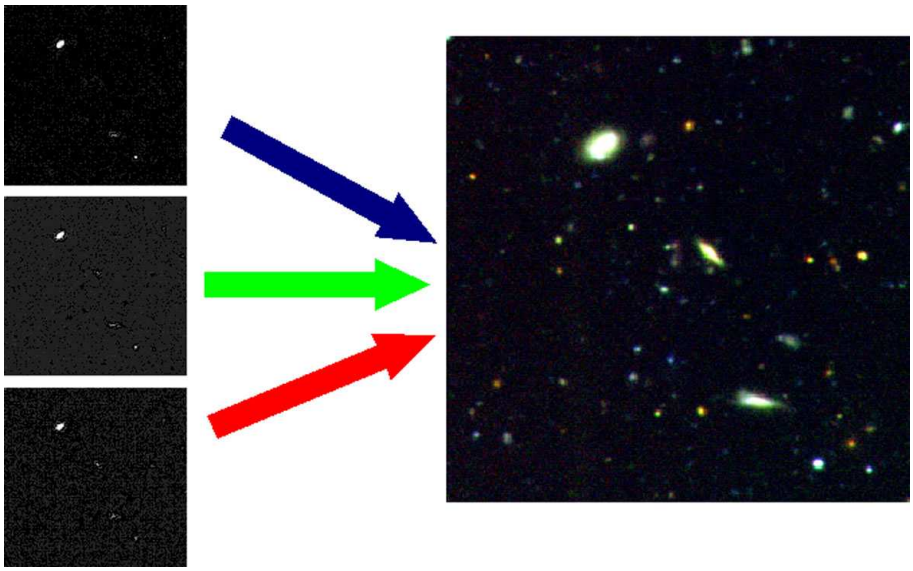

Figure 9.10: Example of colour combination. This images, from the field of GRB 030329 where obtained with the 2.2m telescope at Calar Alto and BUSCA camera.

9.7.4 Pointing correction

When used in real time, the information extracted from the astrometry can be fed to the observatory manager which will update the pointing information and introduce corrections if necessary. This is specially interesting for small robotic observatories based on amateur mounts that have considerable pointing uncertainties. JIBARO is optimised for being used with RTS2 (Kubánek et al. 2006) observatory manager.

9.7.5 Object simulator

In order to test the behaviour of the object detection software we created a code that can introduce a simulated point-like object in the image that will have a point spread function of similar shape to the rest of objects from the image (see Fig. 9.11). This has been also found useful to create images and videos for public outreach.

9.8 Working procedures

Being a group of independent codes, JIBARO may be used in many different ways and for many different purposes. Each individual camera will need different reduction techniques. Here we give several examples of the routines that we normally use. A summary of the processing algorithms used for each of them is given in Table. 9.2. General reduction with

[3]http://www.midnightkite.com/color.html

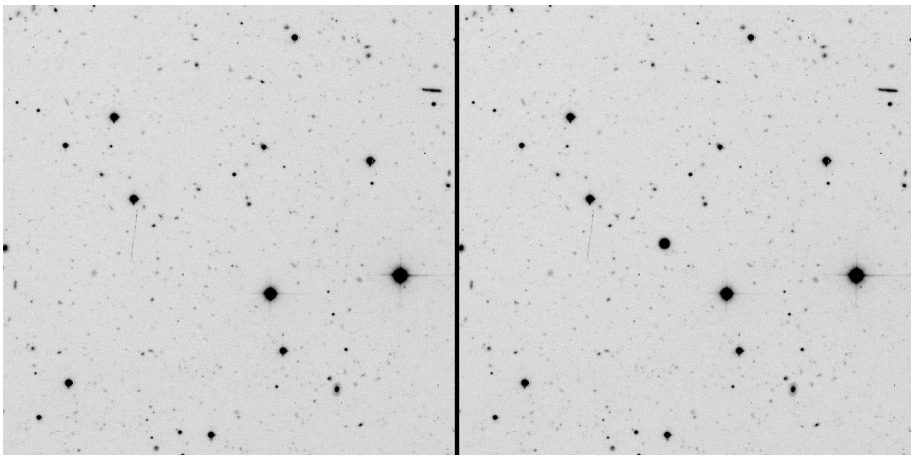

Figure 9.11: Image before (left) and after (right) going through the simulation software, where a new bright object, simulating a GRB, has been added.

JIBARO normally ends with the astrometry of the image. The final phases of photometry and object detection are used in the robotic observatory mode:

Thermoelectrically cooled optical CCD cameras

These cameras are cooled to 30-60°C bellow ambient temperature and their thermal noise is normally very important, specially for long exposures. For these cameras dark frame images must be obtained with the same exposure time as the scientific images. Flat field correction would complete the image reduction.

Nitrogen cooled optical cameras

Professional CCD cameras are normally cooled using liquid nitrogen, which keeps the detector at temperatures close to 77 K, the liquefaction temperature of nitrogen. At this temperature, the thermal noise is usually very small and no dark frame correction is necessary. For these cameras, the images are corrected of bias and then directly of flat field.

Fast readout EMCCD camera

Electron Multiplying CCD (EMCCD, like the one currently being tested in BOOTES-IR) use solid state multipliers to increase weak signals before any readout noise is added, providing very high efficiencies. However, the response does not have the needed linearity to be able to do good photometry. Consequently, images must go through the linearity correction routine to give good photometric results. Although these cameras are thermoelectrically cooled the short exposures do not require dark frame correction.

Near infrared cameras

Detectors operating between 0.9 and 2.5 μm as the one that will be used in BOOTES-IR camera require a unique processing that takes into account the contribution of the

background and its variability. As this background signal is normally very high, we use short exposures of a few seconds that do not require dark subtraction. Observations must be done using the dithering techniques explained in Sect. 9.2.4 so that the sky contribution is correctly removed. This will create individual, corrected images with short exposures that will have to be combined to create the final image with the complete exposure time.

Table 9.2: Processing steps that should be considered for each camera type.

Camera	**Bias**	**Dark**	**Linear.**	**Flat**	**Bckg.**	**Detect**	**Astrom**	**Phot.**	**Obj.det.**
Thermoel. cooled opt.		*		*		*	*	*	*
Nitrogen cooled opt.	*			*		*	*	*	*
Fast readout EMCCD	*		*	*		*	*	*	*
Near infrared cameras	*			*	*	*	*	*	*

9.9 Conclusions

JIBARO has proved its capabilities to handle the output of robotic telescopes in real time over the last 6 years. At this moment it is being shared with other groups. Using our experience they can save time and aim the real efforts to the production of scientific results from the data instead of spending it in caring about the reduction and calibration of the data. The following are some of the institutions that are using our software:

- BOOTES-1 robotic observatory. Estación de Sondeos Atmosféricos (ESAt-INTA), El Arenosillo, Huelva (Spain).
- BOOTES-2 robotic observatory. Estación Experimental de la Mayora (EELM-CSIC), Málaga (Spain).
- BOOTES-IR robotic observatory. Observatorio de Sierra Nevada (OSN), Granada (Spain).
- BART robotic observatory. Ondřejov observatory (Czech Republic).
- FRAM robotic observatory. AUGER observatory (Argentina).
- WATCHER robotic observatory. (South Africa).
- Instituto de Astrofísica de Andalucía (IAA-CSIC), Granada (Spain). Where it is being used by the ARAE (Astrofísica Robótica y de Altas Energías) research group, as well as by other individual astronomers.

Bibliography

Adelman-McCarthy, J. K., et al. 2006, ApJS, 162, 38

Bertin, E., & Arnouts, S. 1996, A&AS, 117, 393

García-Dabó, C. E., & Gallego, J. 1998, Ap&SS, 263, 99

Høg, E., et al. 2000, A&A, 355, L27

Jenkner, H., Lasker, B. M., Sturch, C. R., McLean, B. J., Shara, M. M., & Russel, J. L. 1990, AJ, 99, 2082

Kubánek, P., Jelínek, M., Vítek, S., de Ugarte Postigo, A., Nekola, M., & French, J. 2006, Proc. SPIE, 6274

Mink, D. J. 2002, Astronomical Data Analysis Software and Systems XI, 281, 169

Monet, D. G. 1998, Bulletin of the American Astronomical Society, 30, 1427

Monet, D. G., et al. 2003, AJ, 125, 984

Pence, W. 1999, Astronomical Data Analysis Software and Systems VIII, 172, 487

Skrutskie, M. F., et al. 2006, AJ, 131, 1163

Stetson, P. B. 1987, PASP, 99, 191

Tody, D. 1986, Proc. SPIE, 627, 733

de Ugarte Postigo, A., et al. 2005, JIBARO: Un conjunto de utilidades para la reducción y análisis automatizado de imágenes, in Astrofísica Robótica en España, Ed. A.J. Castro-Tirado, B.A. de la Morena & J. Torres Riera, Madrid, 35

10

X-shooter: A wide band spectrograph for the Very Large Telescope

X-shooter is a second generation spectrograph that will be mounted on the Cassegrain focus of one of the units of the Very Large Telescope (VLT) operated by the European Southern Observatory (ESO). It is capable of obtaining medium resolution spectra (R=4 000-14 000) with an unprecedented wavelength coverage, from 300 to 2,300 nm in a single shot. It is designed to maximise the efficiency throughout this spectral range by splitting the optical beam with dichroics into three arms, each of which has an optimised Echelle spectrograph. The instrument is being built by a Consortium of four European countries and ESO. The current schedule aims at installing the instrument on the telescope by 2008. The author of this Thesis has participated in this project as the diffraction gratings workpackage manager, responsible of the simulation, procurement and testing of the visible and ultraviolet gratings.

10.1 Introduction

The X-shooter spectrograph (D'Odorico et al. 2004; D'Odorico et al. 2006; Covino et al. 2006; Zerbi et al. 2006) was proposed by four international groups in response to the call for proposals for a 2^{nd} generation VLT instruments issued by ESO in November 2001, as the instrument to fill the gap in the capability of the current suite of VLT instruments in operation or under construction at ESO (Fig. 10.1). Following a phase of negotiations among the different proponents and ESO, a Consortium was formed to make a feasibility study and the project was finally approved by ESO Scientific and Technical Committee in December 2003 (Moorwood & D'Odorico 2004). The X-shooter consortium is composed by institutes from Denmark, France, Italy and the Netherlands together with ESO. Each of the partners contributes in manpower and to the hardware cost receiving in return guaranteed time. Each nation has a Principal Investigator or PI (P.K. Rasmussen, F. Hammer, R. Pallavicini and L. Kaper) and a Project Manager or PM (P.K. Rasmussen, I. Guinouard, F.M. Zerbi and R. Navarro). The board of PIs is coordinated by S. d'Odorico (ESO) and the group of PMs by the Instrument Project Manager, H. Dekker (ESO). X-shooter

passed the Preliminary Design Review in December 2004 and the Final Design Review in February 2006. The assembly of the instrument began on late 2006 and testing of the overall instrument is planned to begin during the summer of 2007. Commissioning of the instrument at the telescope is planned for 2008.

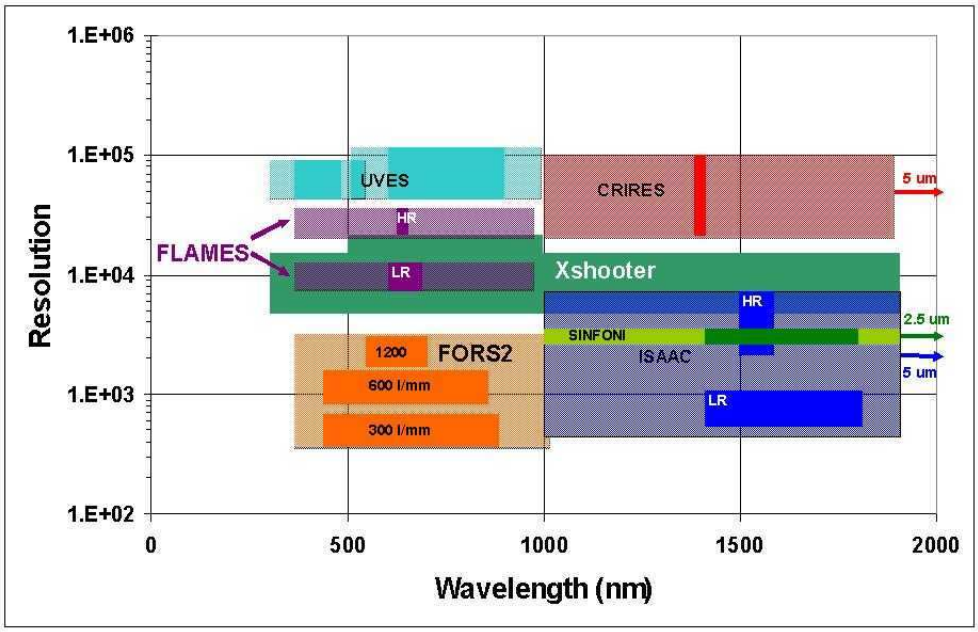

Figure 10.1: Properties of present and future VLT spectrographs, showing the spectral resolution versus wavelength coverage. Note that by the time that X-shooter will be in operation, the FORSes and ISAAC will be beyond their guaranteed lifetime.

10.2 Optics

The initial requirements on the instrument can be synthesised as follows:

- Very wide wavelength coverage (from U to K'-band) in one single observation
- Optimisation of the efficiency by using the Cassegrain focus of one of the VLT units and splitting the optical beam into three spectrographs, optimising coatings, gratings and detectors for each wavelength range.
- Operate at a spectral resolution of R=5,000-10,000, depending on the spectral band and the selected slit width. This will be sufficient to address a vast number of astrophysical applications while operating in a background limited S/N regime.
- Make use of technology that can be rapidly deployed, to be able to reach commissioning at the telescope in 2008.

From the beginning it was clear that in order to achieve the desired spectral coverage with intermediate resolution several spectrographs working in parallel would be needed

and the division was decided as follows: ultraviolet/blue (UV/Blue, 300-550 nm), visible (VIS, 550-1,000 nm) and near infrared (NIR, 1,000-2,300 nm). Each spectrograph would be optimised for its spectral range by means of customised optics, coatings and detectors. A design of the arrangement of the spectrographs in the Cassegrain focus is shown in Fig. 10.2 together with a picture of the VLT telescopes at Paranal Observatory.

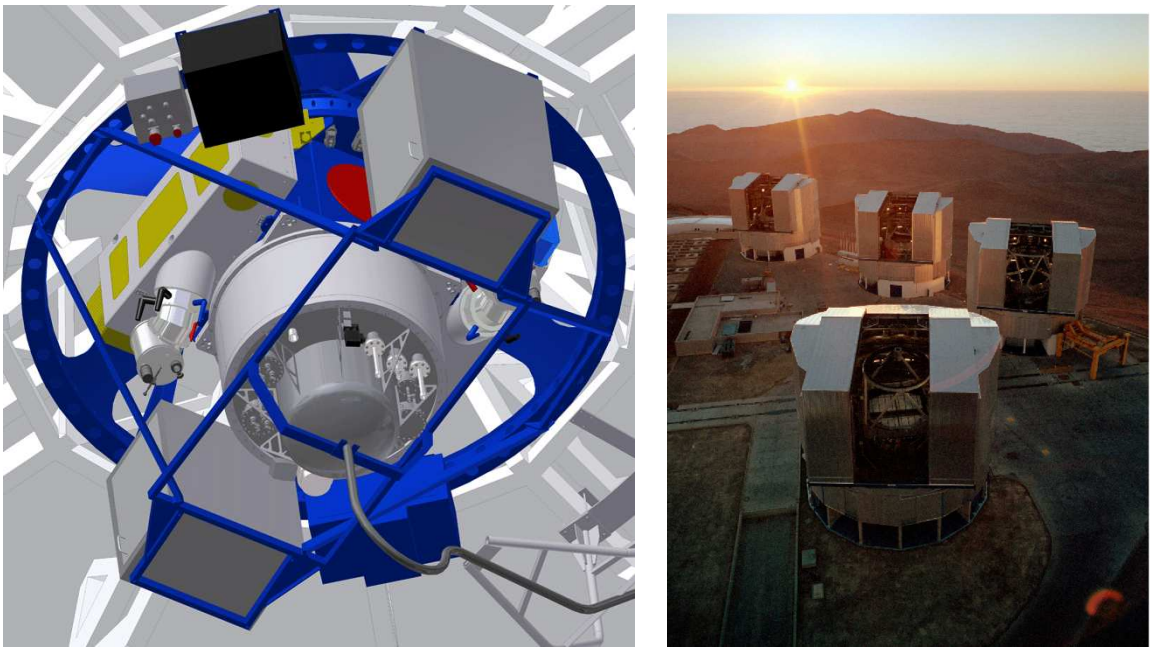

Figure 10.2: X-xhooter (left) is a three arm spectrograph that will simultaneously cover the 300-2,300 nm spectral range with intermediate resolution. It will be mounted on one of the units of the Very Large Telescope (right), in Paranal, Chile.

10.2.1 Pre-slit optics

Pre-slit optics were designed based on the mechanical concept of the backbone structure (Michaelsen et al. 2006), that will hold the three spectrographs together. The light from the Cassegrain focus is split into three channels via two dichroics placed after the focal plane in the divergent beam. The light is then refocused by relay optics onto each spectrograph entrance slit. UV/Blue and VIS relay optics are based on lenses, while NIR uses only mirrors (See Fig 10.3).

Dichroics have been specifically designed to maximise the efficiency in each arm while minimising the width of the transition region. The first dichroic reflects light towards the UV/Blue spectrograph and transmits the redder wavelengths. The second dichroic divides the light again, reflecting light towards the VIS spectrograph and transmitting to the NIR one.

Due to its very wide wavelength range, X-shooter suffers a very strong atmospheric dispersion, which can not be corrected by a unique device. The NIR atmospheric dispersion

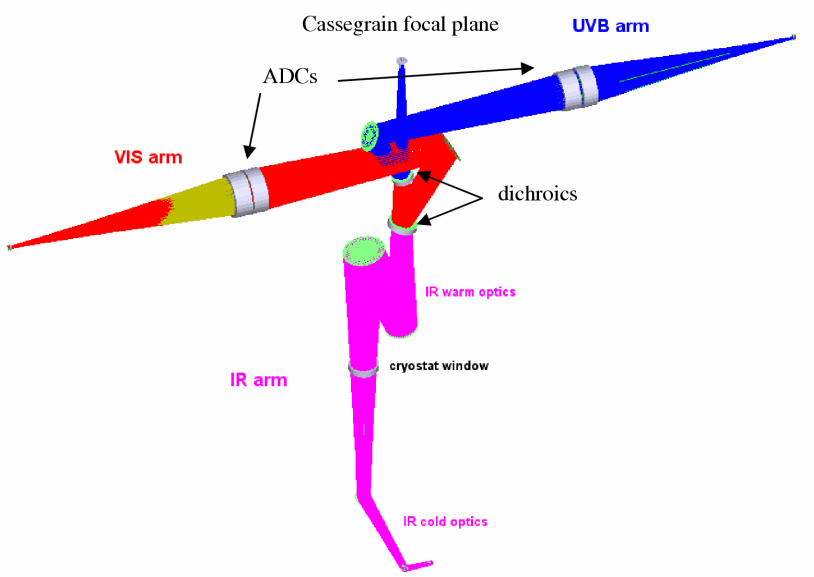

Figure 10.3: Pre-slit optical design.

is only 0.4 arcseconds at 60° zenith angle and no correction is foreseen. Two different atmospheric dispersion correctors (ADC) have been optimised for the UV/Blue and the VIS arms respectively, this minimises the correction residuals. The ADC consist of two counter-rotating double prisms that are cemented onto the two doublets that make the relay optics to reduce the air-glass interfaces.

10.2.2 Auxiliary optics

The acquisition and guiding system (A&G, see Fig. 10.4) is located at the level of the Cassegrain focal plane. It consists of a CCD camera, focal reducer optics, filter wheel (U, B, V, R, I and z bands) and a mirror carriage which places into the focal plane one of the following: A three position mirror, a pellicle and the integral field unit (IFU). The main purpose of the mirror is to detect and centroid objects onto the entrance slits. Once the object is centred there is a second position that will allow to monitor the exposure by showing the field around the object, leaving a hole of $10'' \times 15''$ that is used to feed the spectrographs. The third position has a $0.5''$ pinhole that may be used as an artificial star during daytime for maintenance. The pellicle is used to view the slits of the spectrograph. It is semitransparent, so a calibration lamp can be used to illuminate the slits while viewing them. Selecting the different filters one would have access to each of the slits. The IFU divides a field of $1.8'' \times 4''$ arcseconds into three slices along the slit (Guinouard et al. 2006).

10.2.3 Spectrographs

Different spectrograph designs (ESI-like, UVES-like, 4C-like) were considered during the feasibility study and the preliminary design phases. A comparative analysis identified the 4C layout (*Collimator Compensation of Camera Chromatism*, Delabre et al. 1989) as the

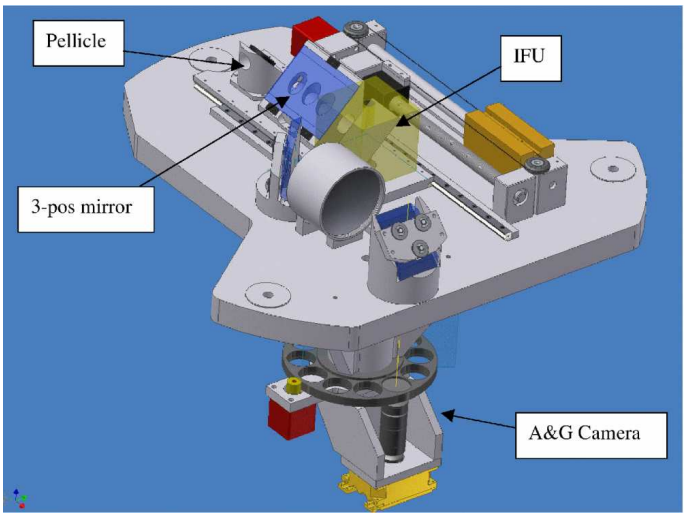

Figure 10.4: Acquisition and guiding system.

optimal choice for X-shooter. In this design, the camera chromatism is compensated by the use of the chromatic effect introduced by a Maksutov-type collimator, greatly simplifying the design of the camera. Moreover, the camera is smaller and less expensive than those required by the other designs. The UV/Blue and VIS spectrographs share a very similar optomechanical design (Spanò et al. 2006), while the 4C spectrograph design of the NIR arm has been modified to fit the requirements of a cryogenic system (Navarro et al. 2006).

Fig. 10.5 shows the optical layout of the UVB spectrograph. Light comes from behind the plane of the drawing through the entrance slit and is directed by 'folding mirror 1' to the main mirror. The light goes through the corrector lens, producing a collimated beam that is directed to the main dispersing element, an Echelle grating. As cross disperser we use a prism in double pass which is placed between the corrector lens and the grating. The light beam returns through the corrector lens once more to the main mirror, which creates an intermediate spectrum near the entrance slit. There, a second folding mirror which acts as a field relay mirror, redirects the light to the camera. The dioptric camera (1 aspherical surface) reimages the spectrum onto a tilted detector. The collimated beam is of 100 mm and the camera optics are smaller than 80 mm. The VIS spectrograph is very similar to this one.

The NIR spectrograph is shown in Fig. 10.6. In this case the 4C design has been modified to decrease the overall size by using a two-mirror collimator. The camera has three elements with mild aspherical surfaces, enhancing the overall efficiency while minimising the ghosts. As cross dispersers it will be using a series of three prisms, one of Silica and two of ZnSe, that provide a more uniform dispersion, maximising the spectral coverage in the fixed detector area.

Table 10.1 displays the main parameters of the three spectrographs. The spectral formats have been computed via ray tracing with the optical model of each spectrograph. Line tilt and inter-order separation have been optimised to avoid overlapping and to ensure well calibrated spectra.

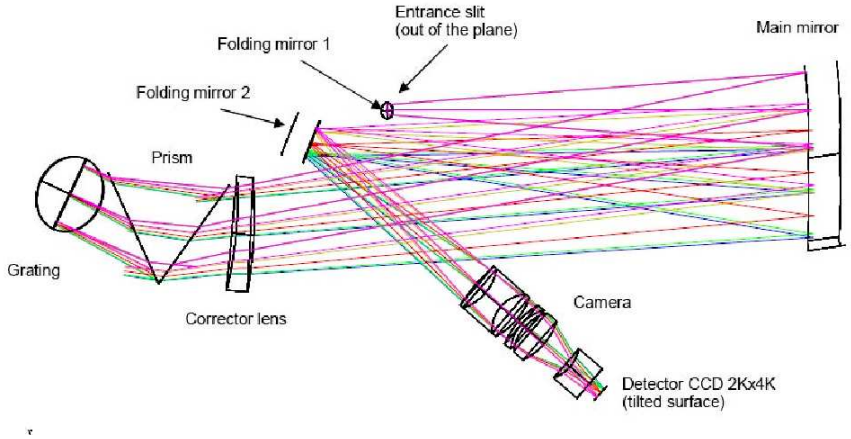

Figure 10.5: Optical layout of the UV/Blue spectrograph. The VIS spectrograph has a very similar design.

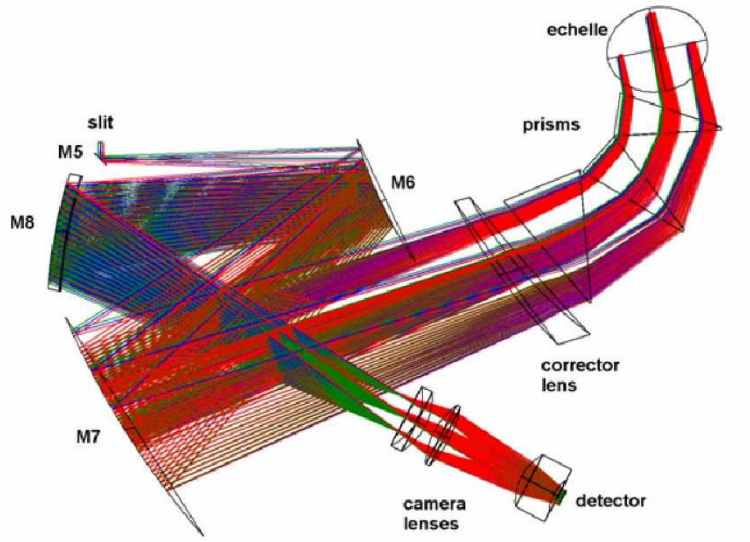

Figure 10.6: Optical layout of the NIR spectrograph. The 4C design has been modified to reduce the size so it can be fitted in the cryostat.

10.2.4 Performance analysis

One of the key features of X-shooter at the time of the definition was the need of the highest possible thoughoutput. Great efforts were made in order to optimise the overall efficiency, including the selection of custom made dichroics, optics, coatings and gratings. Fig. 10.7 shows the simulated efficiency of the instrument, detector included. X-shooter will be one of the most efficient spectrographs on 8m-class telescopes, specially below 370nm.

Table 10.2 shows an estimate of the limiting magnitude that will be achieved by X-

Table 10.1: Parameters of the spectrographs.

	UV/Blue	**VIS**	**NIR**
Collimator Focal Ratio	F/6.5	F/6.5	F/13.4
Slit length	12 arcsec (3.06 mm)	12 arcsec (3.06 mm)	12 arcsec (6.36 mm)
Spectral range	300-550 nm	550-1,000 nm	1,000-2,300 nm
Resolution-slit prod.	4,500 (arcsec)	7,000 (arcsec)	4,500 (arcsec)
Camera free diameter (max)	80 mm	80 mm	70 mm
Camera magnification	0.41	0.42	0.2
Camera output focal ratio	F/2.64	F/2.7	F/2.1
Detector	4k×2k, 15μm/pixel	4k×2k, 15μm/pixel	2k×1k, 18μm/pixel
Detector scale	7 pixel/arcsec	7 pixel/arcsec	5 pixel/arcsec
Gratings	180 gr/mm, 41.8° blaze	99.4 gr/mm, 54.0° blaze	55.0 gr/mm, 46.1° blaze
Cross disperser prisms	60° Si	49° SF6	35° Infrasil + 2×22° ZnSe

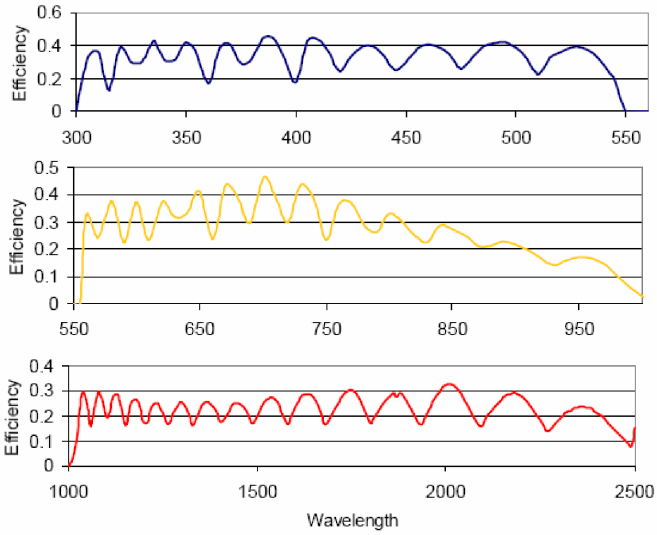

Figure 10.7: Expected efficiency of the UV/Blue (top), VIS (middle) and NIR (bottom) spectrographs, considering from the focal plane to the detector. The ripples are due to the grating efficiencies.

shooter, considering a signal to noise ratio (SNR) of 10 and an exposure time of 1 hour. Two emissivity values have been considered (ε=10.5% and ε=25%). The instrument will have dedicated software tools for controlling the instrument (Vidali et al. 2006) and for reducing the data (Goldoni et al. 2006). Fig. 10.8 shows an example of a simulation of the spectral format of the VIS spectrograph that has been created to feed the reduction software during the development phase.

10.3 Diffraction gratings

In this section we present the contribution of the author to the X-shooter project, the design, procurement and testing of the Echelle diffraction gratings, the main dispersive elements of the spectrographs. The design and manufacture procedure are decisive in the overall

Table 10.2: Limiting magnitudes of X-shooter for 1 hour exposure and a SNR of 10.

Wavelength	Limiting AB-magnitude
330	21.27
370	21.61
440	21.79
540	21.75
650	21.55
810	21.14
930	20.26
1260	20.49
1670	20.77
2100 (ε=0.10)	19.38
(ε=0.25)	18.77
2200 (ε=0.10)	18.60
(ε=0.25)	17.77
2300 (ε=0.10)	17.76
(ε=0.25)	16.87
2400 (ε=0.10)	16.91
(ε=0.25)	16.00

Figure 10.8: Simulated spectrum of a ThAr lamp through the VIS spectrograph.

efficiency of the grating and consequently of the instrument, as Echelle spectrographs can normally loose about 50 % of the light in their main dispersive element. The effect of ghosts can also greatly complicate the analysis and interpretation of the spectra. The selection of a good grating can help to minimise these ghosts and light losses.

10.3.1 Efficiency of the diffraction gratings

During the design phase of X-shooter we performed multiple theoretical simulations of the behaviour of the gratings, in order to have an idea of the performance that could be expected from the final product. The simulations were made using PCGrate-S 6.0 software[1],

[1] http://www.pcgrate.com/

which is based on the modified method of integral equations (Goray & Seely 2002; Goray & Sadov 2002; Goray 2005; Goray et al. 2006a; Goray et al. 2006b), that solve the periodic boundary value problems which describe the incidence of a light beam on the profile of a diffraction grating. The way in which the light is diffracted will depend on the profile and shape of the grating, the coating(s), the surface quality and the incident light. The light waves are assumed to arrive parallel and the diffraction is characterised by the wavelength and incident angle, which we define by the polar and azimuth angles (see Fig. 10.9).

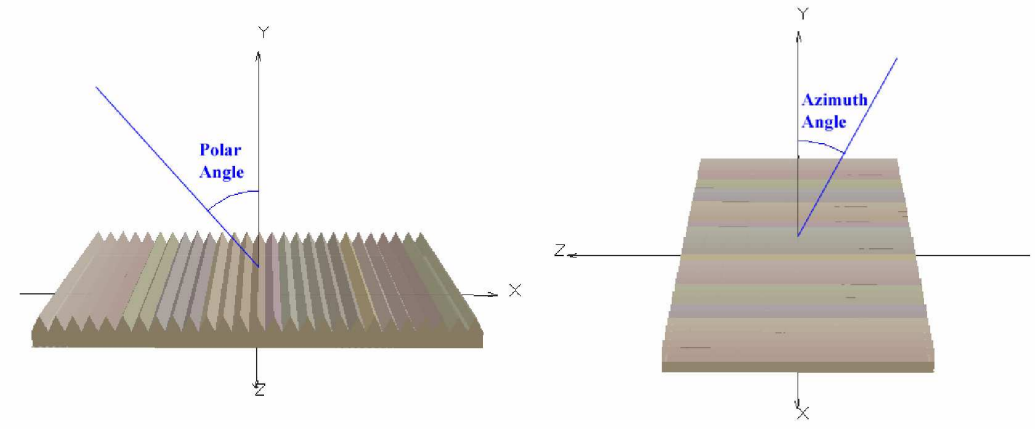

Figure 10.9: Definition of incident angles of the light beam on the gratings.

For the efficiency calculation of our gratings, we have used PCGrate in its *normal* calculation mode (as the alternative *resonance* mode does not allow azimuth angle variation). We also used a *finite* low border conductivity to better simulate the absorptions in the surface of the gratings.

The result of the first simulations showed that the gratings could, in theory, be produced in the desired efficiency range. We then studied the effect of the incident angle in the final throughoutput. This was used to decide the best way in which the grating could be tilted without loosing efficiency in the design of the spectrographs. We found that the variation in polar angle is slightly asymmetrical, being more tolerant if we vary the incident angle by increasing it (see Fig 10.10). However the increase of polar angle also implies a fast rise of the size of the grating. On the other side azimuth angle variations shows less effects in the efficiency of the grating for small angles, but increasing rapidly when we go over $6^\circ - 7^\circ$. A slight deviation in the azimuth angle ($\sim 2^\circ$) was finally used in the design of the spectrographs.

A second study was made searching for factors that could reduce the final performance of the grating. One of the elements that showed up was the surface roughness, that can specially affect the bluest orders, where the roughness of the surface is greater in comparison with the wavelength. In Fig. 10.11 we show the effect of the surface quality on the efficiency curves of the VIS grating by varying the value from 0 to 21 nanometre r.m.s. (root mean square). We find a difference of up to 25% in the bluemost part of the spectrum, being less apparent in the reddest orders.

In some tests of gratings using overcoatings of MgF_2 it was noticed that there was a

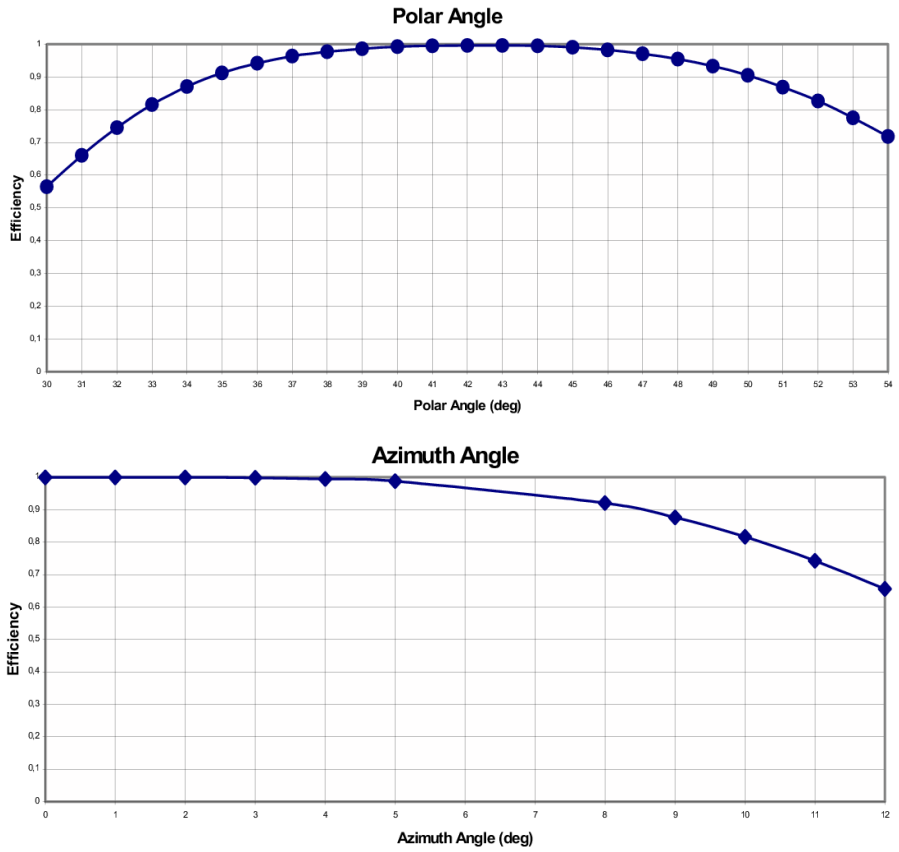

Figure 10.10: Effect of the variation of the polar and azimuth incidence angles in the efficiency of the grating.

decrease in the efficiency due to an excess in the thickness of the layer. As one of the gratings of X-shooter was expected to have such an overcoat, we did several simulations to find the best value. The results are shown in Fig. 10.12. We find that there is not a single thickness that behaves best at all wavelengths. The thickness has to be selected in order to enhance the orders in which we are more interested (because of lower efficiency due to other factors, etc.) without excessively harming the others.

Next we study the possibility of changing the groove profile. Although the demonstration code that we are using gives limited possibilities for this tests, we used it to change the top angle of the gratings, keeping the triangular shape. The tests were done with the VIS grating of X-shooter, which has a blaze angle of 54°. As standard we accepted a top angle of 90°, implying a right angle of 36° (see Fig. 10.13). We varied this right angle from 26 to 38° (the maximum value accepted by the version of PCGrate that we had). The result of this test indicates that the efficiency increases as we increase the sharpness of the groove. Furthermore, the polarisation seems to gain stability as the hidden face of the grating becomes steeper. Throughout this work, we use TE (Transverse Electric) and TM (Transverse Magnetic) to refer to the polarisation of the incident light wave. TE mode is considered when the linearly-polarised light hits the grating with the electric-field

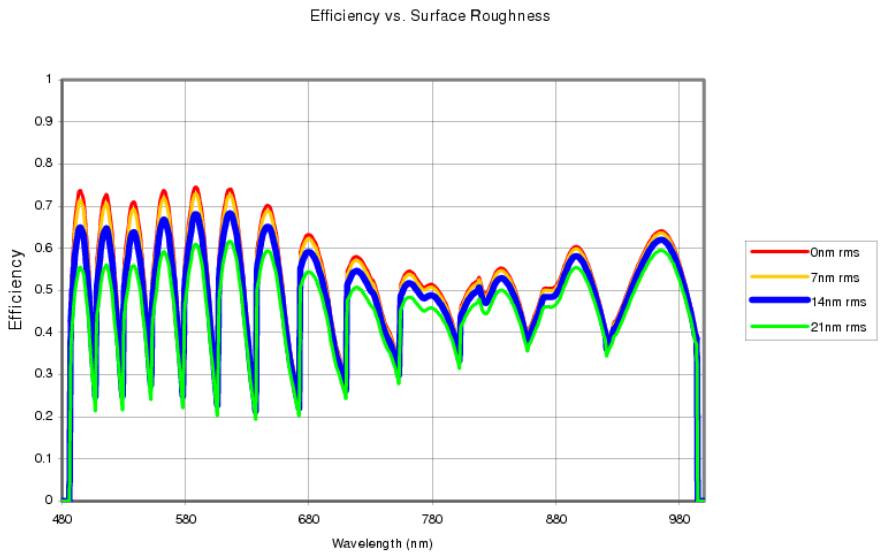

Figure 10.11: Effect of the surface roughness on the efficiency of the grating.

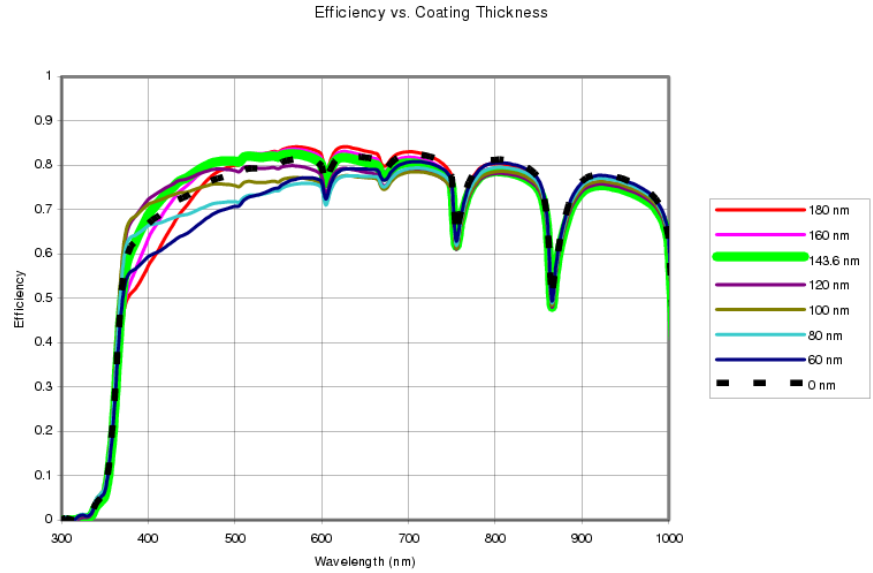

Figure 10.12: Effect of the overcoat thickness on the efficiency of the grating.

vector perpendicular to the plane of incidence, while TM corresponds to the case where the magnetic-field hits perpendicular. These modes are also referred to as P mode (TE) or S mode (TM). When we talk about non polarised light (NP) the numbers are made with an incident angle of 45°.

In conclusion we find that there are several factors that have to be considered when simulating a grating and that can make the results significantly different from a ideal

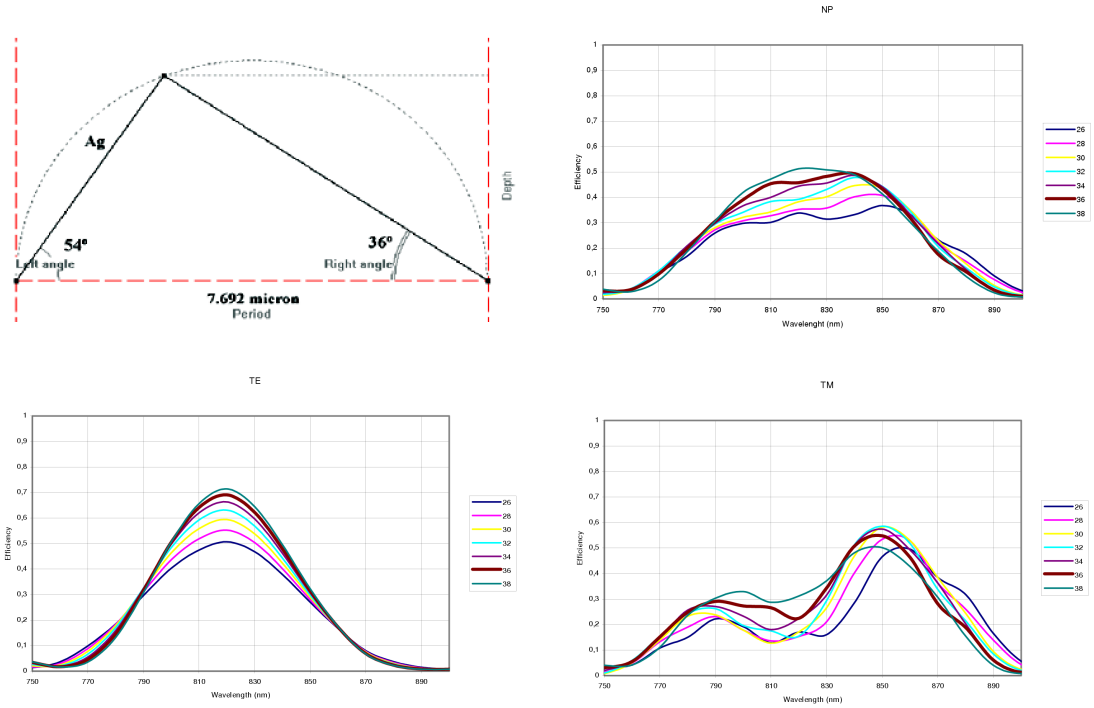

Figure 10.13: Effect of the groove profile in the efficiency of the grating. Top left: Definition of the shape of the studied groove, light arrives from the left. Top right: Efficiency of the 15^{th} order of the VIS grating as a function of the right angle. Bottom left: Efficiency of the Transverse Electric mode (TE or P). Bottom right: Efficiency of the Transverse Magnetic mode (TM or S).

scenario. Some of this factors however, will be dependant on the manufacture and not on the design of the gratings. A good communication with the providers is important in order to be able to get the best achievable product.

10.3.2 Gratings Specifications

In this section we present the specifications for the UV/Blue and VIS gratings as sent to the manufacturer in the final request for quotation, together with the simulated efficiencies and the drawings of the grating blanks. The simulations give an idea of the expected values for the performance of the final product.

UV/Blue

Table 10.3: UV/Blue grating specs

UV/Blue Grating	
Groove Density	180 ± 2 gr/mm
Blaze Angle	42 ± 1 deg
Min. Ruled Area	120 × 150 mm
Average Efficiency 300-500 nm (unpolarised light, surface average, averaged over free spectral range of the orders)	>48%
Average Peak Blaze Efficiency 300 - 500 nm (unpolarised light, surface average, average of peak blaze efficiencies of the orders)	>60%
Maximum ghost level	10^{-4}
Coating	Al
Illumination	
Wavelength Range	300 - 500 nm unpolarised
Orders	14-24
Off-Litrow Angle	0 deg
Off-Plane Angle	2.2 deg
Blank	
Shape	Octagonal, see drawing
Material	Zerodur or equivalent
Wavefront Quality	< 32 nm r.m.s. < 158 nm P-V

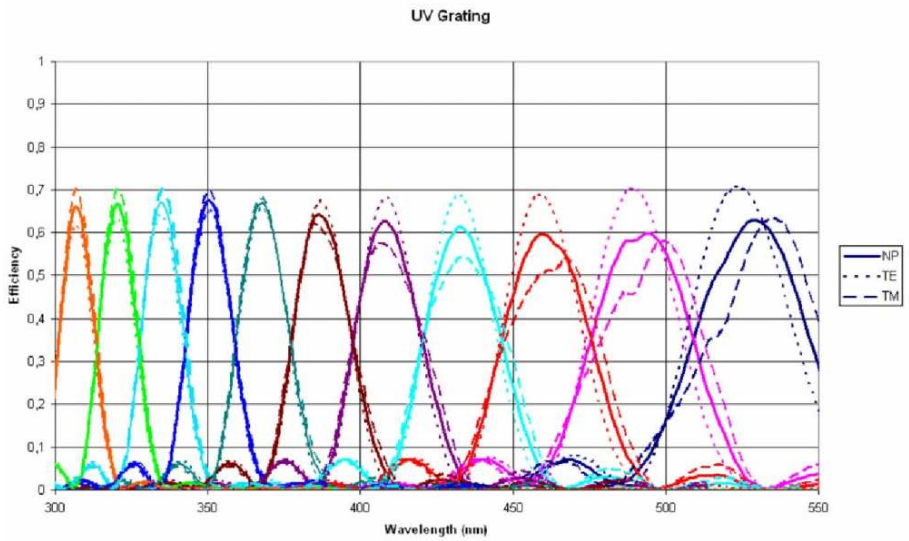

Figure 10.14: Simulation of the efficiency of the UV/Blue grating.

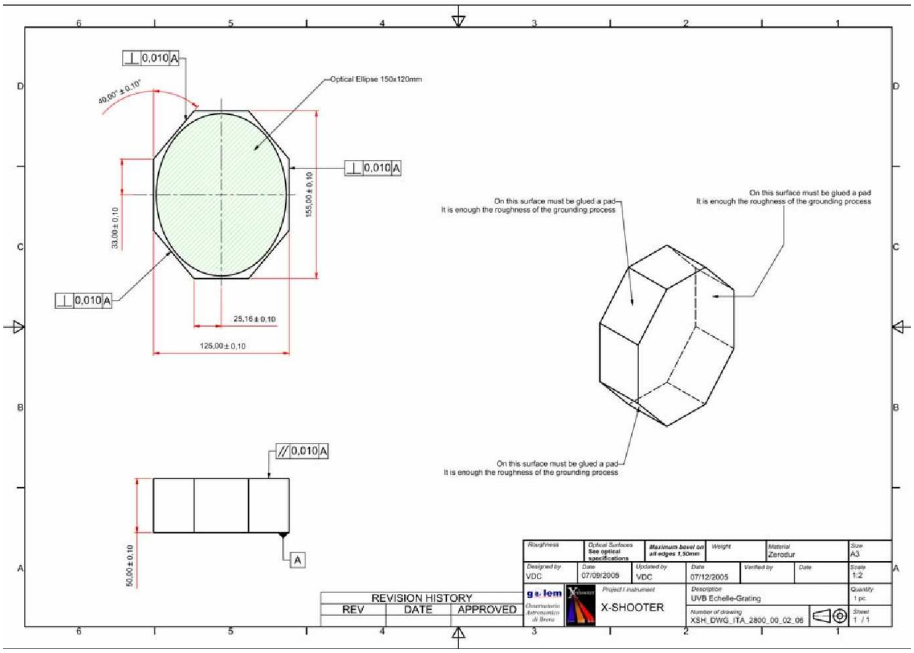

Figure 10.15: Design of the UV/Blue grating blank.

VIS

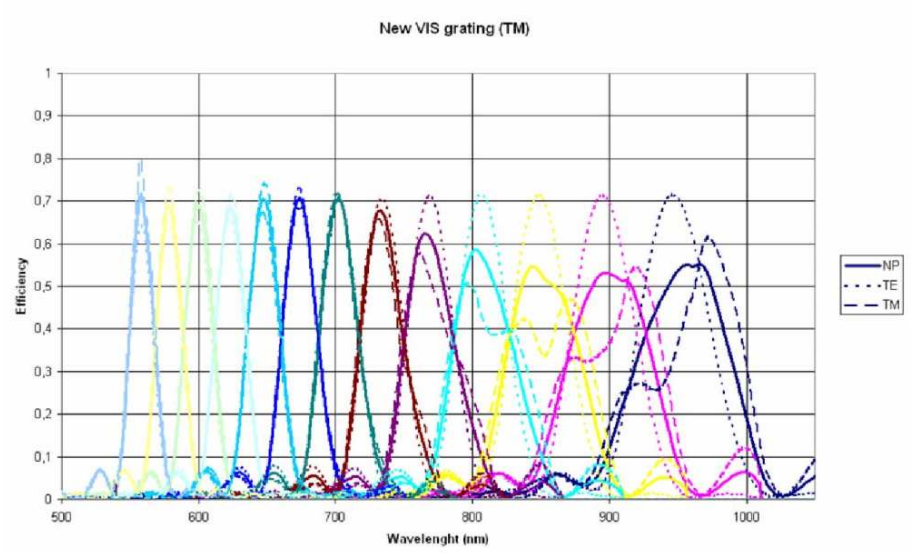

Figure 10.16: Simulation of the efficiency of the VIS grating.

Table 10.4: VIS grating specs

VIS Grating	
Groove Density	99.4 ± 1 gr/mm
Blaze Angle	54 ± 1 deg
Min. Ruled Area	120 × 194 mm
Average Efficiency 550 - 1000 nm (unpolarised light, surface average, averaged over free spectral range of the orders)	>50%
Average Peak Blaze Efficiency 550 - 1000 nm (unpolarised light, surface average, average of peak blaze efficiencies of the orders)	>60%
Maximum ghost level	10^{-4}
Coating	Ag+MgF_2
Illumination	
Wavelength Range	550 - 1000 nm unpolarised
Orders	17-29
Off-Litrow Angle	0 deg
Off-Plane Angle	2.0 deg
Blank	
Shape	Octagonal, see drawing
Material	Zerodur or equivalent
Wavefront Quality	< 63 nm r.m.s. < 315 nm P-V

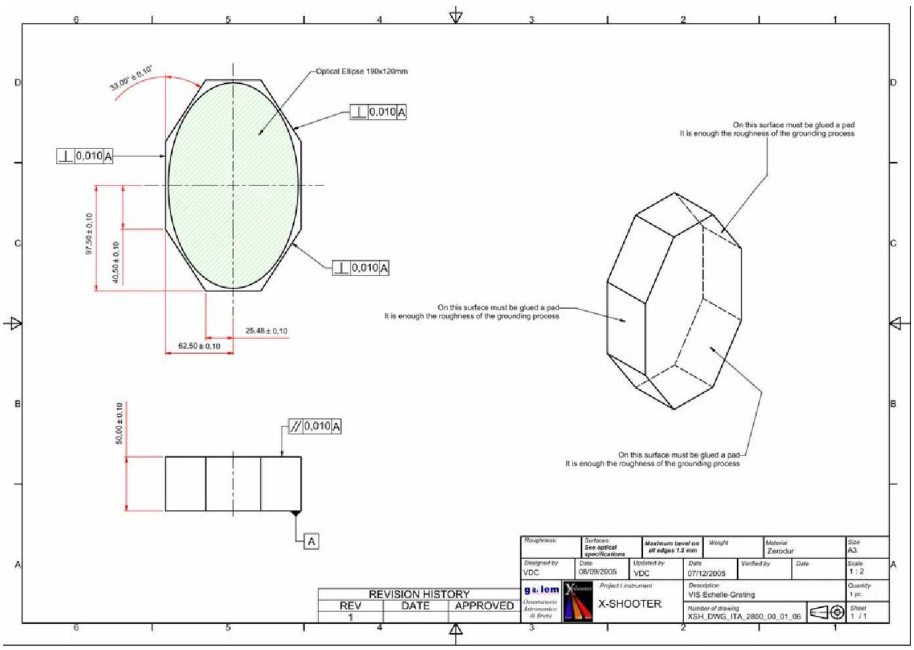

Figure 10.17: Design of the VIS grating blank.

10.3.3 Procurement

Several grating manufacturers were contacted prior to the Preliminary Design Review (PDR) in order to identify how many companies would be able to meet the specifications of the X-shooter project:

- Richardson Grating Lab (RGL). Which after being absorbed by Newport is now named Newport-Rochester. www.newport.com
- Zeiss. www.zeiss.com
- Bach Research Corporation. www.bachresearch.com
- ELAN. www.elan.spb.ru
- Tydex. www.tydex.ru

Only 3 of these (Newport-Rochester, Zeiss and Bach Research Corporation) were found to be capable of producing the size and ruling characteristics required. After the instrument passed the PDR and, being the gratings one of the items with a longer lead time, a request for quotation was sent to these 3 vendors. At this point Zeiss was discarded as a possible provider due to a problem with their ruling engine which had delayed their schedule to the pointo of not being able to produce the gratings in the desired schedule. The two remaining quotations were presented in the Optical Final Design Review (OFDR), which was celebrated on June 2005. There it was decided to choose Newport-Rochester as final provider and proceed with the order.

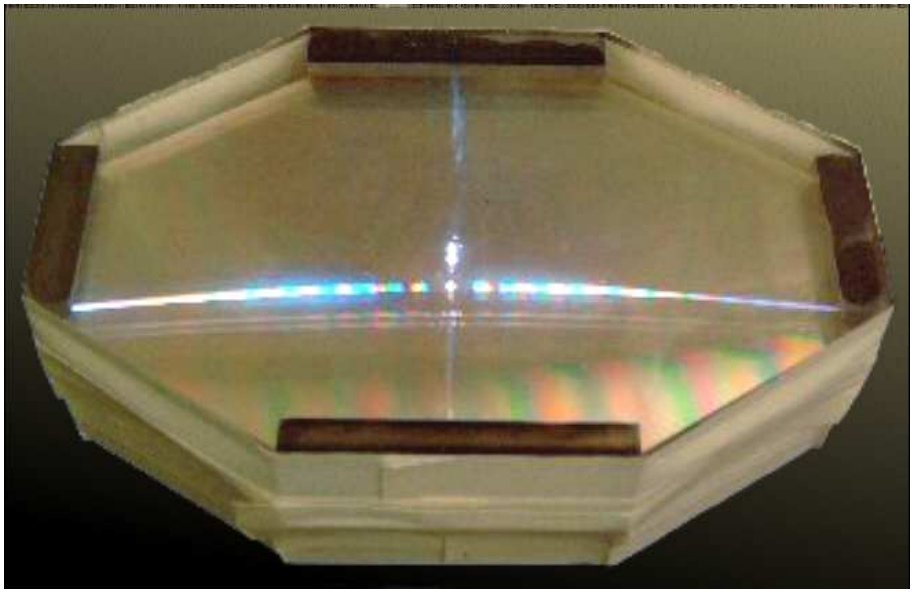

Figure 10.18: VIS grating opened for inspection after delivery in Merate.

As the manufacture of the gratings is one of the most time consuming processes in the project an alternative plan was proposed in case that the gratings would be delivered later

than the rest of the spectrographs. For this case, we proposed several rulings that were available in the catalogue of Newport-Rochester and that could be obtained in a much shorter time. They could be useful at the time of assembly and testing of the optical setup of the spectrographs and would be substituted by the final ones once they arrived.

From OFDR on, further contact was maintained with Newport-Rochester in order to produce a final quotation and arrange the conditions of the two contracts that should be signed (one for each grating). The final quotation was given in November 2005 and an agreement was finally reached in December 2005. The orders of purchase were sent in the December 2005 (VIS) and January 2006 (UV/Blue) respectively. At the Final Design Review (FDR) of the instrument the grating orders had already being signed. The final products were delivered to Brera Observatory (Italy) at the beginning of December 2006 (see Fig. 10.18), where the integration of the VIS and UV/Blue spectrographs is taking place.

10.3.4 Acceptance tests

For the final acceptance of the gratings several tests were requested in order to prove that the specifications had been achieved. These included an interferogram of the surface of the gratings to check the wavefront quality, a ghost level study and an eficiendy test. In this section we show the result of these tests.

UV

Fig. 10.19 shows an interferogram of the grating that tells us about the waferwont quality. The specifications allowed a peak to valley (P-V) deviance across the grating of 158 nm (0.250 waves, as they used a 632.8 nm ligh source for the interferogram) and a root mean square (r.m.s.) deviation of 32 nm (0.051 waves). From the test we obtain a P-V value of 0.208 waves (132 nm) and a r.m.s. deviation of 0.0484 waves (31 nm), being 100% of the points of the grating within wavefront quality specs.

The near order ghost trace shown in Fig. 10.23 (left) is a test to check for the Rowland ghosts, which are due to spurious lines due to large-scale periodic errors in the spacing of the gooves. These lines are usually located symmetrically with respect to each strong line. The spectral distance from it depends on the period of the error, with an intensity that depends on the amplitude of this error. For X-shooter gratings, Newport-Rochester used the MIT B-engine, which uses a double interferometer control system, based on a frequency-stabilized laser, that virtually elliminates Rowland ghosts (Palmer 2005). From the near order trace of the UV grating we can see that ghosts are negligible.

The inter order ghost trace checks for Lyman ghosts. These are the result from compounded periodic errors in the spacing of the grating grooves. From Fig. 10.23 (right) we see that they are $\sim 10^{-5}$, one of magnitude better than the limits imposed by the specifications.

Fig. 10.21 shows the result from the efficiency tests even orders from the 16^{th} to the 24^{th}. We can see that the peak efficiency of all orders is well above of the minimum 60% efficiency specified in the specifications and even above the values extracted from our simulations. This is probably due a better than specified surface quality and a well constructed groove profile.

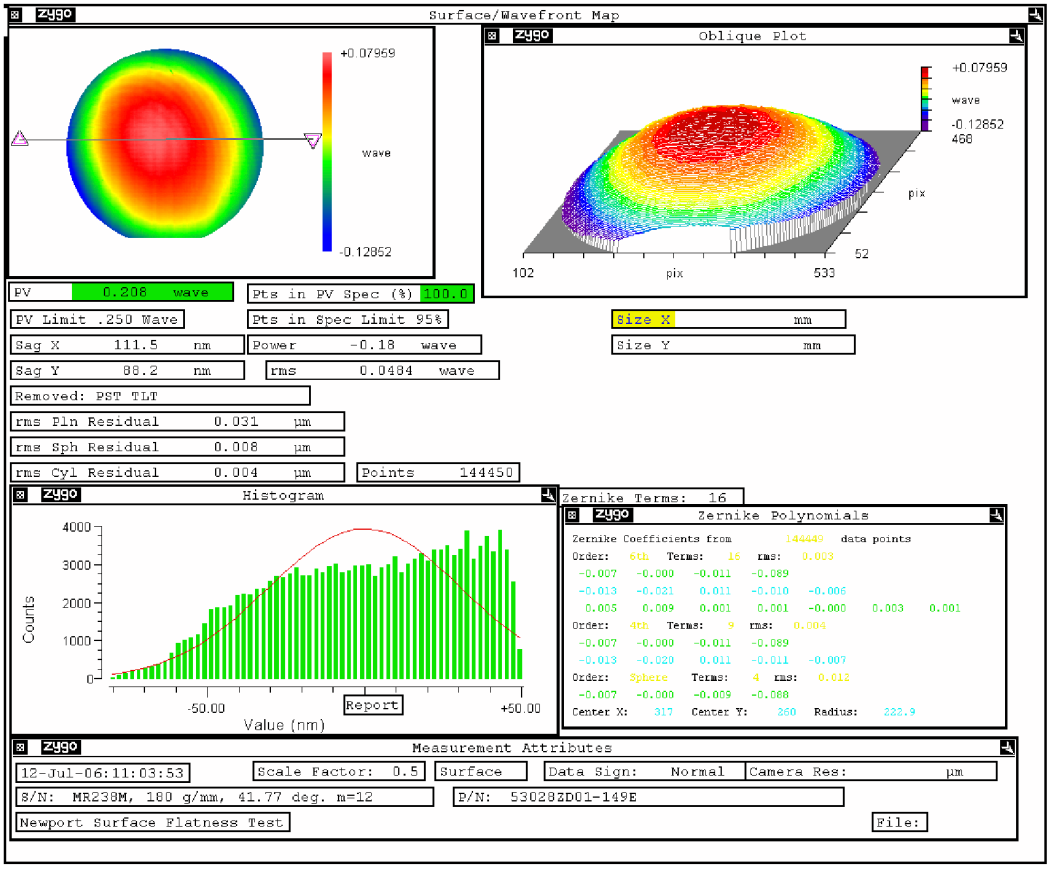

Figure 10.19: Interferogram study of the wavefront of the UV grating.

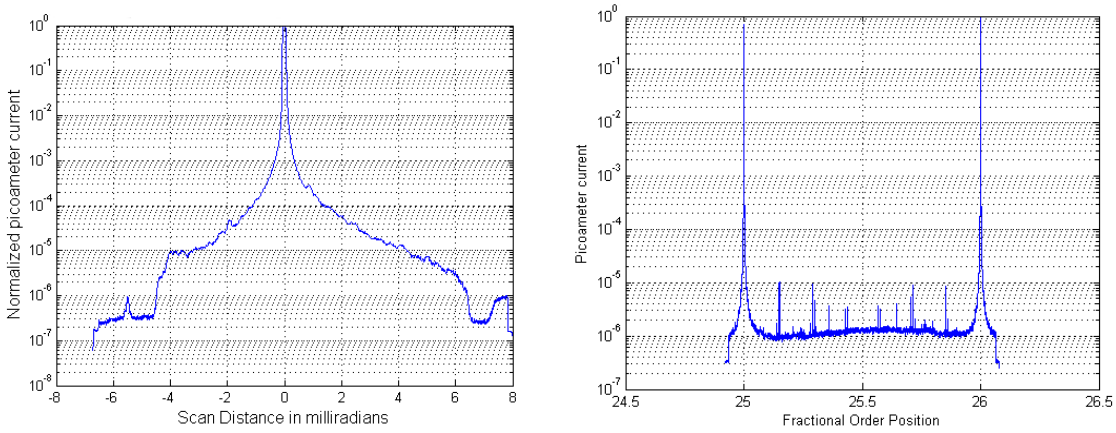

Figure 10.20: Left: Trace of the near order ghost level of the UV grating. Right: Trace of the inter order ghost level of the UV grating.

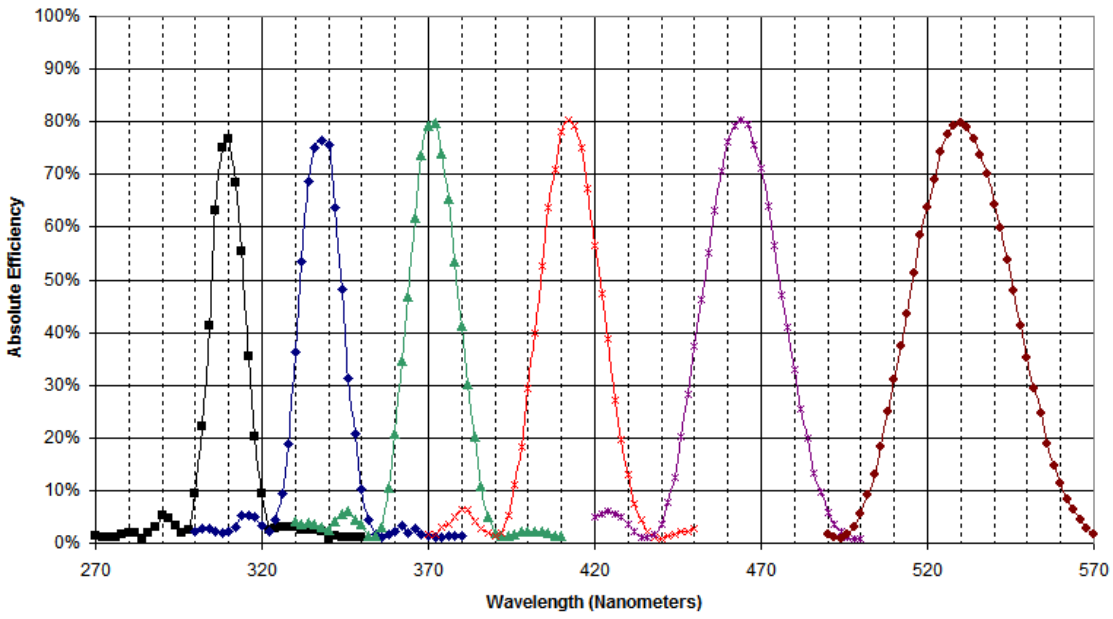

Figure 10.21: Efficiency test of the UV grating provided by Newport-Rochester.

VIS

Fig. 10.22 shows the result of the interferogram test for the VIS grating. In this case the tolerances were of 315 nm P-V and 63 nm r.m.s. and the meassured values 209 nm (0.303 waves) and 45 nm (0.0707 waves), well within specifications.

As in the case of the UV grating the near order ghost trace shown in Fig. **??** and the inter order ghost trace shown in Fig. **??** show negligible Rowland ghosts and Lyman ghosts one order of magnitude bellow the specification values.

The master ruling for the VIS grating was the first one to be produced and this gave us some extra time to experiment with the coatings. The first tests of the grating, using an aluminum coating (see Fig. 10.24) returned a similar efficiency (although slightly higher) to the one given by our simulations, above the specification levels. However, from the experience of ESO, a silver coating with an MgF_2 overcoat could give better results. When the new coating was tested, the efficiency was increased between 5 and 10%, being specially significant the improvement in the reddest orders, where a polarisation effect has shown the TM mode would be pulling down the response. The results of the tests with the new coating, which was used in the final delivered product is shown in Fig. 10.25

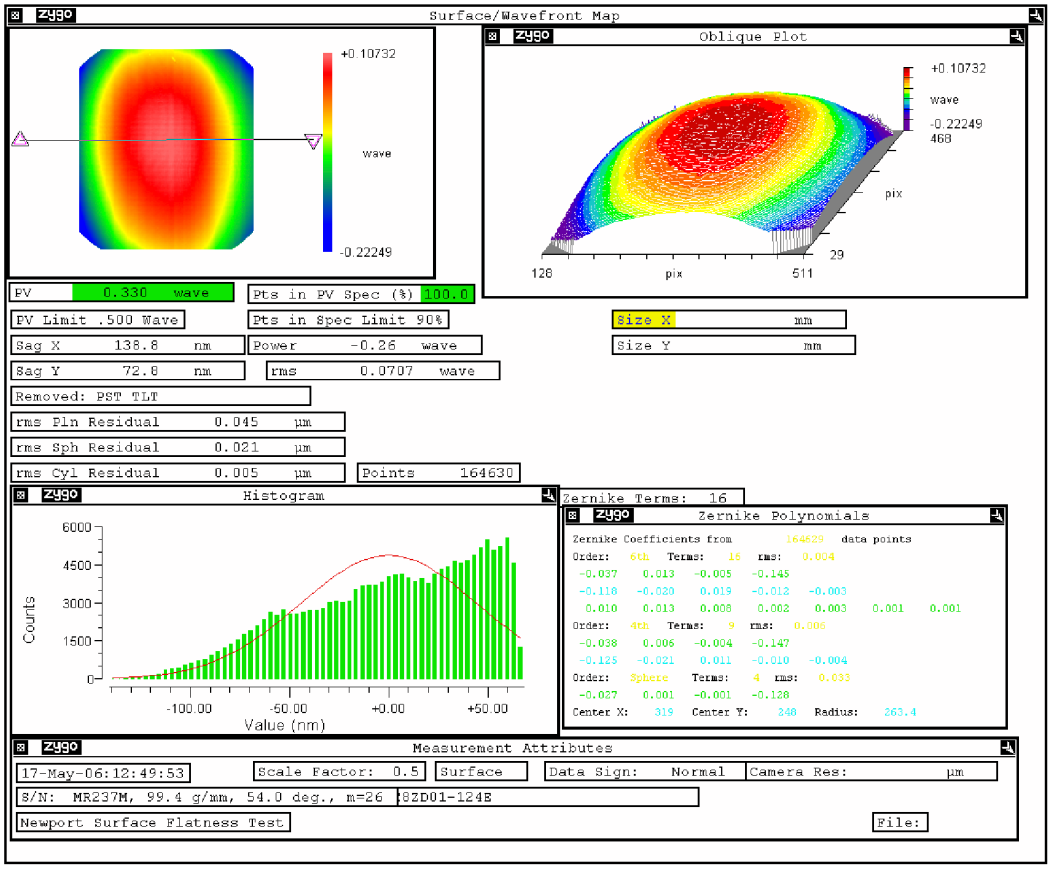

Figure 10.22: Interferogram study of the wavefront of the VIS grating.

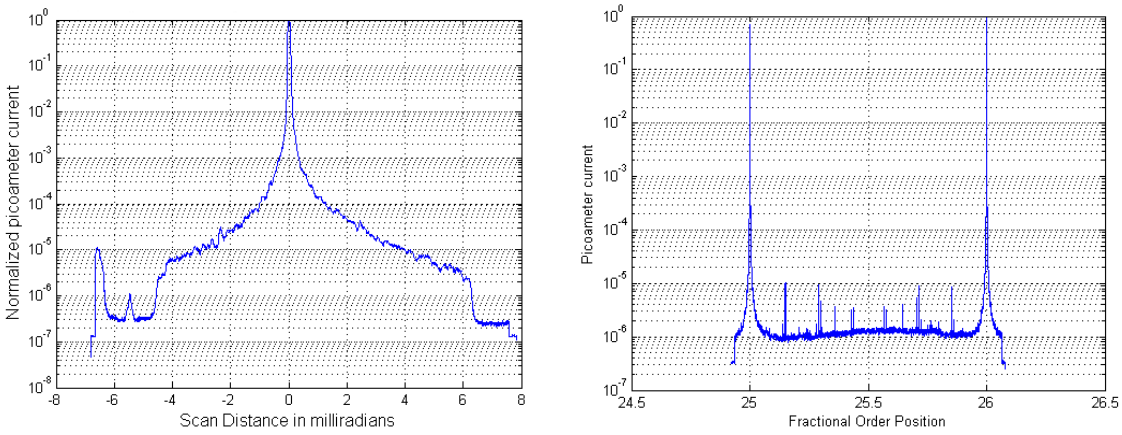

Figure 10.23: Left: Trace of the near order ghost level of the VIS grating. Right: Trace of the inter order ghost level of the VIS grating.

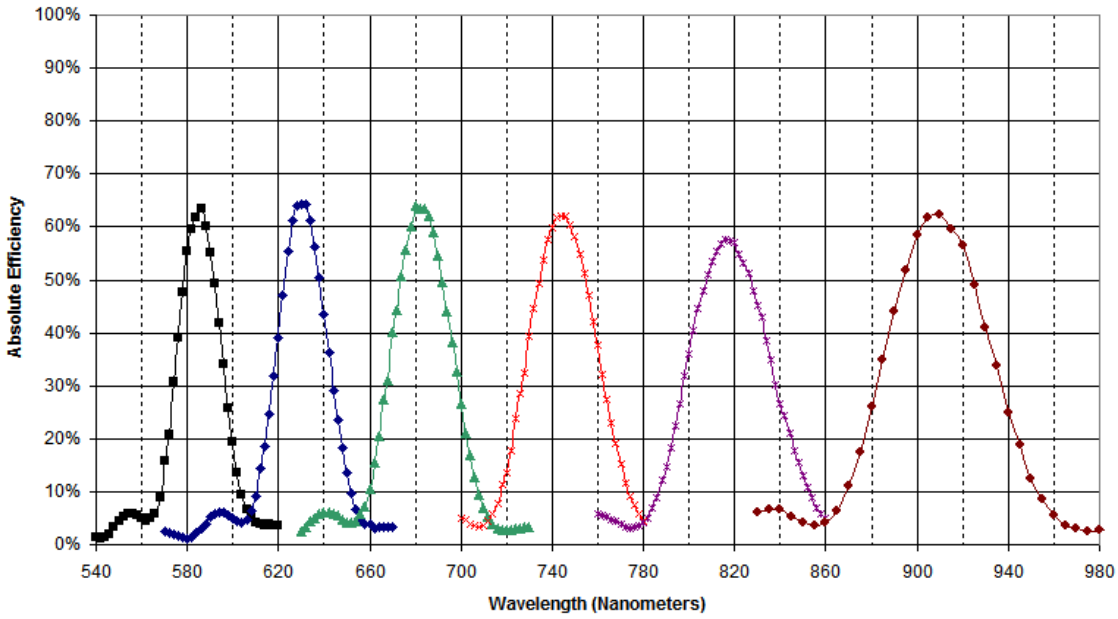

Figure 10.24: Efficiency of the VIS grating with an aluminum coating. Test provided by Newport-Rochester.

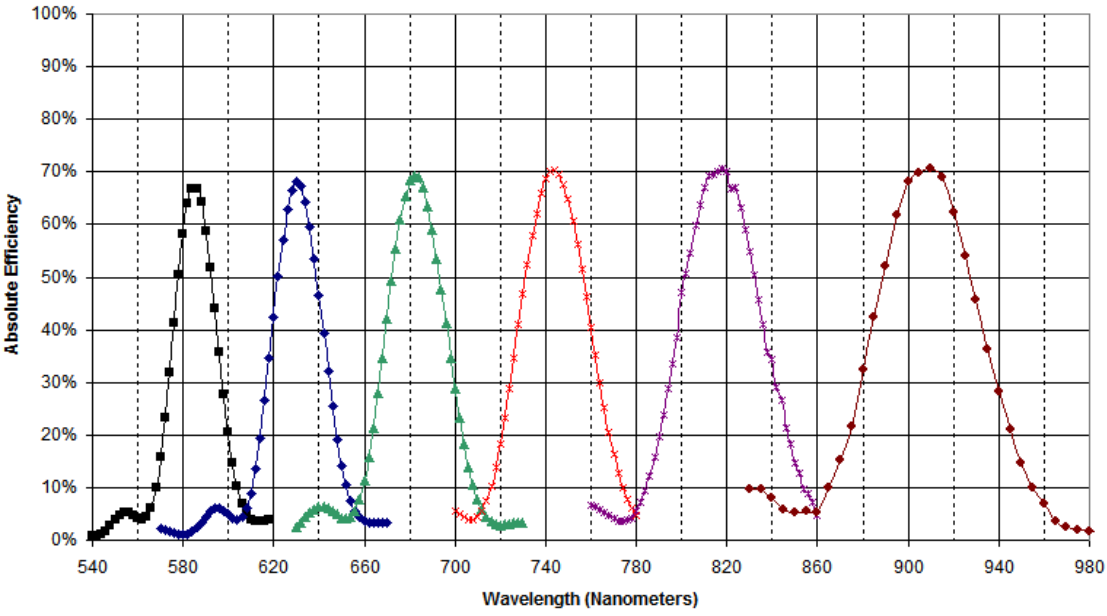

Figure 10.25: Efficiency of the VIS grating with an Ag+MgF_2 coating. Test provided by Newport-Rochester.

10.4 Science with X-shooter

X-shooter is a multi-purpose instrument that can be used to study numerous astrophysical phenomena. A driving science case based in five key topics were used to define the instrument requirements as summarised below:

- **Brown dwarfs**. X-shooter will serve to understand the mechanism of formation of the population of these cold sub-stellar objects and to explore, through a significant statistical sample, their properties and compare them with those of giant planets and low mass stars. This requires simultaneous observations in red and near infrared light to study the accretion and ejection rates, intermediate resolution to follow emission lines and high efficiency to detect young and fading brown dwarfs in star forming regions.

- **Stellar remnants in compact binaries**. The goal is to study the physics of accretion disks by measuring abundances in the secondary stars of mass-transferring binaries to obtain clues about the primaries. For this, UV, Visible and near infrared observations at intermediate resolution are needed in order to study the evolution of narrow emission lines and to measure abundances from absorption lines.

- **High-z emission line galaxies**. By collecting spectra of high redshift, low metallicity HII regions amplified by massive galaxy clusters it will be possible to study the properties of the first stellar populations by measuring the relative emission line and continuum strengths. For this project, a UV-NIR medium resolution spectrophotometry is needed.

- **Quasar absorption lines**. Studying the Lyman-α forest in the line of sight to quasars separated by angular distances of less than 5 arcminutes one can measure the size of intervening clouds through correlations. Ultimately one can derive the cosmological constants Ω_Λ and Ω_m. The above requires high efficiency UV-VIS bands to obtain moderate resolution spectra of absorption lines in the line of sight of intrinsically faint targets ($m_b \sim$21-22).

- **Gamma-ray bursts**. We intend to study the physics of GRBs, to investigate the regions of star formation in which they originate and to probe the intergalactic medium with the unique possibility to do so in the redshift range $6 < z < 10$. The above requires UV to NIR spectroscopy in a single exposure (as the timescales of variation are very rapid) with the highest possible efficiency. The studies of the velocity structure of the absorption lines close to the source and in the intervening medium requires at least medium resolution spectroscopy. Minimum operation overheads are required to observe these targets with rapidly decaying light curves.

10.5 Conclusions

X-shooter is a second generation instrument that is currently being built and that will be mounted on the Cassegrain focus of one ot the VLT 8.0 m units at Paranal observatory. It is being developed by a collaboration of four nations plus ESO and should see first light during the Summer of 2008. It will obtain a complete medium resolution spectrum from 300 to 2500 nm in a single shot through the use of three independent spectrographs that are simultaneously fed by the use of dichroics. It will have an unprecedented efficiency for such an instrument, opening new windows for research in many branches of Astrophysics, including GRBs.

The author of this Thesis has participated with the project as workpackage manager responsible of the testing, procurement and testing of the diffraction gratings of the UV and VIS spectrographs. Different tests were performed during the development phase which served to choose the appropriate gratings and to choose their best arrangement inside the spectrographs. Several manufacturers were contacted and the final products were ordered to Newport-Richardson, who delivered the gratings at the end of 2006. The gratings are now being assembled into the spectrographs at Brera Observatory, in Merate (Italy). Once the spectrographs have been assembled and tested they will travel to ESO Headquarters in Garching (Germany), were the complete instrument will be assembled starting in August 2007. Current schedule foresee that the instrument will travel to Chile during the Spring of 2008.

Bibliography

Covino, S., et al. 2006, Chinese Journal of Astronomy and Astrophysics Supplement, 6, 361

Delabre, B., Dekker, H., D'Odorico, S., & Merkle, F. 1989, Proc. SPIE, 1055, 340

D'Odorico, S., et al. 2004, Proc. SPIE, 5492, 220

D'Odorico, S., et al. 2006, Proc. SPIE, 6269

Goldoni, P., Royer, F., François, P., Horrobin, M., Blanc, G., Vernet, J., Modigliani, A., & Larsen, J. 2006, Proc. SPIE, 6269

Goray, L. I. & Seely, J. F. 2002, Appl. Opt., 41, No. 7, 1434

Goray, L. I. & Sadov, S. Yu 2002, OSA Diffractive Optics & Micro-Optics, 75, 265

Goray, L. I. 2005, Nuclear Inst. and Methods in Physics Research A, 536, No. 1-2, 211

Goray, L. I., Kuznetsov, I. G., Sadov, S. Yu. & Content, D. A. 2006a, J. Opt. Soc. Am A, 23, No. 1, 155

Goray, L. I., Seely, J. F. & Sadov, S. Yu. 2006b, J. Appl. Phys., 100, No. 9, 094901-1-13

Guinouard, I., Horville, D., Puech, M., Hammer, F., Amans, J.-P., Chemla, F., Dekker, H., & Mazzoleni, R. 2006, Proc. SPIE, 6273,

Michaelsen, N., et al. 2006, Proc. SPIE, 6269

Moorwood, A., & D'Odorico, S. 2004, The Messenger, 115, 8

Navarro, R., et al. 2006, Proc. SPIE, 6273

Palmer, C. 2005, "Diffraction Grating Handbook" (6th edition) Newport Corporation.

Spanò, P., et al. 2006, Proc. SPIE, 6269

Vidali, M., Di Marcantonio, P., Santin, P., Vernet, J., & Zacchei, A. 2006, Proc. SPIE, 6274

Zerbi, F. M., et al. 2006, Memorie della Societa Astronomica Italiana Supplement, 9, 419

Part IV

Conclusions and future work

11

Gamma-ray burst science

During the years of Thesis work, the author has actively participated in the follow-up of over 80 gamma-ray bursts that have resulted in more than 100 GRB Coordinates Network (GCN) circulars and 25 refereed publications, being first author of 3 of them. He has been discoverer or codiscoverer of 5 GRB optical afterglows. From all these bursts four of them have been selected (two long bursts and two short bursts) as a significant sample of the two distinct categories and an extensive study has been made for them, which constitutes chapters 4, 5, 6 and 7 of this Ph.D. Thesis.

GRB 021004 is a classical long burst with a very complete multiband follow-up from radio to X-rays. Its detailed light curve shows a great amount of structure that we have attempted to model. GRB 050408 is an X-ray rich burst, the type between classical long GRBs and X-ray flashes, the softest family of events. We studied and modelled the light curve of its afterglow, which we discovered, and searched for the relation between long gamma-ray bursts, X-ray rich bursts (XRR) and X-ray flashes (XRF). GRB 050509B was the first short GRB for which *Swift* gave a precise localisation. In chapter 6 we presented an intensive study of this paricular burst for which no afterglow was detected and derived some implications from its study. Finally, GRB 060121 happened when astronomers had began to think that they knew what short GRB afterglows would look like, and appeared as a different kind of event: A bright short burst happening in the distant Universe.

In this chapter we present our conclusions from the work that we are presenting on gamma-ray bursts and propose future work that we consider that should be done.

11.1 Conclusions

GRB 021004

This burst is an example of a classical long burst at a redshift of $z = 2.3293$ with an early detection, a relatively rapid follow-up and a dense multiband sampling that reveals a vast amount of structure in the light curve. The detailed observations give important constrains in the nature of the bumpy light curve.

We observed the event from 11 optical and near infrared telescopes and in millimetre wavelengths from Plateau de Bure interferometer, providing over 100 datapoints for the

multiband light curve. Using these datapoints together with the previously published data we put together one of the most detailed GRB light curves to date and modelled it. The densely sampled light curve produced important constrains in the models that could explain its behaviour. The model that we fitted to the data is based on an initial burst followed by 7 refreshed shocks that are emitted through a collimated jet with a half opening angle $\theta_j = 1\overset{\circ}{.}8$ adding to a total released energy of 7.8×10^{51} ergs. The energy injections arrive to the front shock between 0.046 and 48.61 days after the burst onset, although we postulate that they were all produced during the GRB explosion and were released with lower velocities than the shock that initially drove the afterglow.

From the several spectral flux distributions that were studied during the evolution of the afterglow we derived a low extinction that followed a Small Magellanic Cloud (SMC) template with an optical extinction $< A_V >= 0.20 \pm 0.08$. A study of the host through late photometry reveals a bright ($M_B = -22.0 \pm 0.3$) starburst galaxy with very low extinction ($< A_V >= 0.06 \pm 0.08$). Both SMC-like extinction and a starburst host galaxy are expected from what it had been observed in other long GRB events.

GRB 050408

In this case we studied an X-ray rich burst, for which we discovered the afterglow and carried out an intense multiwavelength follow-up campaign. We produced the best sampled multicolour optical light curve of an X-ray rich burst to date, that is completed with near infrared, millimetre and X-ray observations.

GRB 050408 is a bright burst, with an observed peak energy of ∼20 keV and an isotropic equivalent energy release in γ-rays $E_{\gamma,iso} \gtrsim 1.3 \times 10^{52}$ erg, at a redshift of $z = 1.236$. This is at least 6 times brighter than the prediction that would be made through the Amati ($E_{peak} - E_{\gamma,iso}$) relation.

The spectral flux distribution in optical and near infrared follows a SMC extinction law with an $< A_V >= 0.73 \pm 0.18$, while late observations show an underlying starburst host galaxy. Both SMC extinction law and starburst host galaxy are typical of classical long GRBs, favouring the models that unify XRF, XRR and long GRBs.

With the data that we gathered we performed a complete modelling of the afterglow in the context of a collimated fireball model. This model includes an energy injection of the order of the initial shock that arrives to the front shock that is producing the afterglow 2.9 days after the burst. A flattening that is observed during the first hours of the burst can be explained through different scenarios, including an additional energy injection, a low initial Lorentz factor or an off-axis viewed jet. This last option results in a slightly better fit and we adopt it as our preferred option.

GRB 050509B

GRB 050509B was the first short burst precisely localised by *Swift* through the X-ray camera (XRT). It was intensively studied from the very early moments after the trigger down to almost 19 days after but that showed no observable optical afterglow in spite of the reported X-ray afterglow.

An elliptical galaxy was found at the edge of the error box, lying at a redshift of $z = 2.225$. A spectral flux distribution study of this host reveals that this galaxy has

an evolved dominant stellar population, with a mean age of 720 Myr, unlike the galaxies that are found harbouring classical long GRBs. Late deep observations do not reveal any underlying supernova component down to very restrictive limits. If the burst was in fact produced in this elliptical galaxy, the compact merger progenitor hypothesis is reinforced, both by the old dominant population of the galaxy and the non detection of supernova. In such scenario, a long travel distance from the place of birth could be expected and the burst would be produced in the outskirts of the host, where it would find a low density environment that would also explain the faint X-ray afterglow and the non detection of its corresponding component at optical and near infrared wavelengths.

However, in the deep images that were obtained, several other faint galaxies were detected, so a higher redshift hypothesis can not be completely ruled out.

GRB 060121

This is a $\sim$2 second duration burst that was classified as a short event. We did an intense multicolour follow-up campaign that began shortly after the trigger. It was a rather different burst from the first short GRBs afterglows that were detected during 2005.

Observations were carried out in U, B, V, R, I and K bands. From a spectral flux distribution we obtained the first (and up to date the only) direct measure of the redshift of a short burst afterglow. We detect a sharp break in the between V and R bands, that indicates 2 possible solutions: A very high redshift, of $z = 4.6$, with a 68% probability and lower one, but still high of $z = 1.7$ with a 35% probability. This latter case would explain the break as due to strong extinction. In any of the 2 cases, GRB 060121 is the furthermost short GRB afterglow ever observed.

It is also significantly different from previous short burst afterglows. This would be an indication that short bursts are not formed by a unique type of events. We suggest the existence of an emerging population of short bursts at high redshift, significantly brighter than previously detected afterglows.

We also study the possibility that GRB 060121 would be part of the intermediate population of bursts, lying between the short and long groups. However, recent observations of other definitively short GRBs have shown similar characteristics and the high redshift population of short events has been confirmed by other groups.

11.2 Prospects for the future

In the years that will follow this Thesis we would like to continue working in the field of GRBs, advancing in the work lines that we have already started and learning new techniques. In the following paragraphs we cite several of the topics which gather our interest and summarise the way in which we think that our contribution could be productive.

Multirange studies of GRB afterglows

Most of the work that we have been doing during the Thesis work has been in the multirange study of individual afterglows, from radio to X-rays. We would like to continue this research, adding polarimetric and spectroscopic observations that will give further clues on

the environment of the bursts, on the burst geometry and on the way in which the observed light curve fluctuations are produced.

Fast photometry

A field that is still hardly unexplored is the fast photometric observations of the afterglows of GRBs. Cameras like the EMCCD mounted on BOOTES-IR will provide observations with unprecedented details of the early emission of relatively bright bursts. The features observed during the initial moments of the GRB will teach us about the initial processes that power the light curves and the circumburst media.

Short GRBs

During the next years a great amount of discoveries are still to be done in the area of short gamma-ray bursts. Almost two years have passed since the discovery of the first counterpart of a short GRB and we have still not obtained a useful optical spectra of an afterglow. This is one of the most immediate aims that should be accomplished in the forthcoming months. Although the physics that drive the afterglows seem to be very similar for long and short GRBs, the environments are expected to be very different. A search for signatures of such different environments in spectroscopy will give us important clues on the nature of the progenitors. As short GRBs can be observed in bright low redshift galaxies we will have the opportunity of comparing the spectra of short GRB galaxies and their afterglows.

From our observations of GRB 060121 we proposed the existence of different subpopulations of short GRBs, with different observational characteristics. We would like to continue working on this area to learn about the physical differences that would separate these populations. The frontier between short and long bursts needs to be defined by observational signatures other than just the duration in order to be able to break the degeneracy. The study of any physical differences in the intermediate population of bursts is still pending.

High redshift GRBs

With GRB 050904 it was demonstrated that GRBs can be observed up to extreme redshifts, and will probably soon become the furthermost objects detected in the Universe. Robotic telescopes with infrared cameras (such as BOOTES-IR) are needed to detect such events, as the Lyman break is redshifted over visible wavelengths. The observation of these events and, in particular, spectroscopy of their afterglows with giant telescopes such as the spanish 10.4 m GTC is crucial and will give us fundamental information of the early Universe.

12

Instrumentation

Gamma-ray bursts are one of the branches of Astrophysics whose advances have been most determined by the advances in instrumentation. They were discovered serendipitously when gamma-ray detectors were placed in space. However, instrumental limitations to give fast and precise positions prevented almost any observational advances for almost 3 decades. It was not until the advent of a new generation of satellites with better gamma-ray detectors, combined with X-ray cameras and a fast network of coordinate distribution that the first optical, near infrared and radio counterparts were detected. Then came the development of robotic observatories that were capable to autonomously point and observe the counterparts in just a few seconds. In the next years, new instrumentation will become available, opening new interesting windows to study these exciting events.

In this chapter we present the conclusions of the work in which we have been participating over the last years related with instrumentation:

1. The development of BOOTES robotic observatories and their instrumentation.
2. The creation of JIBARO, a package of software for the automatic reduction and analysis of observations, optimised for robotic observatories.
3. The participation in the different phases of X-shooter, a second generation instrument for the Very Large Telescope.

12.1 Conclusions

BOOTES

Almost nine years have gone by since the first BOOTES telescope saw first light. After this time BOOTES is now composed of three observatories separated by a baseline of 300 km which are equipped with 5 telescopes and 9 cameras. In order to make the observatories work autonomously, several technological developments have been accomplished. An automatic dome system based on the data supplied by a weather station takes decisions regarding the opening and closing of the observatories. A control software has been written to take care of the communications between the different elements of the observatories

(telescope, cameras, GRB alert system, reduction pipelines, etc.). A near infrared camera is now passing final tests and will be soon installed on the 0.6m BOOTES-IR telescope.

The author has collaborated in most of the phases of development of the different observatories. Amongst these contributions it is worth highlighting the design of a wide field spectrograph that was installed on BOOTES-1 and the leadership of the development of the image reduction and analysis software that is detailed in the following section.

BOOTES has been providing results almost since first light, responding to over 100 GRB alerts, detecting several counterparts and discovering the afterglow of GRB 060707 located at a redshift of $z = 3.43$ (the GRB 000313 optical transient can not be firmly related to the short GRB). It has also worked for other branches of Astrophysics, with a significant contribution to the study of meteors.

JIBARO

Robotic observatories must not only be able to do autonomous observations but must also be able to process and analyse its own data. With this idea in mind JIBARO (**J**oined ut**I**lities in **B**OOTES for the **A**nalysis and **R**eduction of **O**bservations) was created in the context of BOOTES observatories. It is capable of doing the reduction of optical and near infrared observations, with specific routines for bias, dark frame, flat field, background and linearity corrections.

Once the images are reduced, they each go through a detection routine that extracts all the objects. These objects are used to calculate an astrometric solution for the image. By comparing the objects to a catalogue, the photometry of each of the objects is obtained. A further utility searches for new, uncatalogued objects in the image, trying to identify possible GRB counterparts.

Additional utilities include the following: A fits header corrector that adapts images from several observatories to the JIBARO standard, so they can be analysed by it. Image combination, correcting for different scale, rotation and distortion. Combination of images obtained through different filters to create a colour composite. An output to the observatory manager that allows to dynamically correct the pointing. An object simulator to introduce objects in an image, which is used to test the software and to create outreach material.

X-shooter

X-shooter is a second generation spectrograph that will be mounted on the Cassegrain focus of one of the 8m units of ESO's Very Large Telescope. It will obtain a complete medium resolution spectra from 300 to 2,300 nm in a single shot. It is designed to maximise the efficiency through all the spectral range by splitting the optical beam with dichroics into 3 arms, each optimised for a different range.

The author has participated as workpackage manager responsible for the simulation, procurement and testing of the visible and ultraviolet gratings. The gratings have been simulated using PCGrate software. We performed several tests that included studies on the polarisation, incident angle, coating, surface quality and groove profile. The results were used to choose the final design and arrangement of the gratings, that according to the simulations should be capable of meeting the requirements of X-shooter.

After the final design was fixed, several possible providers were contacted and between them Newport-Rochester was selected. The final gratings were ordered at the begining of 2006 and finally delivered in December of the same year. The tests carried out on the delivered material show that the efficiency is consistent with our simulations.

The integration of the ultraviolet and visible spectrographs is now taking place in Brera Observatory (Italy) and the complete instrument will be integrated in the headquarters of ESO in Garching (Germany), beginning in August 2007. The first light of the instrument is foreseen in Chile during 2008.

12.2 Prospects for the future

Robotic observatories

Robotic observatories have proved to be very useful in detecting the counterparts of bright GRBs and observing their early time light curves. However, *Swift* has shown much fainter counterparts than initially expected and robotic observatories will need to increase their collecting areas in order to improve their efficiency. Furthermore, as more and more observatories start to work around the world it is important to coordinate observations in order to be able to have the best possible coverage of each event and to obtain complementary observations. Instrumentation will have to be developed to produce new observations during the early phases of the emission.

BOOTES observatories will soon be upgraded to include larger telescopes (0.6 m) and faster mounts. The different BOOTES observatories, together with other robotic telescopes willing to collaborate will form a unique network that will communicate and automatically plan coordinated observations. New instrumentation is being developed and will be installed on the new generation of telescopes.

Ultimately robotic telescopes should be extended to create 2-4 m class observatories dedicated to do extensive follow-ups of GRBs. These telescopes should be probably funded by space missions as associated ground facilities that will follow-up their alerts.

Software

JIBARO will be soon updated to include spectroscopic and polarimetric analysis, as well as to combine multiband observations of a single or different telescopes in order to make predictions on the evolution of the afterglow and give the necessary information to the observatory planner to dynamically modify upcoming observations.

X-shooter and further instrumentation for large telescopes

During the next year the assembly of X-shooter will be completed and it will travel to Chile to be mounted on one of the 8m VLT units. The author will continue to work on the final phases of the project. Once the instrument is installed and working it would be very interesting to use it for gamma-ray burst research as it will offer new and unique capabilities to study the afterglows.

We would also like to get involved in further instrumentation projects for large telescopes, even more now that Spain has just incorporated to the European Southern Obser-

vatory and the 10.4m GTC telescope will soon see first light at Roque de los Muchachos Observatory in La Palma.

A

Publications

In this appendix we present our publication list. It is divided into four sections: Refereed papers, refereed proceedings, non refereed proceedings and astronomical circulars.

A.1 Refereed papers

1. **'The nature of the X-Ray Flash of August 24 2005'**
   Sollerman, J., Fynbo, J. P. U., Gorosabel, J., Halpern, J. P., Hjorth, J., Jakobsson, P., Mirabal, N., Watson, D., Xu, D., Castro-Tirado, A. J., Feron, C., Jaunsen, A. O., Jelinek, M., Jensen, B. L., Kann, D. A., Ovaldsen, J. E., Pozanenko, A., Stritzinger, M., Thoene, C. C., **de Ugarte Postigo, A.**, Guziy, S., Ibrahimov, M., Jaervinen, S. P., Levan, A., Rumyantsev, V., & Tanvir, N.
   2007, A&Aaccepted DOI: 10.1051/0004-6361:20066683

2. **'Extensive multiband study of the X-ray rich GRB 050408. A likely off-axis event with an intense energy injection'**
   de Ugarte Postigo, A., T.A. Fatkhullin, G. Jóhannesson, J. Gorosabel, V.V. Sokolov, A.J. Castro-Tirado, Yu.Yu. Balega, O.I. Spiridonova, M. Jelínek, S. Guziy, D. Pérez-Ramírez, J. Hjorth, P. Laursen, D. Bersier, S.B. Pandey, M. Bremer, A. Monfardini, K.Y. Huang, Y. Urata, W.H. Ip, T. Tamagawa, D. Kinoshita, T. Mizuno, Y. Arai, H. Yamagishi, T. Soyano, F. Usui, M. Tashiro, K. Abe, K. Onda, Z. Aslan, I. Khamitov & T. Ozisik
   2007, A&A, 462, L57

3. **'X-ray flashes or soft gamma-ray bursts?. The case of the likely distant XRF 040912'**
   G. Stratta, S. Basa, N. Butler, J. L. Atteia, B. Gendre, A. Pelangeon, F. Malacrino, Y. Mellier, D. A. Kann, S. Klose, A. Zeh, N. Masetti, E. Palazzi, J. Gorosabel, A. J. Castro-Tirado, **A. de Ugarte Postigo**, M. Jelinek, J. Cepa, H. Casta, D. Martinez-Delgado, M. Boer, J. Braga, G. Crew, T. Q. Donaghy, J-P. Dezalay, J. Doty, E. E. Fenimore, M. Galassi, C. Graziani, J. G. Jernigan, N. Kawai, D. Q. Lamb, A. Levine, J. Manchanda, F. Martel, M. Matsuoka, Y. Nakagawa, J-F. Olive,

G. Pizzichini, G. Prigozhin, G. Ricker, T. Sakamoto, Y. Shirasaki, S. Sugita, M. Suzuki, K. Takagishi, T. Tamagawa, R. Vanderspek, J. Villasenor, S. E. Woosley, M. Yamauchi & A. Yoshida
2007, A&A, 461, 485

4. **'HI column densities of z > 2 Swift gamma-ray bursts'**
Jakobsson, P., Fynbo, J. P. U., Ledoux, C., Vreeswijk, P., Kann, D. A., Hjorth, J., Tanvir, N. R., Reichart, D., Gorosabel, J., Klose, S., Priddey, R. S., Watson, D., Sollerman, J., Fruchter, A. S., **de Ugarte Postigo, A.**, Wiersema, K., Björnsson, G., Thöne, C. C., Pedersen, K. & Jensen, B. L.
2006, A&A, 460, L13

5. **'Detection of optical linear polarization in the SN 2006aj/GRB 060218 non-spherical expansion'**
J. Gorosabel, V. Larionov, A. J. Castro-Tirado, S. Guziy, L. Larionova, A. Del Olmo, M. A. Martinez, J. Cepa, B. Cedres, **A. de Ugarte Postigo**, M. Jelinek, O. Bogdanov & A. LLorente
2006, A&A, 459, L33

6. **'GRB 051028: an intrinsically faint gamma-ray burst at high redshift?'**
A. J. Castro-Tirado, M. Jelinek, S. B. Pandey, S. McBreen, J. de Jong, D. K. Sahu, P. Ferrero, J. A. Caballero, J. Gorosabel, D. A. Kann, S. Klose, **A. de Ugarte Postigo**, G. C. Anupama, C. Gry, S. Guziy, S. Srividya, L. Valdivieso, S. Vanniarajan & A. A. Henden
2006, A&A, 459, 763

7. **Multi-wavelength afterglow observations of the high redshift GRB 050730**
S. B. Pandey, A. J. Castro-Tirado, S. McBreen, M. D. Perez-Ramirez, M. Bremer, M. A. Guerrero, A. Sota, B. E. Cobb, M. Jelinek, **A. de Ugarte Postigo**, J. Gorosabel, S. Guziy, C. Guidorzi, C. D. Bailyn, T. Munoz-Darias, A. Gomboc, A. Monfardini, C. G. Mundell, N. Tanvir, A. J. Levan, B. C. Bhatt, D. K. Sahu, S. Sharma, O. Bogdanov & J. A. Combi
2006, A&A, 460, 415

8. **'Orbital Elements of 2004 Perseid Meteoroids Perturbed by Jupiter'**
Trigo-Rodriguez, J. M., Vaubaillon, J., Ortiz, J. L., Castro-Tirado, A., Llorca, J., Lyytinen, E., Jelínek, M., **de Ugarte Postigo, A**., Sanz, P. S., Castro, F. J. A., Caso, A. S., González, A. B., Erades, J. P. & Ocaña, F.
2006, Earth Moon and Planets, 22

9. **'GRB 060121: Implications of a Short-/Intermediate-Duration γ-Ray Burst at High Redshift'**
de Ugarte Postigo, A., Castro-Tirado, A. J., Guziy, S., Gorosabel, J., Jóhannesson, G., Aloy, M. A., McBreen, S., Lamb, D. Q., Benitez, N., Jelínek, M., Pandey, S. B., Coe, D., Pérez-Ramírez, M. D., Aceituno, F. J., Alises, M., Acosta-Pulido, J. A., Gómez, G., López, R., Donaghy, T. Q., Nakagawa, Y. E., Sakamoto, T., Ricker, G. R., Hearty, F. R., Bayliss, M., Gyuk, G. & York, D. G.
2006, ApJ, 648, L83

10. **'Physics of the GRB 030328 afterglow and its environment'**
Maiorano, E., Masetti, N., Palazzi, E., Savaglio, S., Rol, E., Vreeswijk, P. M., Pian, E., Price, P. A., Peterson, B. A., Jelínek, M., Amati, L., Andersen, M. I., Castro-Tirado, A. J., Castro Cerón, J. M., **de Ugarte Postigo, A.**, Frontera, F., Fruchter, A. S., Fynbo, J. P. U., Gorosabel, J., Henden, A. A., Hjorth, J., Jensen, B. L., Klose, S., Kouveliotou, C., Masi, G., Møller, P., Nicastro, L., Ofek, E. O., Pandey, S. B., Rhoads, J., Tanvir, N. R., Wijers, R. A. M. J. & van den Heuvel, E. P. J.
2006, A&A, 455, 423

11. **'The bright optical flash from GRB 060117'**
Jelínek, M., Prouza, M., Kubánek, P., Hudec, R., Nekola, M., Řídký, J., Grygar, J., Boháčová, M., Castro-Tirado, A. J., Gorosabel, J., Hrabovský, M., Mandát, D., Nosek, D., Nožka, L., Palatka, M., Pandey, S. B., Pech, M., Schovánek, P., Šmída, R., Trávníček, P., **de Ugarte Postigo, A.** & Vítek, S.
2006, A&A, 454, L119

12. **'Multi-wavelength analysis of the field of the dark burst GRB 031220'**
Melandri, A., Gendre, B., Antonelli, L. A., Grazian, A., **de Ugarte Postigo, A.**, Gorosabel, J., Piro, L., Kosugi, G., Kawai, N., de Pasquale, M. & Garmire, G. P.
2006, A&A, 451, 27

13. **'Revealing the Jet Structure of GRB 030329 with High-Resolution Multi-color Photometry'**
Gorosabel, J., Castro-Tirado, A. J., Ramirez-Ruiz, E., Granot, J., Caon, N., Cairós, L. M., Rubio-Herrera, E., Guziy, S., **de Ugarte Postigo, A.** & Jelínek, M.
2006, ApJ, 641, L13

14. **'The short-duration GRB 050724 host galaxy in the context of the long-duration GRB hosts'**
Gorosabel, J., Castro-Tirado, A. J., Guziy, S., **de Ugarte Postigo, A.**, Reverte, D., Antonelli, A., Covino, S., Malesani, D., Martín-Gordón, D., Melandri, A., Jelínek, M., Elias de La Rosa, N., Bogdanov, O. & Castro Cerón, J. M.
2006, A&A, 450, 87

15. **'A photometric redshift of z = 6.39 ± 0.12 for GRB 050904'**
Haislip, J. B., Nysewander, M. C., Reichart, D. E., Levan, A., Tanvir, N., Cenko, S. B., Fox, D. B., Price, P. A., Castro-Tirado, A. J., Gorosabel, J., Evans, C. R., Figueredo, E., MacLeod, C. L., Kirschbrown, J. R., Jelinek, M., Guziy, S., Postigo, A. D. U., Cypriano, E. S., Lacluyze, A., Graham, J., Priddey, R., Chapman, R., Rhoads, J., Fruchter, A. S., Lamb, D. Q., Kouveliotou, C., Wijers, R. A. M. J., Bayliss, M. B., Schmidt, B. P., Soderberg, A. M., Kulkarni, S. R., Harrison, F. A., Moon, D. S., Gal-Yam, A., Kasliwal, M. M., Hudec, R., Vitek, S., Kubanek, P., Crain, J. A., Foster, A. C., Clemens, J. C., Bartelme, J. W., Canterna, R., Hartmann, D. H., Henden, A. A., Klose, S., Park, H.-S., Williams, G. G., Rol, E., O'Brien, P., Bersier, D., Prada, F., Pizarro, S., Maturana, D., **de Ugarte Postigo, A.**, Alvarez, A., Fernandez, A. J. M., Jarvis, M. J., Moles, M., Alfaro, E., Ivarsen, K. M., Kumar,

N. D., Mack, C. E., Zdarowicz, C. M., Gehrels, N., Barthelmy, S. & Burrows, D. N.
2006, Nature, 440, 181

16. **'The GRB 030329 host: a blue low metallicity subluminous galaxy with intense star formation'**
Gorosabel, J., Pérez-Ramírez, D., Sollerman, J., **de Ugarte Postigo, A.**, Fynbo, J. P. U., Castro-Tirado, A. J., Jakobsson, P., Christensen, L., Hjorth, J., Jóhannesson, G., Guziy, S., Castro Cerón, J. M., Björnsson, G., Sokolov, V. V., Fatkhullin, T. A. & Nilsson, K.
2005, A&A, 444, 711

17. **'GRB 021004 modelled by multiple energy injections'**
de Ugarte Postigo, A., Castro-Tirado, A. J., Gorosabel, J., Jóhannesson, G., Björnsson, G., Gudmundsson, E. H., Bremer, M., Pak, S., Tanvir, N., Castro Cerón, J. M., Guzyi, S., Jelínek, M., Klose, S., Pérez-Ramírez, D., Aceituno, J., Campo Bagatín, A., Covino, S., Cardiel, N., Fathkullin, T., Henden, A. A., Huferath, S., Kurata, Y., Malesani, D., Mannucci, F., Ruiz-Lapuente, P., Sokolov, V., Thiele, U., Wisotzki, L., Antonelli, L. A., Bartolini, C., Boattini, A., Guarnieri, A., Piccioni, A., Pizzichini, G., del Principe, M., di Paola, A., Fugazza, D., Ghisellini, G., Hunt, L., Konstantinova, T., Masetti, N., Palazzi, E., Pian, E., Stefanon, M., Testa, V. & Tristram, P. J.
2005, A&A, 443, 841

18. **'GRB 050904 at redshift 6.3: observations of the oldest cosmic explosion after the Big Bang'**
Tagliaferri, G., Antonelli, L. A., Chincarini, G., Fernández-Soto, A., Malesani, D., Della Valle, M., D'Avanzo, P., Grazian, A., Testa, V., Campana, S., Covino, S., Fiore, F., Stella, L., Castro-Tirado, A. J., Gorosabel, J., Burrows, D. N., Capalbi, M., Cusumano, G., Conciatore, M. L., D'Elia, V., Filliatre, P., Fugazza, D., Gehrels, N., Goldoni, P., Guetta, D., Guziy, S., Held, E. V., Hurley, K., Israel, G. L., Jelínek, M., Lazzati, D., López-Echarri, A., Melandri, A., Mirabel, I. F., Moles, M., Moretti, A., Mason, K. O., Nousek, J., Osborne, J., Pellizza, L. J., Perna, R., Piranomonte, S., Piro, L., **de Ugarte Postigo, A.** & Romano, P.
2005, A&A, 443, L1

19. **'The search for the host galaxy of the gamma-ray burst GRB 000214'**
Guziy, S., Gorosabel, J., Castro-Tirado, A. J., **de Ugarte Postigo, A.**, Jelínek, M., Pérez Ramírez, M. D., Castro Cerón, J. M., Klose, S., Palazzi, E. & Wiersema, K.
2005, A&A, 441, 975

20. **'Radio, millimeter and optical monitoring of GRB 030329 afterglow: constraining the double jet model'**
Resmi, L., Ishwara-Chandra, C. H., Castro-Tirado, A. J., Bhattacharya, D., Rao, A. P., Bremer, M., Pandey, S. B., Sahu, D. K., Bhatt, B. C., Sagar, R., Anupama, G. C., Subramaniam, A., Lundgren, A., Gorosabel, J., Guziy, S., **de Ugarte Postigo, A.**, Castro Cerón, J. M. & Wiklind, T.
2005, A&A, 440, 477

21. **'GRB 050509b: the elusive optical/nIR/mm afterglow of a short-duration GRB'**
Castro-Tirado, A. J., **de Ugarte Postigo, A.**, Gorosabel, J., Fathkullin, T., Sokolov, V., Bremer, M., Márquez, I., Marín, A. J., Guziy, S., Jelínek, M., Kubánek, P., Hudec, R., Vitek, S., Mateo Sanguino, T. J., Eigenbrod, A., Pérez-Ramírez, M. D., Sota, A., Masegosa, J., Prada, F. & Moles, M.
2005, A&A, 439, L15

22. **'GRB 040403: A faint X-ray rich gamma-ray burst discovered by INTEGRAL'**
Mereghetti, S., Götz, D., Andersen, M. I., Castro-Tirado, A., Frontera, F., Gorosabel, J., Hartmann, D. H., Hjorth, J., Hudec, R., Hurley, K., Pizzichini, G., Produit, N., Tarana, A., Topinka, M., Ubertini, P. & **de Ugarte Postigo, A.**
2005, A&A, 433, 113

23. **'The Development of the Spanish Fireball Network Using a New All-Sky CCD System'**
Trigo-Rodríguez, J. M., Castro-Tirado, A. J., Llorca, J., Fabregat, J., Martínez, V. J., Reglero, V., Jelínek, M., Kubánek, P., Mateo, T. & **de Ugarte Postigo, A.**
2004, Earth Moon and Planets, 95, 553

24. **'Probing a Gamma-Ray Burst Progenitor at a Redshift of z = 2: A Comprehensive Observing Campaign of the Afterglow of GRB 030226'**
Klose, S., Greiner, J., Rau, A., Henden, A. A., Hartmann, D. H., Zeh, A., Ries, C., Masetti, N., Malesani, D., Guenther, E., Gorosabel, J., Stecklum, B., Antonelli, L. A., Brinkworth, C., Castro Cerón, J. M., Castro-Tirado, A. J., Covino, S., Fruchter, A., Fynbo, J. P. U., Ghisellini, G., Hjorth, J., Hudec, R., Jelínek, M., Kaper, L., Kouveliotou, C., Lindsay, K., Maiorano, E., Mannucci, F., Nysewander, M., Palazzi, E., Pedersen, K., Pian, E., Reichart, D. E., Rhoads, J., Rol, E., Smail, I., Tanvir, N. R., **de Ugarte Postigo, A.**, Vreeswijk, P. M., Wijers, R. A. M. J. & van den Heuvel, E. P. J.
2004, AJ, 128, 1942

25. **'BOOTES: A stereoscopic robotic ground support facility'**
Castro-Tirado, A. J., Jelínek, M., Mateo Sanguino, T. J., **de Ugarte Postigo, A.** & the BOOTES team
2004, Astronomische Nachrichten, 325, 679

26. **'On the Afterglow of the X-Ray Flash of 2003 July 23: Photometric Evidence for an Off-Axis Gamma-Ray Burst with an Associated Supernova?'**
Fynbo, J. P. U., Sollerman, J., Hjorth, J., Grundahl, F., Gorosabel, J., Weidinger, M., Møller, P., Jensen, B. L., Vreeswijk, P. M., Fransson, C., Ramirez-Ruiz, E., Jakobsson, P., Jørgensen, S. F., Vinter, C., Andersen, M. I., Castro Cerón, J. M., Castro-Tirado, A. J., Fruchter, A. S., Greiner, J., Kouveliotou, C., Levan, A., Klose, S., Masetti, N., Pedersen, H., Palazzi, E., Pian, E., Rhoads, J., Rol, E., Sekiguchi, T., Tanvir, N. R., Tristram, P., **de Ugarte Postigo, A.**, Wijers, R. A. M. J. & van den Heuvel, E.
2004, ApJ, 609, 962

27. **'GRB 030227: The first multiwavelength afterglow of an INTEGRAL GRB'**
Castro-Tirado, A. J., Gorosabel, J., Guziy, S., Reverte, D., Castro Cerón, J. M., **de Ugarte Postigo, A.**, Tanvir, N., Mereghetti, S., Tiengo, A., Buckle, J., Sagar, R., Pandey, S. B., Mohan, V., Masetti, N., Mannucci, F., Feltzing, S., Lundstrom, I., Pedersen, H., Riess, C., Trushkin, S., Vílchez, J., Lund, N., Brandt, S., Martínez Núñez, S., Reglero, V., Pérez-Ramírez, M. D., Klose, S., Greiner, J., Hjorth, J., Kaper, L., Pian, E., Palazzi, E., Andersen, M. I., Fruchter, A., Fynbo, J. P. U., Jensen, B. L., Kouveliotou, C., Rhoads, J., Rol, E., Vreeswijk, P. M., Wijers, R. A. M. J. & van den Heuvel, E.
2003, A&A, 411, L315

28. **'Detection of an optical transient following the 13 March 2000 short/hard gamma-ray burst'**
Castro-Tirado, A. J., Castro Cerón, J. M., Gorosabel, J., Páta, P., Soldán, J., Hudec, R., Jelinek, M., Topinka, M., Bernas, M., Mateo Sanguino, T. J., **de Ugarte Postigo, A.**, Berná, J. Á., Henden, A., Vrba, F., Canzian, B., Harris, H., Delfosse, X., de Pontieu, B., Polcar, J., Sánchez-Fernández, C., de la Morena, B. A., Más-Hesse, J. M., Torres Riera, J. & Barthelmy, S.
2002, A&A, 393, L55

A.2 Refereed proceedings

1. **'Characteristics and Performance of the GAW Experiment for a Large Field of View Cerenkov Gamma-ray Telescope'**
Cusumano, G., Agnetta, G., Assis, P., Biondo, B., Brogueira, P., Catalano, O., Celi, F., Costa, J., Delgado, C., Di Cocco, G., Espirito Santo, M. C., Galeotti, P., Giarrusso, S., La Barbera, A., La Rosa, G., Maccarone, M. C., Mangano, A., Mineo, T., Moles, M., Pimenta, M., Prada, F., Russo, F., Sacco, B., Sanchez, M. A., Segreto, A., Tomé, B., **de Ugarte Postigo, A.**, Vallania, P., & Vigorito, C.
2006, Chinese Journal of Astronomy and Astrophysics Supplement, 6, 369

2. **'RTS2: a powerful robotic observatory manager'**
Kubánek, P., Jelínek, M., Vítek, S., **de Ugarte Postigo, A.**, Nekola, M. & French, J.
2006, SPIE, 6274,

3. **'The optical design of the X-shooter for the VLT'**
Spanò, P., Delabre, B., Norup Sørensen, A., Rigal, F., **de Ugarte Postigo, A.**, Mazzoleni, R., Sacco, G., Conconi, P., De Caprio, V., & Michaelsen, N.
2006, SPIE, 6269,

4. **'BOOTES-IR: a robotic nIR astronomical observatory devoted to follow-up of transient phenomena'**
Castro-Tirado, A. J., Cunniffe, R., **de Ugarte Postigo, A.**, Jelínek, M., Vitek, S., Kubánek, P., Gorosabel, J., Castillo Carrión, S., Mateo Sanguino, T. J., Riva, A.,

Conconi, P., di Caprio, V., Zerbi, F., Amado, P., Cárdenas, C., Claret, A., Guziy, S., Martín-Ruiz, S., Sánchez, M. A., García Teodoro, P., Castro Cerón, J. M., Díaz Verdejo, J., Hudec, R., López Soler, J. M., Berná Galiano, J. Á., Casares, J., Fabregat, J., Páta, P., Sánchez Fernández, C., Sabau-Graziati, M. D., Trigo-Rodríguez, J. M., & Vitali, F.
2006, SPIE, 6267,

5. **'BOOTES-IR: Near IR follow-up GRB observations by a robotic system'**
Castro-Tirado, A. J., **de Ugarte Postigo, A.**, Jelínek, M., Castillo Carrión, S., Mateo Sanguino, T. J., Kubánek, P., Zerbi, F., Amado, P., Cárdenas, C., Claret, A., Gorosabel, J., Martín, S., Sánchez, M. A., García Teodoro, P., Castro Cerón, J. M., Díaz Verdejo, J., López Soler, J. M., Berná Galiano, J. Á., Casares, J., Fabregat, J., Sánchez Fernández, C., Conconi, P., Guziy, S., & Vitaly, F.
2005, Nuovo Cimento C Geophysics Space Physics C, 28, 719

6. **'Simultaneous and optical follow-up GRB observations by BOOTES'**
Castro-Tirado, A. J., Jelínek, M., Mateo Sanguino, T. J., **de Ugarte Postigo**, A., Kubánek, P., Hudec, R., Vitek, S., Páta, P., Bernas, M., Castro Cerón, J. M., Gorosabel, J., Berná Galiano, J. Á., Soldán, J., Soria, T., Fernández, R., de La Morena Carretero, B., & Torres Riera, J.
2005, Nuovo Cimento C Geophysics Space Physics C, 28, 715

7. **'The GRB 030328 host: Another case of a blue starburst galaxy'**
Gorosabel, J., Jelínek, M., **de Ugarte Postigo, A.**, Guziy, S., & Castro-Tirado, A. J.
2005, Nuovo Cimento C Geophysics Space Physics C, 28, 677

8. **'Spectro-photometric study of the GRB 030329 host galaxy'**
Gorosabel, J., Pérez-Ramírez, D., Sollerman, J., **de Ugarte Postigo, A.**, Fynbo, J. P. U., Castro-Tirado, A. J., Jakobsson, P., Christensen, L., Hjorth, J., Jóhannesson, G., Guziy, S., Castro Cerón, J. M., Björnsson, G., Sokolov, V. V., & Fatkhullin, T. A.
2005, Nuovo Cimento C Geophysics Space Physics C, 28, 673

9. **'Multiwavelength chase of GRB 031220 afterglow'**
Melandri, A., Gendre, B., Antonelli, L. A., Grazian, A., **de Ugarte Postigo, A.**, Gorosabel, J., Piro, L., Kosugi, G., & Kaway, N.
2005, Nuovo Cimento C Geophysics Space Physics C, 28, 537

10. **'The earliest spectroscopy of the GRB 030329 afterglow with SAO RAS 6-m telescope and early spectra of core-collapse supernova'**
Kurt, V. G., Sokolov, V. V., Fatkhullin, T. A., Komarova, V. N., Lebedev, V. S., Sokolova, T. N., Castro-Tirado, A. J., **de Ugarte Postigo, A.**, Gorosabel, J., & Guziy, S.
2005, Nuovo Cimento C Geophysics Space Physics C, 28, 521

11. **'Modelling GRB 021004 by multiple energy injections'**
de Ugarte Postigo, A., Gorosabel, J., Castro-Tirado, A. J., Jóhannesson, G.,

Björnsson, G., Gudmundsson, E. H., Bremer, M., Castro Cerón, J. M., Guzyi, S., Jelínek, M., & Pérez-Ramírez, D.
2005, Nuovo Cimento C Geophysics Space Physics C, 28, 287

12. **'The 2004 Perseid fireball night over Spain'**
Trigo-Rodriguez, J. M., Castro-Tirado, A., Jelinek, M., **de Ugarte Postigo, A.**, Llorca, J., Mateo Sanguino, T. J., Sanchez Caso, A., Ocaña, F., Pineda, C., Torrell, S., del Castillo, A., Bullon Lahuerta, J. M., Bernal Gonzalez, A., Lahuerta, L., Lahuerta, S., Patiño, J., Villares, F., Pastor Erades, J., Gomez, C., Garcia Marin, F., & Millan Lopez, J. C.
2005, WGN, Journal of the International Meteor Organization, 33, 5

13. **'Robotic Observatory Tools for Wide-Field Observations'**
de Ugarte Postigo, A., Castro-Tirado, A. J., Mateo Sanguino, T. J., Fernández Palomo, M. T., Berná Galiano, J. Á., Castro Cerón, J. M., Páta, P., Soldán, J., Bernas, M., Hudec, R., Jelínek, M., Vitek, S., Kubánek, P., McBreen, S., Gorosabel, J., García Dabó, C. E., Soria, T., de la Morena Carretero, B. A., & Torres Riera, J.
2004, Baltic Astronomy, 13, 696

14. **'A superbolide recorded by the Spanish Fireball Network'**
Trigo-Rodriguez, J. M., Castro-Tirado, A., Llorca, J., **de Ugarte Postigo, A.**, Sanguino, T. M., & Galvez, F.
2003, WGN, Journal of the International Meteor Organization, 31, 49

15. **'Spanish Fireball Network: Current Status and Recent Orbit Data'**
Trigo-Rodriguez, J. M., Fabregat, J., Llorca, J., Castro-Tirado, A., del Castillo, A., **de Ugarte Postigo, A.**, Lopez, A. E., Villares, F., & Ruiz-Garrido, J.
2001, WGN, Journal of the International Meteor Organization, 29, 139

16. **'Two 1999 Perseid Orbits from Spain'**
Trigo-Rodriguez, J. M., Castellano-Roig, J., **de Ugarte Postigo, A.**, Ruiz-Garrido, J., Fabregat, J., & Llorca, J.
2000, WGN, Journal of the International Meteor Organization, 28, 120

A.3 Non refereed proceedings

1. **'GRB follow-up with BOOTES Optical Chapter 5: The Swift Era'**
Jelínek, M., Castro-Tirado, A. J., Kubánek, P., Vítek, S., **de Ugarte Postigo, A.**, & Hudec, R.
2006, American Institute of Physics Conference Series, 836, 688

2. **'BOOTES-IR: The extension of BOOTES towards the near-IR'**
de Ugarte Postigo, A., Castro-Tirado, A. J., Jelínek, M., Kubánek, P., Cunnife, R., Gorosabel, J., Vitek, S., Castillo-Carrión, S., Guziy, S., Pandey, S. B., Mateo Sanguino, T. D. J., Castro Cerón, J. M., Zerbi, F. M., Conconi, P., Covino, S., Riva, A., de Caprio, V., Amado, P., Claret, A., Cardenas, C., Martín, S., Trigo-Rodriguez,

J. M., Sánchez-Fernández, C., Sabau-Graziati, M. D., Díaz-Verdejo, J., & Vitali, F.
2006, American Institute of Physics Conference Series, 836, 668

3. **'The latest two GRB detected by Hete-2: GRB 051022 and GRB 051028'**
Castro-Tirado, A. J., McBreen, S., Jelínek, M., Pandey, S. B., Bremer, M., **de Ugarte Postigo, A.**, Gorosabel, J., Guziy, S., Bihain, G., Caballero, J. A., Ferrero, P., de Jong, J., Misra, K., & Sahu, D. K.
2006, American Institute of Physics Conference Series, 836, 79

4. **'The X-shooter Spectrograph for the VLT .'**
Zerbi, F. M., Pallavicini, R., Conconi, P., Cosentino, R., De Caprio, V., **de Ugarte Postigo, A.**, Di Marcantonio, P., Riva, M., Santin, P., Spanó, P., & Zacchei, A.
2006, Memorie della Societa Astronomica Italiana Supplement, 9, 419

5. **'JIBARO: Un conjunto de utilidades para la reducción y análisis automatizado de imágenes'**
de Ugarte Postigo, A., Jelínek, M., Gorosabel, J., McBreen, S., García-Dabó, C. E., Mateo Sanguino, T. J., Martín Gordón, D. and Castro-Tirado, A. J.
2005, Astrofísica Robótica en España, edited by A.J. Castro-Tirado, B.A. de la Morena and J. Torres, Madrid, pp. 35-50

6. **'Modelling the afterglow of GRB 021004 with multiple energy injections .'**
de Ugarte Postigo, A., Gorosabel, J., Castro-Tirado, A. J., Jóhannesson, G., Björnsson, G., Gudmundsson, E. H., Bremer, M., Castro Cerón, J. M., Guzyi, S., Jelínek, M., Pérez-Ramírez, D., & A larger collaboration
2005, Memorie della Societa Astronomica Italiana, 76, 655

7. **'GRB 030913: Hunting the Afterglow'**
de Ugarte Postigo, A., Guziy, S., Gorosabel, J., Castro-Tirado, A. J., Castro Cerón, J. M., Mateo Sanguino, T. J., Jelínek, M., Kubánek, P., Hudec, R., Páta, P., Amado, P., Fathkullin, T., Herrería, A., Méndez, J., Ruiz-Lapuente, P., Sokolov, V. V., Zurita, A., & the GRACE collaboration
2004, ESA SP-552: 5th INTEGRAL Workshop on the INTEGRAL Universe, 663

8. **'BOOTES: A Stereoscopic and Robotic Ground-Support Facility for the INTEGRAL Era'**
Castro-Tirado, A. J., Mateo Sanguino, T. J., **de Ugarte Postigo, A.**, Castro Cerón, J. M., Jelínek, M., Kubánek, P., Hudec, R., Vítek, S., Páta, P., Bernas, M., Berná, J. A., Soldán, J., Gorosabel, J., Soria, T., de la Morena, B., Reglero, V., & Torres, J.
2004, ESA SP-552: 5th INTEGRAL Workshop on the INTEGRAL Universe, 637

9. **'BOOTES: Technological Developments and Scientific Results by a Stereoscopic System with two Stations Spaced by 240 km'**
Mateo Sanguino, T. D. J., Castro-Tirado, A. J., **de Ugarte Postigo, A.**, Fernández Palomo, M. T., Castro Cerón, J. M., Berná Galiano, J. A., Páta, P., Soldán, J., Bernas, M., Hudec, R., Jelínek, M., Vítek, S., Kubánek, P., McBreen, S., Gorosabel,

J., García Dabó, C. E., Soria, T., de La Morena Carretero, B. A., & Torres Riera, J.
2004, AIP Conf. Proc. 727: Gamma-Ray Bursts: 30 Years of Discovery, 727, 761

10. **'RTS2 – Remote Telescope System, 2nd Version'**
Kubánek, P., Jelínek, M., Nekola, M., Topinka, M., Štrobl, J., Hudec, R., Mateo Sanguino, T. D. J., **de Ugarte Postigo, A.**, & Castro-Tirado, A. J.
2004, AIP Conf. Proc. 727: Gamma-Ray Bursts: 30 Years of Discovery, 727, 753

11. **'The GRB 030227 Detected by INTEGRAL: Another Sign of Compton Scattering in X-rays'**
Castro-Tirado, A. J., Gorosabel, J., Guziy, S., Reverte, D., Castro Cerón, J. M., **de Ugarte Postigo, A.**, Tanvir, N., Mereghetti, S., Tiengo, A., Pandey, S. B., Masetti, N., Pedersen, H., Péréz Ramírez, M. D., & GRACE Collaboration
2004, AIP Conf. Proc. 727: Gamma-Ray Bursts: 30 Years of Discovery, 727, 491

12. **'BOOTES: Recent Technical Developments and Scientific Results'**
Mateo Sanguino, T. J., de La Morena, B. A., Riera, J. T., Castro-Tirado, A. J., **de Ugarte Postigo, A.**, Gorosabel, J., Castro Cerón, J. M., Dabó, C. E. G., Galiano, J. A. B., Vitek, P. P. S., Bernas, M., Kubánek, M. J. P., Hudec, R., McBreen, S., & Soria, T.
2004, Astronomical Society of the Pacific Conference Series, 312, 536

13. **'Summer 2002 photometric multisite campaign on the open cluster NGC 6633'**
Martín, S., Alonso, R., Rodríguez, E., Ashley, M., Hidas, M., Kim, S.-L., Jeon, Y.-B., Akan, C., Poretti, E., Irwin, M., **de Ugarte Postigo**, A., Bossi, M., Zerbi, F. M., Suárez, J. C., & Hintz, E. G.
2004, ESA SP-538: Stellar Structure and Habitable Planet Finding, 349

14. **'The last born at La Silla: REM, The Rapid Eye Mount'**
Chincarini, G., Zerbi, F., Antonelli, A., Conconi, P., Cutispoto, G., Covino, S., D'Alessio, F., **de Ugarte Postigo, A.**, Molinari, E., Nicastro, L., Tosti, G., Vitali, F., Mazzoleni, R., Sciuto, G., Stefanon, M., Jordan, B., Burderi, L., Campana, S., Danziger, J., di Paola, A., Fernandez-Soto, A., Fiore, F., Ghisellini, G., Goldoni, P., Israel, G. L., Lorenzetti, D., Mc Breen, B., Masetti, N., Messina, S., Meurs, E., Monfardini, A., Palazzi, E., Paul, J., Pian, E., Rodono, M., Stella, L., Tagliaferri, G., Testa, V., & Vergani, S. D.
2003, The Messenger, 113, 40

15. **'Recent Developments in the BOOTES Experiment'**
de Ugarte Postigo, A., Mateo Sanguino, T. J., Castro Cerón, J. M., Páta, P., Bernas, M., Jelinek, M., Hudec, R., McBreen, S., Berná, J. Á., García Dabó, C. E., Gorosabel, J., Más-Hesse, J. M., Soria, T., de La Morena, B. A., Torres Riera, J., & Castro-Tirado, A. J.
2003, AIP Conf. Proc. 662: Gamma-Ray Burst and Afterglow Astronomy 2001: A Workshop Celebrating the First Year of the HETE Mission, 662, 553

16. **'The BOOTES experiment in support of the Gran Telescopio Canarias (GTC) in the study of the high energy Universe'**
Castro Cerón, J. M., **de Ugarte Postigo, A.**, García-Dabó, C. E., Mateo Sanguino, T. J., Páta, P., Bernas, M., Jelínek, M., Hudec, R., Berná, J. Á., Gorosabel, J., Más-Hesse, J. M., & Castro-Tirado, A. J.
2003, Revista Mexicana de Astronomia y Astrofisica Conference Series, 16, 77

17. **'Earliest spectroscopy of the GRB 030329 optical transient'**
Sokolov, V. V., Fatkhullin, T. A., Komarova, V. N., Kurt, V. G., Lebedev, V. S., Castro-Tirado, A. J., Guziy, S., Gorosabel, J., **de Ugarte Postigo, A.**, Cherepaschuk, A. M., & Postnov, K. A.
2003, Bull. Special Astrophys. Obs., 56, 5

18. **'Two years of gamma-ray burst follow up observations with BOOTES-1'**
Castro Cerón, J. M., Castro-Tirado, A. J., Soldán, J., Hudec, R., Bernas, M., Páta, P., Mateo Sanguino, T. D. J., **de Ugarte Postigo, A.**, Berná, J. A., Nekola, M., Gorosabel, J., de La Morena, B. A., Más-Hesse, J. M., Giménez, A., & Torres Riera, J.
2001, ESA SP-459: Exploring the Gamma-Ray Universe, 407

19. **'Search for gamma ray burst quasi simultaneous optical emission with BOOTES-1'**
Castro Cerón, J. M., Castro-Tirado, A. J., Soldán, J., Hudec, R., Bernas, M., Páta, P., Mateo Sanguino, T. J., **de Ugarte Postigo, A.**, Berná, J. Á, Nekola, M., Gorosabel, J., de la Morena, B. A., Más-Hesse, J. M., Giménez, Á., & Torres Riera, J.
2001, Highlights of Spanish astrophysics II, 37

20. **'Gamma-Ray Burst Follow Up Observations with BOOTES in 1998–2000'**
Castro Cerón, J. M., Castro-Tirado, A. J., Hudec, R., Soldán, J., Bernas, M., Páta, P., Sanguino, T. J. M., **de Ugarte Postigo, A.**, Berná, J. Á., Nekola, M., Gorosabel, J., de La Morena, B. A., Más-Hesse, J. M., Giménez, Á., & Torres Riera, J.
2001, Gamma-ray Bursts in the Afterglow Era, 53

21. **'First Results from the Burst Observer and Optical Transient Exploring System Station 1 (BOOTES-1)'**
Castro-Tirado, A. J., Soldán, J., Bernas, M., Páta, P., Hudec, R., Mateo Sanguino, T. J., de La Morena, B., Berná, J. A., **de Ugarte Postigo, A.**, Gorosabel, J., Más-Hesse, J. M., & Giménez, A.
2000, AIP Conf. Proc. 526: Gamma-ray Bursts, 5th Huntsville Symposium, 526, 260

A.4 Astronomical circulars

1. **'GRB 070223: NIR observations at WHT.'**
Castro-Tirado, A. J., **de Ugarte Postigo, A.**, Jelinek, M., Gorosabel, J., Licandro, J., & Bramich, D.
2007, GRB Coordinates Network, 6168

2. **'GRB 070219: i-band observations.'**
de Ugarte Postigo, A., Castro-Tirado, A. J., Gorosabel, J., Jelinek, M., Rodriguez-Gil, P., & Lopez, S.
2007, GRB Coordinates Network, 6110

3. **'GRB 070706B: watcher upper limit.'**
French, J., Melady, G., Jelinek, M., **de Ugarte Postigo, A.**, & Kubanek, P.
2006, GRB Coordinates Network, 5247

4. **'GRB 061222B: BOOTES-IR optical observations.'**
de Ugarte Postigo, A., Jelinek, M., Castro-Tirado, A. J., Casanova, V., Gorosabel, J., Cunniffe, R., Vitek, S., Kubanek, P., Hudec, R., & Sabau-Graziati, L.
2006, GRB Coordinates Network, 5968

5. **'GRB 061217: confirmation of host candidate.'**
de Ugarte Postigo, A., Castro-Tirado, A. J., Gorosabel, J., Jelinek, M., Aceituno, J., Guijarro, A., Monreal, A., Alfonso, J., & Caballero, J. A.
2006, GRB Coordinates Network, 5951

6. **'GRB 061217: optical observations at calar alto.'**
Jelinek, M., Castro-Tirado, A. J., Aceituno, J., Guijarro, A., Monreal, A., Alfonso, J., **de Ugarte Postigo, A.**, & Gorosabel, J.
2006, GRB Coordinates Network, 5933

7. **'GRB 060930: near-IR afterglow candidate retraction.'**
de Ugarte Postigo, A., Jelinek, M., Castro-Tirado, A. J., & Gorosabel, J.
2006, GRB Coordinates Network, 5701

8. **'GRB 060930: near-IR afterglow candidate.'**
de Ugarte Postigo, A., Jelinek, M., Castro-Tirado, A. J., Gorosabel, J., Pinilla-Alonso, N., de, J. L. C., & Licandro, J.
2006, GRB Coordinates Network, 5682

9. **'GRB 060929: TNG k-band observations.'**
Covino, S., **de Ugarte Postigo, A.**, Pinilla, N., & Licandro, J.
2006, GRB Coordinates Network, 5661

10. **'GRB 060929: BART observation.'**
Nekola, M., Munz, F., Strobl, J., **de Ugarte Postigo, A.**, Kubanek, P., & Markwardt, C. B.
2006, GRB Coordinates Network, 5658

11. **'GRB 060929: BOOTES-IR & OSN observations.'**
de Ugarte Postigo, A., Kubanek, P., & Castro-Tirado, A.
2006, GRB Coordinates Network, 5656

12. **'GRB 060926: BOOTES-IR observations.'**
de Ugarte Postigo, A., & Kubanek, P.
2006, GRB Coordinates Network, 5616

13. **'GRB060904B: watcher observations.'**
de Ugarte Postigo, A., French, J., & Kubanek, P.
2006, GRB Coordinates Network, 5510

14. **'GRB 060904 BOOTES-IR and 1.5m OSN observations.'**
de Ugarte Postigo, A., Aceituno, F., Castro-Tirado, A. J., & Kubanek, P.
2006, GRB Coordinates Network, 5509

15. **'GRB060825: BOOTES-IR optical observations.'**
de Ugarte Postigo, A., Gorosabel, J., Jelinek, M., Cunniffe, R., Vitek, S., Castro-Tirado, A. J., Kubanek, P., & Sabau-Graziati, L. D.
2006, GRB Coordinates Network, 5472

16. **'GRB 060801: optical observations at hanle and calar alto.'**
Castro-Tirado, A. J., Anupama, G. C., Srividya, S., Ramya, S., **de Ugarte Postigo, A.**, Sanchez, S., Montoya, L., Castillo, A., Munoz-Mateos, J. F., Jelinek, M., & Gorosabel, J.
2006, GRB Coordinates Network, 5384

17. **'GRB 060707: OA fading and redshift.'**
Jakobsson, P., Tanvir, N., Jensen, B. L., Fynbo, J. P. U., **de Ugarte Postigo, A.**, Gorosabel, J., Klose, S., & Vreeswijk, P.
2006, GRB Coordinates Network, 5298

18. **'GRB 060707: BOOTES-IR optical afterglow candidate.'**
de Ugarte Postigo, A., Gorosabel, J., Jelinek, M., Cunniffe, R., Kubanek, P., Vitek, S., Castro-Tirado, A. J., & Sabau-Graziati, M. D.
2006, GRB Coordinates Network, 5290

19. **'GRB 060707: BOOTES-IR optical observation.'**
de Ugarte Postigo, A., & Gorosabel, J.
2006, GRB Coordinates Network, 5288

20. **'GRB 060604: redshift.'**
Castro-Tirado, A. J., Amado, P., Negueruela, I., Gorosabel, J., Jelinek, M., & **de Ugarte Postigo, A.**
2006, GRB Coordinates Network, 5218

21. **'GRB 060413: watcher UBVR observations.'**
French, J., Melady, G., Hanlon, L., McBreen, B., McBreen, S., Meintjes, P., Hoffman, M., Calitz, H., Smith, N., Jelinek, M., **de Ugarte Postigo, A.**, Castro-Tirado, A. J., Hudec, R., & Kubanek, P.
2006, GRB Coordinates Network, 4960

22. **'GRB 060218: optical/nIR observations at La Palma.'**
de Ugarte Postigo, A., Castro-Tirado, A. J., Pandey, S. B., Barrado Y Navascues, D., Montesinos, B., Mishra, K., & Dehaes, S.
2006, GRB Coordinates Network, 4790

23. **'GRB 060213: optical afterglow candidate.'**
Guziy, S., Jelinek, M., Castro-Tirado, A. J., Pandey, S. B., **de Ugarte Postigo, A.**, Vitek, S., Gorosabel, J., Viironen, K., Caballero, J. A., & Sabin, L.
2006, GRB Coordinates Network, 4771

24. **'GRB 060204C: OSN limits.'**
Jelinek, M., Martinez, D., Guziy, S., Vitek, S., & **de Ugarte Postigo, A.**
2006, GRB Coordinates Network, 4668

25. **'GRB 060204C: BOOTES-IR optical limits.'**
Guziy, S., Vitek, S., Jelinek, M., Castro-Tirado, A. J., **de Ugarte Postigo, A.**, Pandey, S. B., Gorosabel, J., Cuniffe, R., Castillo, S. C., Kubanek, P., Sabau-Graziati, M. D., & Hudec, R.
2006, GRB Coordinates Network, 4666

26. **'GRB 051221B: Bootes optical observations.'**
de Ugarte Postigo, A., Jelinek, M., Vitek, S., Castro-Tirado, A. J., Gorosabel, J., Pandey, S. B., Guziy, S., Kubanek, P., & Hudec, R.
2005, GRB Coordinates Network, 4379

27. **'GRB 051211B: optical afterglow.'**
Jelinek, M., **de Ugarte Postigo, A.**, Castro-Tirado, A. J., Casanova, V., Martinez, D., Guziy, S., Castillo, S., Pandey, S. B., & Gorosabel, J.
2005, GRB Coordinates Network, 4358

28. **'GRB 051211: IAC80 optical observations.'**
de Ugarte Postigo, A., Fernandez-Acosta, S., Guziy, S., Jelinek, M., Pandey, S. B., Gorosabel, J., & Castro-Tirado, A. J.
2005, GRB Coordinates Network, 4335

29. **'GRB 051211A and GRB051211B: Bootes simultaneous observations.'**
Jelinek, M., Castro-Tirado, A. J., Vitek, S., **de Ugarte Postigo, A.**, Kubanek, P., & Hudec, R.
2005, GRB Coordinates Network, 4333

30. **'GRB 051211:IAC80 optical observations.'**
de Ugarte Postigo, A., Fernandez-Acosta, S., Guziy, S., Jelinek, M., Pandey, S. B., Gorosabel, J., & Castro-Tirado, A. J.
2005, GRB Coordinates Network, 4325

31. **'GRB 051109a: Bootes R & I-band detection of the early afterglow.'**
Jelinek, M., **de Ugarte Postigo, A.**, Castro-Tirado, A. J., Vitek, S., Gorosabel, J., Pandey, S. B., Guziy, S. S., Kubanek, P., & Hudec, R.
2005, GRB Coordinates Network, 4227

32. **'GRB 051105a, observation from naini tal and OSN.'**
de Ugarte Postigo, A., Pandey, S. B., Jelanek, M., Castro-Tirado, A. J., Casanova, V., Gorosabel, J., Guziy, S., Mishra, K., & Kamble, A.
2005, GRB Coordinates Network, 4204

33. **'GRB051028: confirmation of the afterglow.'**
Pandey, S. B., Jelinek, M., Guziy, S. S., Gorosabel, J., **de Ugarte Postigo, A.**, Vitek, S., & de Jong, J. T. A.
2005, GRB Coordinates Network, 4176

34. **'GRB051028: WHT optical candidate.'**
Jelinek, M., Pandey, S. B., Guziy, S. S., Gorosabel, J., **de Ugarte Postigo, A.**, Vitek, S., & de Jong, J. T. A.
2005, GRB Coordinates Network, 4175

35. **'GRB 051022, refined optical astrometry.'**
de Ugarte Postigo, A., Aceituno, F. J., & Guziy, S.
2005, GRB Coordinates Network, 4164

36. **'GRB 051022, j & k-band observation.'**
Castro-Tirado, A. J., **de Ugarte Postigo, A.**, Bihain, G., Guziy, S., Pandey, S. B., Jelinek, M., & Gorosabel, J.
2005, GRB Coordinates Network, 4143

37. **'GRB 051021: optical observations.'**
Tristram, P., Zealand, N., Guziy, S., **de Ugarte Postigo, A.**, Pandey, S. B., Castro-Tirado, A. J., Jelinek, M., Gorosabel, J., & Yock, P.
2005, GRB Coordinates Network, 4122

38. **'GRB 051006: optical observations at sierra nevada.'**
de Ugarte Postigo, A., Castro-Tirado, A. J., Guziy, S., Casanova, V., Jelinek, M., & Gorosabel, J.
2005, GRB Coordinates Network, 4064

39. **'GRB 051001, optical observations at mt. John.'**
Tristram, P., Jelinek, M., Castro-Tirado, A. J., **de Ugarte Postigo, A.**, Guziy, S., Gorosabel, J., Yock, P., & Krimm, H.
2005, GRB Coordinates Network, 4055

40. **'INT 2.5m limit for GRB050922B.'**
Guziy, S., Jelinek, M., Gorosabel, J., Castro-Tirado, A. J., **de Ugarte Postigo, A.**, Flores, E. R., & Vijanen, K.
2005, GRB Coordinates Network, 4025

41. **'GRB 050911, optical content of Swift/XRT error box.'**
Castro-Tirado, A. J., **de Ugarte Postigo, A.**, Guziy, S., Jelinek, M., Gorosabel, J., Tristram, P., & Yock, P.
2005, GRB Coordinates Network, 3968

42. **'GRB 050911, optical observations.'**
Tristram, P., Castro-Tirado, A. J., Guziy, S., **de Ugarte Postigo, A.**, Jelinek, M., Gorosabel, J., & Yock, P.
2005, GRB Coordinates Network, 3965

43. **'GRB 050904: Bootes early R-band detection.'**
Jelinek, M., Castro-Tirado, A. J., **de Ugarte Postigo, A.**, Kubanek, P., Vitek, S., Gorosabel, J., Guziy, S., Hudec, R., Castro Cerón, J. M., Pata, P., & Bernas, M.
2005, GRB Coordinates Network, 3929

44. **'GRB 050827 : OSN 1.5m optical observations.'**
Guziy, S., Gorosabel, J., Castro-Tirado, A. J., Casanova, V., **de Ugarte Postigo, A.**, & Jelinek, M.
2005, GRB Coordinates Network, 3903

45. **'GRB 050824 optical candidate.'**
Gorosabel, J., Casanova, V., Garrido, R., Castro-Tirado, A. J., Jelinek, M., & **de Ugarte Postigo, A.**
2005, GRB Coordinates Network, 3865

46. **'GRB 050817: optical observations.'**
Tristram, P., **de Ugarte Postigo, A.**, Gorosabel, J., Guzyi, S., Jelanek, M., Castro-Tirado, A. J., & Yock, P.
2005, GRB Coordinates Network, 3823

47. **'GRB 050813: I-band observations.'**
Gorosabel, J., Guziy, S., Sota, A., Castro-Tirado, A. J., **de Ugarte Postigo, A.**, & Jelinek, M.
2005, GRB Coordinates Network, 3796

48. **'GRB 050730, optical candidate.'**
Sota, A., Castro-Tirado, A. J., Guziy, S., Jelinek, M., **de Ugarte Postigo, A.**, Gorosabel, J., Bodganov, A., & Perez-Ramirez, M. D.
2005, GRB Coordinates Network, 3705

49. **'GRB 050724: j-band observations.'**
de Ugarte Postigo, A., Gorosabel, J., Castro-Tirado, A. J., Jelinek, M., Guziy, S., Roeser, H.-J., Aguirre, A., Pedraz, S., & Bogdanov, O.
2005, GRB Coordinates Network, 3680

50. **'GRB 050724: optical and near-IR observations.'**
Castro-Tirado, A. J., Gorosabel, J., **de Ugarte Postigo, A.**, Guziy, S., Jelinek, M., Karrer, M., Roeser, H.-J., Elias-Rosa, N., Bogdanov, O., & Aguirre, A.
2005, GRB Coordinates Network, 3673

51. **'GRB 050716'**
Gorosabel, J., Castro-Tirado, A. J., Lopez, R., Andreuzzi, G., **de Ugarte Postigo, A.**, Guziy, S., Jelinek, M., & Bogdanov, O.
2005, GRB Coordinates Network, 3641

52. **'GRB 050713, r-band observations at NOT.'**
Guziy, S., Castro-Tirado, A. J., **de Ugarte Postigo, A.**, Gorosabel, J., de Cruz, J. L., Bogdanov, O., & Jelinek, M.
2005, GRB Coordinates Network, 3584

53. **'GRB 050626 optical observations.'**
Gorosabel, J., Castro-Tirado, A. J., Tristram, P., Britton, T., Yock, P., Guziy, S., **de Ugarte Postigo, A.**, Jelinek, M., & Bogdanov, O.
2005, GRB Coordinates Network, 3565

54. **'GRB050528: Bootes optical candidate (retraction).'**
Jelinek, M., Castro-Tirado, A. J., **de Ugarte Postigo, A.**, Vitek, S., Guziy, S., Kubanek, P., Hudec, R., Nekola, M., Pata, P., Bernas, M., & Mateo Sanguino, T. J.
2005, GRB Coordinates Network, 3500

55. **'GRB050528: Bootes optical candidate.'**
Jelinek, M., Castro-Tirado, A. J., **de Ugarte Postigo, A.**, Vitek, S., Guziy, S., Kubanek, P., Hudec, R., Nekola, M., Pata, P., Bernas, M., & Mateo Sanguino, T. J.
2005, GRB Coordinates Network, 3498

56. **'GRB 050525A: Bootes simultaneous optical observations.'**
de Ugarte Postigo, A., Jelinek, M., Gorosabel, J., Guziy, S., Kubanek, P., Hudec, R., Vitek, S., Soria, T. J., Fernandez, R., Fabregat, J., & Castro-Tirado, A. J.
2005, GRB Coordinates Network, 3480

57. **'GRB 050520: OSN optical observations.'**
de Ugarte Postigo, A., Castro-Tirado, A. J., Sota, A., Jelinek, M., Gorosabel, J., & Guziy, S.
2005, GRB Coordinates Network, 3432

58. **'GRB 050509b: optical observations.'**
de Ugarte Postigo, A., Castro-Tirado, A. J., Eigenbrod, A., Jelinek, M., Gorosabel, J., & Guziy, S.
2005, GRB Coordinates Network, 3384

59. **'GRB 050505: early time observations.'**
de Ugarte Postigo, A., Jelinek, M., Gorosabel, J., Kubanek, P., Hudec, R., Mateo Sanguino, T. J., Castillo, S., Guziy, S., & Castro-Tirado, A. J.
2005, GRB Coordinates Network, 3376

60. **'GRB 050505, simultaneous optical observation.'**
Jelinek, M., Castro-Tirado, A. J., Gorosabel, J., **de Ugarte Postigo, A.**, Guziy, S., Kubanek, P., Hudec, R., & Vitek, S.
2005, GRB Coordinates Network, 3373

61. **'GRB 050421: BOOTES-2 simultaneous optical observations.'**
Jelinek, M., Castro-Tirado, A. J., Gorosabel, J., **de Ugarte Postigo, A.**, Kubanek, P., Hudec, R., Sanguino, T. J. M., Soria, T., Fernandez, R., & Fabregat, J.
2005, GRB Coordinates Network, 3298

62. **'GRB 050421: optical observations at the INT.'**
de Ugarte Postigo, A., Furnes, J., Corradi, R., Jelinek, M., Gorosabel, J., & Castro-Tirado, A. J.
2005, GRB Coordinates Network, 3297

63. **'GRB 050416B: optical observations.'**
Jelinek, M., **de Ugarte Postigo, A.**, Kubanek, P., Sanguino, T. J. M., Castillo, S., Gorosabel, J., Guziy, S., & Castro-Tirado, A. J.
2005, GRB Coordinates Network, 3285

64. **'GRB 050412: optical observations.'**
Jelinek, M., **de Ugarte Postigo, A.**, Casanova, V., Gorosabel, J., & Castro-Tirado, A. J.
2005, GRB Coordinates Network, 3255

65. **'GRB 050410 R band optical observations.'**
Misra, K., **de Ugarte Postigo, A.**, Jelinek, M., Kamble, A. P., Pandey, S. B., & Castro-Tirado, A. J.
2005, GRB Coordinates Network, 3226

66. **'GRB 050408: steepening of the optical decay.'**
Jelinek, M., Fathkullin, T., Komarova, V., Sokolova, T., Sokolov, V., Vlasyuk, V., Balega, Y., Guziy, S., **de Ugarte Postigo, A.**, Gorosabel, J., & Castro-Tirado, A. J.
2005, GRB Coordinates Network, 3197

67. **'GRB 050408 optical candidate.'**
de Ugarte Postigo, A., Komarova, V., Fathkullin, T., Sokolova, T., Sokolov, V., Vlasyuk, V., Balega, Y., Guziy, S., Jelinek, M., Gorosabel, J., & Castro-Tirado, A. J.
2005, GRB Coordinates Network, 3193

68. **'GRB 050408 optical candidate.'**
de Ugarte Postigo, A., Komarova, V., Fathkullin, T., Sokolova, T., Sokolov, V., Vlasyuk, V., Balega, Y., Guziy, S., Jelinek, M., Gorosabel, J., & Castro-Tirado, A. J.
2005, GRB Coordinates Network, 3192

69. **'GRB050326: optical limit.'**
Tristram, P., Jelinek, M., **de Ugarte Postigo, A.**, Gorosabel, J., Castro-Tirado, A. J., Castro Cerón, J. M., & Yock, P.
2005, GRB Coordinates Network, 3151

70. **'GRB 050223: optical observations.'**
Gorosabel, J., Eguchi, S., **de Ugarte Postigo, A.**, Yock, P., & Castro-Tirado, A. J.
2005, GRB Coordinates Network, 3061

71. **'GRB 050219a, optical observations.'**
de Ugarte Postigo, A., Eguchi, S., Gorosabel, J., Yock, P., & Castro-Tirado, A. J.
2005, GRB Coordinates Network, 3041

72. **'GRB 050215b, BOOTES-2 simultaneous optical observations.'**
Jelinek, M., Castro-Tirado, A. J., Gorosabel, J., **de Ugarte Postigo, A.**, Kubanek, P., Hudec, R., Mateo Sanguino, T. J., Soria, T., Fernandez, R., & Fabregat, J.
2005, GRB Coordinates Network, 3029

73. **'GRB 050215c, BOOTES-1B optical limit.'**
Jelinek, M., Gorosabel, J., Castro-Tirado, A. J., **de Ugarte Postigo, A.**, Kubanek, P., Hudec, R., & Vitek, S.
2005, GRB Coordinates Network, 3023

74. **'short/hard GRB 050202, optical observations.'**
Castro-Tirado, A. J., Bond, I., Kilmartin, P., **de Ugarte Postigo, A.**, Gorosabel, J., Jelinek, M., & Yock, P.
2005, GRB Coordinates Network, 3018

75. **'GRB 050129: optical observations.'**
Gorosabel, J., Castro-Tirado, A. J., **de Ugarte Postigo, A.**, Jelinek, M., & Casanova, V.
2005, GRB Coordinates Network, 3008

76. **'GRB 041224 and GRB 041226: BOOTES-2 simultaneous observations.'**
Castro-Tirado, A. J., Jelinek, M., **de Ugarte Postigo, A.**, Vitek, S., Kubanek, P., Mateo Sanguino, T. J., Castro Cerón, J. M., Soria, T., & Fabregat, J.
2005, GRB Coordinates Network, 2961

77. **'GRB 050117, i-band observations.'**
de Ugarte Postigo, A., Sota, A., Jelinek, M., Gorosabel, J., Castro-Tirado, A. J., & Castro Cerón, J. M.
2005, GRB Coordinates Network, 2957

78. **'GRB 041218: optical candidate.'**
Gorosabel, J., **de Ugarte, A.**, Castro-Tirado, A. J., Jelinek, M., & Pedraz, S.
2004, GRB Coordinates Network, 2861

79. **'GRB 041016: BOOTES-2 simultaneous observation.'**
Jelinek, M., Castro-Tirado, A. J., **de Ugarte Postigo, A.**, Vitek, S., Kubanek, P., Mateo Sanguino, T. J., Soria, T., & Fabregat, J.
2004, GRB Coordinates Network, 2822

80. **'GRB 040924, optical follow-up.'**
Perez-Ramirez, D., Tristram, P., Gorosabel, J., Jelinek, M., Okada, C., Yock, P., **de Ugarte Postigo, A.**, Guziy, S., & Castro-Tirado, A. J.
2004, GRB Coordinates Network, 2739

81. **'XRF 040912, identification of CXO sources.'**
Gorosabel, J., Cepa, J., **de Ugarte Postigo, A.**, Martinez-Delgado, D., Casanova, V., Guziy, S., Jelinek, M., Castro Cerón, J. M., Castaneda, H., Zucker, D., Bell, E. F., & Castro-Tirado, A. J.
2004, GRB Coordinates Network, 2724

82. **'XRF 040916, optical follow-up.'**
de Ugarte Postigo, A., Reverte-Paya, D., Gorosabel, J., Guziy, S., Jelinek, M., Vilchez, J., & Castro-Tirado, A. J.
2004, GRB Coordinates Network, 2717

83. **'GRB 040825B: optical observations.'**
Gorosabel, J., **de Ugarte Postigo, A.**, Miranda, L. F., Castro-Tirado, A. J., Jelinek, M., Pereira, C. B., Castro Cerón, J. M., & Aceituno, J.
2004, GRB Coordinates Network, 2675

84. **'GRB 040825A: optical observations.'**
Tristram, P., **de Ugarte Postigo, A.**, Gorosabel, J., Castro-Tirado, A. J., Jelinek, M., Castro Cerón, J. M., & Yock, P.
2004, GRB Coordinates Network, 2661

85. **'GRB 040730: optical observations.'**
Gorosabel, J., Eguchi, S., Castro-Tirado, A. J., **de Ugarte Postigo, A.**, Kilmartin, P., Yock, P., Jelinek, M., Gotz, D., & Castro Cerón, J. M.
2004, GRB Coordinates Network, 2635

86. **'XRF 040701, optical observations.'**
de Ugarte Postigo, A., Tristram, P., Gorosabel, J., Yock, P., & Castro-Tirado, A. J.
2004, GRB Coordinates Network, 2621

87. **'GRB 040624: r-band observations.'**
Gorosabel, J., Casanova, V., Verdes-Montenegro, L., Jelinek, M., **de Ugarte Postigo, A.**, Castro-Tirado, A. J., & Castro Cerón, J. M.
2004, GRB Coordinates Network, 2615

88. **'GRB 040403, deep optical observations.'**
de Ugarte, A., Sota, A., Gorosabel, J., Castro-Tirado, A. J., & Castro Cerón, J. M.
2004, GRB Coordinates Network, 2571

89. **'GRB 040323, a dark GRB ?'**
Castro-Tirado, A. J., Gorosabel, J., **de Ugarte, A.**, Tristram, P., Yock, P., Jelinek, M., Perez-Ramirez, M. D., & Castro Cerón, J. M.
2004, GRB Coordinates Network, 2553

90. **'GRB 2974 follow-up observations.'**
Strobl, J., Kubanek, P., Jelinek, M., Hudec, R., Topinka, M., Munz, F., Nekola, M., Castro-Tirado, A. J., Sanguino, T. M., & **de Ugarte Postigo, A.**
2003, GRB Coordinates Network, 2491

91. **'GRB 031111, optical observations.'**
Fernandez-Acosta, S., Guziy, S., Casanova, V., **de Ugarte, A.**, Gorosabel, J., & Castro-Tirado, A. J.
2003, GRB Coordinates Network, 2446

92. **'GRB 030913, optical candidate.'**
Guziy, S., **de Ugarte Postigo, A.**, Castro-Tirado, A. J., Gorosabel, J., Amado, P., Herrero, A., Ruiz-Lapuente, P., Mendez, J., Castro Cerón, J. M., & Zurita, A.
2003, GRB Coordinates Network, 2391

93. **'GRB 030913, Bootes observations.'**
de Ugarte Postigo, A., Kubanek, P., Jelinek, M., Mateo Sanguino, T. J., Hudec, R., Soria, T., Guziy, S., & Castro-Tirado, A.
2003, GRB Coordinates Network, 2389

94. **'XRF 030723, optical observations.'**
de Ugarte, A., Tristram, P., Sekiguchi, T., Jelinek, M., Gorosabel, J., Guziy, S., Kilmartin, P., Castro Cerón, J. M., Kilmartin, P., Yock, P., & Castro-Tirado, A. J.
2003, GRB Coordinates Network, 2314

95. **'GRB 030519B: optical observations.'**
Gorosabel, J., Levan, A., **de Ugarte Postigo, A.**, Castro-Tirado, A. J., Fruchter, A., Guziy, S., Castro Cerón, J. M., Guijarro, A., Aguirre, A., & Alises, M.
2003, GRB Coordinates Network, 2263

96. **'GRB 030329 optical observations.'**
Gorosabel, J., **de Ugarte Postigo, A.**, Castro-Tirado, A. J., Fruchter, A., Levan, A., Guziy, S., Castro Cerón, J. M., Guijarro, A., & Aguirre, A.
2003, GRB Coordinates Network, 2242

97. **'GRB 030324, optical observations.'**
Guzyi, S., Castro-Tirado, A. J., Cardiel, N., Pedraz, S., Huferath, S., Worseck, G., Greiner, J., Klose, S., **de Ugarte, A.**, & Gorosabel, J.
2003, GRB Coordinates Network, 1945

98. **'GRB 030227 optical afterglow.'**
Gorosabel, J., Castro-Tirado, A. J., Reverte, D., Vilchez, J., Castro Cerón, J. M., **de Ugarte Postigo, A.**, Guziy, S., & Martinez, S.
2003, GRB Coordinates Network, 1915

99. **'GRB 030227, possible optical counterpart of XMM-newton source.'**
Castro-Tirado, A. J., Reverte, D., Vilchez, J., Gorosabel, J., Castro Cerón, J. M., **de Ugarte, A.**, & Guziy, S.
2003, GRB Coordinates Network, 1904

100. **'GRB 030226 simultaneous optical observations.'**
Castro-Tirado, A. J., **de Ugarte Postigo, A.**, Mateo Sanguino, T. J., Fernandez Palomo, M. T., Jelinek, M., Kubanek, P., Hudec, R., Vitek, S., Pata, P., & Berna, J. A.
2003, GRB Coordinates Network, 1887

101. **'GRB 030115, simultaneous observations by BOOTES-1.'**
Castro-Tirado, A. J., Mateo Sanguino, T. J., **de Ugarte Postigo, A.**, Jelinek, M., Kubanek, P., Hudec, R., Vitek, S., Pata, P., & Berna, J. A.
2003, GRB Coordinates Network, 1826

102. **'GRB 030115, no optical candidate.'**
Castro-Tirado, A. J., Gorosabel, J., Casanova, V., Garcia-Lobo, E., Castro Cerón,

J. M., **de Ugarte, A.**, Fynbo, J., & Rol, E.
2003, GRB Coordinates Network, 1807

103. **'GRB 030115, optical candidate.'**
Castro-Tirado, A. J., Gorosabel, J., Casanova, V., Garcia-Lobo, E., Castro Cerón, J. M., & **de Ugarte, A.**
2003, GRB Coordinates Network, 1805

104. **'GRB 021201: Bootes simultaneous optical observations.'**
Castro-Tirado, A. J., **de Ugarte Postigo, A.**, Mateo Sanguino, T. J., Jelinek, M., Kubanek, P., Hudec, R., Vitek, S., Pata, P., & Berna, J. A.
2002, GRB Coordinates Network, 1720

105. **'GRB 020531, simultaneous optical observations.'**
Castro-Tirado, A. J., Castro Cerón, J. M., **de Ugarte Postigo, A.**, Hudec, R., Jelinek, M., Bernas, M., Pata, P., & Berna, J. A.
2002, GRB Coordinates Network, 1430

106. **'GRB 000313 - optical transient in the BATSE error box.'**
Castro-Tirado, A., Soldan, J., Hudec, R., Pata, P., Bernas, M., Gorosabel, J., Castro Cerón, J. M., Mateo Sanguino, T. J., **de Ugarte, A.**, Angel Berna, J., Henden, A., Vrba, F., Canzian, B., Harris, H., Delfosse, X., & Barthelmy, S.
2000, GRB Coordinates Network, 612